Proceedings of the 1999 CCSS Workshop held in Dublin, Ireland

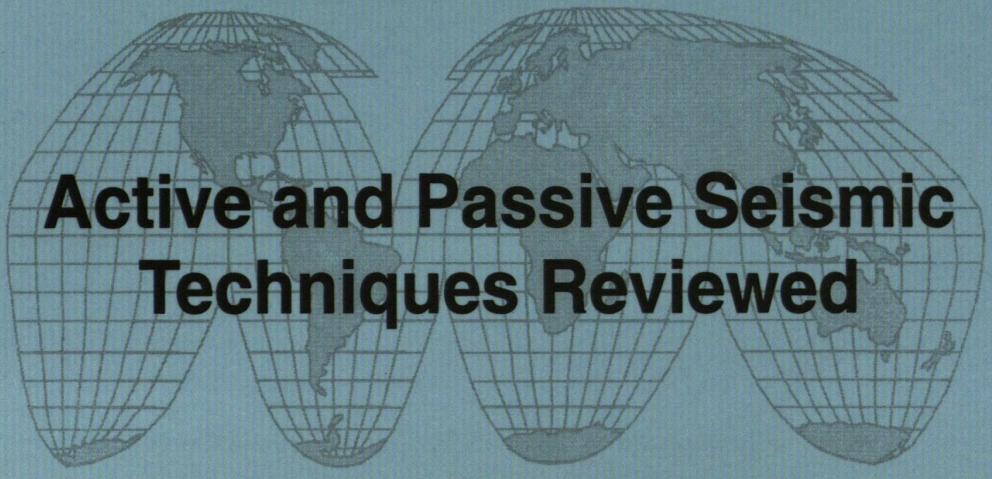

Active and Passive Seismic Techniques Reviewed

In honour of Robert Mallet, 19th Century Irish Seismologist

Editors: A. W. Brian Jacob, Christopher J. Bean, Stephen T. F. Jacob

COMMUNICATIONS OF THE DUBLIN INSTITUTE FOR ADVANCED STUDIES
Series D, Geophysical Bulletin No. 49

DUBLIN

Price: IR£31.50 / €40

Proceedings of the 1999 CCSS Workshop held in Dublin, Ireland

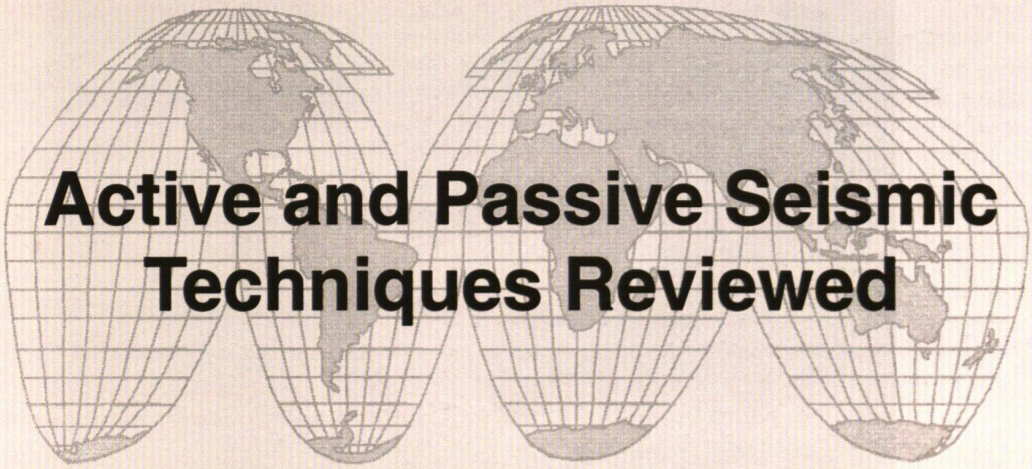

Active and Passive Seismic Techniques Reviewed

In honour of Robert Mallet, 19th Century Irish Seismologist

Editors: A. W. Brian Jacob, Christopher J. Bean, Stephen T. F. Jacob

COMMUNICATIONS OF THE DUBLIN INSTITUTE FOR ADVANCED STUDIES
Series D, Geophysical Bulletin No. 49

DUBLIN

Price: IR£31.50 / €40

COMMUNICATIONS OF THE

DUBLIN INSTITUTE FOR ADVANCED STUDIES

Series D, Geophysical Bulletin No. 49

DUBLIN 2000

DUBLIN INSTITUTE FOR ADVANCED STUDIES

ISBN 1-85500-958-7

Robert Mallet

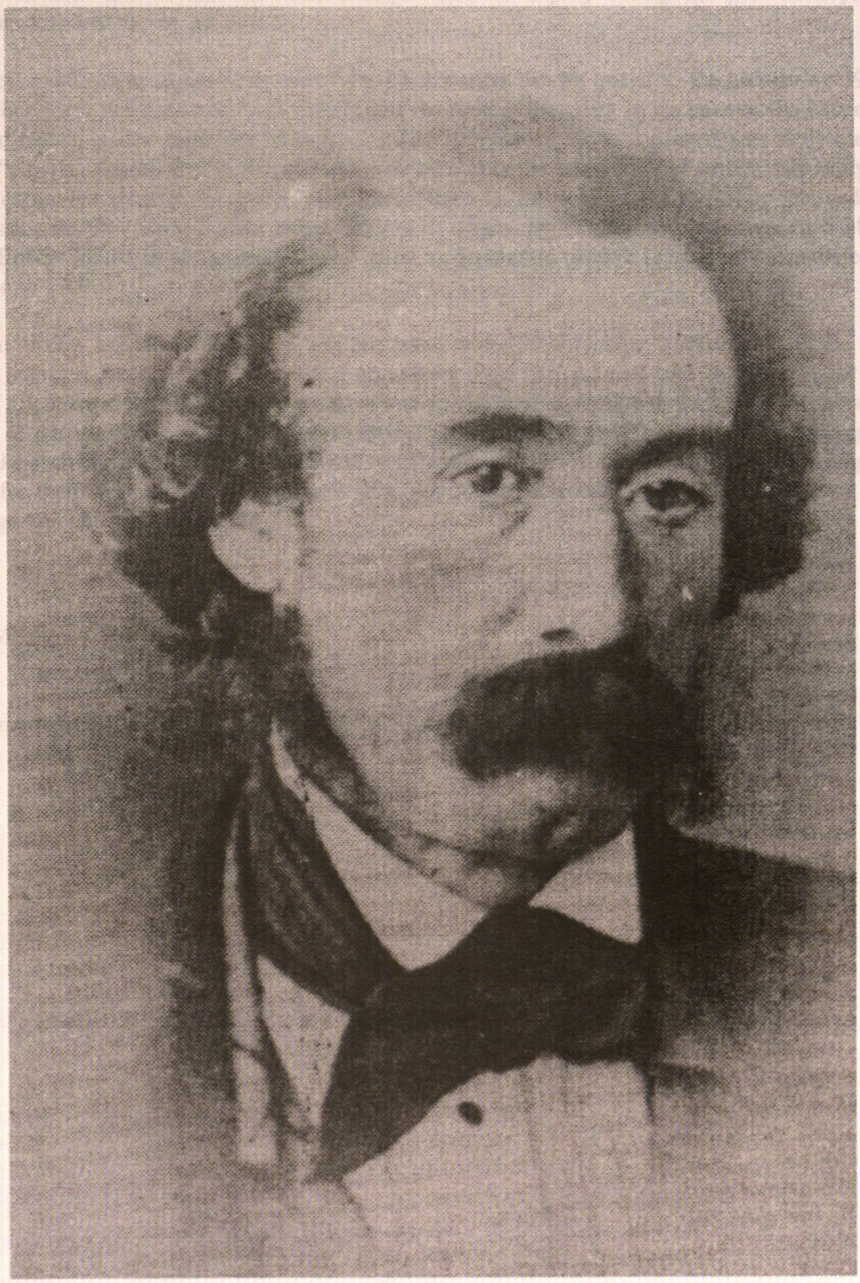

Robert Mallet, MRIA, FRS, 1810-1881
From a photograph in the possession
of the *Old Dublin Society*

Foreword

The Earth has several physical attributes that are unique within our Solar System. The existence of life is the most conspicuous attribute, which in turn is related to the Earth's oceans and continents. An understanding of the origin of continents and oceans has been a major field of inquiry during the past century, and further investigations will continue in this century.

Seismological exploration of the structure of the Earth's crust can be traced to the pioneering 1909 study by Andrija Mohorovicic in Croatia that first determined the base of the crust. In his honour, the boundary between the crust and mantle is now called the Mohorovicic discontinuity, or Moho for short. This study can properly be considered "passive seismology" in that Mohorovicic used only the traveltimes of natural seismicity, rather than man-made, controlled sources. As noted in the Introduction to this volume, the workshop returned the focus of the Commission on Controlled Source Seismology to its origins by: (1) honouring the invention of this field of science by Robert Mallet in 1849, and (2) once again incorporating passive seismology, as initiated by Andrija Mohorovicic in 1909.

A great deal of new and exciting science was presented at the 1999 Dublin Workshop. Both the speakers and others who attended are indebted to the local organizers, Prof. Brian Jacob and Dr. Christopher Bean. Their selection of scientific topics and keynote speakers was an essential ingredient to the success of the workshop. As well, many of the staff of the Dublin Institute for Advanced Studies contributed their time, energy, and good cheer to make each participant feel welcome and comfortable. Finally, it is a pleasure to acknowledge the People of Ireland, for their warm hospitality and rare gifts, not only as scientists, such as Robert Mallet, but as warm human beings and philosophers of life.

Walter D. Mooney

Chairman
Commission on Controlled Source Seismology (CCSS)

Contents

Introduction

This volume is the Proceedings of the Workshop, sponsored by the IASPEI Commission on Controlled Source Seismology (CCSS), held in Dublin, Ireland, in the Dublin Institute for Advanced Studies (DIAS) 6-8 October 1999. This Workshop took a different form to any that preceded it. There have been rapid developments in all aspects of seismology in the recent past and the organisers considered that the scope of this Workshop should be widened to include passive techniques as well as the active ones exclusively considered previously. The feedback we received from participants (and our own observations) gave us the impression that the Workshop was successful in its aim to bring passive methods to the attention of the "active" community. We hope it was also illuminating to those who have been developing and using passive techniques. We hope, too, that the balance of experiment and theory suited most tastes.

Another feature of this Workshop was that it was in honour of Robert Mallet, a nineteenth century Irish scientist and engineer who was the first to carry out a controlled source seismic experiment. This was on a beach just south of Dublin in late October and early November 1849. The Workshop was thus almost exactly 150 years after Mallet's pioneering experiment. Mallet could even be said to have presaged the mixing of active and passive techniques in that his experiments were part of a much wider systematic plan of research to study earthquakes in all their aspects. There was a poster on his controlled source experiment and there is a brief account in the last paper in this volume.

The Workshop took place in DIAS. We are grateful to the Institute for providing the facilities and, especially, to many willing helpers who gave their time to help make the Workshop a success. We would also like to thank the Royal Irish Academy for hosting a meeting in the Academy during the Workshop, at which the Chairman of the Commission, Walter Mooney, gave a paper. There was a full house and the Academy held a reception afterwards which was enjoyed by those attending the Workshop. The Workshop closed with a dinner, which was enlivened by an "Awards Ceremony", conducted by Chairman Mooney who was ably assisted by Gemma Mussachio. Any outsider who wants to know more about this event should contact a participant. Your editors will keep a low profile on this one. On the day after the Workshop there was a field trip to the site of Robert Mallet's first experiments in Controlled Source Seismology on Killiney Beach and afterwards through the Leinster Granites via the historical site of Glendalough. The entertaining and informative leader of this field trip was Padhraig Kennan. To him we owe the thanks of all the Workshoppers who went on the trip.

The papers follow the same sequence as did the talks in the Workshop, with the posters at the back of the volume. As the papers were in thematic groups, there is a pattern to the layout. The abstract for the talk given as a Discourse by Walter Mooney in the Royal Irish Academy on the evening of Thursday 7 October is also in its chronological position.

The intention in this volume was to produce a written record quickly, before memories of the Workshop have faded, which would reinforce what participants took away with them. Unfortunately the illness of one of us (BJ) has caused some delays and we hope that we have been rapid enough to be useful. We would like to thank all those authors who polished their original extended abstracts. A very high proportion have done so. Generally we have printed the papers exactly as received, except for reformatting, mostly merely correcting what we considered to be some obvious typographical errors. We hope we have got those right and will take the blame if we have not. Because of certain technical restrictions resulting from the need to get the volume out quickly, some of the figures may be not be as clear as the authors would like. We suggest that, where a reader finds this a problem, they contact the author in question for a better rendering.

During the meeting we had a total of thirty-eight contributions, including posters. These covered a diverse range of material including active-passive studies, theoretical work, borehole high-resolution controlled source studies, acquisition methods and environmental issues. As expected the majority of contributions concentrated on the development of new models for a broad spectrum of geographical locations and tectonic settings. This theme got off to a flying start with an excellent overview of deep lithospheric structure based on receiver functions. Presentations on passive-active experiments in Tibet, Greece, Ireland, Italy, Mexico, Central Europe, Brazil, Russia and the East Pacific also formed part of this theme. Particularly striking was the multi-disciplinary nature of many of these experiments. In all such cases, clear net benefit can be demonstrated with reflection (and some high resolution refraction) measurements offering good structural control, with refraction profiling and passive studies leading to better estimation of physical properties and depth of investigation respectively. There were

some noteworthy examples of tomographic imagery in volcanic regions, demonstrating the effectiveness of combined ocean bottom and land based recording instruments when used in conjunction with a highly repeatable, closely spaced (120m) air gun source with 360 degree coverage. The array was also used to record local seismicity.

Theoretical contributions covered five basic themes: I) Forward modelling versus inversion II) Stochastic modelling and wave scattering III) Full wavefield versus travel time inversion IV) Statistical versus deterministic deconvolution and V) Resolution issues. Most models of the continental crystalline crust contain mid-crustal first or higher order velocity steps. These discontinuities are mainly based on observed wide-angle reflections on refraction profiles. Stochastic modelling has shown that this interpretation may not be unique. A variety of statistically defined, non-layered crustal models are capable of producing similar arrival patterns at wide angle. There is still no broad consensus on this issue. Stochastic modelling is also challenging traditional interpretations of Pn. It can be shown that in the presence of fine scale structure in the lithospheric mantle, a Pn phase can still exist in the presence of a negative velocity gradient in the uppermost mantle. This has important implications for petrophysical models of the lower lithosphere. It is clear that, with recent advances in clustered arrays of desktop computers, full-wavefield tomography is now computationally feasible for problems of practical interest in 2D and, to a lesser extent in 3D. Models derived through current fast travel time modelling routines can be used as starting models for such schemes, acting as an ideal compliment to the computationally more expensive full wavefield methods. This area looks very promising, especially with the current trends in distributed memory computing.

Resolution is always a key issue in seismology. In travel time tomography although we often take the Fresnel zone as a measure of lateral resolution, in practice it can be shown that the effective resolution is significantly better than this theoretical limit. The inclusion of full waveforms clearly further improves resolution. The detrimental role of near surface wave attenuation in influencing resolution was brought to our attention by results of controlled source experiments carried out in a petroleum reservoir borehole. The seismic quality factor (Q) was effectively infinite at 1000Hz at reservoir level. This points to a need for a greater use of borehole seismometers for improved data fidelity.

Survey design and acquisition methods are of paramount importance in CSS. We were reminded how, in the space of thirty years, refraction surveys have gone from having as few as two recording stations to twelve hundred stations; with the ratio of personnel-to-equipment reduced by a factor of thirty-six! Despite this move to greater data coverage, we were shown how it is possible to achieve low-fold 3-D coverage from 2-D seismic surveys, if nature is obliging enough to force us into crooked line survey geometries.

Finally, the growing issue of the competing needs of the seismologist and the environmentalist were very nicely illustrated in an account of two experiments, one in Puget Sound, Washington state, the other off the coast of southern California. While the Puget Sound experiment was carried out to the satisfaction of all interested parties, the southern California project was severely restricted. The principle ingredient missing from the operation in southern California was an early, intensive public relations campaign.

A. W. Brian Jacob (DIAS)
Christopher J. Bean (University College Dublin)
Stephen T. F. Jacob (DIAS)

Editors

Probing Deep Lithospheric and Upper Mantle Structures with Receiver Functions

Rainer Kind and Stephan Sobolev
GeoForschungsZentrum Potsdam
kind@gfz-potsdam.de
stephan@gfz-potsdam.de

Although the basic idea to use P to S converted teleseismic phases underneath a single station or an array of stations to determine the structure in the crust and upper mantle is quite old, it took a few decades to realise the full potential of this technique. Its history should therefore be described here briefly. An early attempt to use P to S converted teleseismic phases in an industrial style to map crustal and upper mantle horizons was made in the former Soviet Union starting in the fifties. A summary of similar work in northeast Germany is given by Pomeranceva et al. (1970) and Hoffmann et al. (1989). Phinney (1964) has introduced 'crustal transfer functions' in the frequency domain, which have been revived by Burdick and Langston (1977) in the time domain and called later 'Receiver Functions'. Vinnik (1977) has included delay and sum techniques into the method and used it to study upper mantle discontinuities. In the last years the Receiver Function method has further been extended to include move out corrections and migration methods, as they are used traditionally in steep angle reflection methods (Yuan et al. 1997, Kosarev et al. 1999, Bostock and Rondenay 1999, Duecker and Sheehan 1997). Identification of multiples is a problem (as in reflection seismics). Both methods are primarely useful for mapping topography, rather than determining velocities. Ryberg and Weber (1999) have compared both methods in detail, using 2D theoretical seismograms. They showed that it is possible to achieve lateral resolutions better than the size of the Fresnel zone. The improved form of the Receiver Function method is now used with increasing success and may play in the near future the same role in the mantle as reflection seismics in the crust.

Applications of the new version of the technique are summarized as follows:

Kind and Vinnik (1988) have studied the upper mantle discontinuities underneath the Graefenberg (GRF) Array using Vinnik's delay and sum technique. Petersen et al. (1993) have attempted to determine the sharpness of the upper mantle discontinuities using summation traces of P to S conversions. The use of wave forms of summation traces to determine the sharpness of seismic discontinuities seems, however, in many cases doubtful since possible topography of the discontinuity will be interpreted into reduced sharpness of the discontinuity (Yuan et al. 1997, Li et al. 1999). Stammler et al. (1991) and Stammler et al. (1992) have tried, in a first global study (mainly using continental stations), to identify a possible correlation or anticorrelation of the upper mantle discontinuities at 410 and 660 km depth. An anticorrelation due to lateral temperature changes in the mantle transition zone would be expected as a consequence of phase changes in olivine (e.g. Schubert et al. 1975). Kind et al. (1995) have determined the crustal structure and Moho depth at the stations of the German Regional Seismic Network (GRSN) using Receiver Functions.

Kosarev et al. (1999), Yuan et al. (1997) and Kind et al. (1996) have imaged the crustal thickness and detached Indian and Asian mantle lithospheres underneath Tibet to 250 km depth using data from temporary deployments of broadband stations (INDEPTH and PASSCAL experiments). Yuan et al. (1999) have, in a very similar way, imaged the entire upper mantle underneath the Andes using data from several temporary station deployments (Sonderforschungsbereich 267 'Deformation Processes in the Andes' and PASSCAL). A low velocity zone in the upper crust was found in both of these two largest high plateaus in the world. This zone has been interpreted as a zone of partial melt resulting from underthrusting of several 100 km of Indian shield under the Tibetan upper crust and of Brasilian shield under the Andean upper crust. Yuan et al. (1999) imaged the Nazca crust down to 120 km depth beneath the Andes, and the south American Moho across the entire Andean orogen. Comparing results of the steep angle experiment ANCORP in northern Chile and Bolivia (ANCORP Working Group 1999) with Receiver Function results, it was found that the steep angle reflector at 80 km depth originates from the top of the subducted oceanic crust. Receiver Functions have been able to image clearly the crust-mantle boundary in both of these extreme regions, where controlled source methods are not always successful in transporting sufficient energy to large depths.

Gossler et al. (1999) have used Receiver Functions to study the crustal structure between the Harz Mountains and the Scandinavian Shield to the south of Stockholm across the Sorgenfrei-Tornquist Zone.

The resulting crustal thicknesses confirm most earlier results obtained with different seismic methods. North of the Elbe river there is a disagreement about the Moho depth between industrial steep angle reflection data (Hoffmann et al. 1996) and wide angle data (Thybo et al. 1998). Receiver function data confirm the larger crustal thickness indicated by steep angle reflections. They also found a structure penetrating the entire crust just north of the Caledonian Deformation Front (CDF), which separates the Caledonian Orogen from the Scandinavian Shield. Gossler et al. (1999) also compared Receiver Function observations with steep angle reflection results in the north German Basin (DEKORP-BASIN Research-Group 1999). The Moho depth in both methods is in good agreement. It is remarkable that in both methods a structure is visible in the lower crust near the Baltic Shores, which was interpreted as a piece of the Baltic crust underneath the Caledonian upper crust. This is in agreement with large zircon ages observed in boreholes in the same region.

Li et al. (1999) have used Receiver Functions to study the conduit of the Hawaiian Plume in the upper mantle. They used data from a permanent station on Oahu and a temporary deployment on the Island of Hawaii. Two indications of the plume conduit have been found: a very low velocity zone underneath the central part of the Island of Hawaii at about 120 km depth, and a thinning of the upper mantle transition zone several hundred kilometers to the southwest of the Island of Hawaii. The latter observation is an indication of the lower mantle origin of the Hawaii Plume.

In conclusion, Receiver Functions have proved to be very useful in imaging the entire upper mantle from deeper than the 660 km discontinuity to the surface. The main structures, even within the crust can be seen.

References:

ANCORP Working Group, 1999. *Seismic reflection image of Andean subduction zone revealing offset of intermediate-depth seismicity into oceanic mantle.* Nature, 397: 341–344, 1999.

Bostock, M. and S. Rondenay, 1999. *Migration of scattered teleseismic body waves.* Geophys. J. Int., 137: 732–746.

Burdick, L. J. and Ch. L. Langston, 1977. *Modeling crustal structure through the use of converted phases in teleseismic body-wave forms.* Bull. Seism. Soc. Am., 67: 677–691.

DEKORP-BASIN Research-Group, 1999. *The deep crustal structure of the Northeast German Basin: New DEKORP-BASIN'96 deep-profiling results.* Geology, 27, 1, 55–58.

Duecker, K. G. and A. F. Sheehan, 1997. *Mantle discontinuity structure from midpoint stacks of converted P to S waves across the Yellowstone hotspot track.* J. Geophys Res., 12: 8313–8327.

Gossler, J., R. Kind, S. V. Sobolev, H. Kaempf, K. Wylegalla, M. Stiller and TOR Working Group, 1999. *Major crustal features from the Harz Mountains to the Baltic Shield derived from receiver functions.* Tectonophysics, in press.

Hoffmann, N., Stiewe, H., Pasternak, G., 1996. *Struktur und Genese der Mohorovicic--Diskontinuitaet (Moho) im Norddeutschen Becken--ein Ergebnis langzeitregistrierter Steilwinkelseismik.* Z. Angew. Geol., 42: 138–148.

Hoffmann, H., J. Boelsche, W. Horst, W. Lange, F. Palesch, V. Pomeranceva and K. Wruck, 1989. *Tiefenseismische Untersuchungen in der DDR durch den VEB Geophysik – Stand und Ergebnisse.* Z. angew. Geol., 35, 10/11: 308–314.

Kind R. and L. P. Vinnik, 1988. *The upper-mantle discontinuities underneath the GRF array from P-to-S converted phases.* J. Geophys., 62: 138–147.

Kind R., G. L. Kosarev and N. V. Petersen, 1995. *Receiver functions of the stations of the German Regional Seismic Network (GRSN).* Geophys. J. Int., 121: 191–202.

Kind R., J. Ni, Wenjin Zhao, Jianxin Wu, Xiaohui Yuan, Lianshe Zhao, E. Sandvol, Ch. Reese, J. Nabelek and T. Hearn, 1996. *Evidence from earthquake data for a partially molten crustal layer in southern Tibet.* Science, 274: 1692–1694.

Kosarev, G., R. Kind, S. V. Sobolev, X. Yuan, W. Hanka and S. Oreshin, 1999. *Seismic evidence for detached Indian lithospheric mantle beneath Tibet.* Science, 283: 1306–1309.

Li, X., R. Kind, K. Priestley, S. V. Sobolev, F. Tilmann, X. Yuan, and M. Weber, 1999. *Mapping the Hawaii plume conduit with converted seismic waves.* Nature, submitted.

Petersen, N., L. Vinnik, G. Kosarev, R. Kind, S. Oreshin and K. Stammler, 1993. *Sharpness of*

the mantle discontinuities. Geophys. Res. Let., 20: 859–862.

Phinney, R. A., 1964. *Structure of the Earth's crust from spectral behaviour of long-period body waves*. J. Geophys. Res., 69: 2997–3017.

Pomeranceva, I. V., A. N. Mozzenko, Ch. Junge und W. Lange, 1970. *Die Methode 'Zemlja'-Ein neues Verfahren zur regionalen Untersuchung des Krustenbaues*. Z. Geologie, 19 (2): 125–136.

Ryberg, T. and M. Weber, 1999. *Receiver function arrays – a reflection seismic approach*. Geophys. J. Int., in press.

Schubert, G., D. A. Yuen and D. L. Turcotte, 1975. *Role of phase transitions in a dynamic mantle*. Geophys. J. R. Astron. Soc., 42: 705–735.

Stammler, K., R. Kind, G. L. Kosarev, A. Plesinger, J. Horalek, Liu Qiyuan and L. P. Vinnik, 1991. *Broadband observations of PS conversions from the upper mantle*. Geophys. J. Int., 105: 801–804.

Stammler, K., R. Kind, N. Petersen, G. Kosarev, L. Vinnik and Liu Qiyuan, 1992. *The upper mantle discontinuities: correlated or anticorrelated?* Geophys. Res. Let., 19: 1563–1566.

Thybo, H., Perchuc, E., Gregersen, S., 1998. *Interpretation in Statu Nascendi of seismic wide-angle reflections based on EUGENO-S data*. Tectonophysics 289: 281–294.

Vinnik, L. P., 1977. *Detection of waves converted from P to SV in the mantle*. Phys. Earth Planet. Int., 15: 294–303.

Yuan, X., J. Ni, R. Kind, J. Mechie, E. Sandvol, 1997. *Lithospheric and upper mantle structure of southern Tibet from a seismological passive source experiment*. J. Geophys. Res., 102: 27491–27500.

Yuan, X., S. V. Sobolev, R. Kind, O. Oncken and Andes Seismology Group, 1999. *New constraints on subduction and collision processes in the central Andes from comprehensive observations of P to S converted seismic phases*. In preparation.

Case Studies in the New Lithospheric Seismology: Projects INDEPTH and URALS

Larry D. Brown

(Institute for the Study of the Continents, Cornell University, Ithaca, N.Y. 14853, USA, brown@geology.cornell.edu)

The new lithospheric seismology is characterized by the integrated acquisition and analysis of near-vertical reflection profiling for structural detailing, wide-angle reflection/refraction recording for physical property estimation and passive recording of local and teleseismic events for extended penetration and independent measurement of bulk lithospheric properties. New recording technologies and instrument pools can be exploited in experimental design to enhance scientific productivity and operational cost effectiveness. The potential and limitations of a fully integrated seismic experiment are illustrated by the experience in Project INDEPTH, a program of geophysical and geological transects across the Himalayas and Tibet Plateau. Project INDEPTH (**IN**ternational **DEep** **P**rofiling of **T**ibet and the **H**imalaya) began in 1992 with a modest pilot experiment to test the feasibility of multichannel reflection profiling to probe the doubly thick crust of the Himalaya region. The core reflection profiling was carried out with a standard oil industry recording system and explosive sources. A small piggyback of three component recording at wide-angles with refraction equipment (PASSCAL REFTEKS) at fixed locations was added to provide both additional crustal P velocity and S wave information to complement reflection imagery at minor additional cost, and met with modest success. The wide-angle program was expanded in Phase II (1994) to provide greater density and longer offsets, and augmented by equipping an interspersed subset of stations with broadband sensors for natural source recording. The complementary nature of the various seismic components proved especially critical for the intepretation of key features of the Tibetan crust in this phase. For example, interpretation of a strong reflector detailed by reflection profiling beneath the southern Tibet Plateau as a fluid was confirmed by shear wave observations on the wide-angle refraction stations, as well as on receiver functions derived from teleseismic recordings by the stations equipped with broadband sensors. Subsequent detailed analysis of both the near-vertical and wide-angle reflection results have fueled a new debate over the nature (magma vs water) of deep crustal fluids worldwide. Where the reflection profiling failed to penetrate to the base of the crust, teleseismic data (receiver functions) provided key constraints on Moho geometry. Where the teleseismic data alone was tenuous, reflection profiling confirmed structure (e.g. MFT) and ties of surface geology (e.g. **Figure 1**) Where the reflection profiling could not be carried out (e.g. Zangbo Suture), wide-angle recording filled the gap.

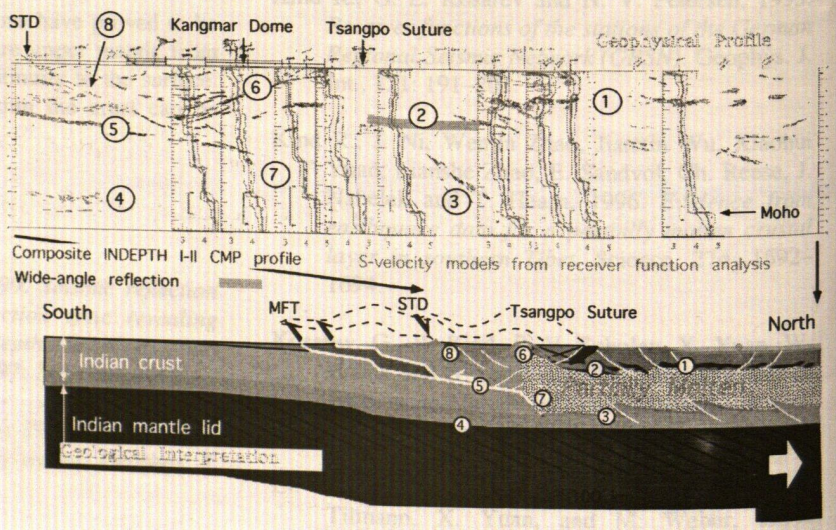

Figure 1: Integration of reflection and receiver functions results from Project INDEPTH to define crustal structure of Himalaya-southern Tibet Plateau region. Note that reflection provides structural details in upper crust only hinted at by teleseismic data, but receiver functions constrain depth Moho where reflection penetration is lacking. Numbers refer to features discussed in Nelson et al. (1996)

Experience in Phase II was a major influence in the design of Phase III, which went forward in spite of a greatly reduced budget. Probing of the central Tibet Plateau was built around a core profile of broadband stations to provide gross structural control to mantle depths, a deployment that was also exploited to record both crustal refraction and reflection information from a program of specially designed shots (**Figure 2**). Moreover, integrated use of a portable, 24 channel "engineering" seismic system provided key tests of crustal reflectivity at minimal cost. Numerous local earthquakes also recorded by this core array promise an additional source of both tectonic and structural information. Analysis of the passive component of this experiment has just gotten underway.

Simutaneous tomographic inversion of controlled source (reflection AND wide-angle), local event and teleseismic recordings could lead to much more robust models of velocity structure with overlapping scales of resolution.

A deep reflection profile in another part of Eurasia, the Southern Urals, was collected by Project URSEIS in 1995 using both vibroseis and dynamite sources (an integration issue of some interest in itself) and augmented by co-incident refraction recording. Key results of that experiment were the confirmation of a Uralian crustal "root" (though one whose dimensions are still debated) and the discovery of a number of sub-Moho reflectors (e.g. Berzin et al. 1996). Although passive seismic recording was not carried out during URSEIS,

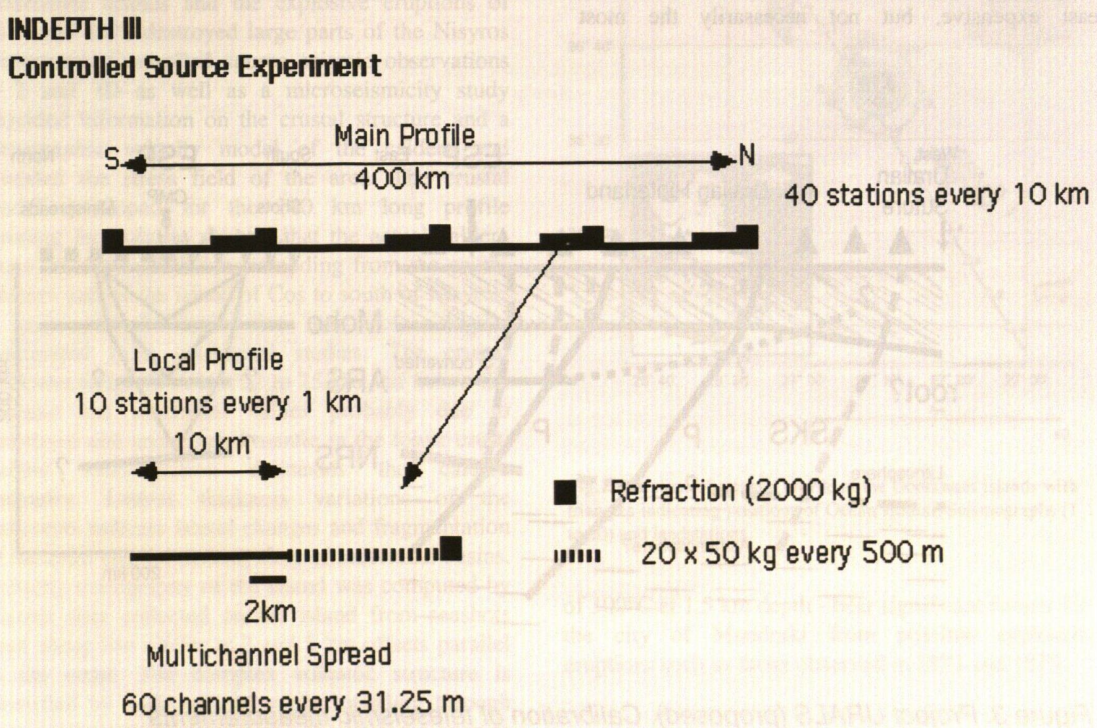

Figure 2. Experimental design for INDEPTH III, in which a core array of broadband stations is also used for crustal reflection and refraction.

However, the analysis of INDEPTH's various types of seismic (and other geophysical) data has yet to exploit the full potential of integration. To date the observations of these respective methods have been independently analyzed and the subsequent results compared. True integration should include integrated inversion and modeling. For example, the "shallow" velocity structure provided by crustal reflection and refraction could constrain the lithospheric velocity estimates of receiver function inversion. primarily for logistical reasons, the reflection profile has led to the proposal of a new active/passive experiment to exploit the presence of sub-lithospheric marker reflectors to estimate interval anisotropy. Project URALS (Ultradeep Reflectors, Anisotropy and Lithospheric Stratigraphy) represents an attempt to "calibrate" passive methods (receiver functions, SKS splitting estimates) against independent estimates of deep lithospheric properties provided by a controlled source ESP (e.g. **Figure 3**).

If successful, it opens new doors for mapping of lithospheric deformation at depth by integrated recording of teleseismic and near-vertical shear wave information. Like INDEPTH, Project URALS represents a strategy for combining the best of controlled-source and passive seismic techniques in a cost-effective manner to answer important geological questions which have proven resistant to "traditional" exploration approaches.

Such growing experience in simultaneous active/passive recording for lithospheric structure has also revealed the limitations of the current infrastructure available to support such major initiatives. These increasingly large and logistically complex experiments make greater demands upon both limited instrument pools and funding resources. Budgetary pressures can result in a bias toward the least expensive, but not necessarily the most effective, selection of options from the available geophysical "toolkit". In short, effective implementation of lithospheric experiments will continue to place a premium on long term international cooperation by funding agencies, instrument pools as well as individual researchers.

References

Nelson et al., 1996, Partially molten middle crust beneath southern Tibet: Synthesis of Project INDEPTH Results, **Science, 174**, 1684-1688.

Berzin et al., 1996, URSEIS '95 - New views of orogenic evolution from the Ural Mountains, **Science, 274**, 220-221.

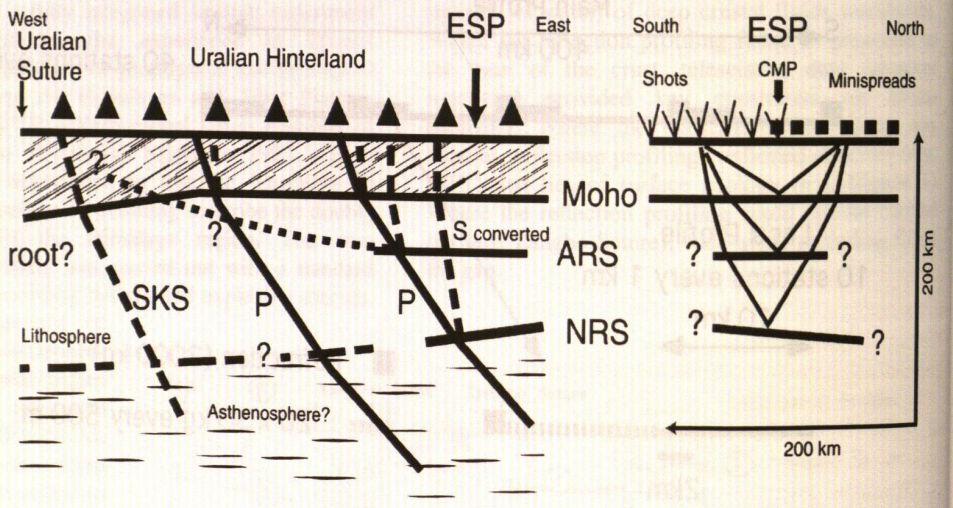

Figure 3. Project URALS (proposed). Calibration of teleseismic measurements (receiver function+SKS splitting) with 3 component, controlled-source expanding spread.

Active and Passive Seismic Studies of Nisyros Volcano – East Agean Sea

Jannis Makris, Tatiana Chonia
Institute of Geophysics, University of Hamburg, Bundesstraße 55, 20146 Hamburg, Germany.
E-mail: makris@dkrz.de, tatiana@gpm.dkrz.de

Abstract

The explosive nature of the volcanic activity of the island of Nisyros has been geologically and historically documented. The ignimbritic eruption of 145 000 ± 5 000 years BP covered most of the Dodecanes islands and the explosive eruptions of 1871 and 1873 destroyed large parts of the Nisyros settlements. Controlled source seismic observations in 2 and 3D as well as a microseismicity study provided information on the crustal structure and a tomographic velocity model of the caldera and revealed the stress field of the area. The crustal model developed for the 140 km long profile crossing the volcano showed that the actual caldera has a diameter of 30 km, extending from the south-western part of the island of Cos to south of Nisyros. It has a much larger size than volcanologists anticipated from geological studies. The crustal thickness ranges between 22 to 25 km and below the volcano has maximum values probably due to mobilised and underplated mantle in the lower crust. Recent sedimentation delineates the caldera geometry. Lateral thickness variations of the sediments indicate lateral changes and fragmentation of the crust and the development of individual basins. Velocity tomography of the island was computed by seismic data collected on the island from seashots fired along two circles at 2 and 5 km offsets parallel to the coast. The complex volcanic structure is identified by high velocity rocks intruding through the upper crust and penetrating the volcanic cone to depths of approx. 1.0 km to 1.8 km below surface. A particularly high magma position was identified below the island of Yali and the central caldera of Nisyros.

The seismicity observed over a period of three months, allowed us to locate 1600 events with magnitudes ranging from 1.2 to 3.2 ML. They are located within the caldera and are mostly of shallow depth. One active linear fault extends from the island of Tilos to Nisyros and to Yali, striking NW-SE. The fault is displaced at Yali to the E-NE and continues along the NW-SE trend over western Cos. The high tectonic activity of this fault, crossing the Nisyros caldera at its western side, and the existence of an overheated aquifer in the caldera - water temperature of 300°C at 1.5 km depth - bear significant danger for the city of Mandraki from possible explosive eruptions such as those observed in 1871 and 1873.

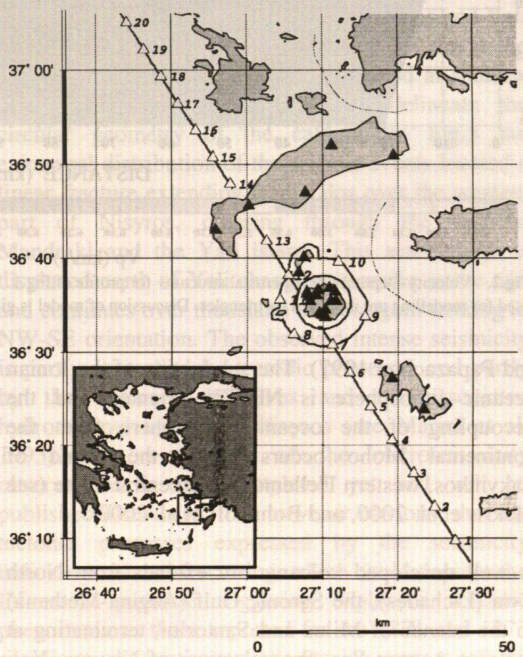

Fig.1. Location of seismic profile at the Dodecanes islands with triangles indicating positions of Ocean Bottom Seismographs (1 to 20) and landstations.

Introduction

The deformation of the Aegean Sea is dominated by wrench-faulting of NE-SW orientation, inducing transtension and subsidence of the continental crust and developing sedimentary basins, e.g. the North Aegean Trough (Makris et al. 1986) and the Cretan Sea (Makris et al. 1975, Hartung 1988, Götz 1997). The Aegean crust is in general stretched (Makris 1978, Angelier et al. 1982) and its deformation is expressed by intense seismic activity, while the external Hellenides are exposed to compression, producing crustal shortening and subduction of oceanic lithosphere, accompanied by very high seismicity (e.g. McKenzie 1972, Makris 1978, Le Pichon et al. 1981, Taymaz et al. 1990, Papazachos

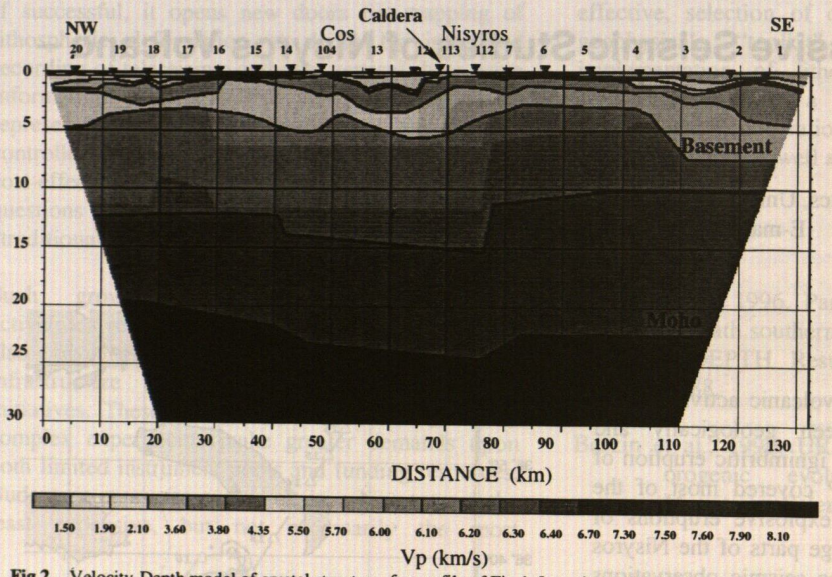

Fig.2. Velocity-Depth model of crustal structure for profile of Fig.1. Locations of traveltime sections used for modelling are indicated by triangles. Discussion of model is given in text

and Papazachou 1997). The subduction of the Ionian oceanic lithosphere is NE-SW oriented and the decoupling of the oceanic lithosphere from the continental Moho occurs below the island of Zakynthos, western Hellenides and central Crete (see Makris et al. 2000, and Bohnhoff et al. 2000).

A well developed volcanic arc extends from North Evia (Lichades), the Saronic Gulf (Aegina-Methana) to the islands of Milos and Santorini, terminating at the east Aegean Sea, the volcanoes of Nisyros, Yali and Cos. The east Aegean volcanic activity has been described by e.g. Keller 1969, Marini et al. 1993, Papanikolaou et al. 1998, while geophysically only local studies of the geothermal field of Nisyros have been published (Marini at al. 1993), without referring to the crust or the volcanic structure at depth.

In the following we will present results of an active seismic experiment, a tomographic velocity study and a seismicity investigation conducted in the autumn of 1997 in order to better understand the crustal and volcanic structures of the south-eastern Aegean Sea.

Data acquisition and crustal structure

In autumn 1997 an active and passive seismic experiment was conducted along a 140 km long profile extending from the islands of Chalki to that of Leros, striking NW-SE. The volcanoes of Nisyros, Yali and south-western Cos were occupied by a dense network of seismic stations (10 in total) and 20 Ocean Bottom Seismographs (OBS) were deployed at sea. Shots were fired by a 48 lt. airgun array at 120 m intervals along the seismic line and in two circles around Nisyros, one at 2 km and the other at 5 km parallel to the coast (see Fig.1). The local seismicity was observed for a period of 3.5 months by a microseismicity array of 22 stations.

The data were evaluated along the profile by two-point ray tracing. The velocity model obtained is presented in Fig.2. The crust is stretched continental of 22 km thickness at the NW end of the line near Leros thickening to the south-east. It is nearly 25 km thick bellow Nisyros and about 22 km at the south-east end near the island Chalki. Between Cos and Nisyros the geometry of the neogene sediments revealed the structure of the caldera, extending between south Cos to Nisyros. The volcanic edifices of Cos, Yali, and Nisyros are part of this major structure of nearly 30 km in diameter providing an explanation for the large volumes of the ignimbrits extruded 145 000 BP (Keller 1969). The identified volcanic structure is nearly twice the size of the Santorini caldera developed by the 1350 BC eruption, which destroyed the Minoan civilisation (Galonopoulos 1971). The

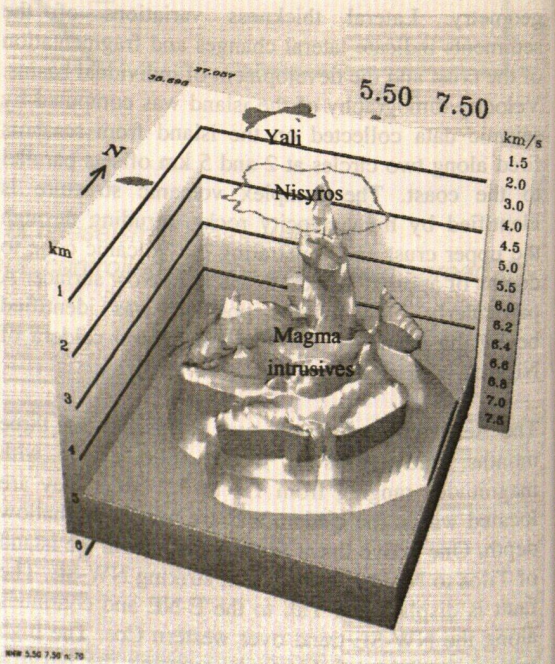

Fig. 3. 3D tomographic velocity model of the magma intrusion at the Nisyros volcano.

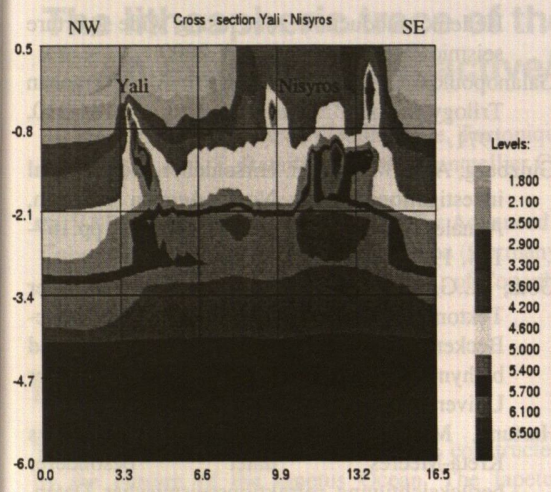

Fig.4. A NW-SE cross-section across the velocity tomography of the islands of Yali and Nisyros. For further details see text.

thickness of the sediments show significant lateral changes, particularly south of OBS position 4 and constrain the geological and tectonic models of the south-eastern Aegean Sea.

A tomographic 3D velocity model of Nisyros deduced from active seismic observations

We used observations obtained by 5 OBS and 12 stations on Nisyros and Yali to develop the 3D velocity structure of the upper part of the volcano. The shots were fired at two circles parallel to the coast of Nisyros, which is nearly of circular geometry, at 2 and 5 km offsets from the coast. The software used for the data inversion is developed by P. Ditmar, M. Tchernychev and J. Roslov 1994 (personal communication) based on a non-linear inversion algorithm with 3D ray tracing that uses first arrivals as input.

The program is very efficient and the inversion was accomplished in 2 steps. First we used the inner circle (300 shots). This model revealed the shallow structure of the volcano and was used as input for the second inversion of the external circle (500 shots).

The results obtained are very interesting and are presented in Figs.3 and 4. It is obvious that magma has intruded at a very shallow depth in the caldera, which explains the very high temperature of 300°C observed in the lower aquifer in the caldera at 1.5 km depth as confirmed by drilling (Marini et al. 1992). In Fig.4 we present a cross- section of NW-SE orientation and one can see that the intrusives below Nisyros have a complicated 3D geometry with several apophytic branches. The velocity model of Fig.2 shows that large scale subsidence controls the sedimentation and deforms the complete crust to the Moho.

Local seismicity

Twenty-two seismic stations were placed on Cos, Yali, Nisyros and Tilos and observed the microseismic activity for 3.5 months. In this period 1600 events were located, using in most cases P and S arrivals. The accuracy of the hypocentral locations is better than 2 km for events below Nisyros and Yali - central part of the array - and 3 to 4 km at the periphery. The events are mostly located at shallow to intermediate crustal depth and delineate the circular geometry of the caldera. In Fig.5 the epicentral distribution of the seismic events located a linear fracture extending from Tilos over the western part of Nisyros, crossing through the city of Mandraki and the Yali island. This active fault is displaced north of Yali changing its strike to the east and continues over the island of Cos again striking in NW-SE orientation. The observed intense seismicity is partly controlled by tectonic processes and partly by the volcanic intrusives and the associated hydrothermal system of Nisyros (see Marini et al. 1993). The evaluation of the microseismicity observations is not completed yet and will be published elsewhere. It is however obvious, that the tectonic processes expressed by the seismicity indicate tensional fracturing, which could depress the lithostatic pressure triggering explosive volcanic phenomena as those reported for the 1871 and 1873 eruptions. A continuous monitoring system of the

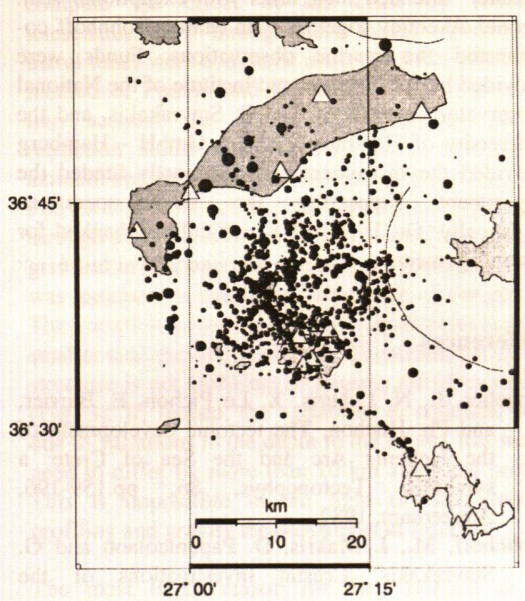

Fig.5. Location of 1600 earthquakes located by a temporary array of 22 stations that recorded the microseismicity for 100 days.

seismic activity and its real-time evaluation are necessary for a warning procedure that can increase the safety of inhabitants and tourists that visit the island.

Discussion and conclusions

The crustal velocity model of the Dodecanes Islands, a velocity tomography model of the islands of Nisyros and Yali and seismicity data from passive microseismicity observations helped in identifying a much larger caldera than had been previously anticipated by onshore geological observations only. Most parts of the caldera of 30 km diameter is underwater, extending from Cos to south of Nisyros. This explains the large volume of ignimbrits erupted 145 000 years BP. The tomographic evaluation of 3D active seismic observations revealed several apophytic intrusions and the deep structure of the volcano. The seismicity on the other hand, is induced by tectonic deformation and volcanic processes. It my be used as a direct indicator for the volcanic activity that could be induced by explosive eruptions of overheated aquifers. Further data collection is in progress and we hope by combining geophysical, geochemical and geodetic information in real-time to develop a "CEOWARN" system for the island of Nisyros.

Acknowledgements

We thank the civil authorities of Nisyros for their support during the field work. The crew of R/V "Iskatel" attended their tasks with exceptional zeal. Leonid Akentiev together with Marco Bohnhoff co-ordinated the marine observations. Funds were provided by the Geodynamic Institute of the National Observatory of Athens, Dr. G. Stavrakakis, and the University of Hamburg. GeoPro GmbH - Hamburg provided the instrumentation and partly funded the experiment supporting the field operations logistically. Dr. F. Egloff is particularly thanked for his engagement

References

Angelier, J., N. Lyberis, X. Le Pichon, E. Barrier, and Ph. Huchon, The tectonic development of the Hellenic Arc and the Sea of Crete: a synthesis, Tectonophys, 86, pp.159-196, Amsterdam, 1982.

Bohnhoff, M., J. Makris, D. Papanicolaou and G. Stavrakakis, Crustal investigations of the Hellenic subduction zone using wide aperture seismic data (in preparation), 2000.

Galanopoulos, A.G., The Eastern Mediterranean Trilogy in the Bronze Age, Acta, pp.184-210, 1971.

Ginzburg, A., J. Makris, H. Hirschleber, Geophysical investigations in the North Aegean Through, Annales Geophysicae, 1987, 5B, (2), pp.167-174, 1986.

Götz, L.G., Beschreibung und Vergleich der Tektonik pazifischer und mediterraner Backarc-Becken hergeleitet aus echographischen und bathymetrischen Vermessungen, ZMK der Universität Hamburg, IfG, 1996.

Hartung, M., Geophysikalische Vermessung des Kreta-Meeres unter besonderer berücksichtigung refraktionsseismischer Daten, Diplomarbeit, Institut für Geophysik der Universität Hamburg, 1987.

Keller, J., Origin of rhyolites by anatectic melting of granitic crustal rocks. The example of rhyolitic pumice from the island of Kos (Aegean Sea), Bull. volcanol., 33, pp. 942-959, Napoli, 1969.

Le Pichon, X., J. Angelier, The Aegean Sea, Philos. Trans. R. Soc. London, Seria A, 300, pp. 357-372, 1981.

Makris, J., Crustal structure of the Aegean Sea and the Hellenides obtained from geophysical surveys, J. Geophys. Res., 41, pp. 441-443, 1975.

Makris, J., Some geophysical considerations on the geodynamic situation in Greece, Tectonophys 46, pp. 251-268, 1978.

Makris, J., The crust and upper mantle of the Aegean region obtained from deep seismic soundings, Tectonophysics, 46, pp. 269-284, 1978.

Makris, J., F. Egloff, V.Kamberis and F. Marmeris, A seismic on- and offshore study of Western Greece, (in preparation), 2000

Marini, L., C. Principe, G. Chiodini, R. Cioni, M.Fyticas, and G. Marinelli, Hydrothermal eruptions of Nisyros (Dodecanese, Greece). Past events and present hazard, Journal of Volcanology and Geothermal Research, 56, pp. 71-94, 1993.

McKenzie, D., Active tectonics of the Mediterranean region, Geophys. J.P.. Astron Soc., 30, pp.109-185, 1972.

Papanikolaou D.J. et al., Newsletter of the European Centre on Prevention and Forecasting of Earthquakes, Issue No2, 1998.

Papazachos, B., C. Papazachou, The Earthquakes of Greece, Editions ZITI, Thessaloniki, 1997.

Taymaz, T., J. Jackson and R. Westaway, Earthquake mechanisms in the Hellenic Trench near Crete, Geophysical Journal International, 102, pp. 695-731, 1990.

The lithospheric trace of the Iapetus Suture in SW Ireland: An example of an active/passive seismic experiment

F. Masson (Laboratoire de Géophysique, Tectonique et Sédimentologie, CNRS and Université Montpellier 2, CC 060, 4 pl. E. Bataillon, 34095 Montpellier Cedex 05, France. E-mail: fmasson@dstu.univ-montp2.fr
and
the VARNET Group (Dublin Institute for Advanced Studies (Ireland), University College Dublin (Ireland), NUI Galway (Ireland), University of Karlsruhe (Germany), GeoForschungsZentrum Potsdam (Germany), University of Copenhagen (Denmark))

Introduction

The British and Irish Caledonides were constructed by the closure of the Iapetus Ocean. The Iapetus Suture is the tectonic boundary which resulted from the amalgamation in a three-plate configuration of Laurentia and Baltica with Avalonia, which is a continental fragment of Gondwanan affinity. The British and Irish parts of the Iapetus Suture are bounded by the Laurentian and Avalonian continents. Despite the expected differences between these two continents, the location of the Iapetus suture, particularly in Ireland, remains a matter of discussion. It is traditionally placed along the Solway-Navan-Silvermines line (Fig. 1). A set of deep seismic reflection offshore profiles (Klemperer and Hobbs, 1991) seems to confirm this location. Nevertheless this line is only one possible solution (McKerrow and Soper 1989; Todd et al., 1991).

The VARNET (VARiscan NETwork) project was designed to carry out a multi-disciplinary study of the "Variscan Front" in Ireland. It included the acquisition of new wide-angle seismic data. Two profiles were recorded in June 1996 in south-western Ireland (Fig. 1). Line A crosses both the Variscan Front and the Iapatus Suture Zone. Line B extends across the westernmost peninsulas of Ireland and crosses the Variscan Front near Dingle Bay. During the acquisition of the wide-angle data the seismic field recorders were set into continuous recording mode whenever possible. Six earthquakes (Fig. 2a) and a Chinese nuclear test (Fig. 2b) were recorded during these periods. Because of the close station spacing of about 1 km this data set is a unique teleseismic record. The data set is used here to carry out a residual travel time analysis of the mantle structure beneath the wide-angle profiles.

Residual time analysis: heterogeneity in the mantle

Absolute travel-time residuals are the difference between theoretical and observed travel-times. They contain both hypocenter parameters errors and uncertainties due to slight, along-raypath differences between the reference and the actual spherical earth models. These two sources of error are removed by using relative residuals which are computed by removing the mean value of the residuals. Relative residuals contain only information about lateral heterogeneities along the raypaths and are usually taken to be indicative of the velocity structure beneath the seismic array. The accuracy of the relative arrival times is estimated to be better than 0.05 s (the digital sample rate is 0.01 s). Figure 3 shows relative residual times for two events.

The peak-to-peak variation is about 0.5 s which is an unexpectedly high value in a passive tectonic region. This is at variance with the general idea that teleseismic travel-time residuals are lower in the passive than in the active tectonic regions. There are a number of possible explanations for the residual time variations observed along line A and some of the major ones are discussed below. Because the crustal structure has been defined by the wide-angle seismic profile (Landes et al., 1999) it is possible to compute the effect of the crust by shooting teleseismic rays through this model. Theoretical travel times were computed using the finite difference method of Podvin and Lecomte (1991). This takes into account the lateral heterogeneities of the refraction model along the profile as well as the azimuth and the epicentral distance of the events. The Podvin and Lecomte method computes travel times through a 3D velocity model represented by a regular grid and in this study the 2D refraction seismic model was assumed to extend to either side of the profile. The variation of the calculated residual times is much smaller than the observed ones. Therefore, the crustal structure is not sufficient to explain the observations (Fig. 3). If, indeed, the variations in residuals were due to variations in the depth to the Moho, this would need to differ by more than 10 km along the profile. This is impossible in the light of both seismic profiling and gravity measurements in Ireland.

The most likely reason for the variation in the observed residual times is the existence of a velocity contrast in the mantle, below the Moho. This contrast has to be sharp in order to explain the large variation

of the residual times from 52.2° to 52.5°, a zone which is only about 30 km wide.

Modelling and Discussion

A precise determination of the three-dimensional velocity structure of the mantle is not achievable from two recorded events. However, it should be noted that these two events have been recorded on a large number of closely-spaced digital seismic stations (about 150), with the waves crossing the profile at two different azimuths. Moreover, there must be significant variations in the mantle structure to produce the observed variations in residual times. It is therefore worthwhile to try and model these structures, even with very simplistic assumptions.

The model shown in figure 4, combined with the crust determined from the wide-angle seismic experiment, explains the residual time curves between latitudes 51.9° and 52.6° for both events. Event A1 is well matched from 52.6° to the northern end of the profile whereas only the general trend of event A5 is explained in this segment. South of 51.8°, both events show observed residual times which are lower than the computed ones. This observation could be explained by introducing a relatively high velocity mantle at the southern end of the profile.

The residual time curves suggest that a sharp velocity contrast exists beneath the Moho near the southern edge of the Shannon River Estuary. Modelling indicates that this velocity contrast extends to over 100 km depth and dips to the South at a steep angle of about 13° from the vertical.

Subcrustal velocity contrasts are often observed in active tectonic regions. Oceanic subduction zones, mantle plumes or continental collision zones show subcrustal velocity contrasts with variable depth extension. In passive tectonic regions, such velocity contrasts are more rarely observed. The velocity model obtained for SW Ireland shows a velocity contrast of about 3% with a depth extension of about 100 km. It is tempting to attribute its origin to a former collision zone. In fact, the sharp contrast can be interpreted as a deep trace of the Palaeozoic Iapetus Suture Zone and several arguments support this conclusion. First, such a velocity contrast has to be created by a significant tectonic event. The Variscan orogen is unlikely to be responsible because Variscan deformation close to the Shannon River Estuary is shallow (Landes et al., 1999, Masson et al., 1998) and generally, Variscan deformation in Ireland is associated with thin-skinned tectonics. The other major tectonic event which effected Ireland is the closure of the Iapetus Ocean. The plate tectonic models for this event could generate such a horizontal velocity contrast by juxtaposing dissimilar lithospheric blocks next to each other. Second, the location of the velocity contrast, between the Solway-Navan-Silvermines line and the Shannon River Estuary, is consistent with previous locations of the Iapetus suture zone, which were based on geological field observations as well as geophysical methods.

Such a velocity contrast has also been proposed in the Urals. Poupinet et al. (1997) suggest that this is probably due to a modification of the lithosphere by the continental subduction process and by orogeny. This is compatible with the model obtained in our study which shows also a fast dipping block. The roughly consistent depth for these two models could indicate that a continental collision induces thermal and/or compositional heterogeneities deep into the upper mantle. After the end of the collisional event this disturbed mantle gradually returns to a more homogeneous state. After this homogenisation, mainly crustal velocity variations are observable, as seen in Central Finland, which result from very ancient Palaeozoic events.

References

Klemperer, S.L. and Hobbs, R., 1991. The BIRPS Atlas: Deep seismic reflection profiles around the British Isles. Cambridge University Press, Cambridge.

Landes, M., Prodehl, C., Hauser, F., Jacob, A.W.B., Vermeulen, N.J. and Mechie. J., 1999. VARNET-96: Influence of Variscan and Caledonian orogenies on crustal structure in SW Ireland. Submitted to Geophys. J. Int.

Masson, F., Jacob, B., Prodehl, C., Readman, P., Shannon, P., Schulze, A. and Enderle, U., 1998. A wide-angle seismic traverse trough the Variscan of SW Ireland. Geophys. J. Int., 134: 689-705.

McKerrow, W.S. and Soper, N.J., 1989. The Iapetus Suture in the British Isles. Geological Magazine, 126: 1-8.

Podvin, P. and Lecomte, I., 1991. Finite difference computation of traveltime in very contrasted velocity models: a massively parallel approach and its associated tools. Geophys. J. Int., 105: 271-284.

Poupinet, G., Thouvenot, F., Zolotov, E.E., Matte, P., Egorkin, A.V. and Rackitov, V.A., 1997. Teleseismic tomography across the middle Urals: lithospheric trace of an ancient continental collision. Tectonophysics, 276: 19-33.

Todd, S.P., Murphy, F.C. and Kennan, P.S., 1991. On the trace of the Iapetus suture in Ireland and Britain. J. Geol. Soc. London, 148: 869-880.

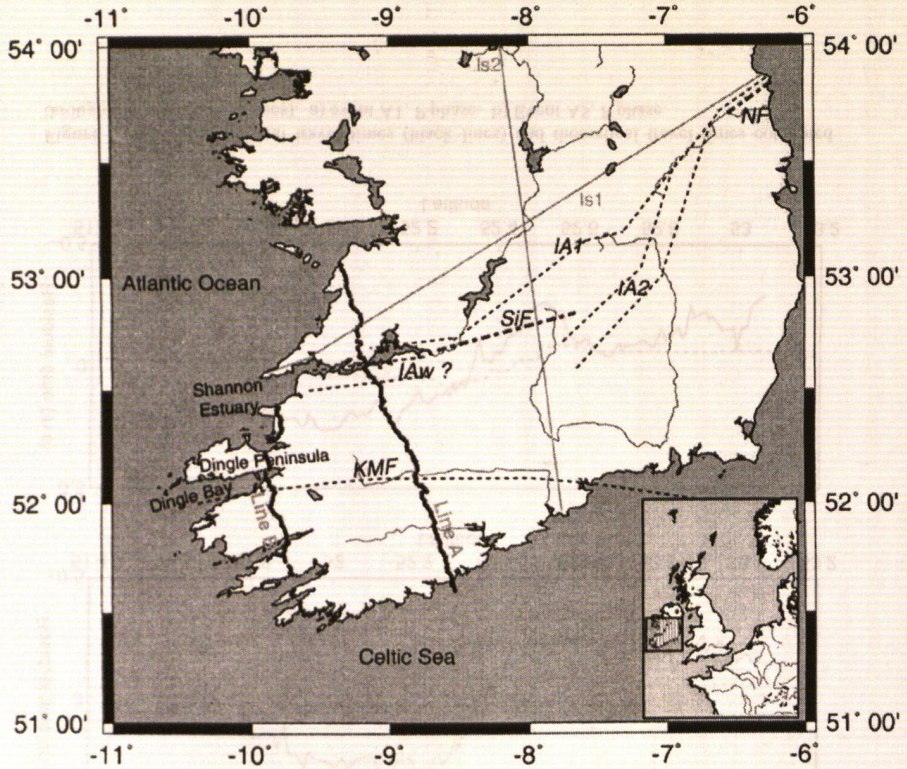

Figure 1: Map of southern Ireland. Line A and line B are the two wide-angle seismic lines recorded during the VARNET experiment. Is1 and Is2 are two older refraction seismic lines. The dotted lines IA indicate the possible locations of the Iapetus Suture. Iaw is the possible location of the Iapetus Suture in western Ireland, along the Solway Line (from Todd et al., 1991). Two Caledonian faults are indicated: the Navan Fault (NF) and the Silvermines fault (SiF) (from Todd et al., 1991).

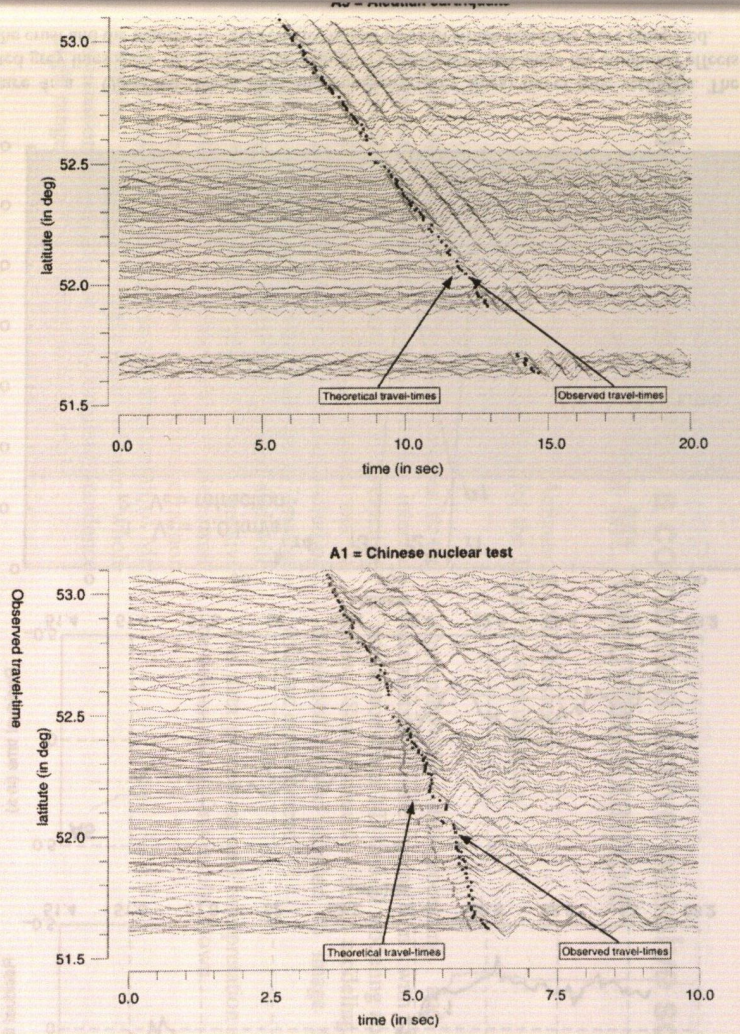

Figure 2: Teleseismic events recorded along line A. No signal-enhancing processing has ben applied. A – Event A5 earthquake from the Aleutian Islands. B – Event A1, Nuclear Test in China. Black squares indicate the picked travel times. Grey squares indicate theoretical travel times.

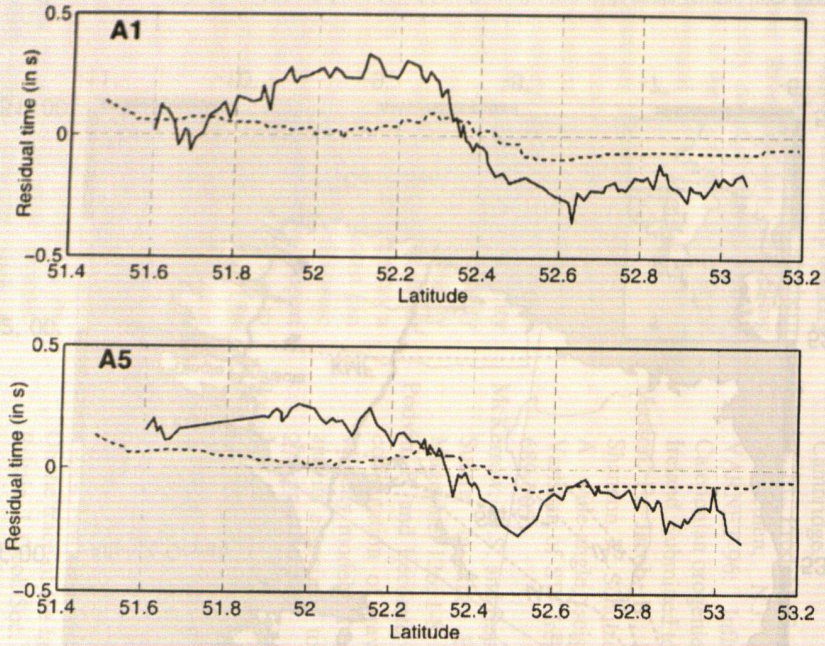

Figure 3: Observed residual travel times (black lines) and theoretical travel times computed through the crust (dotted lines). a) event A1, P phase. b) Event A5, P phase.

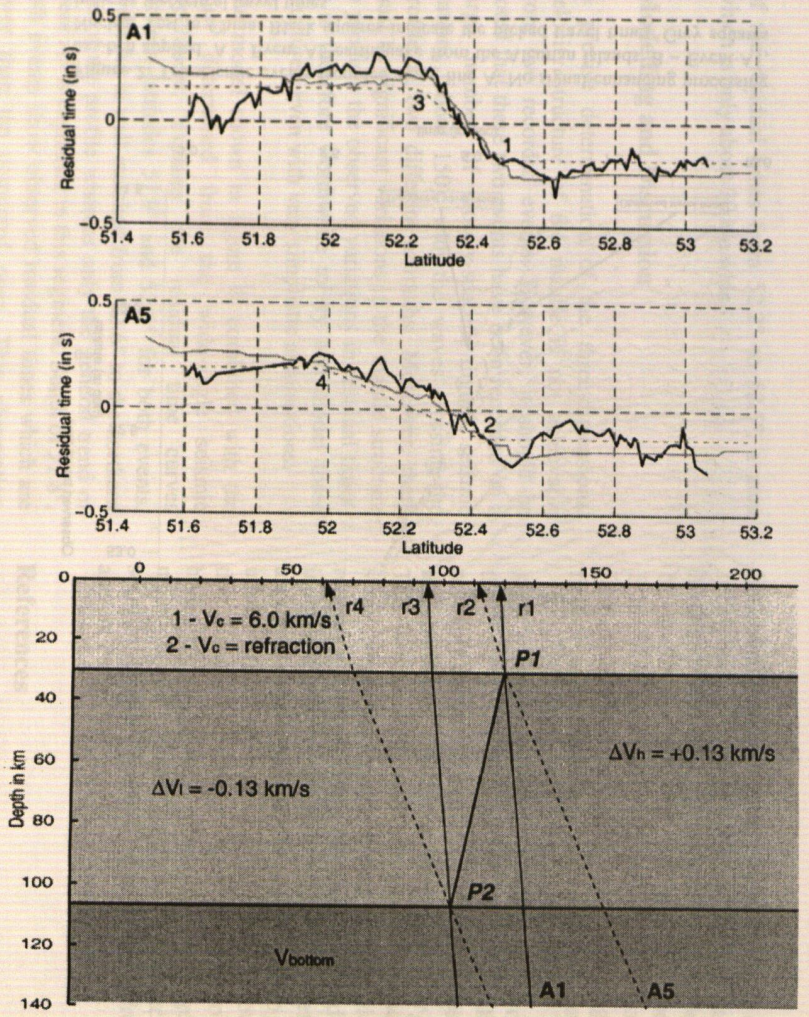

Figure 4: a – Observed (black line) and computer (grey lines) travel time residuals. The dotted grey lines show the effect of the mantle. The full grey lines show the combined effects of the crust and the mantle. b – 2D velocity model through which residuals were computed.

Studying a volcano by a combined active-passive source project: the Mt. Vesuvius example

Uli Achauer, EOST Strasbourg
Reporter for the TomoVes working group

The aim of the EC-funded project TomoVes is the construction of detailed models of the internal structure of Mt. Vesuvius based on seismic velocities and attenuation. The field project, carried out in 1994, 96 and 97, consisted of 3 phases including controlled sources experiments with energy sources on land and offshore recorded both on land and with OBS, as well as a 2-3 month duration passive experiment aiming at recording local and teleseismic events. The active part was a reflection/refraction type experiment of profiles across the summit of Mt. Vesuvius, which will make use of the whole information retrievable in the complete incidence angle range from near vertical to wide-angle.

Currently the data-processing and first data interpretations are going on with the gradual procession from 1-D to 3-D modeling and shallow to deep. Simultaneously new modeling tools are developed and/or adapted to image the complex volcanic environment.

The data processing and interpretation strategy will be discussed and first results shown.

When Should We Resort to Stochastic Modelling?

Christopher J. Bean
Dept. of Geology, University College Dublin, Belfield, Dublin 4, Ireland.
Phone: +353-1-7062140, E-mail: Chris.Bean@ucd.ie

Introduction

The complex patterns on most seismograms are testament to the highly heterogeneous nature of geological materials. In seismology we aim to determine the elastic properties of the subsurface, based on such seismograms. In refraction/wide angle reflection work the traditional approach to achieving this aim is to invert travel time picks and amplitudes of the main phases for geological structure. This leads to 'smooth, large scale' crustal velocity models. That is, although shot generated 'noise' is usually significantly more energetic than the background noise, traditionally it has been regarded as largely uninterpretable and is not used.

In order to glean more information from these incoherently scattered wavelets, which constitute most of this shot related noise, we need to focus on 'smaller' scale geological variability. However due to limited resolution this cannot be achieved deterministically. That is, we cannot spatially position known fine scale structures based on their seismic response. This lack of resolution coupled with the need to incorporate finer scale structure into geophysical models has led to hybrid stochastic-deterministic crustal models, where gross crustal structure is defined deterministically, internal small scale variability is quantified stochastically.

Controls on stochastic parameters

Information on small-scale geological variability can be obtained from detailed observations of geological outcrops/maps and from high-resolution borehole logging runs (wire-line logs). While geological maps allow us to quantify small-scale lithological fluctuations, borehole elastic/acoustic logs capture fine scale variability associated with both lithological and fracture related heterogeneity. A surprising result has been the striking similarity between fracture and lithological related heterogeneity for a wide variety of geological settings and histories, almost all of which exhibit 1/f type scaling. However, in stark contrast, there is no consensus yet on the bandwidth of this scaling, a point which I will address in this talk. One model/viewpoint leads to the suggestion that the bandwidth is very large, perhaps of crustal dimensions. If this is true then it has important implications for our deterministic description crustal velocity models.

Does the stable crystalline crust have a deterministic velocity structure?

Will any two independent interpretations of a seismic section be the same? If we image a given geographical location at two different spectral windows will they converge on the same geological model? If not, why not? Is there anything fundamentally different about 'large scale' and 'small scale' velocity fluctuations. If not, then where do we draw the distinction between stochastic and deterministic modelling? Is this distinction merely based on a subjective point of view or an apparent data resolution?

In order to address some of these questions I will look at controls on the velocity structure in the crystalline crust. The analysis of 9km deep borehole data indicates that fractures may dominate the seismic response of the material, at least in the upper 1/3 of the crust, with lithology playing a secondary role. Fractures are known to have power law number-length distributions and are 'patchy' (analogous to clouds). No individual scale length can be singled out and there is no fundamental distinction between 'small' and 'large'. Finite difference wave field modelling in materials with these types of statistics bares many of the hallmarks of real data, including correlatable phases, without any built in 'deterministic' structure.

Hence it seems as if it may sometimes be possible to obtain a 'complete' description of the observed seismic wavefield based on stochastic modelling (of broad band heterogeneity) alone. I suggest that this should not be viewed as a poor relation of the deterministic approach as it allows us to capture some essential characteristics of the geology which we cannot obtain with a band limited deterministic perspective (obvious exceptions exist such as hydrocarbon reservoir characterisation, where 'deterministic' features , e.g. shale smears/thin layers, can have significant effects on fluid migration pathways). From this perspective, a deterministic model can be viewed as the long spatial wavelength components of a material with broad band scaling heterogeneity. The 'stochastic part' is not merely a 'filling in' of the 'little bits' which we cannot resolve deterministically, as that methodology will lead to a resultant model with breaks in scaling, which may not exist in the underlying geology.

The effect of sets of small sloping crustal reflectors on the geometry and complexity of the wide-angle reflection fields

R.F. Mereu, Department of Earth Sciences, University of Western Ontario,
London, Ontario, Canada, N6A5B7, E-mail: r.mereu@seis.gp.uwo.ca

Abstract

In the conventional method of incorporating heterogeneity into crustal models of the earth, small indeterministic velocity fluctuations are added to a deterministic seismic velocity field. In this paper we investigate an alternative method of adding heterogeneity to earth models. Sets of small sloping seismic reflectors are "embedded" in a uniform seismic velocity field in which the velocity increases linearly with depth. This alternative approach allows us to focus our attention on the effect of both the slope, velocity contrast and geometric distribution of the small scale reflectors on the observed wide-angle reflection field. It is also computationally much faster than the finite difference approach and hence may be employed to test a lot of models in a short time. When a seismic wave travels through a heterogeneous crust, two separate filtering actions are assumed to take place. The seismic slowness (inverse velocity) is filtered with a linear low pass smoothing filter. The reflectors are filtered using a highly non-linear filter which depends on the actions of the reflection coefficients. The effect of the velocity gradient is to make the reflective field for down going waves much greater than for up going waves. The method tests the hypothesis that much of the complexity in the observed Pg coda is due to the on/off switching ("light bulb effect") characteristics of the plane wave reflection coefficients. On/off switching of totally reflected light waves may easily be observed when one looks at waves sparkling on the surface of the sea. The numerical experiments revealed that the geometry of the wide-angle reflection field and the presence or absence of the PmP travel-time branch may be related to the random orientations and velocity contrasts of the small scale reflectors. These experiments also predict that first arrival Pg waves should be shingled and also confirm earlier studies on crustal heterogeneity which indicate that that long intra-crustal discontinuities such as the Conrad may be illusions of the inversion procedure. The complexity of the record sections which is predicted from the above analysis was compared to that of real data obtained from recent Canadian Lithoprobe seismic coincident near-vertical and wide angle reflection experiments which were conducted across the Canadian Shield. A new method of obtaining crustal images from wide-angle data is suggested. These images may be used to complement velocity anomaly images.

Introduction

Images from most near-vertical reflection experiments indicate that the earth's crust is usually composed of numerous short sloping reflectors of various lengths with occasional regions of low reflectivity. On the other hand seismic images from seismic refraction experiments tend to favour simple layered or block type models. The fact that most intra-crustal discontinuities of the refraction models are in general not visible in the near vertical reflection models is a problem which is addressed in this paper. In the past, the complexities of crustal models have been studied with conventional methods in which heterogeneity is introduced into crustal models using a velocity field with small indeterministic velocity fluctuations.(e.g. Levander and Holliger 1992). In this paper we investigate an alternative method of adding heterogeneity to earth models. This alternative approach allows us to focus our attention on the effect of the slope, velocity contrast, and geometric distribution of the small scale reflectors on the observed wide-angle reflection field. Further details of this new method are given by Mereu (1999).

Basic Assumptions

1. The crustal model is composed of a field of sloping small scale thin seismic reflectors which are "embedded" in a uniform seismic velocity field in which the velocity increases linearly with depth. Each reflector in general has a different location, a different orientation, a different thickness and a different velocity contrast with the surrounding medium. This assumption should be looked upon as an end member of a gross simplification of reality as are all earth models. This assumption is also very similar to the ones made for near-vertical reflection analysis.

2. The reflection coefficient associated with each reflector is a variable and will depend not only on the velocity and density contrasts but also on the reflector thickness. Very thin reflectors will have very low apparent reflection coefficients as they will

not be "seen" by the seismic waves. The areal size and thickness of the reflectors are large enough such that plane wave reflection coefficients may be used to determine if a reflection from each reflector is supercritical or sub-critical.

3. The velocity contrasts used in computing the plane wave reflection coefficients were assumed to be as large as 0.8 km/s in the crust and 1.2 km/s for the Moho transition zone. The actual contrasts used are under the control of random numbers.

4. In the initial starting model, one horizontal reflector of length 1 km is placed at the centre of each 1x1 km square grid of the cross section of the model. Each reflector is then moved about within the square grid also under the control of a set of random numbers.

5. The slope angle of the reflectors are assumed to lie within given limits. The actual orientation of each reflector is controlled by a set of 2 dimensional random numbers. To give the field structure these numbers are first filtered using a 2-dimensional Butterworth filter which smooths the random numbers. This has the effect of giving the model different vertical and horizontal correlation distances. The orientation of the reflectors effects the angle of incidence and hence may also have an effect in determining the nature of the reflection, the length of the travel path and time.

6. The velocity gradient represents that of an average crust in which the velocity increases linearly from 6.1 km/s at the surface to 7.0 km/s just above the Moho transition zone.

7. Ray theory may be used to compute the arrival time at the surface of energy from each of the embedded reflectors. Since the velocity increases linearly with depth, all ray paths to each reflector will form arcs of circles. The resulting travel time field may be computed quickly with few calculations. When computing the two way travel-time to a particular reflector, the presence of all other reflectors is ignored. This assumption follows from the fact that any ray which encounters a reflector in supercritical mode will also strike upper reflectors along its path at smaller angles of incidence and hence will find them effectively transparent. Multiples are therefore likely to be insignificant.

8. Scattered and diffracted waves will contribute to the overall background noise level. Since they will not likely be associated with a "light bulb" effect, their presence was ignored. To obtain a complete full wave solution for this problem one would have to resort to a finite difference approach.

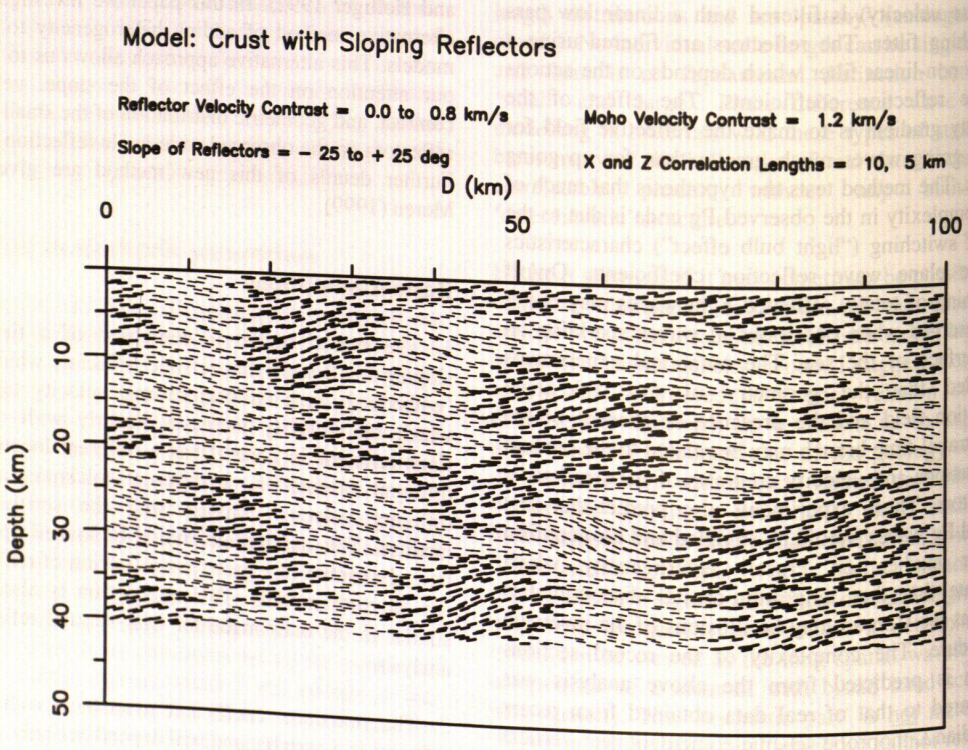

Figure 1: Model crust with small sloping reflectors
Positive slopes ––– bold lines
Negative slopes ––– thin lines

Conclusions (See Figures 1 and 2)

Figure 1 shows an example of one of the models which was studied. Only the first 100 km is illustrated in the diagram. In this model the reflector slopes have been filtered such that the correlation lengths in the X and Z direction are 10 and 5 km respectfully. Reflectors with positive slopes are plotted with bold lines. This enables the viewer to see the vertical and lateral structures of the model more readily. Velocity contrasts as large as 0.8 km/s were used within the crust while contrasts as large as 1.2 km/s were used within the Moho transition zone. The aim was to produce a seismic model which is similar to a typical model from near vertical reflection experiments.

The upper part of Figure 2 shows the reduced travel-time (T-D) plot (reducing velocity 6.0/km/s) for the Figure 1 model while lower part shows the corresponding Depth-D plot. As a result of the constant velocity gradient there is a one to one correspondence of the points in the upper figure to those in the lower figure. Reflectors which were observed in supercritical mode are plotted with a thick bold short line segment. This allows us to view the wide-angle reflection field more readily. Gaps in the Depth-D plot are an indication that the rays striking the reflectors do not return to the surface. This leads to corresponding gaps or small shadow zones on the travel-time sections. The severe geometric distortion which occurs when one maps the points in the lower diagram to the upper T-D travel-time section leads to anomalous linear zones of large amplitudes which could easily be misinterpreted as a PcP branch from a large intra-crustal discontinuity. Such a discontinuity may therefore be an illusion of the interpretation procedure. This may explain why long intra-crustal discontinuities are seldom seen in near vertical reflection experiments. The study confirms that first arrival Pg signals are usually shingled. Further experiments such as the one illustrated here showed that the overall geometry of the wide-angle reflection fields as well as the presence or absence of the PmP branch are sensitive to the slope and velocity contrast which were assumed for the reflectors. The PmP branch is predicted to be clear for one shot point and almost non existent for a shot a few km away as is often seen in real data.

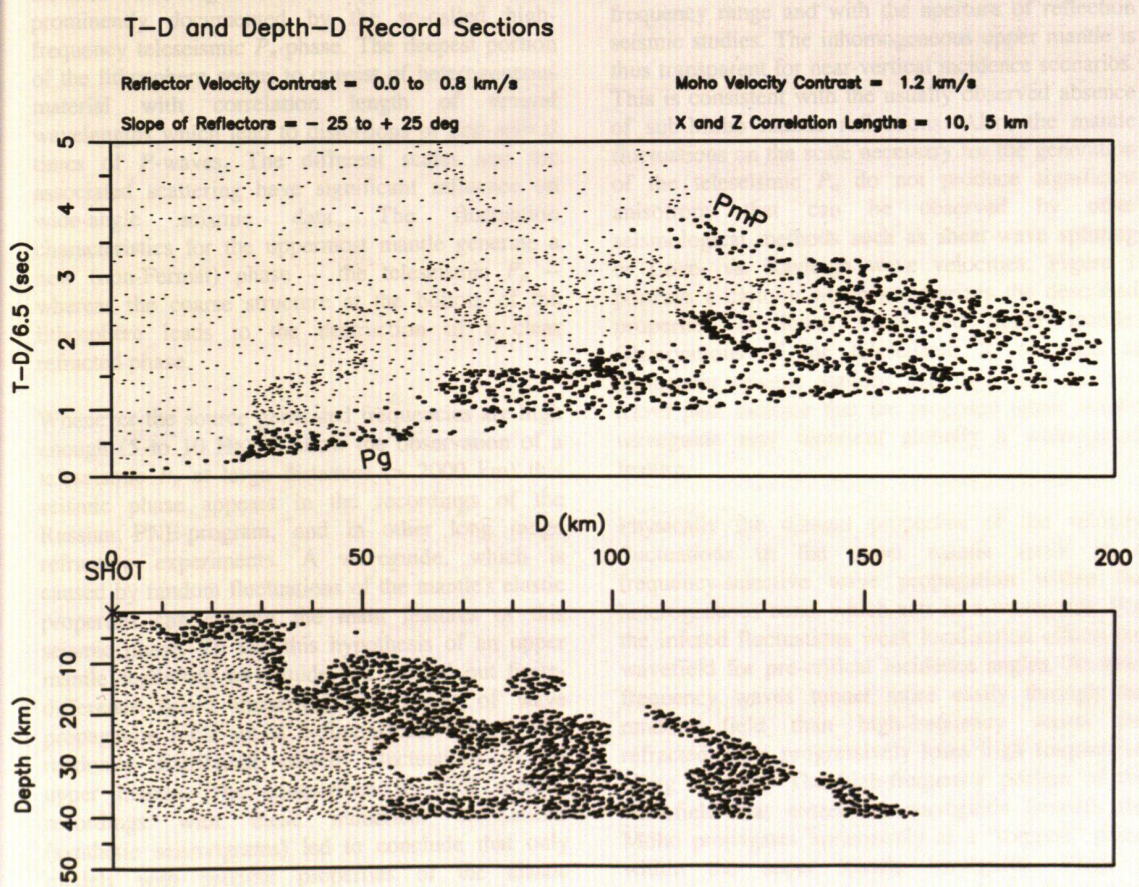

Figure 2: T–D and Depth–D record sections for model in Figure 1
Supercritical reflectors ---- bold lines Subcritical reflectors ---- thin lines

Acknowledgements

This study was supported by the Natural Sciences and Engineering Research Grant A1793.

References

Levander, A.R., and Holliger, K., 1992. Small-scale heterogeneity and large scale velocity structure of the continental crust. *Journal of Geophysical Research*, 97: 8797-8804.

Mereu, R.F., 1999. The effect of small random crustal reflectors on the complexity of Pg and PmP coda. *Physics of the Earth and Planetary Interiors*. (In press).

Imaging the fine-scale structure of the lithospheric mantle – wave propagation in the earth's uppermost mantle

Marc Tittgemeyer[1], Trond Ryberg[2] and Friedemann Wenzel[1]

[1] Geophysikalisches Institut, Universität Karlsruhe, Hertz Str. 16, 76187 Karlsruhe, Germany.
[2] GeoForschungsZentrum, Telegrafenberg, 14473 Potsdam, Germany.

Seismological data presented to date indicate that the Earth crust/mantle system shows conspicuous fluctuations of elastic parameters at different scales. Reflection seismic data show a layered or reflective lower crust with velocity inhomogeneities as high as 10 %. Typically the spatial distribution of lower crustal impedance fluctuations is fractal and self-affine over a scale of at least 0.1 to 1 km. At the crust/mantle boundary (Moho) the scale of heterogeneity changes rapidly.

Most models of the Earth's upper mantle had previously assumed a homogeneous elastic structure. In contrast many seismological data sets show conclusive evidence for strong scattering. For instance scattering within the uppermost mantle is prominently documented by the so-called high-frequency teleseismic P_n-phase. The deepest portion of the lithosphere seems to consist of heterogeneous material with correlation length of several wavelengths which lead to distortions of first-arrival times of P-waves. The different scales and the associated scattering have significant influence on wide-angle seismic data. The fluctuation characteristics for the uppermost mantle generate a new (non-Fermat) phase -- the teleseismic P_n -- whereas the coarse structure at the bottom of the lithosphere leads to the destruction of a clear refracted phase.

Whenever the source generated frequencies are high enough (5 to 10 Hz) to allow the observation of a teleseismic P_n at large distances (> 2000 km) this seismic phase appears in the recordings of the Russian PNE-program, and in other long range refraction experiments. A waveguide, which is caused by random fluctuations of the mantle's elastic properties can explain the main features of this seismic phase. To test this hypothesis of an upper mantle scattering waveguide, we carried out finite-difference based numerical simulations of wave propagation for a set of 2-dimensional models with randomly distributed velocity fluctuations in the upper mantle. The comparison of PNE seismic recordings with these numerical simulations (synthetic seismograms) led to conclude that only models with specific properties of the elastic structure are capable to propagate seismic energy comparable to the observations.

We focus on the statistical properties of the upper mantle's velocity fluctuations acting as scatterers. Randomly distributed velocity fluctuations in the uppermost mantle shall have a predominantly elongated shape with a horizontal and vertical correlation length around 20 km and 0.5 km, respectively. A small, but significant amount of velocity fluctuations of 1.5 to 2 % located within a sufficiently thick heterogeneous zone ($L \geq 100$ km) is necessary to produce synthetic seismograms similar to the observations. Furthermore, our modeling tests have shown that if these fluctuations in the upper mantle are smooth enough (compared to the velocity fluctuations in the lower crust) they do not generate significant reflections if probed by the frequency range and with the aperture of reflection seismic studies. The inhomogeneous upper mantle is thus transparent for near-vertical incidence scenarios. This is consistent with the usually observed absence of sub-Moho mantle reflections. Also, the mantle fluctuations on the scale necessary for the generation of the teleseismic P_n do not produce significant anisotropy that can be observed by other seismological methods such as shear-wave splitting or Love- vs. Rayleigh wave velocities. Figure 1 portrays a cartoon which summarizes the described properties of lower crust and upper mantle. Observations of the teleseismic S_n recorded at permanent seismic stations and data with oceanic travel path indicate that the proposed upper mantle waveguide may represent globally a wide-spread feature.

Physically the distinct properties of the velocity fluctuations in the upper mantle result in a frequency-selective wave propagation within the heterogeneous zone, which acts as a waveguide. For the infered fluctuations weak localisation effects the wavefield for pre-critical incidence angles. As low-frequency waves tunnel more easily through the random field than high-frequency waves the refracted wave progressively loses high frequencies along its path. The high-frequency portion of the wavefield that enters the waveguide beneath the Moho propagates horizontally as a "trapped" phase within the upper mantle waveguide. From a petrophysical point of view the velocity fluctuation in the upper mantle can be explained by

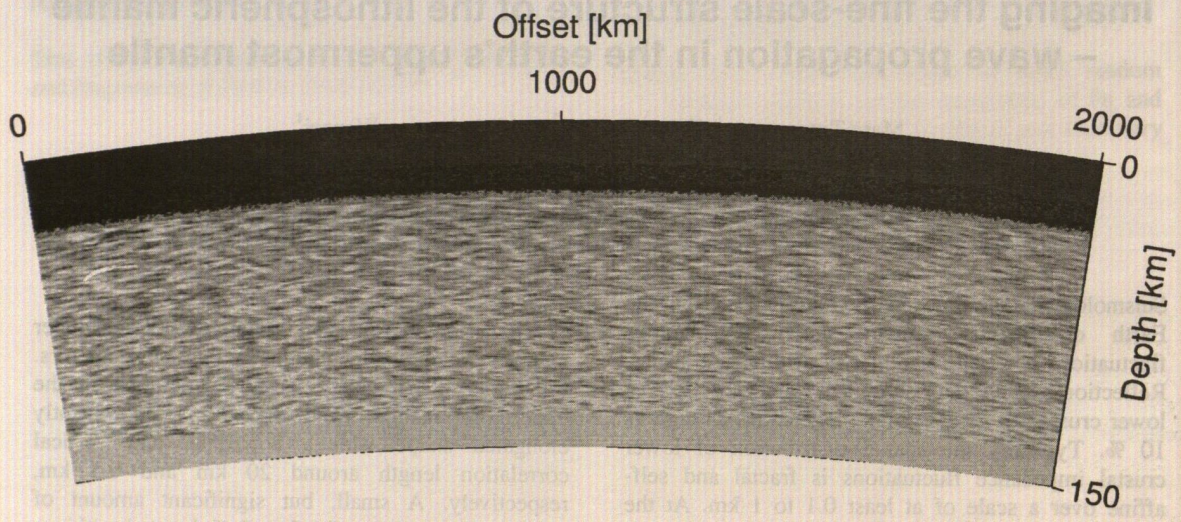

Figure 1: Long distance wave propagation of the teleseismic *Pn* and S_n is achieved by statistical fluctuations of elastic parameters in the uppermost mantle, which differs remarkable in the scale of structure and in the magnitude of variation from the overlaying lower crust. A typical lower crustal structure is characterized by a bimodal velocity distribution of 5 % with a fractal dimension of 2.7 and with a horizontal and vertical correlation length of 800 m and 200 m, respectively. Mantle heterogeneities have a gaussian distribution with a horizontal and vertical correlation length of 20 km and 0.5 km, respectively. The standard deviation of the velocity fluctuations is 2 %. Both targets, lower crust and upper mantle provide a generic description of geologic heterogeneity. (The figure is plotted with a radial exaggeration of 1:4).

compositional changes at a given scale length and by models with spatially varying intrinsic anisotropy of the upper mantle mineral content. Questions concerning the geodynamic processes that generate the upper mantle velocity fluctuations have not been addressed yet. These questions form a significant interdisciplinary challenge for the future.

The proposed model of fluctuations in the elastic properties of the Earth's upper mantle has some adverse consequences for the standard understanding of a refracted wave in that zone. A crust/mantle boundary (Moho), as documented by wide-angle reflections, is globally present beneath the entire surface of the Earth. Observations of refracted waves (P_n) from the uppermost mantle are wide-spread and are usually interpreted as the result of compressional velocities increasing beneath the Moho. We show that this conclusion is erroneous, and only valid within the class of smooth models. Realistic models of the Earth that include velocity perturbations just below the Moho allow the propagation and observation of refracted waves even if the gradient upon which the fluctuations are superimposed becomes negative. The size of the fluctuations can be as small as 1 %.

Consequently, (1) the average velocity gradient beneath the Moho could be negative in the majority of tectonic settings; (2) the measurement of a phase velocity in a scattering medium may not represent the average compressional velocity; (3) long-range refraction profiles should be re-interpreted with the newly established facts in mind. A variety of regional upper mantle models may not be correct.

Popular Tools for Interpreting Seismic Refraction / Wide-Angle Reflection Data

J. Mechie
GeoForschungsZentrum Potsdam (GFZ), Department 2,
Telegrafenberg, 14473 Potsdam, Germany.
E-mail: jimmy@gfz-potsdam.de

This abstract is not meant to be an exhaustive treatise on the methods available for interpreting seismic refraction / wide-angle reflection data. It is meant to give an overview of the most commonly used methods which one can find in the literature, and includes what I hope will be a useful bibliography.

Since its introduction about 25 years ago, ray-tracing has become the almost universal method used to interpret seismic refraction / wide-angle reflection data. The first available computer programs solved the kinematic aspects of the problem for two-dimensional laterally heterogeneous elastic isotropic media i.e. rays and travel-times were calculated based on solving differential equations derived from the eikonal equation numerically with e.g. the Runga-Kutta method (Červený et al. 1974, Červený et al. 1977).

Today most ray-tracing programs are also capable of calculating the dynamic aspects of the wavefield. Thus amplitudes can also be modelled, usually in the later stages of the interpretation after the travel-times have been fitted. The most common methods of calculating amplitudes include ray-theoretical seismograms (Červený et al. 1977) and Gaussian beam seismograms (Červený 1985). It should be noted that the latter method also works in regions e.g. critical points, caustics, head waves and diffracting edges, where the ray method alone fails.

Over the years the ray-tracing method has been extended so that anelastic media and three-dimensional anisotropic media can be modelled. The latter extension is most useful when one has areally distributed data or for studying the effects of anisotropy (Gajewski and Pšenčík 1987). In programs which handle three-dimensional media the two-point shooting method (the most common method in programs handling two-dimensional media) is often replaced and/or supplemented by the paraxial method (Červený et al. 1984).

Since its introduction about 10 years ago (Vidale 1988) ray-tracing using a finite-difference approximation of the eikonal equation has become very popular. Initially it was introduced as a way of calculating first arrival travel-times and rays through three-dimensional laterally inhomogeneous elastic isotropic media. Over the years the method has been extended and/or improved both from the numerical point of view (e.g. Podvin and Lecomte 1991, Schneider et al. 1992) and also so that reflected arrivals (Hole and Zelt 1995) and second arrival refractions from prograde travel-time branches can be calculated.

Full wavefield methods also exist for calculating synthetic seismograms. The most common and accurate of these methods is the reflectivity method which was first introduced about 30 years ago (Fuchs and Müller 1971, Kennett 1974, Müller 1985). The main limitation of this method is that only horizontally homogeneous layers can be modelled. However, anisotropic media can also be included in the model (Booth and Crampin 1983a, b, Nolte et al. 1992). A method for calculating the full wavefield in horizontally inhomogeneous media is the finite-differences method. Although the theory to do this has been around for almost 25 years (e.g. Kelly et al. 1976, Reynolds 1978) only in the past 5-10 years has it been possible in practice to make such calculations for refraction / wide-angle reflection data on a crustal/lithospheric scale over several hundreds of kilometres and at realistic frequencies (see e.g. Gibson and Levander 1988, Mechie et al. 1994).

So far only forward modelling procedures have been discussed. One of the earliest and most popular methods for inverting refraction data is the time-term method (Willmore and Bancroft 1960, Bamford 1977). In this method, which can also handle areally distributed data, refractor velocity and geometry are solved for and optionally weak refractor anisotropy can also be included. Since the early nineties with the introduction of partial derivatives for the travel times with respect to the velocity field and layer boundaries, inversion of travel-time data in laterally heterogeneous media has been possible (Lutter and Nowak 1990, Lutter et al. 1990, Zelt and Smith 1992, Hole et al. 1992). Today also various tomographic methods exist (e.g. Hole 1992, Zelt and Barton 1998). In these methods the forward problem is generally solved with finite-differences ray-tracing while the inverse problem is generally solved using back projection techniques.

Lastly, in the past few years commonly used methods e.g. normal moveout correction and migration, in the processing of near-vertical incidence seismic reflection data have been applied to refraction / wide-angle reflection data (e.g. Lafond and Levander 1995, Patzwahl 1998). A pre-requisite for using these processing techniques on wide-angle data is a good velocity model.

In the future I believe that three-dimensional seismic refraction / wide-angle reflection surveys will play a more important role than up to now. These surveys will probably produce so much data that trial and error forward modelling alone will be impracticable and undesirable. Schemes to invert both travel times and amplitudes for both velocity distribution and interface geometries will be required. For reliable phase correlation especially of secondary arrivals these areal surveys should be configured so that some data in profile form is recorded. Finally, imaging methods including those particularly suited to array configurations e.g. beam forming methods (Scherbaum et al. 1997) will probably also become more important and could find pertinent application in the delineation of fault zone geometry.

References

Bamford, D., 1977. Pn anisotropy in a continental upper mantle. Geophys. J.R. astr. Soc., 49: 29-48.

Booth, D.C. and Crampin, S., 1983a. The anisotropic reflectivity technique: theory. Geophys. J.R. astr. Soc., 72: 755-766.

Booth, D.C. and Crampin, S., 1983b. The anisotropic reflectivity technique: anomalous reflected arrivals from an anisotropic upper mantle. Geophys. J.R. astr. Soc., 72: 767-782.

Červený, V., 1985. Gaussian beam synthetic seismograms. J. Geophys., 58: 44-72.

Červený, V., Langer, J. and Pšenčík, I., 1974. Computation of geometric spreading of seismic body waves in laterally inhomogeneous media with curved interfaces. Geophys. J.R. astr. Soc., 38: 9-19.

Červený, V., Molotkov, I.A. and Pšenčík, I., 1977. Ray Method in Seismology. University of Karlova, Prague. 214 pp.

Červený, V., Klimeš, L. and Pšenčík, I., 1984. Paraxial ray approximations in the computation of seismic wavefields in inhomogeneous media. Geophys. J.R. astr. Soc., 79: 89-104.

Fuchs, K. and Müller, G., 1971. Computation of synthetic seismograms with the reflectivity method and comparison with observations. Geophys. J.R. astr. Soc., 23: 417-433.

Gajewski, D. and Pšenčík, I., 1987. Computation of high-frequency seismic wavefields in 3-D laterally inhomogeneous anisotropic media. Geophys. J.R. astr. Soc., 91: 383-411.

Gibson, B.S. and Levander, A.R., 1988. Lower crustal reflectivity patterns in wide-angle seismic recordings. Geophys. Res. Lett., 15: 617-620.

Hole, J., 1992. Nonlinear high-resolution three-dimensional seismic travel time tomography. J. Geophys. Res., 97: 6553-6562.

Hole, J.A. and Zelt, B.C., 1995. 3-D finite-difference reflection traveltimes. Geophys. J. Int., 121: 427-434.

Hole, J.A., Clowes, R.M. and Ellis, R.M., 1992. Interface inversion using broadside seismic refraction data and three-dimensional travel time calculations. J. Geophys. Res., 97: 3417-3429.

Kelly, K.R., Ward, R.W., Treitel, S. and Alford R.M., 1976. Synthetic seismograms: a finite difference approach. Geophysics, 41: 2-27.

Kennett, B.L.N., 1974. Reflections, rays and reverberations. Bull. Seismol. Soc. America, 65: 1643-1651.

Lafond, C.C. and Levander, A., 1995. Migration of wide-aperture onshore-offshore seismic data, central California: Seismic images of late stage subduction. J. Geophys. Res., 100: 22231-22243.

Lutter, W.J. and Nowack, R.L., 1990 Inversion for crustal structure using reflections from the PASSCAL Ouachita experiment. J. Geophys. Res., 95: 4633-4646.

Lutter, W.J., Nowack, R.L. and Braile, L.W., 1990. Seismic imaging of upper crustal structure using travel times from the PASSCAL Ouachita experiment. J. Geophys. Res., 95: 4621-4631.

Mechie, J., Keller, G.R., Prodehl, C., Gaciri, S., Braile, L.W., Mooney, W.D., Gajewski, D. and Sandmeier, K.-J., 1994. Crustal structure beneath the Kenya Rift from axial profile data. In: C. Prodehl, G.R. Keller and M.A. Khan (Editors), Crustal and upper mantle structure of the Kenya rift. Tectonophysics, 236: 179-200.

Müller, G., 1985. The reflectivity method: a tutorial. J. Geophys., 58: 153-174.

Nolte, B., Frazer, N.L. and Mallick, S., 1992. Seismogram synthesis for azimuthally anisotropic media with a single slowness integration. Geophys. J. Int., 111: 127-140.

Patzwahl, R., 1998. Plattengeometrie und Krustenstruktur am Kontinentalrand Nord-Chiles aus weitwinkelseismischen Messungen. Berliner Geowissenschaftliche Abhandlungen, Reihe B, 30: 1-150.

Podvin, P. and Lecomte, I., 1991. Finite difference computation of traveltimes in very contrasted velocity models: a massively parallel approach and its associated tools. Geophys. J. Int., 105: 271-284.

Reynolds, A.C., 1978. Boundary conditions for the numerical solution of wave propagation problems. Geophysics, 43: 1099-1110.

Scherbaum, F., Krueger, F. and Weber, M., 1997. Double beam imaging: mapping lower mantle heterogeneities using combinations of source and receiver arrays. J. Geophys. Res., 102: 507-522.

Schneider, W.A., Ranzinger, K.A., Balch, A.H. and Kruse, C., 1992. A dynamic programming approach to first arrival traveltime computation in media with arbitrarily distributed velocities. Geophysics, 57: 39-50.

Vidale, J., 1988. Finite-difference calculation of travel times. Bull. Seismol. Soc. America, 78: 2062-2076.

Willmore, P.L. and Bancroft, A.M., 1960. The time-term approach to refraction seismology. Geophys. J.R. astr. Soc., 3: 419-432.

Zelt, C.A. and Smith, R.B., 1992. Seismic traveltime inversion for 2-D crustal velocity structure. Geophys. J. Int., 108: 16-34.

Zelt, C.A. and Barton, P.J., 1998. Three-dimensional seismic refraction tomography: A comparison of two methods applied to data from the Faeroe Basin. J. Geophys. Res., 103: 7187-7210.

Modelling Strategies and Model Assessment for Wide-Angle Data: Solving Inverse Problems by Exploring Model Space

Colin A. Zelt
Rice University, Houston, TX, USA
E-mail: czelt@rice.edu

Wide-angle traveltime modeling and inversion for velocity and interface structure can provide us with a model of a physical property of the earth which can be rigorously assessed, whether the data be 2D, 3D, sparse, noisy, or recorded over complex structure. A velocity model can be interpreted in terms of composition, metamorphic grade, temperature, age, porosity, rheology, etc. Wide-angle data can be acquired relatively inexpensively, as compared to reflection data, and the derived models can be the starting models for higher-resolution waveform processing and inversion techniques. When using traveltimes, it makes sense to use the traveltimes from all phases we can confidently identify in order to best constrain the model. This means refraction, wide-angle reflection, zero- and near-vertical-offset data, as well as multiples, *S*-waves and converted arrivals if available.

Both forward and inverse methods can be used to construct velocity and interface models. The reasons in favour of forward modeling are usually related to a sense that it is easier to ensure a more geologically meaningful result: it is more likely the reasons are related to the limitations of the inverse method at hand. The important reasons in favour of applying an inverse method can be summarized around one concept: the nonuniqueness of the problem means that there is no realistic chance of fitting the data through forward modeling, particularly a large dataset, without introducing unnecessary structure into the model. An inverse method has a reasonable chance of avoiding this problem, while also incorporating various forms of prior/geologic information. This means it is possible to find the simplest model that fits the data without over or under fitting, and therefore, avoid over interpreting or under utilizing the data. To construct other models consistent with the data that are not minimum structure is also important, and an inverse approach is best for this task as well since many alternate models can be constructed relatively quickly as compared to using forward modeling. Finally, for large 2D and 3D datasets, it is unlikely that forward modeling will be able to provide a single model that satisfactorily fits all of the data.

When solving an inverse problem, an attempt should be made to determine model structure that is required by the data, as opposed to merely being consistent with the data. This is especially important for real problems with noisy and insufficient data in which case there will be significant model nonuniqueness. If a wide range of models or model features satisfy the data, should any weight be given to a geological interpretation of a particular model or model feature that is consistent with the data? The inversion of wide-angle traveltime data is a nonlinear problem, so there are no theoretical means for quantitatively assessing the solutions in terms of model resolution and nonuniqueness. An effective approach for assessing a solution to a nonlinear problem is the exploration of model space by varying the free parameters of the inversion and the prior constraints to establish a set of models that satisfy the data, particularly end-member models that emphasize a particular model characteristic. If done in a systematic fashion, this approach is superior to any form of indirect or linearized method of model assessment.

This talk focuses on inverse methods for obtaining 2D and 3D velocity and interface models from wide-angle traveltime data and methods to asses the models, primarily by exploring model space. Before this, some pre-modeling considerations will be discussed, including arrival picking, data uncertainties, traveltime reciprocity, and the selection of a starting model. An effective means for identifying and picking later arrivals is a "bootstrap" approach in which predicted times from progressively more refined models are overlain on the observed data. Pick uncertainties are necessary to avoid over- or under-fitting the data and to allow the appropriate up- and down-weighting of the contribution to the derived model from relatively certain and uncertain picks, respectively. For source-receiver pairs that are reciprocal or nearly reciprocal, the corresponding traveltimes of any arrival type should agree to within the assigned uncertainties, regardless of earth structure. For a linearized, iterative inverse approach, as advocated in this talk, a starting model is necessary and, at least as one end-member approach, it makes sense to incorporate as

much reliable prior information as possible. It is therefore important to use a model parameterization and inverse technique that allows different forms of prior information to be incorporated into the model and possibly maintained during the inversion iterations.

Given the unique characteristics of each dataset and the local earth structure, there is no single approach to inverting wide-angle data that is best. We can classify the end-member styles of wide-angle data inversion according to the model parameterization and the goal of the inversion: uniform/fine-grid parameterization versus non-uniform/coarse-grid parameterization, and minimum-structure model versus non-minimum-structure model. The uniform/fine-grid parameterization and the non-uniform/coarse-grid parameterization can usually be considered the over-parameterized and minimum-parameter model, respectively. A non-minimum-structure model will be consistent with the wide-angle data, but will satisfy more prior information than the minimum-structure model. A non-minimum-structure model may be minimum structure over the set of all models which must include the additional structure associated with the prior information; we call this the prior-structure model.

The over-parameterized, minimum-structure approach uses a starting model that is usually laterally homogeneous using a fine enough grid to represent the expected model heterogeneity. Little or no prior information is used. Over parameterization is not a concern since a regularized inversion that includes perturbation, flatness and/or smoothness constraints will ensure a stable inversion by keeping the model from achieving too much structure. This is an excellent approach to identify the minimum-structure model required by the data.

Seeking a minimum-parameter/prior-structure model is at the opposite end of the spectrum compared to the previous approach. The starting model may be simple or relatively complex, depending on the prior information. Given the relatively few model parameters and the irregular node distribution, a regularized inversion which minimizes the model perturbation at each iteration is appropriate since the modeling goal of honouring the prior information, and perhaps other ideas of what is geologically reasonable, can be monitored and controlled at each iteration. For a simple starting model, the model may be developed by adding model parameters as needed laterally and downward in a layer stripping fashion, called the "across-and-down" approach. For a complex starting model, the gross model structure is assumed to be contained in the starting model and few if any model parameters will be added as the inversion proceeds, and all model parameters are solved for simultaneously in a "whole-model" approach. Both the across-and-down and whole-model approaches are excellent methods for incorporating geologic information into a final model. Both approaches may be applied like automated forward modeling if a parameter-selective inversion algorithm is used. If the local structure is complex or there are reflected and refracted phases with overlapping regions of constraint, the whole-model approach should perform best.

The two intermediate strategies (over-parameterized/prior-structure model and minimum-parameter/minimum-structure model) are useful for incorporating or assessing prior information and particular model features. In some cases, which of the four modeling strategies to apply will be dictated by the earth structure. Aspects of the modeling approach may be data dependent; for example, the shot and receiver spacing, marine data recorded by deep ocean bottom receivers, and onshore-offshore geometries. Traveltimes picked from coincident reflection data can be (1) used to develop the starting model, (2) inverted simultaneously with the wide-angle data, or (3) inverted after modeling the wide-angle data to constrain interfaces that are not tied to the velocity structure. Although the limitations of ray theory in predicting finite frequency effects must be considered, a final model must predict traveltimes of the correct arrival type over the offset range of the picks. Care must be taken during each iteration, particularly with layered and blocky model parameterizations, that all relevant raypaths are traced since there is no known inversion algorithm that can exploit the fact that the model predicts no arrivals where there is observed data.

One advantage of using an inverse method as compared to trial-and-error forward modeling is the time saved to develop an acceptable model that satisfies the data. Ideally, this time should be used to assess the final model, something that cannot be done rigorously through forward modeling. Model assessment establishes the reliability of the final model. Presenting model statistics, traveltime fits, ray diagrams, ray coverage, resolution values and kernels is useful, but can only indirectly address this issue. Direct model assessment techniques that derive alternative models that satisfactorily fit the real data are the best means for establishing the absolute bounds on model parameters and whether a particular model feature is required by the data or merely consistent with the data. This is because of the nonlinearity of the problem and therefore the need to "see" other models that fit the data equally well to be certain of the bounds estimated for particular model features and to establish the associated model parameter trade-offs involved. If the solution of a problem is poorly constrained, or equivalently, very

nonunique, it means the solution presented as the preferred final model may have no special significance. Indirect methods are easier and quicker to apply than direct methods. Direct methods require more time and thought to apply and the tests to run will usually be unique for each dataset.

Consider the difference between the results of processing reflection data and modeling wide-angle data. With most reflection data, the final section can be presented in uninterpreted form so that the reader can assess the interpretation provided and objectively establish their own interpretation. Reflection data do not have the same potential for possessing a highly unpredictable spatial dependence of the reliability of the image, as with a velocity model derived from wide-angle data. This is because the effects related to signal-to-noise ratio, frequency content, low fold, coherent noise, and the increase of the Fresnel zone with two-way time, are normally evident in a reflection section. With wide-angle traveltime data, the goal is to produce a velocity model that predicts the observed traveltimes. Thus, the final result of the modeling approach, the model, is fundamentally different than that from the processing approach, since it looks nothing like the data. It is therefore left to the modeler to establish the credibility of the model using indirect and direct model assessment techniques.

For minimum-parameter models, single-parameter resolution and uncertainty tests are powerful nonlinear means for establishing spatial resolution centered about a specific node and the absolute bounds on a single node value. The former involves inverting synthetic data obtained by perturbing one parameter value in the final model, and the latter involves inverting the real data in the manner in which the final model was obtained, except fixing the value of one node to determine how much it may be perturbed yet still allow an acceptable fit the data. Nonlinear checkerboard resolution tests are an effective means for establishing the spatial resolution at all model nodes in one or a few runs. Synthetic data from the background or final model with an alternating pattern of high and low velocity or depth anomalies superimposed are inverted. The resolution at different length scales can be estimated by testing anomaly patterns with different sizes.

Direct model assessment techniques are based on deriving alternate models that fit the data. The drawback of such techniques is the number of additional tests necessary, and the inability to explore all possibilities in model space. The above mentioned single-parameter uncertainty test is an example of a direct technique. A multi-parameter form of model assessment can be used to test whether a particular model feature is required by the data, and to place bounds on it. Regularized inversion techniques can be used for direct assessment by spatially varying the weighting of perturbation, flatness and smoothness constraints. Direct model assessment should be applied to model features that contain the most "structure", e.g. low-velocity zones, lateral velocity variations within a layer, and the largest magnitude velocity and interface perturbations relative to the starting model. Even if these features are not important to the primary geologic interpretation of the model, their presence may involve parameter trade-offs in other regions of the model that are geologically important. In addition, any model features that are central to the geologic interpretation should be tested by direct model assessment. Direct model assessment can be applied without focusing on a single node or model feature, but rather with the intent of exploring model space to gain insight into general model nonuniqueness and parameter trade-offs. To do this in a systematic way one can vary within reasonable limits all of the parameters that comprise the inversion. For example, the prior uncertainties assigned to velocity and depth nodes, the trade-off parameters in the objective function that weight the model perturbation and roughness, the model parameterization in terms of node spacing or locations and number of layers, comparing the results of a layer stripping and whole-model approach, different starting models, and omitting or down-weighting the prior information.

The modeling strategies and methods for model assessment discussed in the first half of this talk will be demonstrated using real data examples: (1) assessment of a minimum-parameter model for a 2D profile from the southeastern Canadian Cordillera, (2) minimum-structure inversion and assessment of 3D data from the Faeroe Basin, (3) 3D simultaneous refraction and reflection tomography and assessment of data from the Chilean margin, (4) "tomographic assessment" of a geologically-constrained, minimum-parameter model for a 2D profile from India, (5) a comparison of a minimum-parameter, simultaneous wide-angle and zero-offset traveltime inversion with a minimum-structure, first-arrival tomographic inversion for a 2D profile from the Iberia margin, and (6) 3D tomography and assessment of onshore-offshore data from southwestern British Columbia. The results from these and other studies suggest: (1) a grid search technique applied to the free parameters of an inverse approach is an effective method for exploring model space and assessing the effect of the free parameters and prior information on the solution, (2) end-member models which satisfy the data may not be geologically reasonable, adding a subjective element into the model assessment, (3) a subjective, geologically-constrained, minimum-parameter 2D model can be assessed using an objective, minimum-structure, first-arrival, tomographically-derived

model, (4) simultaneous refraction and reflection tomography allowing spatially-varying weights on the perturbation and roughness of slowness and interface depth is effective for modeling and assessing 3D data, and (5) minimum structure does not imply required structure.

Selected References:

Hole, J.A., 1992. Nonlinear high-resolution three-dimensional seismic travel time tomography, *J. Geophys. Res.*, 97, 6553-6562.

Lailly, P., & Sinoquet, D., 1996. Smooth velocity models in reflection tomography for imaging complex geological structures, *Geophys. J. Int.*, 124, 349-362.

Lanz, E., Maurer, H. & Green, A.G., 1998. Refraction tomography over a buried waste disposal site, *Geophysics*, 63, 1414-1433.

Lutter, W.J., Fuis, G.S., Thurber, C.H. & Murphy, J., 1999. Tomographic images of the upper crust from the Los Angeles Basin to the Mojave Desert, California: Results from the Los Angeles Region Seismic Experiment, *J. Geophys. Res.*, in press.

McCaughey, M. & Singh, S.C., 1997. Simultaneous velocity and interface tomography of normal-incidence and wide-aperture traveltime data, *Geophys. J. Int.*, 131, 87-99.

Sain, K., Zelt, C.A. & Reddy, P.R., 1999. Tomographic assessment of geologically-constrained, minimum-parameter velocity models obtained from refraction/wide-angle reflection data: Hirapur-Mandla profile, India, *Geophys. J. Int.*, submitted.

White, D.J., & Boland, A.V. , 1992. A comparison of forward modeling and inversion of seismic first arrivals over the Kapuskasing Uplift, *Bull. Seism. Soc. Am.*, 82, 304-322.

Zelt, B.C., Ellis, R.M., Clowes, R.M., & Hole, J.A., 1996. Inversion of three-dimensional wide-angle seismic data from the southwestern Canadian Cordillera, *J. Geophys. Res.*, 101, 8503-8529.

Zelt, C.A., 1998. Lateral velocity resolution from three-dimensional seismic refraction data, *Geophys. J. Int.*, 135, 1101-1112.

Zelt, C.A., 1999. Modelling strategies and model assessment for wide-angle seismic traveltime data, *Geophys. J. Int.*, 139, 183-204.

Zelt, C.A. & Barton, P.J., 1998. Three-dimensional seismic refraction tomography: A comparison of two methods applied to data from the Faeroe Basin, *J. Geophys. Res.*, 103, 7187-7210.

Zelt, C.A., Hojka, A.M., Flueh, E.R. & McIntosh, K.D., 1999. 3D simultaneous seismic refraction and reflection tomography of wide-angle data from the central Chilean margin, *Geophys. Res. Lett.*, 26, 2577-2580, 1999.

Zhang, J., ten Brink, U.S. & Toksöz, M.N., 1998. Nonlinear refraction and reflection traveltime tomography, *J. Geophys. Res.*, 103, 29743-29757.

Resolution Issues in Travel Time Tomography

John A. Hole and Matthias G. Imhof
Virginia Tech, Department of Geological Sciences,
4044 Derring Hall, Blacksburg, VA, 24061-0420;
hole@vt.edu, mgi@vt.edu

Prior to communicating the results of seismic travel time analysis, the interpreter must assess the reliability of the velocity model. Of primary importance is the ability to resolve the presence or absence and spatial dimensions of a feature within the model. This can be expressed as spatial resolution or as resolution of a model parameter. This article reviews and discusses factors affecting the resolution limits of models derived from travel time data.

Optimum Spatial Resolution and the Fresnel Zone

The optimum spatial resolution of travel time tomography is usually assumed to be the Fresnel zone. Resolution is defined in this case as the ability to distinguish two nearby small objects. The travel time from the source to any diffracting point within the Fresnel zone plus the travel time from the same point to the receiver is within a half of the dominant period (period is 1/frequency) of the Fermat ray's travel time. This ensures constructive interference between waves travelling along the diffraction path and the ray path. The Fresnel zone forms a beam around the ray path. The beam is widest at a point approximately midway along the ray path between the source and receiver, with strong dependence upon the velocity structure. For reflected ray paths at normal incidence, the Fresnel zone defines the familiar lateral resolution limit on the reflector.

For seismic refraction data, the width of the Fresnel zone is depressingly large. As an example, Fresnel zones were computed for a 1-D velocity model from northern California. The vertical gradient of the model is fairly typical, while the velocity is lower than average, producing a smaller Fresnel zone. A ray recorded at an offset of 50 km turns in a seismic velocity of 5.8 km/s at 8 km depth. For a dominant frequency of 20 Hz, the Fresnel zone diameter at the turning point is over 3 km. This is much larger than the 300-m wavelength. This Fresnel zone indicates 3 km vertical resolution at 8 km depth. Rays recorded at less than 13 km offset have Fresnel zones that extend to the surface. This suggests that 20 Hz travel times cannot resolve any vertical variations in the upper 1.5 km, regardless of how many traces are recorded. A lower dominant frequency, as is often the case for crustal refraction data, results in wider Fresnel zones. These examples suggest that crustal refraction data have very poor depth resolution.

The concept of the Fresnel zone is based upon the ability to distinguish two wavelets arriving at similar travel times. If the wavelets arrive within a half period of one another, they will interfere constructively to produce a single peak. The shape and amplitude of the combined wavelet, however, are different from a single wavelet. This distortion of the wavelet allows reflection data to detect thin beds as small as 1/32 of a wavelength. The detection limit is practical, not theoretical, and depends on the signal quality and knowledge of the wavelet.

Of interest in transmission data is the ability of an object to produce a travel time effect at the receiver that can be distinguished from energy that has diffracted around the object. Wavefront healing can eliminate the effect of a small object as observed at a distant receiver. If the object is smaller than a Fresnel zone, energy that travelled around the object will arrive within a half period of energy that travelled through the object. The object and diffractions around it will not be distinct arrivals, as they will constructively interfere. If the peak of a zero-phase wavelet is picked, the detection limit is the Fresnel zone. However, travel time picking based upon the first break of a causal minimum-phase wavelet is limited by the maximum frequency, not the dominant frequency. Realistic picking accuracy is about a quarter-period of the maximum frequency in the signal that is sufficiently above the noise level. Detection is primarily a signal-to-noise issue, as there is no theoretical limit to picking accuracy if noise is absent. Wavefront healing is asymptotic, never perfect, and hence small objects can theoretically be detected. Since the first arrival time can be picked more accurately than a half period, objects smaller than the Fresnel zone can be detected. The half-period Fresnel beam should be replaced by a narrower beam that represents the true picking accuracy.

The amplitude of the arrival caused by the small object is also critical to detection. In order to be detected, the energy of the arrival must be larger than the noise in the data. The amplitude of arrivals due to an object smaller than the Fresnel zone but larger than a wavelength is reduced proportional to the cross-sectional area of the object. Objects smaller than a wavelength act as forward scatterers, with greater signal loss.

For transmission data, the velocity and along-ray extend of the object are also important to detection. A sufficiently high velocity or a thin, fast object that is elongated parallel to the ray can channel the energy, producing a much earlier arrival. Such an object reduces the width of the Fresnel zone relative to the background because diffractions from outside the object arrive too late. A slow object also narrows the Fresnel zone for the ray that travels directly through it. However, faster rays diffract around the slow object, which produces a local triplication in the travel time curve. Identification and picking of secondary phases within the triplication is subject to the Fresnel zone limit, where the Fresnel zone is defined including the low velocity body. Since it is difficult in practice to pick secondary arrivals close to the primary, the resolution of low velocity bodies is limited by the loss of information within local triplications.

The above discussion indicates that objects smaller than a Fresnel zone may be detected by seismic travel times. This is analogous to the detection in reflection data of a very thin bed by changes in the wavelet. Similarly, small gaps in a reflector can be detected by the observation of diffraction tails. Detection, however, does not imply that the location of such objects can be resolved to better than a Fresnel zone.

In a stacked seismic reflection section, equivalent to a zero-offset normal-incidence gather, the spatial resolution along the reflector is limited to a Fresnel zone. The resolution can be improved by migration, which is an inversion process that collapses the diffraction hyperbolae to the location of the diffractor. Migration acts by downward continuation of the wavefield through the velocity model, reducing the distance to the reflector and thus the width of the Fresnel zone. The lateral resolution is then limited by migration considerations. Assuming sufficient spatial sampling of the shots and receivers and an accurate velocity model, lateral resolution in the migrated section is approximately a wavelength. This is usually a substantial improvement.

Travel time tomography is an inversion process analogous to migration. It acts by back-projection of wavefronts through the velocity model to locations where they constructively interfere. If the sources and receivers are sufficiently sampled in space, the shape of the wavefront healing curve can be used to back-propagate the arrival times towards the anomalous object. Analogous to migration, tomography will reduce the size of the effective Fresnel zone. Both migration and tomography require that the velocity model be well known away from the object of interest. In practice, both inversions must iteratively improve the image as the true ray locations become better known.

As a thought exercise, consider two sub-parallel rays with overlapping Fresnel zones. Somewhere within the Fresnel zone of the first ray is an object that produces a detectable travel time effect at the receiver. The object does not lie within the Fresnel zone of the second ray. Combining information from the two rays, it is clear that the location of the anomalous body must be in the portion of the first ray's Fresnel zone that does not overlap with that of the second ray. With multiple overlapping Fresnel zones, the location of the body can be accurately determined.

Travel time data are capable of detecting the presence of anomalous bodies smaller than the width of a Fresnel zone. Through tomography or any other travel time inversion, this detected information is sufficient to spatially resolve objects smaller than a Fresnel zone. The resolution limit is instead controlled by detectability, ray coverage, and shadow zone effects. Detectability depends upon the data frequency, the size of the travel time perturbation, and the amplitude of the wave through the body. Ray coverage determines the spatial resolution of detectable small objects in the same manner as for large objects. Ideal resolution requires dense ray sampling, complete azimuthal coverage at the target to define all its dimensions, plus sufficient ray coverage elsewhere to determine all portions of the model that affect the rays of interest.

Resolution and the Model Parameterization

In a linear inversion, the resolution of a model parameter is formally defined as a vector $\mathbf{r}_i$ that relates the dependence of the inversion result upon the true value of all of the model parameters:

$$m_i = \mathbf{r}_i \cdot \mathbf{m}^t$$

where m_i is the model parameter of interest and $\mathbf{m}^t$ is the true earth model expressed as a vector of parameters. The resolution vectors for all parameters are usually combined as the rows of a resolution matrix $\mathbf{R}$. Standard procedures exist for computing this matrix. For travel time inversion, the resolution matrix depends upon the ray geometry, the model parameterization, and the inversion algorithm. It does not depend upon the travel time data.

The resolution matrix is frequently misused as an indicator of image reliability. The diagonal terms of the matrix are often plotted to indicate well constrained parameters. Diagonal values close to unity indicate that the value of the model parameter is similar to the true value. However, the off-diagonal terms are also important, for they indicate the dependence of each parameter upon the other

parameters. The off-diagonal terms should have four attributes: they should be small; they should be non-negative; the largest values should be clustered at parameters physically close to the parameter of interest (which are sometimes, but not always, near the diagonal); and the non-zero values should produce an average physically centered at the parameter of interest. Non-zero values in physically distant parts of the model indicate the possible creation of artifacts due to under-parameterization or non-uniqueness. Negative terms indicate a strong trade-off between parameters and possible artificial oscillations in the model. Non-centered terms indicate that objects may be offset from their true location. Instead of plotting the diagonal terms, several of the resolution vectors $\mathbf{r}_i$ should be plotted in physical space. The plot should indicate a narrow peak centered at the parameter of interest. The spread approximates the spatial resolution.

The resolution matrix is strongly affected by the model parameterization. The choice of parameters to represent the model places extra constraints on the set of non-unique models that adequately match the data. The subset of models that match the data but cannot be expressed by the parameterization are eliminated from consideration. This may eliminate the true model, and may even eliminate all models that match the data. For an inappropriate parameterization, the true earth may not be adequately represented by $\mathbf{m}^t$.

The example of gridded tomography models is used, where the model parameters are the velocity in each grid cell. The concepts apply equally to layers, polygons, or any other model parameterization. If very large grid cells are chosen, then each cell is sampled by numerous rays and becomes over-constrained in the inversion. The resolution matrix will express great confidence in the value of each model parameter. However, true heterogeneity within a cell may be sampled by the data but cannot be expressed by the model. Even large-scale heterogeneity cannot be represented if the true heterogeneity does not conform in shape and position to the large cells. This concept can be expressed as model fidelity, or the ability of the model parameterization to represent expected and constrained earth structure. The resolution matrix gives false confidence in the under-parameterized, poor-fidelity inversion results.

The inability of a parameterization to represent constrained structures means that the grid cell will contain incorrect values from the perspective of some of the rays that travel through the cell. It is hoped that the velocity represents some average over the cell. Travel time misfits within a cell will affect the model in other cells. If poorly constrained cells exist somewhere along the ray path, then the misfit can be relocated at great distance from the cell that caused it. Such artifacts of the parameterization are difficult to recognize. A partial test for artifacts can be performed by comparison of inversion results with the grid cells shifted in position by fractions of the grid cell dimension. Inversion for the locations of the corners of large blocks allows the blocks to deform to their optimal shape for improved fidelity, but cannot guarantee a sufficient number of blocks. A mix of parameter types, such as velocity plus position of a grid node, can produce strong non-linear tradeoffs between parameters, even in the linear seismic inversion problem with fixed rays.

Tomography using grid cells much smaller than the expected spatial resolution provides perfect model fidelity. The grid cells are under-constrained, and the resolution matrix will have small diagonal terms. In order to stabilize the inversion and reduce high-frequency oscillations in the model, smoothing constraints or damping are required during inversion. Smoothing should be minimized in order to optimize spatial resolution. The off-diagonal terms of the resolution matrix will have the desired attributes and will represent the interdependence of neighbouring grid cells. The resolution vector for an individual parameter plotted in physical space will accurately represent the spatial resolution that can be obtained from the data.

Two ideal parameterizations thus exist: blocks approximately the size of the true spatial resolution with locations of the grid nodes as extra parameters, or cells much smaller than the true spatial resolution with smoothing constraints. Inversion with mid-size floating blocks introduces highly nonlinear velocity-position tradeoffs. Inversion with small cells and smoothing creates a very large matrix to be inverted. There is no formal technique to fully assess resolution of the nonlinear travel time inversion problem, but the concepts of model fidelity and over- and under-constrained parameters remain valid. Linearized estimates of nonlinear resolution will always be over-confident.

Full Waveform Inversion of Seismic Data: Frequency versus Time Domain

Y. Freudenreich, R. Shipp, S. C. Singh

Dept. of Earth Sciences, Bullard Laboratories, University of Cambridge, Cambridge, England

Summary

Full waveform inversion of seismic data provides a detailed velocity structure of the sub-surface. Full waveform inversion can either be performed in the frequency or in the time domain. The frequency domain method can be more efficient than the time method, provided only a few discreet frequencies are used. In this paper, we investigate the applicability of the two methods by applying them to a simple synthetic example. We show that the frequency domain approach works fine for large offset data but fails in the case of limited offset range and also show that the time domain approach appears more robust.

Introduction

Traveltime of seismic data contains the information about the large-scale feature of sub-surface whereas the detailed information is contained in the waveforms. Waveform inversion of seismic data is an extremely non-linear problem, which can be linearized by starting from a good initial model. The waveform inversion has been successfully applied to several 1-D problems (Singh *et al.*, 1993; Singh *et al.*, 1998), but applications to 2-D problems has had limited success. Mora (1988) developed a 2-D elastic inversion method using a finite difference solution of the wave equations in the time domain and tested on a synthetic near-offset data. Crase *et al.* (1990) applied this approach on near-offset to a real seismic data set. Sun and McMechan (1992) extended this approach and showed the feasibility of this method on synthetic wide-angle data. Shipp *et al.* (1997) applied this approach to the sub-basalt imaging problem. In parallel, Pratt *et al.* (1999) and Forgues *et al.* (1998) proposed a formulation in the temporal frequency domain in order to carry out the inversion of one discreet frequency at a time and showed that one can recover the sub-surface structure by inverting a few discreet frequencies. And, as only a few discreet frequencies are used, the method is very efficient.

A single frequency of seismic data is sinusoidal and the inversion of a single frequency should lead to ringing in the final velocity model, that correspond to the wave number associated with that frequency. By successively increasing the frequency of data to be inverted and using results from the previous frequency as a starting model, cancellation of this ringing may be achieved. However to the best of our knowledge no investigation has been made to assess the conditions under which the inversion of single discrete frequency data might provide accurate representation of the model. By applying both time domain and frequency domain methods to a simple example, we examine the applicability of these two methods.

We begin this paper with a brief review of the full waveform inversion method in the time domain and apply it to band-limited or single-frequency data. In this case we are not explicitly performing frequency domain inversion in the manner of Pratt *et al.* but rather simulating such a scheme by the introduction of a sinusoidal source into our time domain scheme. The use of a sinusoidal source wavelet allow us to invert for a single frequency component rather than a band frequency.

Synthetic Examples

Our test model consists of a layer, 500 m thick, over a half space of velocities 2.4 km/s and 2.5 km/s, respectively. A 200 m thick layer with a velocity of 2.7 km/s is placed in the half-space at a depth of 2 km. A ricker source wavelet with a dominant frequency of 3 Hz and a band width of 1-6 Hz was used. Synthetic data were computed at 100m offset interval in the range of 0-10 km and a 4 ms time interval. The starting model was the model without the thin layer.

The first example shows the results of inverting a maximum of 1 km, 3 km and 10 km offset using the time domain method and with a ricker wavelet (1-6 Hz) as the source wavelet. As expected, the inversion of near offset data (figure a) gives a response which is equivalent to a ricker wavelet (Neves and Singh, 1996). However the inversion recovers the correct position and impedance contrast of the reflectors. Including the long offsets (figure c) improves the inversion result. The amplitude of the side-lobes is decreased and the model is well recovered.

In the second experiment, we inverted a single frequency and assumed that the source wavelet is a sinusoidal wave of 3 Hz, which is the central frequency for the ricker wavelet. For 3 km offset data (figure d), the inversion produces strong ringing in the inverted velocity model. For 7km to 10km offset (figure e) the inversion still not provide a good model due to a presence of ringing. These ringing effects decrease with the use of wide-angle data (figures f) in the inversion, but the final result is still far from the true model.

Pratt *et al.* (1999) suggested that if we start to invert with a low frequency and use these results as a starting model for inverting a higher frequency, then the ringing effects will disappear. We inverted the model for a maximum offset of 3 km, 7 to 10 km and finally 10 km. For a 3 km offset data (figure g) we notice that the location of the reflector is not constrain. For 7 km to 10 km offset (figure h) the results show that the inversion has not been able to recover the true model and some ringing still remain. We obtain a better recovery of the data by inverting large range of offset (figure i). By progressively moving up in the frequency spectrum during the inversion process (2 Hz, then 4 Hz and finally 6 Hz) the velocity model is improved, but some ringing still remains which is due to a lack of frequencies that are not included in the inversion. It appears that when we apply a single frequency approach the quality of the results depends on the range of offset.

Conclusion

We have analysed the inversion results for various offsets (1 km, 3 km and 10 km) using a ricker wavelet source or a single frequency source. Our tests illustrate the advantages of inverting wide-angle data. Indeed, for a ricker wavelet source, the use of long offsets improve the quality of the inversion. Whereas, for a single frequency source it is necessary to have long offset data. We also demonstrated that the combination of several inversions initiated with a different discreet frequency is less accurate than moving up in the frequency spectrum during the inversion process. Finally we compared these inversions with an inversion on a band of frequency and show that Shipp's approach provides a powerful tool for full waveform inversion modelling. According to our simulation of the frequency domain approach we conclude that this method works fine for a very large offset data, but fails in the presence of limited offset range. Contrary to this, the time domain approach appears more robust. Although, the frequency domain method is efficient it will require a significant amount of human input in choosing frequencies and offsets which might bias the final model.

References

Crase, E., Pica, A., Noble, M., McDonalds, J., and Tarantola, A., 1990, Robust elastic nonlinear waveform inversion: Application to real data, Geophysics, 55, 527-538.

Forgues, E., Scala, E., Pratt, R., 1998, High resolution velocity model estimation from refraction data, SEG, Expanded Abstracts, 1211-1214.

Mora, P., 1988, Elastic wave-field inversion of reflection and transmission data, Geophysics, 53, 750-759.

Neves, F., Singh, S., 1996, Sensitivity study of seismic reflection/refraction data, Geophys. J. Int., 126, 2, 470-476.

Pratt, R.G., 1999, Seismic waveform inversion in the frequency domain, Part 1: Theory and verification in a physical scale model, Geophysics, 64, 888-901.

Pratt, R.G., Shipp, R., 1999, Seismic waveform inversion in the frequency domain, Part 2: Fault delineation in sediments using crosshole data, Geophysics, 64, 902-914.

Shipp, R., Singh, S., and Barton, P., 1997, Sub-basalt imaging using full wavefield inversion, 67th SEG, Expanded Abstracts, 1563-1566.

Singh, S., Kent, G., Collier, J., Harding, A., Orcutt, J., 1998, Melt and mush variations in crustal magma properties along the ridge crest at the southern East Pacific Rise, Nature, 394, 6696, 874-878.

Singh, S., Minshull, T., Spence, G., 1993, Velocity structure of a gas hydrate reflector, Science, 260, 5105, 204-207.

Sun, R., and McMechan, G., 1992, 2-D Full-wavefield inversion for wide-aperture, elastic, seismic data, Geophys. J. Int., 111, 1-10.

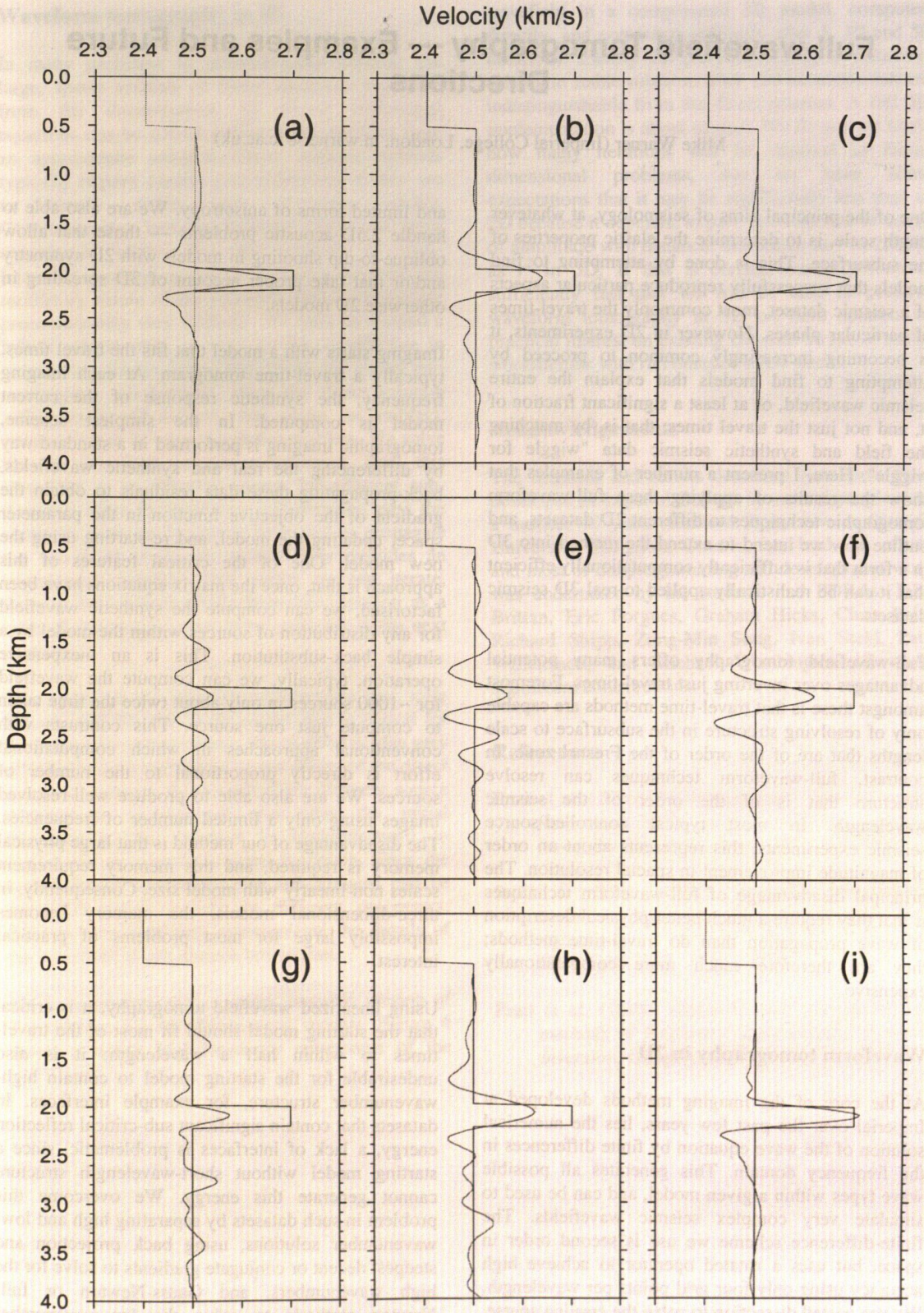

Figure: Inversion results obtained using three different approaches. (a,b,c) inversion in the time domain with a ricker wavelet source, (d,e,f) inversion with a sinusoidal source of 3 Hz, and (g,h,i) inversion with a variation of the frequency: first 2 Hz, then 4 Hz and finally 6 Hz. The first column display the results of inversions for a maximum offset of 3 km. In the second column inversions from 7 km to 10 km offset. And in the third column inversions on 10 km offset.

Full-wavefield Tomography — Examples and Future Directions

Mike Warner (Imperial College, London, m.warner@ic.ac.uk)

One of the principal aims of seismology, at whatever length scale, is to determine the elastic properties of the subsurface. This is done by attempting to find models that successfully reproduce particular aspects of a seismic dataset, most commonly the travel-times of particular phases. However in 2D experiments, it is becoming increasingly common to proceed by attempting to find models that explain the entire seismic wavefield, or at least a significant fraction of it, and not just the travel times; that is, by matching the field and synthetic seismic data "wiggle for wiggle". Here, I present a number of examples that show the results of applying these full-waveform tomographic techniques to different 2D datasets, and outline how we intend to extend the method into 3D in a form that is sufficiently computationally efficient that it can be realistically applied to real 3D seismic datasets.

Full-wavefield tomography offers many potential advantages over inverting just travel-times. Foremost amongst these is that travel-time methods are capable only of resolving structure in the subsurface to scale lengths that are of the order of the Fresnel zone. In contrast, full-waveform techniques can resolve structure that is of the order of the seismic wavelength. In most typical controlled-source seismic experiments, this represents about an order of magnitude improvement in spacial resolution. The principal disadvantage of full-waveform techniques is that they require a much better physical description of wave propagation than do travel-time methods; they are therefore much more computationally expensive.

Waveform tomography in 2D

At the core of the imaging methods developed at Imperial over the past few years, lies the numerical solution of the wave equation by finite differences in the frequency domain. This generates all possible wave types within a given model, and can be used to simulate very complex seismic wavefields. The finite-difference scheme we use is second order in space, but uses a rotated operator to achieve high accuracy using only four grid points per wavelength. We use nested dissection to solve the ensuing sparse, matrix equation with minimal matrix infill during the direct LU decomposition of the matrix. In 2D, we are able to handle both acoustic and elastic wave equations, and to incorporate anelastic attenuation and limited forms of anisotropy. We are also able to handle 2.5D acoustic problems — those that allow oblique-to-dip shooting in models with 2D symmetry and/or that take proper account of 3D spreading in otherwise 2D models.

Imaging starts with a model that fits the travel times, typically a travel-time tomogram. At each imaging frequency, the synthetic response of the current model is computed. In the simplest scheme, tomographic imaging is performed in a standard way by differencing the real and synthetic wavefields, back-propagating these data residuals to obtain the gradient of the objective function in the parameter space, updating the model, and re-starting using the new model. One of the critical features of this approach is that, once the matrix equations have been factorised, we can compute the synthetic wavefield for any distribution of sources within the model by a simple back-substitution. This is an inexpensive operation; typically, we can compute the wavefield for ~1000 sources in only about twice the time taken to compute just one source. This contrasts with conventional approaches in which computational effort is directly proportional to the number of sources. We are also able to produce well-resolved images using only a limited number of frequencies. The disadvantage of our method is that large physical memory is required, and this memory requirement scales non-linearly with model size. Consequently, in three-dimensional models, the memory becomes impossibly large for most problems of practical interest.

Using linearized wavefield tomography, it is critical that the starting model should fit most of the travel-times to within half a wavelength; it is also undesirable for the starting model to contain high-wavenumber structure, for example interfaces. In datasets that contain significant sub-critical reflection energy, a lack of interfaces is problematic, since a starting model without short-wavelength structure cannot generate this energy. We overcome this problem in such datasets by separating high and low-wavenumber solutions, using back projection and steepest decent or conjugate gradients to solve for the high wavenumbers, and Gauss-Newton or full-Newton methods to solve the low-wavenumber problem. A full mathematical treatment of the forward modelling and inversion schemes are given in Pratt et al. (1996, 1998) and Stekl & Pratt (1998).

Waveform tomography in 3D

In many problems in computational physics, the large, sparse systems of linear equations that arise from the discretization of partial differential equations can be solved indirectly by iterating from an approximate solution. These indirect methods typically require careful preconditioning if they are to remain stable and converge rapidly. Conventionally, iterative methods have not been considered suitable for the solution of high-frequency wave-propagation problems, because the oscillatory nature of the solutions makes appropriate preconditioning very difficult. We have developed a hybrid scheme that, at least in 2D, is effective in overcoming this problem. We divide the model into overlapping sub-domains, using the direct solution within each sub-domain, but using an indirect, iterative solver to solve the global problem. We solve for the wavefield in one sub-domain, treat this wavefield as an effective source for adjacent sub-domains, solve for these new sub-domains, pass the results to their neighbours in turn, and so propagate the wavefield across the model. This provides an approximate solution from which we can iterate, treating the residual errors from one iteration as a suite of effective sources, to be removed, in the next iteration.

This approach has memory requirements that scale linearly with the size of the model; this is critical for three-dimensional problems. The method is also very efficient since it capitalises on the ability of the direct solver to compute the wavefield for different source distributions at minimal cost after the initial factorisation. The method is straightforward to implement on coarsely parallel hardware, since the wavefields in non-overlapping sub-domains can be computed simultaneously on different processors; these in turn need only communicate the details of the wavefield at sub-domain boundaries.

We have implemented a scalar, acoustic version of this scheme, for two-dimensional models. Figure 4 shows a single, high-frequency component of the wavefield in a complicated 2D model, computed directly, and computed indirectly after 5, 10 and 50 iterations. Clearly the pre-conditioning is effective; we obtain stable solutions after ~50 iterations that are indistinguishable from the direct solution. A full 3D implementation is about to start. We do not yet know how many iterations will be required in three-dimensional problems, but we have some expectations that it may be significantly less than in 2D because it depends, in part, upon the rate of decay of amplitude with distance; this varies as r in 2D but as r^2 in 3D. If this is correct, our algorithm is sufficiently fast that we will be able to perform waveform tomography in 3D on field datasets of practical interest on existing Beowulf arrays of scalar workstations with run times of a few weeks.

Acknowledgements

The methods and results described here have been developed at Imperial College by several people over a number of years. Gerhard Pratt, now at Queen's University, Kingston, Ontario, has lead this effort, and most of the programming and development work was undertaken by his students and PDRAs. John Brittan, Eric Forgues, Graham Hicks, Chris Pain, Richard Shipp, Zong-Min Song, Ivan Stekl, Paul Williamson, and Michael Worthington all made significant contributions.

References

Pratt et al. (1996). *Two-dimensional velocity models from wide-angle seismic data by wavefield inversion.* **Geophys. J. Int., 124**, 323–340.

Stekl & Pratt (1998). *Accurate visco-elastic modelling by using frequency-domain finite differences using rotated operators.* **Geophysics, 63**, 1779 – 1974.

Pratt et al. (1998). *Gauss-Newton and full-Newton methods in frequency-space seismic waveform inversion.* **Geophys. J. Int., 133**, 341–362.

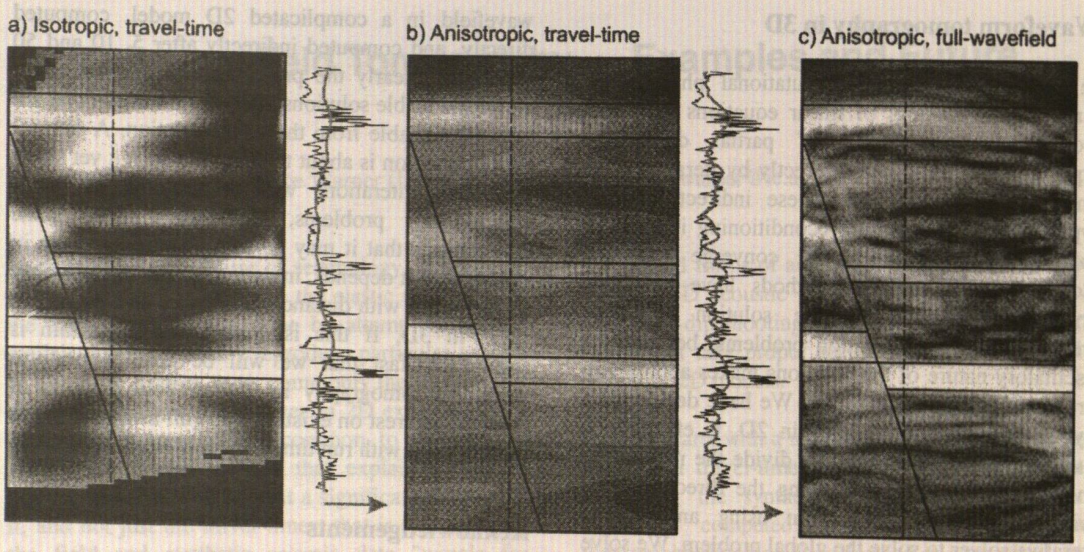

Figure 1 Inversion of wide-angle field data – cross-borehole geometry

In this experiment, sources and receivers were located in vertical boreholes down the sides of the model. Sonic logs from a third borehole, dashed line, can be used as an independent test of the accuracy of the various inversion schemes. **(a)** Tomographic inversion of picked travel-times assuming an isotropic model. The result is poorly imaged, and the absolute velocities are not correct. **(b)** Tomographic inversion of picked travel-times assuming an anisotropic model with transverse isotropy with a vertical axis of symmetry. The figure and sonic log show the vertical component of velocity; the anisotropy is about 22%. The structure is better imaged, and the absolute velocities are now correct. **(c)** Full-wavefield, frequency-doamin, finite-difference, tomographic inversion assuming elliptical anisotropy. There is a significant improvement in resolution over the travel-time models. The associated sonics show that this improved resolution is real.

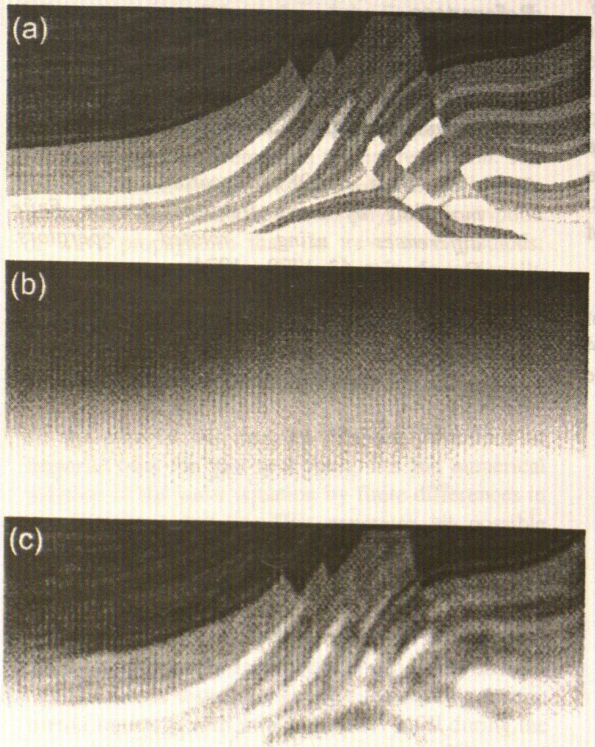

Figure 2 Inversion of combined wide-angle and near-normal-incidence synthetic data

(a) Input Marmousi velocity model. Sources and receivers are located at all positions along the surface of the model; maximum offset 9 km.

(b) The starting model for the wavefield inversion; a smoothed version of the real model.

(c) Tomographic velocity image obtained by full-wavefield inversion of the synthetic data at all times and offsets. Maximum frequency used in the data is 10 Hz. Twenty iterations at six frequencies were used. Note that this is a quantitative image of velocity, it is not a reflection image of acoustic-impedence contrast.

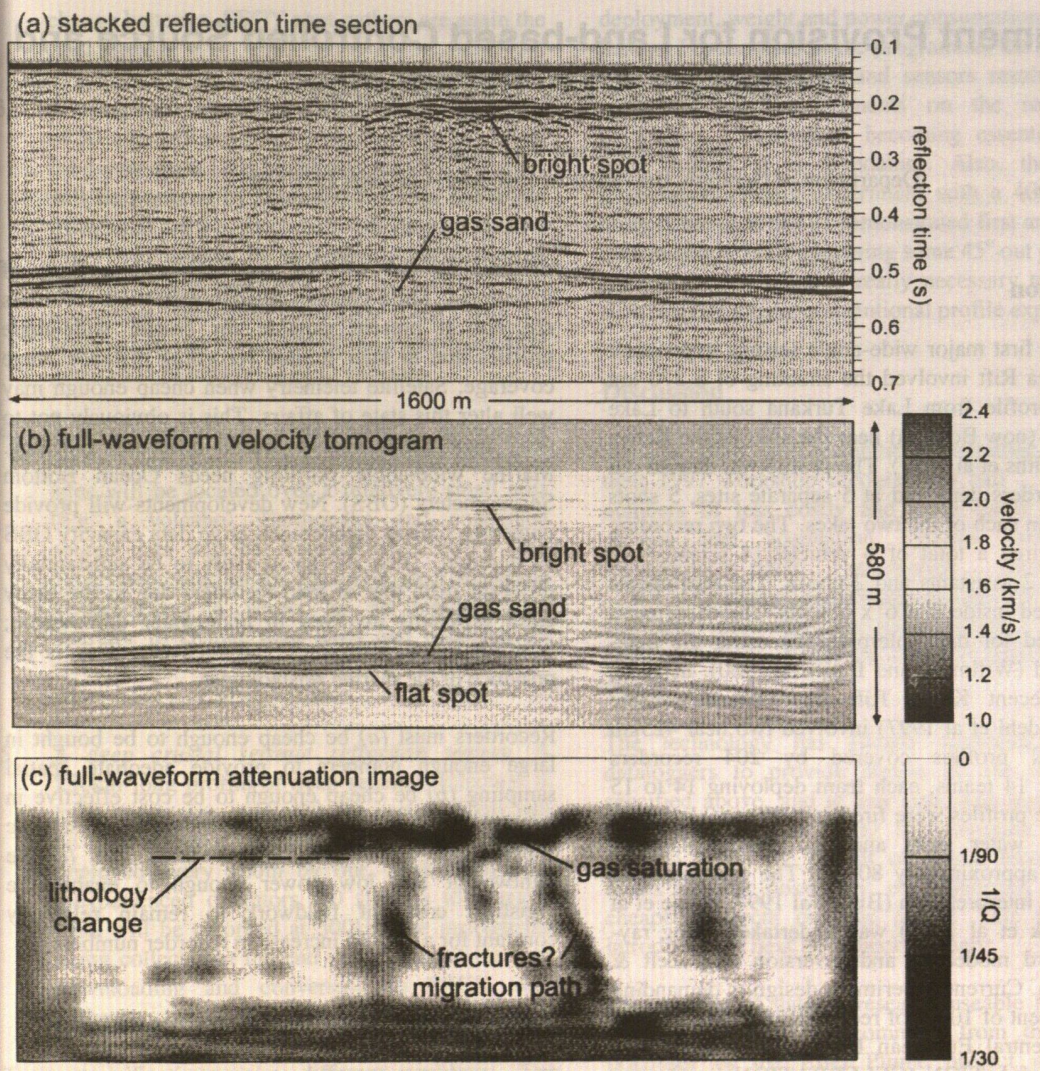

Figure 3 **Inversion of near-normal-incidence, field, reflection data**

The data are from a high-resolution site survey; no wide-angle component was included in the inversion. The reflection section is in time; the tomograms are in depth. The velocity tomogram is able to resolve velocity structure at a resolution comparable to that of the reflection image. The frequency domain formulation allows attenuation to be recovered. These results were obtained by separately inverting for the high and low wavenumbers, using conventional back-propogation to obtain the high wavenumbers, but using Gauss-Newton to obtain the low wavenumbers. If simple back propagation is used alone, errors in the low wavenumber starting model are difficult to remove.

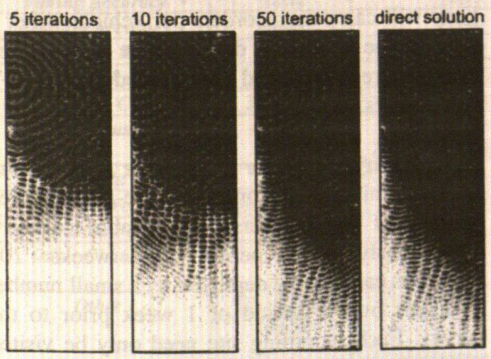

Figure 4 **Comparison of direct and iterative solutions to the wave equation**

High-frequency solution to the acoustic wave equation in a complicated 2D model. Only a single frequency component is shown. The model measures 100 x 300 nodes at 4 nodes/wavelength; it is subdivided into 29 sub-domains. The iterative and direct solutions are indistinguishable after about 50 iterations. This iterative scheme generalises very efficiently into 3D.

Instrument Provision for Land-based Controlled Source and Temporary Array Seismology

Peter Maguire and Paul Denton
Department of Geology, University of Leicester, Leicester LE1 7RH

Introduction

In 1968 the first major wide-angle seismic experiment in the Kenya Rift involved the shooting of a 370 km refraction profile from Lake Turkana south to Lake Hannington (now Bogoria) near the apex of the Kenya dome (Griffiths et al 1971). The profile was carried out with 2 recorders deployed at 5 separate sites, 5 shots being fired in each of the two lakes. The two recording parties required a total of 6 vehicles, 4 scientists, 2 technicians, 2 assistants and 2 cooks. The instruments were operated inside 6' x 6' x 6' tents. The experiment was designed for data interpretation using the time-term method (Willmore and Bancroft 1960). In 1994, the most recent Kenya Rift International Seismic Project (Prodehl et al 1997) involved two near 425km long crustal profiles covered by 204 recorders deployed by 14 teams, each team deploying 14 to 15 stations. The profiles were fired into from 10 borehole shots, three water shots and two quarry blasts at spacings of approximately 80 km. The principal data analysis and interpretation (Birt et al 1997, Byrne et al 1997, Novak et al 1997) was undertaken using ray-trace forward modelling and inversion (e.g. Zelt & Smith 1992). Current experiment design is demanding the deployment of 1000s of recorders; for example, the proposed Central European Lithospheric Experiment Based on RefrAcTION (CELEBRATION) is planned with 1200 recorders (M.Grad, pers. comm.)

The development in equipment that has caused this huge increase in data coverage has resulted from (1) seismologists demanding data suitable for new computing intensive interpretation procedures and (2) manufacturers making use of developments in electronic and computer design to create data-loggers and sensors to satisfy the seismologists' needs.

Controls on equipment design

The academic seismologist needs to record seismic data in the field in a cost-effective and accurate manner. Data loggers are required that can record seismic data in a wide variety of field conditions and experimental configurations and can provide the data in a format ready for processing in an efficient manner.

Survey design constrains the required recording instrument characteristics. The range of seismic methods used and the acquisition environment necessitates the use of more than one type of instrument. Multi-channel seismic reflection recorders are not at present suitable for crustal wide-angle profiles due to their limited recording distance range coverage. Satellite telemetry when cheap enough may well alter this state of affairs. This is obviously not to deny their need in deep crustal reflection profiling. Marine wide-angle profiling needs Ocean Bottom Seismometers (OBS). New developments will provide numerous, cheap, lightweight, large data capacity OBS as required. Their design is likely to be substantially different from that of land recorders due to the many extra problems involved in underwater deployment; position fixing, recording, and recovery. This is the province of the marine seismologist.

Recorders must *(a)* be cheap enough to be bought in large enough numbers to provide adequate spatial sampling *(b)* be cheap enough to be cost effective in relation to the amount of expenditure on seismic experiments by those that use them and *(c)* be lightweight and low power enough to enable the logistical costs of fieldwork to remain relatively constant for a 10 fold increase in recorder numbers.

Hypothetical Experiment Requirements

The principal design criteria that need to be fulfilled for onshore instruments are best illustrated by a number of different hypothetical generic experiments.

1. ***A wide-angle crustal survey.*** A 400km profile is to be shot with 2000 x 3 component 4.5Hz geophones at 200m intervals, shots being fired every 25km. The experiment is to take place over two nights with shots being fired during 3 minute windows activated every 30 minutes. The operators will include inexperienced students. They will carry 50 recorders per vehicle. After 5 days in the field, the data will be downloaded from the recorders and reformatted into SEGY shot gathers.

2. ***A wide-angle onshore - offshore experiment.*** This is similar to the onshore wide-angle survey except that the recorders must be able to record continuously for a period of 4 weeks. 200 recorders can now be deployed by a small number of teams over a period of 1 week prior to the survey. Each recording site need only be visited once per week to check its operation and to

change batteries. SEGY shot gathers are again the final format.

3. ***A teleseismic recording programme***. A network of 30 sites will record a continuous stream of data for 1 year from 120s broadband sensors. The sites will be powered by lead-acid batteries recharged from solar panels. Each site will be visited once every two months by a relatively inexperienced operator. Data cartridges will be swapped and instrument operation checked. Data will be analysed during the course of the experiment after generation of network SEED volumes.

4. ***A local tomography experiment***. A network of 200 x 3 component 1Hz and broadband recording sites will be located over a relatively small area (e.g. a volcano). Earthquake and controlled source data will be recorded at >100Hz. The experiment will last for 3 months, each site being visited every 4 weeks by an inexperienced operator to change data discs and batteries, 20 stations per operator per day. Data will be in either SEGY or SEED format.

5. ***A deep crustal seismic reflection survey.*** A 250km long profile of deep seismic reflection is to be undertaken over a 10 day period. Shots will be fired at 500m intervals, 1000 recorders being deployed every 100m by our, again, relatively inexperienced operators, 50 stations to a team. Data will be recorded at 500Hz, the instruments being collected at the end of the project for data downloading and conversion to SEGY shot gathers.

These specifications raise different problems. For example, for the onshore wide angle survey, ease of deployment, weight and power consumption are critical factors. For the teleseismic programme, the deployment time and use of broadband sensors results in much more stringent requirements on the recorder. 3-component recording is becoming essential. For S-wave studies it is mandatory. Also, the Stanford Exploration Project experiment with a 4000 element array (Cole et al 1989) demonstrated first arrivals from a local quarry blast appearing some 45° out of plane. 3-component recording is really necessary to check on such arrivals during conventional profile experiments.

Discussion

(a) The IRIS instrumentation committee, following their 1997 workshop recognised a call "... for larger numbers of less costly and more easily deployable sensors and acquisition systems (and) greater integration of fixed ... and mobile ... instrumentation ... but with current capabilities as opposed to defining new and more rigorous specifications." While this doctrine has not, in essence, changed, three points need stating:

The technology has already advanced to enable dataloggers to provide almost all the requirements specified above, and at low cost. The biggest change has been the near 1000 fold increase in storage capacity since the advent of digital recording. This opens up the possibility of logistically easier and cheaper projects on vast scales. This immediately introduces the next bottleneck, namely:

The transfer of data to research useable form on the home workstation. A comment from the principal organiser of the Eifel Plume project imaging the lithosphere / asthenosphere boundary beneath the Eifel

Table 1

	(1) Onshore Wide-angle Survey	(2) Onshore – Offshore Wide-angle survey	(3) Teleseismic Recording Project	(4) Local Tomography	(5) Deep Reflection Survey
Number of Instruments	2000	200	30	200	1000
Sensor	3-C 4.5 - 1Hz	3-C 1Hz	3-C 0.01 - 10Hz	3-C 0.01 - 10Hz	1-C 1 – 15Hz
Timing Accuracy	±2ms	±2ms	±5ms	±2ms	±2ms
Position Accuracy	±10m	±10m	±100m	±10m	±10m
Sampling Rate	100Hz	100Hz	20-50Hz	100Hz	500Hz
Dynamic Range	>120dB	>120dB	>120dB	>120dB	>120dB
Data Storage Capacity	20Mbyte	>2Gbytes	>2Gbytes	>2Gbytes	>2Gbytes
Power Consumption	<2 watts	Less critical 2-4 watts + solar panel	Less critical 2-4 watts + solar panel	<2 watts	<2 watts
Weight	<4kg	Less critical	Less critical	<4kg	<4kg
Data Collection	No extraction	Hot-swap discs	Swappable discs	Swappable discs	No extraction
Final Data Format	SEGY	SEGY	SEED	SEED / SEGY	SEGY
Other Channels	No	No	For monitoring mass position and T	For monitoring mass position and T	No
Other	12V to active sensor	12V to active sensor	12V to active sensor Analogue/TTL for calibration / centring	12V to active sensor Analogue/TTL for calibration / centring	

region in northern Europe (J.Ritter, pers.comm) is that "PhD students spend most of their time gathering and reformatting data instead of doing 'real' research". For a seismic equipment pool of 200 autonomous recorders the management of the data recorded is a far harder task than the logistical support of the dataloggers in the field. Each datalogger will be able to record 100Mbytes per day. For many experiments that is a total of 20Gbytes of raw data per day. This amount of data needs to be transformed into research useable form and copied to a backup facility either at the end of a controlled source experiment (e.g. 300Gbytes at the end of 15 days) or during a natural source experiment (e.g. 2 Gbytes per day). This transfer must be as simple and as fast as possible.

A straw poll of experimental seismologists in 1999 suggests that the requirement is still for more recorders but with a much greater link between active and passive recording (the Eifel Plume Project has recorded some 30,000 x 3-component natural event and controlled source seismograms from a mixture of 60 broadband and 170 shortperiod recorders). 'Dream' experiments all involve use of large numbers of broadband and shortperiod instruments. However, the technical requirements of the two, outlined above, suggests that they should have separate datalogger provision. This may not only accommodate the difference in cost (i.e. fewer more expensive data loggers for the more expensive broadband seismometers), but also the different experiment durations, the broadband networks needing to be deployed for very much longer periods of time than the shortperiod arrays. Using the same recorders, will (and has) resulted in instruments being commandeered for short term controlled source experiments at the expense of longer term, ongoing natural source projects.

(b) An addendum to item a(2) above is that explosive communication technology developments will have significant impact on recording technology and in particular data transfer to the home base. In the early 2000s, with the ever decreasing cost of recording technology and the likelihood of a constellation of Low Earth Orbit communication satellites not just 1000 recorders will be deployed in the field, rather 10,000. These will provide spatial sampling enabling very much more robust waveform analysis, processing and interpretation techniques in both profile and 3D surveys.

(c) Science advances via developments in theory, methodology and technology. Crustal or lithospheric seismology has now evolved at sea to enable the highest resolution studies to incorporate near 50m spacing between both shots and receivers over complete 3D surveys. The interpretation schemes have developed accordingly to include for example, full waveform inversion. This has fuelled the geologists expectation of all crustal and lithospheric surveys to provide the same well resolved images. Surveys restricted to a completely onshore locale, while being able to deploy the same number of recorders, cannot accommodate the same shot density because of both cost and, increasingly, environmental concerns. A recent estimate for a combined wide-angle and normal incidence reflection profile in Ethiopia results in nearly two-thirds of the total cost being spent on drilling and the provision of explosives.

While accepting that ocean basin and continental margin study is of immense importance, there is an equivalent, perhaps greater need, for onshore surveys. It is only from these that structures identified in the seismic image can be traced to the surface and matched directly with geology. This implies that the greatest development in the immediate future, if onshore controlled source seismology is to retain its role in studies of the lithosphere, needs not to be in recording technology but rather in improvement of the seismic source.

References

Birt, C.S., Maguire, P.K.H., Khan, M.A., Thybo, H., Keller, G.R. and Patel, J. (1997) The influence of pre-existing structures on the evolution of the southern Kenya Rift Valley - evidence from seismic and gravity studies. *Tectonophysics*, **278**, 211-242.

Byrne, G.F., Jacob, A.W.B., Mechie, J. and Dindi, E. (1997) Seismic structure of the upper mnatle beneath the southern Kenya Rift from wide-angle data. *Tectonophysics*, **278**, 243-260.

Cole, S., Claerbout, J., Nichols, D. and Zhang, L. (1989) The ambient seismic field in three dimensions. *59th Annual Internat. Mtg., Soc. Expl. Geophys., Expanded Abstracts*, 395-413.

Griffiths, D.H., King, R.F., Khan, M.A. and Blundell, D.J. (1971) Seismic refraction line in the Gregory Rift. *Nature*, **229(3)**, 69-71.

Novak, O., Prodehl, C., Jacob, A.W.B. and Okoth, W. (1977) Crustal structure of the southeastern flank of the Kenya Rift deduced from wide-angle P-wave data. *Tectonophysics*, **278**, 171-186.

Prodehl, C., Ritter, J.R.R., Mechie, J., Keller, G.R., Khan, M.A., Jacob, B., Fuchs, K., Nyambok, I.O., Obel, J.D. and Riaroh, D. (1997) The KRISP 94 lithospheric investigation of southen Kenya – the experiments and their main results. *Tectonophysics*, **278**, 121-178.

Willmore, P.L. and Bancroft, A.M. (1960) The time-term approach to refraction seismology. *Geophys. J. Roy. Astr. Soc.*, **3**, 419-432.

Zelt, C.A. and Smith, R.B. (1992) Seismic traveltime inversion for 2-D crustal velocity structure. *Geophys. J. Int.* **108**, 16-34.

The Origin of Continents and Oceans

Walter D. Mooney
U.S. Geological Survey, MS 977, 345 Middlefield Road,
Menlo Park, California 94025, USA

The Earth has several physical attributes that are unique within our Solar System, the existence of continents and oceans being one of the most conspicuous attributes. Here I give a brief historical summary of the major discoveries concerning the Earth's interior, and a modern view of the inner workings of our planet. In doing so, I will also explain the origin of the continents and oceans that support life on Earth.

One physical attribute of the Earth noted by the Chinese and the Greeks was that it possessed a magnetic field. The origin of this magnetic field was debated for more than three centuries, beginning with W. Gilbert (De Magnete, 1600). Another important attribute, the weight and density (5.5 gr/cc) of the Earth, was determined in 1798 by H. Cavendish. Surficial rocks have a density of 2.8 gr/cc, and Cavendish therefore realized that the Earth's interior must consist of dense materials. We now know that the magnetic field and high density are both due to a convecting iron-rich core.

The seismograph was developed in 1889. J. Oldham discovered the Earth's core in 1906, and Sir H. Jeffreys and K. Bullen constructed the first detailed cross-section through the Earth in 1939.

Today we are able to describe the Earth's interior in considerable detail, and to explain conclusively the origin of oceans and continents in terms of plate tectonics. This is one of the great scientific achievements of the Twentieth Century.

Velocity Imaging by tau-p Transformation

P.J. Barton

Bullard Labs, Madingley Road, Cambridge, England CB3 OEZ
barton@esc.cam.ac.uk

Abstract

I present a method for producing a 'brute stack' velocity image rapidly and automatically from travel-times picked from densely sampled refraction data. The procedure involves transformation from the time-offset into the tau-p (slope-intercept) domain. Differences in apparent velocity in the up- and down-dip directions and the approximate turning points are calculated and corrected using simple geometry, by consideration of reciprocal paths. The tau-velocity-turningpoint map distributes phases automatically on the basis of geometry and velocity to give a two-dimensional representation of subsurface structure.

Introduction

Refraction profiling has traditionally sampled the subsurface sparsely. However, it is now possible to sample the seismic wavefield to long offsets at a spatial density similar to that used in conventional seismic reflection profiling, using tens or hundreds of ocean bottom seismometer (OBS) units and an airgun source. As a parallel development, two-ship synthetic aperture profiling (SAP) also allows long offset supergathers to be synthesised. Conventionally, little data processing takes place, and wide-angle data are analysed by the abstraction of parameters (such as travel-times) before a subsurface model is built by forward modelling and iterative inversion. The quantity and quality of wide-angle refraction data now being collected is such that we need a radical look at the way that such data is analysed, both to make the task manageable, and to take advantage of the new data density, which has the potential to allow the processing of an image from the data itself, rather than simply producing a model to fit the data. We describe here a developing approach that results in velocity images being transformed directly and automatically from the wide-angle data. The approach taken is similar to that described by Pavlenkova (1982).

Velocity Images

Consider the seismic data collected from an imaginary wide-angle survey shot across the edge of a bathymetric trough on the continental shelf. A realistic long wavelength velocity model has been compiled (Figure 1(a)), and a synthetic seismic survey performed by sampling the model using sea bed seismic receivers spaced at 5 km intervals along a 200 km long profile using the *RAYINVR* code of Zelt & Smith (1992). We will consider the data as travel-times only, so that they are the equivalent of accurately picked common-receiver gathers at OBS stations (Figure 1 (b)). Each individual pick forms part of a phase of arrivals that have turned or reflected in a particular layer of the model. Adjacent gathers display similar phases indicating lateral continuity of structure in the subsurface. At an appropriate reduction velocity - corresponding to the seismic velocity of the layer in which it has turned - a phase will form an approximately horizontal branch on a time-distance plot. A crude picture of the subsurface structure may be pulled from the data (Figure 1(c)) by applying different reduction velocities to these different phases. The juxtaposition of many such sub-horizontal branches from adjacent receiver gathers causes them to coalesce into a 'horizon' that broadly reflects the lateral geometry of the horizon from which the arrivals originate: compare Figures 1(a) and 1(c).

However, real field data is not so conveniently labelled with phases corresponding to layers. Therefore, instead of dealing with arrivals on a phase-by-phase basis, we next consider each arrival pick individually in terms of its instantaneous apparent velocity. For each individual seismic arrival, the 'reduction' of its travel time by its apparent velocity maps it onto the time scale at a time equivalent to the intercept at zero offset of the tangent to the phase. The necessary information may be extracted from the travel time data by fitting a sliding polynomial curve to the arrival branches, taking the gradient of this curve at each data point to obtain the apparent velocity. In a one-dimensional earth the turning point lies halfway between the shot and the receiver, and the apparent velocity in both directions is the same. A simple map may therefore be created by plotting each individual travel-time pick halfway between shot and receiver, using intercept time (tau) as the vertical scale, and labelling each pick with apparent velocity. This procedure is in effect a tau-p inversion, mapping from the offset-time domain to the slope-intercept domain.

However, where lateral variations exist in the earth (i.e. virtually everywhere) the apparent velocity sampled by a cone of rays propagating from left to

right will be different from that experienced in the opposite direction, forming a phase with low apparent velocity in the 'down-dip' direction and a high apparent velocity in the 'up-dip' direction. The ray turning point will also move 'up-dip' from the midpoint between the shot and the receiver. Two-dimensionality may be detected by separating energy propagating in different directions along the profile (Figure 1 (d) & (e)): note how the two plots show lateral 'down-dip' translations of equivalent features, which also display slightly different velocities. In order to produce a single well-focused image that expresses the two-dimensional information present in the data, the information from the two different propagation directions must be integrated.

The simplest of two-dimensional structures is a dipping interface between two layers of uniform velocity. The true velocity for the second layer, the dip of the interface, and the critical angle at the interface may be calculated from the two apparent velocities in opposite directions, providing the velocity in the upper layer is known (Dobrin, 1976). The proportional displacement of the critical angle reflection point away from the shot-receiver midpoint follows simply. This simple case is of interest because the gross features of the raypath (the true value of the velocity at the turning point, and the proportional displacement of that point from the midpoint) are much better predicted by this model than by the one-dimensional case, for any two-dimensional model in which the lateral variation is approximately linear between shot and receiver. The calculations require knowledge of apparent velocities and intercept times along reciprocal raypaths, but shots and receivers are seldom truly coincident. This problem was addressed by considering bins along the profile and searching for reciprocated bins. In most wide-angle surveys there is an imbalance between the number of shots and receivers, such that the number of reciprocated paths is much less than the total number of observations. This shortcoming was overcome by producing a map of bin-to-bin paths, and interpolating correction factors for paths that were not reciprocated directly. Unconstrained regions of the bin array were defaulted such that the unreciprocated data is included in the final plot unaltered. Figure 1(f) shows the recovered velocity image, for comparison with Figure 1(a).

The method demonstrated here has been tested on several real datasets with data density similar to that used in this example, and excellent results have been achieved.

Discussion and Conclusions

The main advantages of this new method of analysis are its objectivity and speed. Travel-times may be picked semi-automatically using Promax or similar packages, and from that point onwards the procedure is entirely automatic. Each picked travel-time maps onto a single velocity point on the tau map independently of other points, except inasmuch as surrounding points are necessary for the determination of slope (apparent velocity) and intercept time (tau). The tau-velocity-turningpoint map sorts arrivals automatically into phases, grouped on the basis of geometry and velocity, and highlights layers with high velocity gradient (densely sampled on plot). Such phase allocation and relative subsurface geometry could be fed back into forward modelling or inversion schemes.

The final product of this process is an integrated two-dimensional map of seismic velocity plotted against tau, or intercept time (Figure 1(f)). This map contains exactly the same information as displayed in the original picked receiver gathers (Figure 1(b)), but in a much more accessible form. Conversion from tau time to depth or two-way-time requires knowledge of the velocities in the layers above, and a downward continuation approach. Clayton & McMechan (1981) showed the potential for inverting complete seismic records from time-offset into tau-p, and converting them to a one-dimensional velocity-depth curve. By combining their techniques with this robust method for mapping 'true' velocities and turning points from reversed raypaths we will be able to produce a mapping algorithm for transforming wide-angle seismic data into two-dimensional velocity images automatically, without the need for either picking the data or interpreting the phase represented by any particular seismic arrival.

References

Clayton, R. W., & McMechan, G. A., 1981. Inversion of refraction data by wavefield continuation. Geophysics 46, 860-868.

Dobrin, M. B., 1976. Introduction to Geophysical Prospecting. McGraw-Hill.

Pavlenkova, N. I., 1982. The intercept-time method - possibilities and limitations. J. Geophys. 51, 85-95.

Zelt, C. A., & Smith, R. B., 1992. Seismic traveltime inversion for 2D crustal velocity structure. Geophys. J. Int., 108, 16-34.

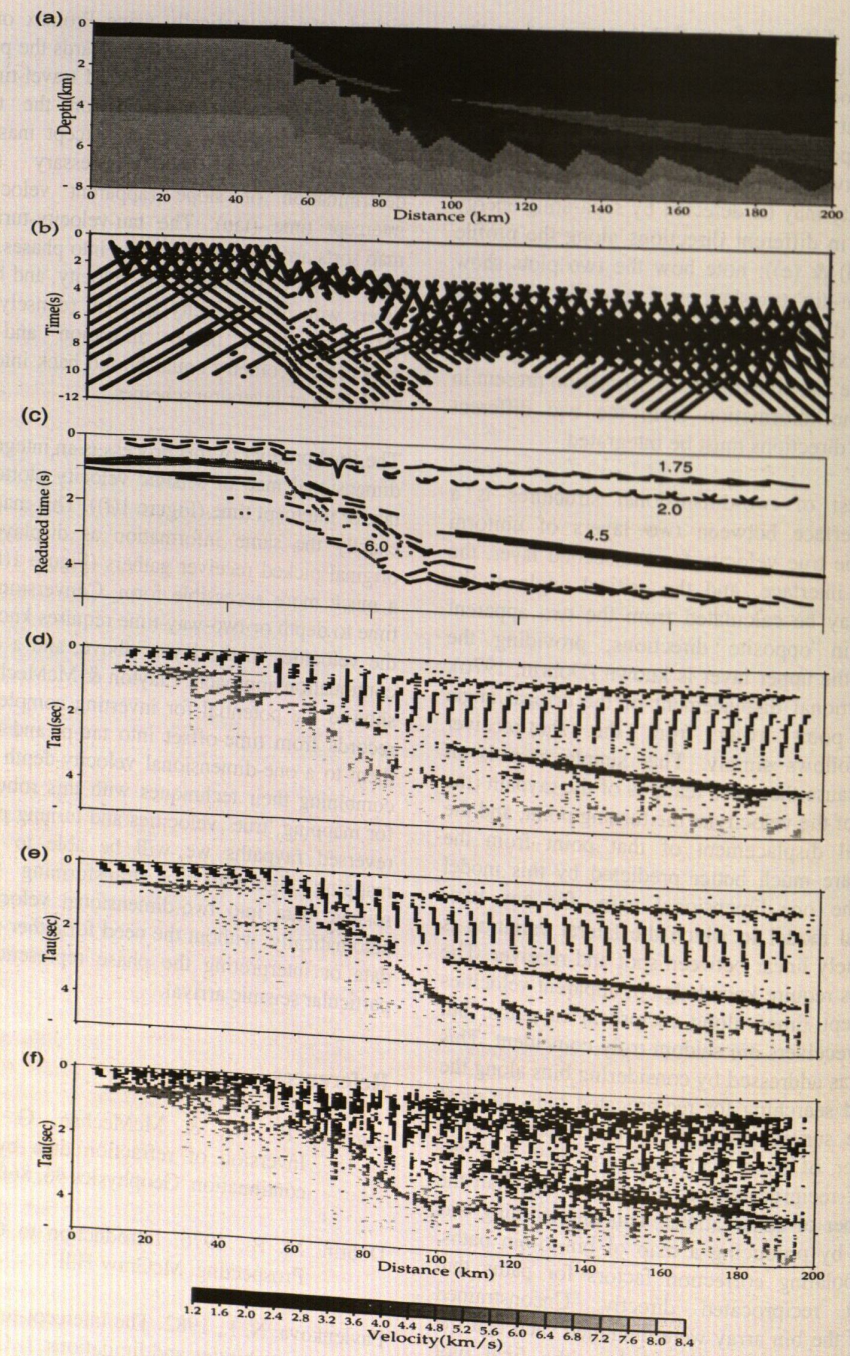

Figure 1. (a) Input velocity model of trough structure on continental shelf. Grey shades show seismic velocities in km/s: velocity scale at bottom applies to all sections. Note variable water depth, sediments, a high velocity, discontinuous basalt flow over further sediments, and faulted basement.

(b) 'Picked' synthetic travel-time receiver gathers from ocean bottom seismometers at 5 km intervals along velocity model shown in (a).

(c) Travel time receiver gathers as shown in (b) (every second gather), with each arrival branch plotted against reduced time, shown on plot in km/s. Arrivals from upper sediments, reduced at 1.75 km/s; arrivals from second sedimentary layer, reduced at 2.0 km/s; arrivals from basalt layer, reduced at 4.5 km/s; arrivals from upper basement, reduced at 6.0 km/s.
(d) & (e) Results from mapping offset-time picks into the tau-velocity-midpoint domain as described in the text.

(d) Energy travelling from right to left.

(e) Energy travelling from left to right.
Note that the two images are offset in distance and show slightly different velocity distributions.

(f) Recovered velocity image. Reciprocated paths from (d) and (e), combined with remaining paths that are not individually reciprocated but have been corrected using interpolated bin-to-bin factors as described in the text.

Aspects of Source Control in Controlled-Source Seismology

A. M. Ziolkowski (Anton.Ziolkowski@glg.ed.ac.uk)
University of Edinburgh, Department of Geology and Geophysics, West Mains Road, Edinburgh EH9, United Kingdom

Scope of the Talk

My aim in this talk is to cover three issues of importance in seismology applied to the exploration and production of hydrocarbons, with particular emphasis on the role of the source in the formulation of the problem and its solution.

The first issue is the classic problem of sea-surface multiples (often incorrectly referred to as water-*bottom* multiples). The sea surface causes all the upgoing seismic waves to be reflected down again and makes the processing and interpretation of seismic data difficult. The theory of seismic migration assumes that the data consist of primary reflections only. If multiples are present, they are treated in the migration process as primary reflections, thus confusing the interpretation. Multiples can also make nonsense of AVO (amplitude versus offset) analysis, which uses subtle variations in the amplitude of primary reflections to deduce contrasts in the elastic properties at a reflecting interface. Thus a solution of the free surface multiple problem is critical not only to the interpretation of the seismic data for basic geological structure, it is essential to the interpretation of more subtle effects caused by variations in fluid content and stratigraphy.

I outline some ideas on a wave-theoretical solution of this problem that require no knowledge of the earth, but do require precise knowledge of the source wavefield. Processing of 2D synthetic data indicate that the application of these ideas appears feasible for ocean bottom cable (OBC) data.

The second issue is the problem of the determination of stratigraphy from seismic data. Seismic stratigraphy has had an honourable and impressive development ever since the publication of the famous AAPG Memoir 26 (Vail, Todd and Sangree, 1977). On a large scale, greater than 100 m, the definition of stratigraphic units is normally very successful, but in the range 20—100 m it is often very difficult to identify individual stratigraphic units, even though the frequency bandwidth of the data should permit a vertical resolution down to about 20m. Intimately related to this difficulty is the problem of precisely tying wells to seismic data. Mis-ties of 20-30 ms are very common at the reservoir level, even though the sea-floor can normally be tied to within a sample (4 ms). I show that lack of knowledge of the source signature forces a processing strategy that introduces lateral variations in the wavelet at depth. If the source wavefield is measured during seismic data acquisition, the processing strategy can be designed to ensure that no lateral variations in the wavelet occur, with the result that any observed lateral variations must be caused by the geology.

The third issue is the determination of the petrophysical parameters of the reservoir at the 1 m scale from seismic data. Seismic attribute analysis has been developed to help obtain petrophysical parameters between wells. It attempts to deduce petrophysical parameters from seismic attributes using relationships established at the wells.

There are at least two very serious issues facing this approach. First, these relationships are based on petrophysical properties measured on the cm scale on the core samples and on seismic parameters measured on the same core samples but using frequencies near 1 MHz – roughly four orders of magnitude higher than the frequencies used in seismic surveys. Since it is well known that seismic properties are frequency-dependent, these relationships may not be particularly reliable, even at the wells. Secondly, the relationships are then assumed to hold for the seismic data, in which the smallest resolvable volume is six to nine orders of magnitude greater than the core samples on which the measurements are based. One must therefore wonder how much confidence to have in this approach.

I outline a more deterministic approach to this problem that uses instrumented boreholes to obtain seismic data with a resolution of about 1 m in the reservoir, plus an extrapolation of petrophysical properties from the cm scale, based on a newly-developing theory of seismic wave propagation in fluid-saturated poro-elastic media.

Multiples

The first rigorous wave-theoretical approach to the

suppression of multiples was formulated for 1-D and 2-D by Riley and Claerbout (1976), who first identified the sea surface as the source of difficulty, as shown in Figure 1. Riley and Claerbout remarked "The solution to eliminating this class of multiples amounts to finding a transformation which converts data recorded with the free surface present to the equivalent data which would have resulted if the free surface were absent." They also identified the requirement that the source wavefield be known and, in the absence of source measurements, proposed a least-squares minimisation of the energy of the multiple wavetrain to estimate the inverse of the far-field source waveform.

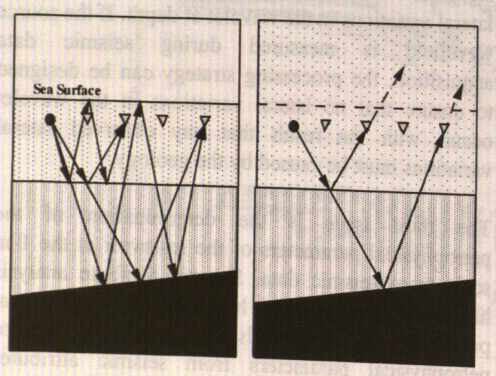

Figure 1. *Subsea reflections, with and without the effect of the sea surface.*

After Riley and Claerbout many geophysicists worked on this problem. Two very important contributions are by Berkhout (1982) and by Fokkema & van den Berg (1990).

Berkhout (1982) showed that the effect of the free surface is essentially a feedback problem, and the reflection response can be recovered by undoing the feedback effect of the free surface by a recursive process of prediction and subtraction. He considered the 2D case with a dipole line source at the water surface for each shot and ignored the direct wave.

Fokkema & van den Berg (1990) formulated an exact wave-theoretical formulation for a monopole source below the sea surface. A complete two-dimensional array of receivers is required for each source and, because reciprocity is an essential part of the formulation, each receiver must also be a monopole, and for each receiver a complete two-dimensional array of monopole sources is required.

In Edinburgh we have developed a new formulation of the 3D problem, based on a plane wave decomposition of the data (Ziolkowski, Taylor, and Johnston, 1999) that solves three problems associated with these earlier formulations.

- we can accommodate source arrays, rather than point sources;
- we can remove the incident field without simultaneously removing part of the scattered field;
- we avoid the minimum energy criterion to find a wavelet.

The additional information required to solve these problems comes from measurements of the source wavefield made during data acquisition. We have also extended our formulation to ocean-bottom cable (OBC) data (Ziolkowski, Taylor and Johnston, 1998) and have shown analytically and numerically that our algorithm works on 2-D data (Taylor and Johnston, 1999). Results will be presented at the meeting.

Seismic Stratigraphy and Well-Ties

The essence of seismic stratigraphy is (1) to correlate stratigraphic interfaces, determined using well logs and core, with identifiable events on seismic reflection data, and (2) to correlate these events away from the well on the seismic data. If everything is working properly, a stratigraphic interface identified at one well should correlate, via the seismic data, to the same interface at the next well (provided of course that the interface is present at both wells). In practice this can very rarely be done. Normally there is a mis-tie, typically of the order of 20-30 ms. Furthermore, the phase of the wavelet at any interface is very rarely what it should be.

Ideally, the seismic wavelet should be zero phase with a positive central peak. At an interface where there is a contrast in acoustic impedance, the peak of the wavelet should occur at the arrival time of the reflection, with the polarity of the reflection corresponding to the polarity of the reflection coefficient. In fact this rarely occurs, even for the major reflections in seismic reflection data and interpreters continually face the problem of how to tie known interfaces at the wells to the seismic reflection data. To understand the problem one must question the data acquisition and processing procedures that purport to give a "zero-phase" wavelet in the data.

In conventional marine seismic data acquisition there are very tight specifications on the acquisition system, to ensure that there is excellent shot-to-shot repeatability. Along a line, provided the ship's speed, the wind and the ocean currents are more or less constant, the shot-to-shot repeatability is normally excellent. When the ship changes direction the drag

on the air gun array is liable to change, depending on the wind and the currents, and this then affects the depth at which the guns tow. The period of oscillation of an air gun bubble is very sensitive to changes in the gun depth and therefore the signature of the source tends to change from line to line. To make sure the wavelet in the processed data is the same from line to line it makes sense to measure the source wavefield (e.g. Ziolkowski et al., 1982) and then equalise the wavelets. It is not industry practice to do this.

A second problem is the duration of the source signature. In marine seismic surveys this signature is typically 200-300 ms long – much longer than the "gap" in the conventional predictive deconvolution filter that is applied to attenuate water-layer multiples (in the absence of a more rigorous approach). The predictive deconvolution filter, which is computed from the autocorrelation of the data, is different on every trace, and therefore changes the wavelet slightly from trace to trace. After CMP stacking the wavelet in the stacked trace is an average of the wavelets in the CMP gather. This wavelet changes slowly from CMP gather to CMP gather, because of the great overlap of the gathers, but over differences of several km large changes can and do occur.

The zero-phase processing usually requires a statistical assumption about the reflection properties of the earth to enable the amplitude spectrum of the wavelet to be estimated from the data, and a further assumption about the properties of the wavelet is required to estimate the phase of the wavelet from the amplitude spectrum. This phase is then removed.

I show using published data (Ziolkowski, Underhill and Johnston, 1998) that none of these assumptions are necessary if the source wavefield is measured. Furthermore the correct polarity and timing of the seismic reflection data can be preserved, and stratigraphy can be identified. In the Inner Moray Firth our approach permitted the Mid Cimmerian Unconformity to be identified on seismic data, for the first time in this part of the North Sea. This has stratigraphic trapping potential.

These results will be presented at the meeting.

Determination of Reservoir Petrophysical Parameters from Seismic Data

The data on which the exploration and production of hydrocarbons is based come from wells and geophysical exploration. Well logs and core provide petrophysical data for reservoir characterisation on the cm scale. Geophysical methods, particularly seismic methods, currently provide data with a resolution at the reservoir level of about 20 m. Figure 2 illustrates the gap between these two kinds of data.

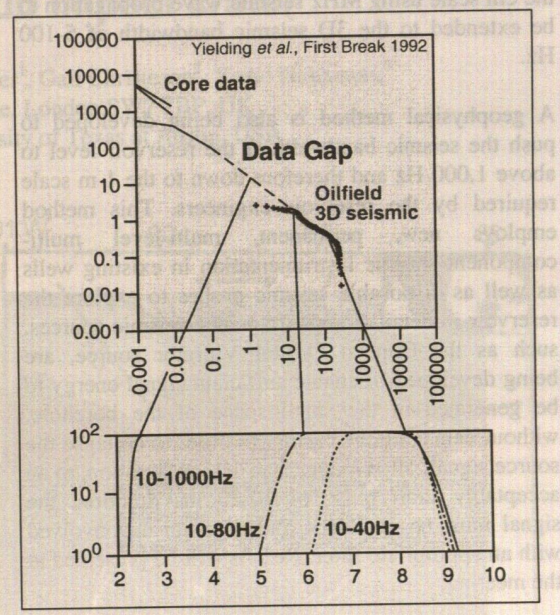

Figure 2. *The upper part shows a log-log plot of the number of faults resolvable per unit volume against the size of the faults that can be seen, in metres. The data show a fall-off, more-or-less on a straight line, but there is a gap of several orders of magnitude between what can be seen with core and well logs in the narrow vicinity of a well, and what can be resolved with 3D seismic data. The lower part shows the seismic bandwidth associated with the structures that can be resolved.*

Hydrocarbon reservoirs are partitioned, structurally and stratigraphically, with internal units typically having dimensions on the 1 m scale. To manage hydrocarbon production from the reservoir, the reservoir engineer needs to model the fluid flow in the complex heterogeneous reservoir at the 1 m scale. The reservoir engineer is working in the dark because this scale length falls right in the data gap. To make a breakthrough in this field and to enable the reservoir engineers to find the by-passed oil and increase the yield, we need to bridge the data gap. This issue is extremely important to the economy of the UK and many other countries as oil fields are currently being closed down with often more than 50% of the original hydrocarbon reserves still in place.

Geophysics, particularly seismic methods, offers the *only* affordable means for exploring the earth below the surface and between wells. An underpinning theory of wave propagation in fluid-saturated poro-elastic rocks is required to relate the petrophysical rock properties, measured with well logs and on cores in the laboratory, to seismic propagation effects. Such a theory is being developed in the

Department of Geology and Geophysics at Edinburgh. The theory will allow the petrophysical-seismic relationships determined on core samples on the cm scale using MHz seismic wave propagation to be extended to the 3D seismic bandwidth of 5-100 Hz.

A geophysical method is also being developed to push the seismic bandwidth at the reservoir level to above 1,000 Hz and therefore down to the 1 m scale required by the reservoir engineers. This method employs new, permanent, multi-level multi-component seismic instrumentation in existing wells as well as disposable seismic probes to explore the reservoir in detail. Swept frequency seismic sources, such as the Conoco Orbital Vibrator source, are being developed to enable sufficient signal energy to be generated in the small space of the borehole, without damaging the casing. In order to collapse the source signal, often longer than 10 s in duration, to an acceptably short pulse of 10-20 ms duration, the signal must be measured and the data deconvolved with an appropriate filter. Results will be presented at the meeting.

Conclusions

Controlled source seismology has an advantage over uncontrolled source seismology in that both the place and start time of the applied source function are known very precisely. For a range of problems that are very important in the exploration and production of hydrocarbons it is also necessary to have precise knowledge of the source time function and the directivity pattern of the source. Normally these source characteristics are not measured, although the means for measuring them have been available for many years. Instead, and partly no doubt for historical reasons, the industry resorts to a variety of methods that rely on statistical assumptions of dubious validity to overcome the problems that arise. Many of the classical problems of exploration and production seismology still remain: the elimination of sea surface multiples, the tying of wells to seismic data, the identification of stratigraphic hydrocarbon traps, and the parameterisation of the reservoir at the 1 m scale. In this talk I show how a deterministic approach to the measurement of seismic sources can lead to solutions of these problems.

References

Berkhout, A.J., 1982, Seismic migration: Imaging of acoustic energy by wavefield extrapolation. A. Theoretical aspects, second edition. *Elsevier Science Publ.*, 211-218.

Fokkema, J.T. and van den Berg, P.M., 1990, Removal of surface-related wave phenomena: the marine case, *60th Ann. Internat. Mtg., Soc. Expl. Geophys., Expanded Abstracts,* 1689-1692.

Riley, D.C. and Claerbout, J.F., 1976, 2-D Multiple reflections: *Geophysics*, **41**, 592-620.

Taylor, D.B. and Johnston, R.G.K., 1999, Fast 2-D synthetic seismograms to test sea surface multiple removal algorithms, *69th Ann. Internat. Mtg., Soc. Expl. Geophys., Expanded Abstracts.*

Vail, P.R., Todd, R.G., and Sangree, 1977, Chronostratigraphic significance of seismic reflections. In *Seismic Stratigraphy – Applications to Hydrocarbon Exploration*, C.E. Payton, ed., pp99-116, AAPG Memoir 26. Tulsa: American Association of Petroleum Geologists.

Ziolkowski, A.M., Parkes, G.E., Hatton, L., and Haugland, T.-A., 1982, The signature of an air gun array: computation from near field measurements including interactions, *Geophysics*, **47**, 1413-1421.

Ziolkowski, A., Taylor, D, Johnston, R., 1998, Multiple wavefields: separating incident from scattered, up from down, and primaries from multiples: *68th Ann. Internat. Mtg., Soc. Expl. Geophys., Expanded Abstracts,* 1499-1502.

Ziolkowski, A., Underhill, J.R., and Johnston, R.G.K., 1998, Wavelets, well ties, and the search for subtle stratigraphic traps: Geophysics, 63, 297-313.

Ziolkowski, A.M., Taylor, D.B., and Johnston, R.G.K., 1999, Marine seismic wavefield measurements to remove sea surface multiples, *Geophysical Prospecting* (in press).

Modelling seismic structure and velocity in 3-D across the Chicxulub impact crater

Jo Morgan[1] (j.morgan@ic.ac.uk), Mike Warner[1], Gail Christeson[2], Yosio Nakamura[2]
[(1)] T.H. Huxley, Imperial College, London SW7 2BP, UK
[(2)] Institute for Geophysics, University of Texas at Austin, USA

The Chicxulub impact crater, which lies partly offshore in Yucatan, Mexico, has been linked to mass extinctions and rapid climate change at the end of the Cretaceous. The crater has been buried on a stable carbonate platform, making it the best-preserved of the three largest impact craters known on Earth, and an ideal target for seismic investigation. Chicxulub provides us with a unique opportunity to understand the dynamics and structure of large impact craters.

In the Autumn of 1996, an international group of scientists from the U.K. (Imperial College, University of Cambridge and University of Leicester), U.S.A. (University of Texas at Austin and Lunar and Planetary Institute, Houston), Canada (Geological Survey of Canada) and México (Universidad Nacional Autónoma de México and Petróleos Méxicanos) acquired a suite of onshore and offshore 2-D seismic reflection and dense 2-D and sparse 3-D wide-angle-seismic data (see figure1).

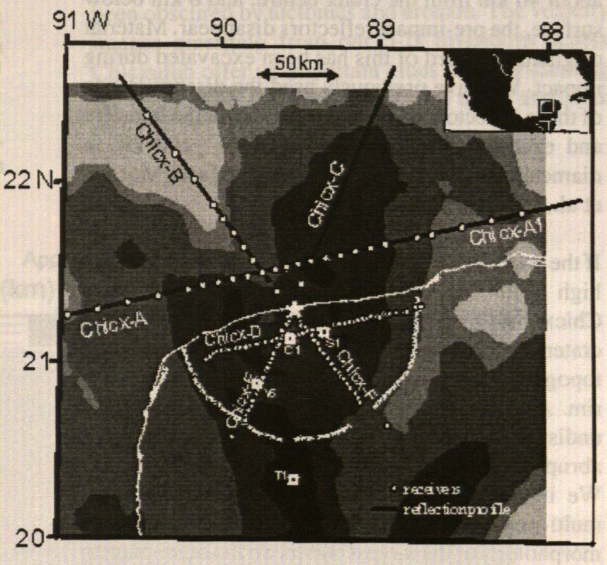

Figure 1

Results from the reflection data

The reflection data were acquired by GECO on a 240-channel 6-km streamer, using a 50 m shot spacing and 18 s recording time. The seismic reflection data image the crater from the K-T boundary, a few hundred metres below the present-day surface, down to the base of the crust at about 35 km depth (see Chicx-A and A1 in figure 2 below).

The present-day K-T surface deepens to ~1 km (1s TWTT) revealing a ~145-km-diameter post-impact basin (coloured grey in figure 2). Reflective pre-impact stratigraphy (at between 1.5 and 3.0 s) can be tracked across the crater; on each line, we see large offsets in the stratigraphy defining a terrace zone (TZ in figure 2) of slumped blocks 20-35 km wide. The total vertical offset of the stratigraphy across this terrace zone is between 3 and 6 km; single offsets can be as large as 2.5 km (figure 3). The head scarp of

Figure 2

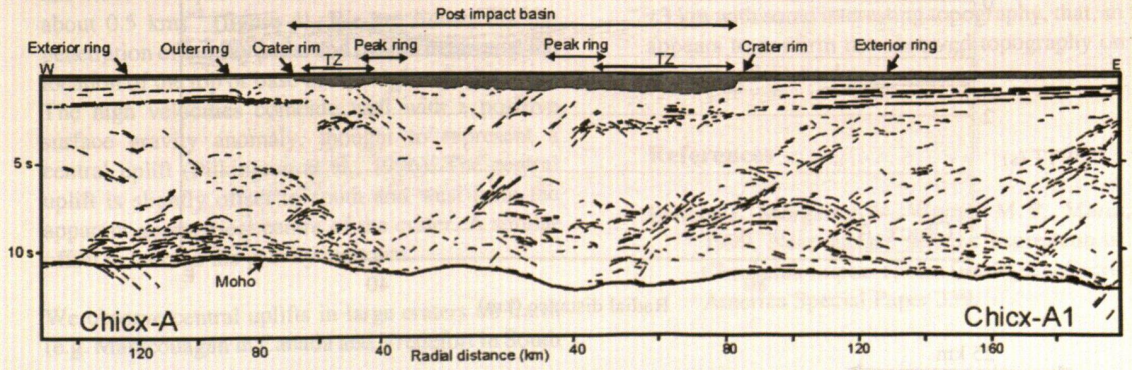

this terrace zone appears to be directly analogous to the crater rim in peak-ring craters. To the east, the crater rim coincides with the ~82-km-radius gravity gradient and the onshore cenote ring (a ring of sinkholes shown as a white dashed line in figure1). The post-impact basin appears to have been structurally controlled by the terrace zone; we observe major faulted offsets in the deeper strata immediately beneath, and apparently controlling, the outer edge of the crater basin (see figure 2 and 3). At about 40 km from the crater centre, and 8 km below surface, the pre-impact reflectors disappear. Material originally inboard of this has been excavated during impact. We have previously used the disappearance of these reflectors to calculate the size of the transient and excavation cavities as measuring ~100 km in diameter at the original Cretaceous surface (Morgan et al., 1997).

If the crater rim were the only significant topographic high with an inward-facing asymmetric scarp Chicxulub would be a 145-km-diameter peak-ring crater. In fact we observe at least one further topographic ring 20 - 30 km outboard of the crater rim. As we move out from the crater rim relatively undisturbed, flat-lying, pre-impact stratigraphy is abruptly offset vertically by 400 - 500 m (figure 3). We interpret this offset as an outer ring within a multi-ring basin, hence Chicxulub has the morphology of the largest craters on the other planets and moons (Morgan et al., 1999). This outer ring forms the outermost significant topographic feature visible on the seismic data, and on that basis, would most closely correspond to the crater diameter that would be measured from photographic or radar images if Chicxulub was located on another planet.

At Chicxulub, topographic offsets and rings seen outside the crater rim are associated with deeper crustal reflectors. These crustal reflectors have a predominant dip of 30 - 40 degrees toward the center of the crater and often turn subhorizontal in the middle crust away from the crater centre (see figure 2). The seismic reflection sections suggest that the middle crust and lower crust have moved inward and downward as part of transient cavity collapse (that is collapse of the initial cavity formed at the end of the compressive stage of impact). This movement appears to have produced a significant offset of the base of the crust at a radial distance of 35 - 55 km (see figure 2). The offsets at the base of the crust do not appear to represent velocity pull-down effects; wide-angle velocity modeling confirms that the Moho is downthrown between 1 and 3 km in this region.

Results from wide-angle data

The 13,000 air-gun shots that were fired to generate the reflection data were also recorded at wide angle on OBS's and land recorders. The OBS data were collected by the University of Texas using their 4-channel (3-component geophones and a hydrophone) instruments, and the land-station data were collected by groups from Imperial College and Universidad Nacional Autonoma de Mexico using PASSCAL three-component instruments. Offshore 23 OBS's were located along line A, 10 OBS's were located along line B, and 2 along line C. Onshore 46 stations recorded data along line D, 25 each along lines E and F (figure 1).

In our preliminary modelling we used the RAYINVR code (Zelt and Smith, 1992) to invert the first arrivals at the 6-km multichannel streamer to obtain the shallow velocity structure (< 2 km depth) along the reflection profile (Brittan et al., 1999). Subsequently, the OBS first-arrival times have been included in 2-D tomographic inversions (code from Zelt and Barton, 1998) to obtain upper crustal velocity structure along

Figure 3

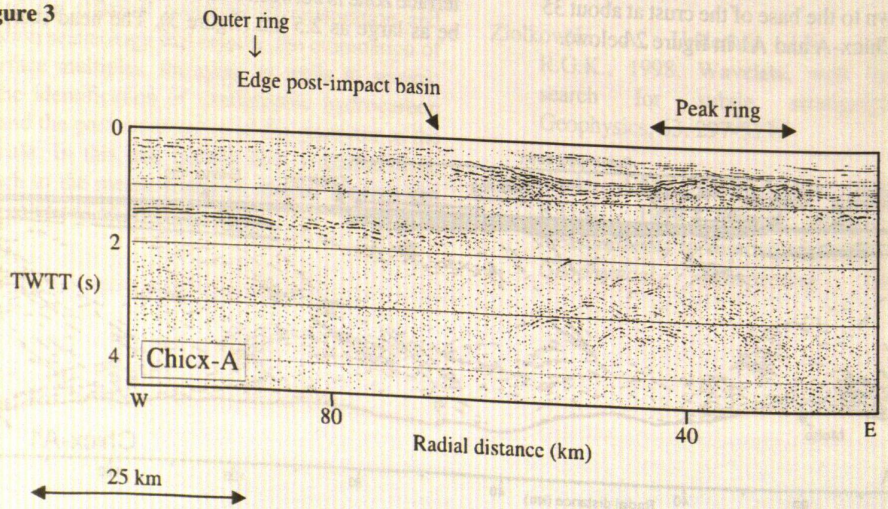

marine lines A, A1 and B (Christeson et al., 1999), and data from the land stations to obtain upper crustal velocity structure along lines B-F, C-E and A-D. Currently researchers at both Imperial College and University of Texas are inverting travel-times for the entire wide-angle dataset in 3-D.

The most prominent feature seen on these tomographic images is the low-velocity Tertiary basin. The post-impact basin is ~1 km deep and shows velocities gradually increasing from 2 to 3.5 kms^{-1}. Surprisingly, we observe the peak ring as a velocity low. Inboard of the peak ring at about 1.6 km depth, a velocity increase with depth from < 4 kms^{-1} to > 5 kms^{-1} coincides with a low-frequency reflector. If we extrapolate well data from onshore to offshore, this boundary coincides with a lithology change from a low-density suevitic breccia to a denser melt breccia. Another prominent feature is the velocity high near the centre of the crater; it is about 40 to 50 km wide, and represents a P-wave velocity contrast of about 0.5 kms^{-1} (figure 4). We are limited by the penetration of our ray paths and cannot determine the location of the top or base of this high velocity zone. The high velocities coincide well with a positive surface gravity anomaly, thought to represent a central uplift (Pilkington et al., 1996). The central uplift is slightly offset to south and west from the apparent geometrical centre of the crater. A similar offset is seen on the gravity contours.

We observe central uplifts in large craters on Earth (e.g. Manicouagan in Canada and Vredefort in South Africa). On the other planets and moons, we observe central uplifts as topographic features on the flat crater floor in medium size craters. However, in larger craters the central uplift appears to evolve into a topographic peak ring; it is thought that in these craters the central uplift becomes gravitationally unstable (during the formation of the crater) and collapses outwards. The relationship between topographic features observed across large craters and the subsurface structure is poorly understood, and hard to understand from craters on Earth that have been obscured by tectonics and erosion. The velocity images emerging from our 3-D inversions across Chicxulub offer us important clues to understanding the relationship between the central uplift and peak ring.

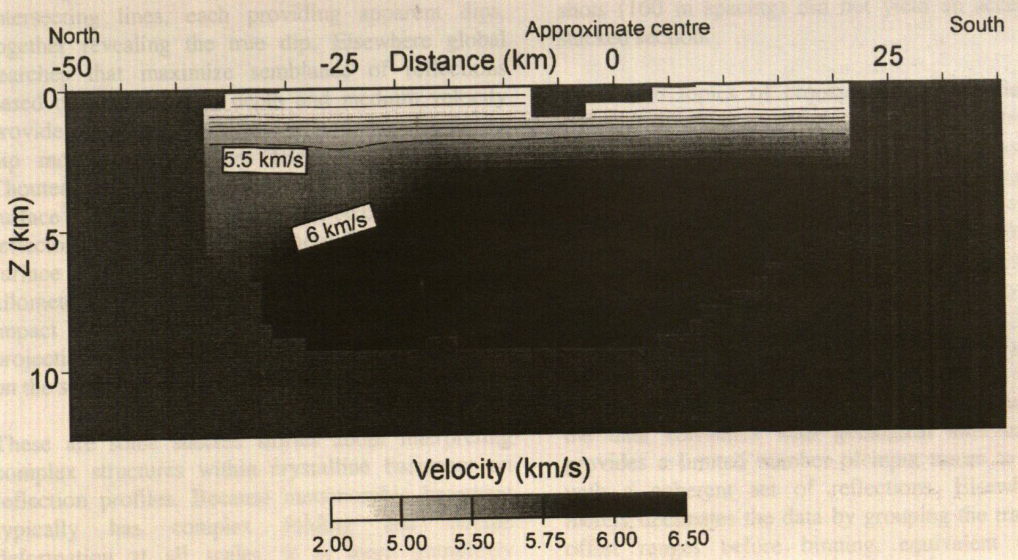

Figure 4 – Velocity image of the central uplift at Chixulub

Bright, clear, PmP reflections are observed on nearly all stations, and weak to very strong Pn refractions are observed on many stations. These data indicate that Moho in this area generally lies at a depth of 35 ±3 km with some interesting topography, that, so far, appears to confirm the observed topography on the seismic reflection data.

References

Brittan, J., Morgan, J. V., Warner, M. R., Marin, L., 1999, Near surface seismic expression of the Chicxulub impact crater: Geological Society of America Special Paper 339.

Christeson, G., Nakamura, Y., Buffler, R., and the Chicxulub Working Group, 1999, Upper crustal structure of the Chicxulub impact crater from wide-angle ocean bottom seismograph data: Geological Society of America Special Paper 339.

Morgan J. V., Warner, M. R., and the Chicxulub Working Group, 1997, Size and morphology of the Chicxulub impact crater: Nature, v. 390, p. 472-476.

Morgan, J and Warner, M., 1999, The third dimension of a multi-ring impact basin: Geology, v. 27, p. 407-410.

Zelt and Smith, 1992, Seismic travel-time inversion for 2-D crustal velocity structure: Geophys. J. Int., v.108, p.16-34.

Zelt and Barton, 1998, Three-dimensional seismic refraction tomography: A comparison of two methods applied to data from the Faeroe Basin: Journal of Geophysical Research, v.103, p. 7187-7210.

Obtaining low-fold 3-D coverage from 2-D seismic surveys

David Snyder, Brian Roberts & Erick Adam
Geological Survey of Canada, 615 Booth Street, Ottawa K1A 0E9, CANADA
snyder@cg.nrcan.gc.ca

Seismologists have long demonstrated the ability to make the best out of what they have in terms of data. Over the past few years, LITHOPROBE seismologists, in particular, have taken advantage of crooked line survey geometries, dictated by rugged topography and limited road access, to provide some cross-dip information and to study out-of-plane reflectors (e.g. Vasudevan, Cook & Maier 1995; Bellefleur, Calvert & Chouteau 1998). At times, the cross-dip information provided is as simple as two intersecting lines, each providing apparent dips, together revealing the true dip. Elsewhere global searches that maximize semblance of reflections based on azimuth, dip, depth and medium velocity provide estimates of structure in a manner similar to dip move-out corrections (Bellefleur, Calvert & Chouteau 1998). In regions with good exposure, surface structural observations can be correlated with reflectors. In one study in northern Quebec, regional surface structures (mostly gneissic layering) tens of kilometers off the profile near the Manicouagan impact were shown to correlate after downdip projection with the attitudes of prominent reflections on the seismic sections (Hynes & Eaton 1999).

These are some success stories about interpreting complex structures within crystalline basement on reflection profiles. Because metamorphic basement typically has complex folding and ductile deformation at all scales, it is more complexly reflective than a sedimentary basin where the common-depth-point (CDP) method was first developed. The restricted lateral extent of prominent or significant reflectors means that limited offset ranges are often more effective in imaging these complex structures than are full fold CDP stacks. In extreme cases, hand editing of individual CDP gathers before stacking can be effective, or more automated range stacks may be more appropriate for large data sets or regions with somewhat less complexity (Nedimovic & West 1999).

Thus limited fold of coverage may or may not be a drawback of these surveys. In another study near a mining camp in Ontario, intersecting 2-D line coverage provided estimates of data degradation due to reduced fold during feasibility studies for a proposed full 3-D survey (Perron, Adam & Roberts 1996). Structures of interest here were ore bodies and mineralized stratigraphic horizons 100-300 m in scale. Even the simple geometry of perpendicular lines provides broadside surveys. By using a shot spacing of 40 m and a receiver spacing of 10 m (nominal 60 fold) to deliberately oversample the target area, it was then possible to decimate the data and reduce the coverage during processing to determine a threshold of acceptable resolution. The study found that a fold of 30 (shot spacing of 80 m) is sufficient to obtain a useful seismic image of stratigraphic horizons in spite of the limited offsets available at some CDPs. Decimating 75% of the shots (160 m spacing) did not yield an acceptable stacked section.

These two topics of crooked line geometries and selective offset range merge nicely in some areas. In regional transects, typical of LITHOPROBE surveys, offsets of nearly twenty kilometers are common. The survey route makes large deviations from a straight line over such distances and provides source-receiver geometries with midpoints several kilometers distant from the actual survey route (Figure 1). The crooked line geometries thus provide limited information from the third (out of the survey plane) dimension, but also this information is also based on limited offset range. In many cases this natural decimation of the data correlates with geological structure and provides a limited number of input traces to stacks with a coherent set of reflections. Elsewhere it merely decimates the data by grouping the traces by offset ranges before binning, equivalent to the method described above.

Another recent Lithoprobe study near Yellowknife, NWT, provides a good example. The crooked line geometry of SNORCLE (Slave-Northern Cordillera Lithospheric Evolution) line 1 provided useful cross-dip information about the true dip of a prominent, shallow reflector (Snyder, Roberts & Bleeker 1999). The additional information enhanced the likelihood of it representing an ultra-mafic sill injected into a thick sequence of meta-turbidites rather than an extensional fault as was initially suggested (Cook et al. 1999). Picking a CDP line much closer to the actual survey route and limiting bin sizes tightened the range of offsets used in stacking and focused near-surface energy to reveal closer correlation between the reflector and a prominent outcrop. Creating a 3-D cube and using prestack equivalent offset migration (Bancroft, Geiger & Margrave 1998) provided a more poorly focused reflection due to the limited fold of coverage, but did reveal the true strike

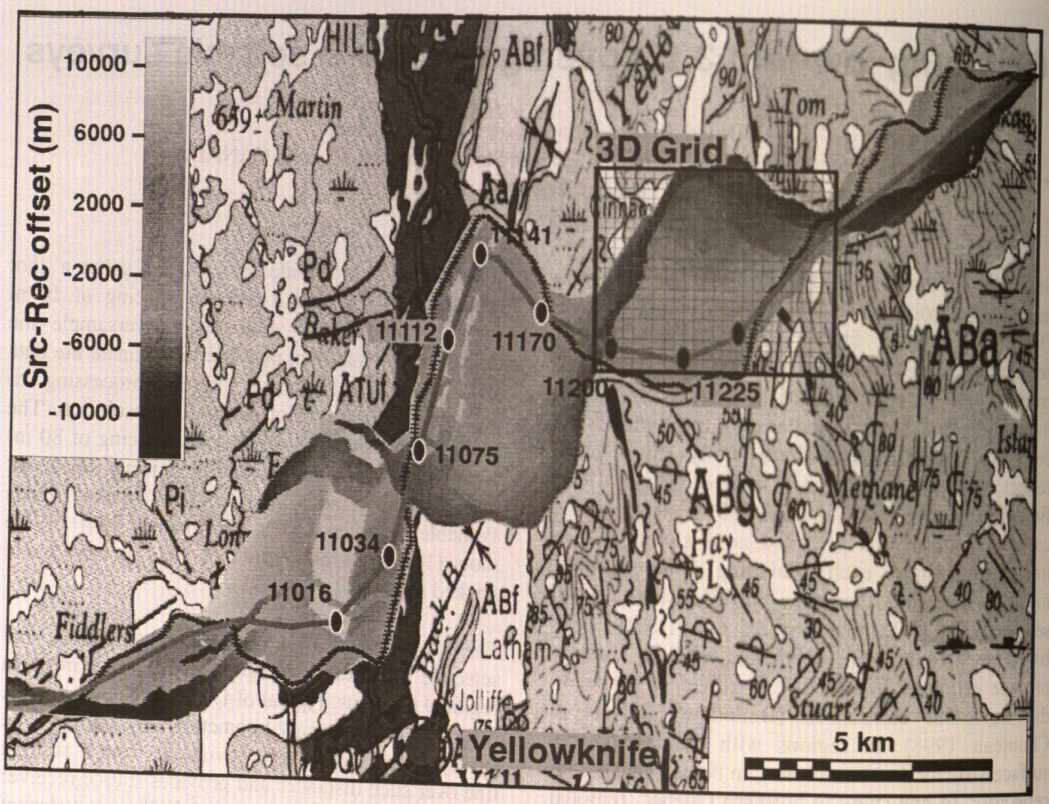

Figure 1. Geological map of the Yellowknife area showing SNORCLE survey route (black crosses) and CDP line (red) used in the reprocessing of the data for better cross-dip information. Black box labelled 3D grid show area of Figure 2 top. The greyscale shows the distribution of source receiver offsets as plotted at their common midpoint. Some midpoints lie nearly 5 km from the survey route. Geological units include Archean meta-turbidites (ABa & ABg), Proterozoic granitic plutons (Pd), and Archean greenstones and pillow lavas (AT). The thin black units near the bottom centerline are ultra-mafic sills that we now correlate with prominent reflections.

of the reflector/sill (Figure 2). The bowl-shaped geometry that was revealed is typical of sills world-wide and strengthened the case for the alternative interpretation. Interpreting more of the prominent crustal reflections observed on the SNORCLE profile as mafic intrusions rather than extensional fault surfaces has important implications for the regional geology and the Archean history of this famous greenstone belt.

A final, more practical, example is drawn from the current Lithoprobe survey. A four-way broadside shot into two crossing profiles was recently proposed for the Tintina Trench area of the Yukon Territories. The Tintina fault is interpreted from regional mapping to represent a crustal, or even lithospheric, scale feature equivalent to the San Andreas fault. The suggested acquisition parameters include use of 750 active channels recorded simultaneously on two roads at roughly right angles to each other. Receiver spacing of 50 m would provide 37.5 km spread lengths and 100 m vibrator point spacing and 100m bin sizes provided greater than 15 fold everywhere in a rectangular area covering the entire width of the Tintina Trench. This presumably covers most, if not all, major splays of the regional strike-slip fault zone coincident with the trench. The survey was costed at $120 K over the costs of the regional 2-D transect. It was not done due to weather and time contraints.

These handicapped or psuedo- 3-D surveys cannot replace a full 3-D survey, especially if one truly requires full volumetric information about a target to locate diffracting bodies or image complete sets of faults, for example. This is the true justification to the large costs associated with full 3-D surveys. Our argument here is that such costs may not be justifiable if it is only 3-D information such as true dip about specific horizons or individual reflectors that is sought. In such cases, the design of 2-D surveys with intentionally crooked lines or pseudo-3D studies using broadside shots and simple cross lines are recommended because they may prove sufficient for many needs.

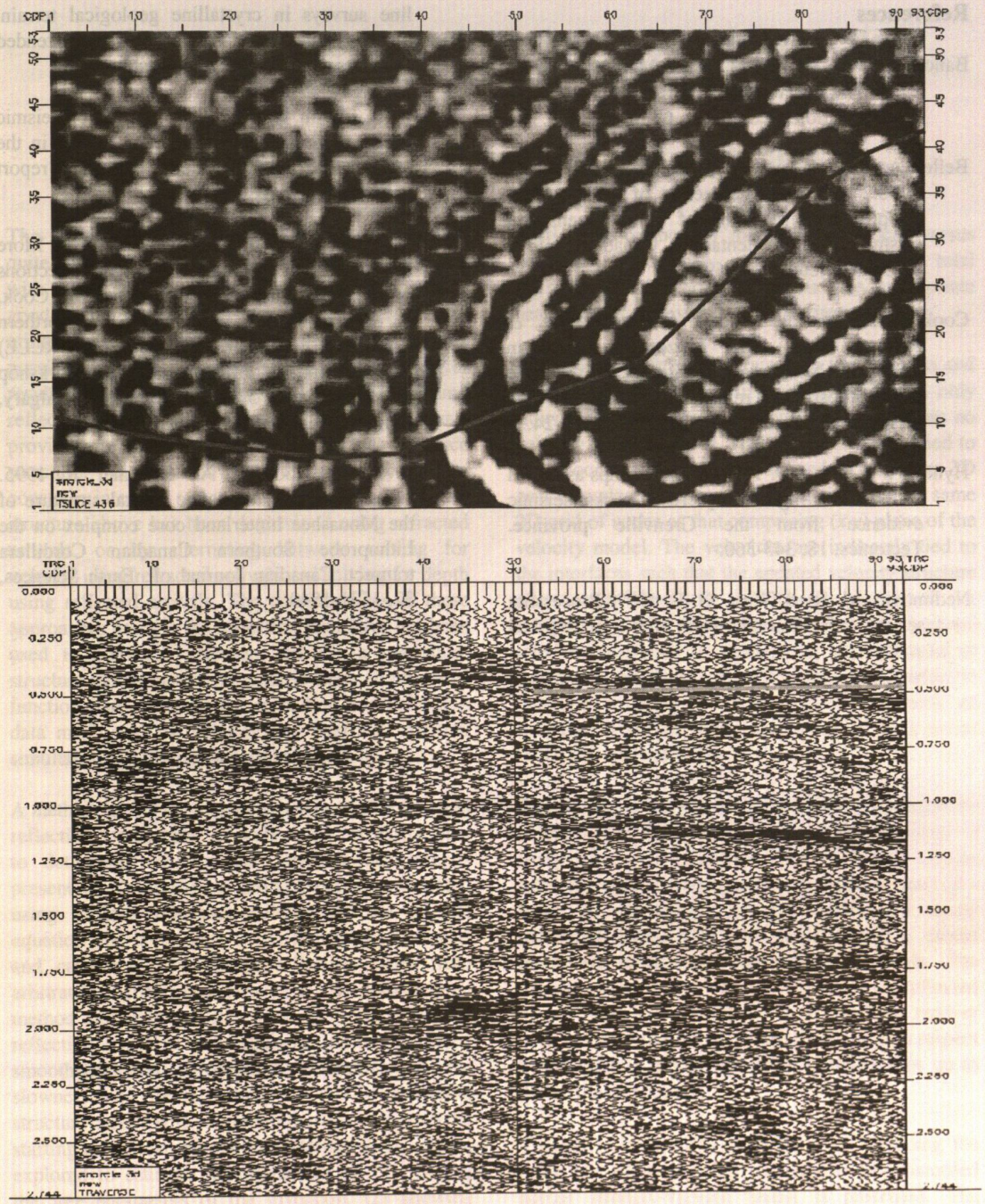

Figure 2. (top) Time slice at 436 ms (map view) from the 3D cube of data marked by the box in Figure 1. Grey line is the CDP line shown in Figure 1. Bin size is 30 m by 30 m. Coherent black and white trends in the right half of the figure are interpreted as the prominent reflections from a 300-m-thick ultramafic sill. The image indicates a dish shape, but a predominantly NE-SW strike of the reflector in this area. (bottom) A vertical slice from the same cube along the CDP line above. The grey arrow indicates the location of the time slice shown above. Note that both images are somewhat fuzzy due to the limited fold available with the small bin size.

References

Bancroft, J. C., Geiger, H. D. & Margrave, G. F., 1998. The equivalent offset method of prestack time migration. Geophysics, 63, 2042-2053.

Bellefleur, G., Calvert, A. J. & Chouteau, M. C. 1998. Crustal geometry of the Abitibi Subprovince, in light of three-dimensional seismic reflector orientations. Canadian Journal of Earth Science, 35, 569-582.

Cook, F. A., van der Velden, A., Hall, K. W. & Roberts, B. J. 1999. Frozen subduction in Canada's Northwest Territories: Lithoprobe deep lithospheric reflection profiling of the western Canadian Shield. Tectonics, 18, 1-24.

Hynes, A. & Eaton, D. 1999. Lateral ramps as an aid to the unroofing of deep-crustal rocks: seismic evidence from the Grenville province. Tectonics, 18, 343-360.

Nedimovic, M. R. & West, G. F. 1999. Processing seismic reflection data from high fold, crooked line surveys in crystalline geological terrain. Society Exploration Geophysics extended abstracts, annual meeting, Houston.

Perron, G., Adam, E. & Roberts, B. 1996. Seismic reflection acquisition parameters testing in the Manitouwadge mining camp. Technical report to Noranda, 8 pages + plates.

Snyder, D., Roberts, B. & Adam, E. 1999. More thoughts about the nature of bright reflections in the upper crust near Yellowknife. *In:* Cook, F. & Erdmer, P. (compilers) Slave-Northern Cordillera Lithospheric Evolution (SNORCLE) Transect and Cordilleran Tectonics workshop meeting (March 5-7), University of Calgary, Lithoprobe Report No. 69, 37-39.

Vasudevan, K., Cook, F. A., & Maier, R. 1995. Three dimensional seismic crustal structure of the Monashee hinterland core complex on the Lithoprobe Southern Canadian Cordillera transect. Canadian Journal of Earth Sciences, 32, 1531-1540.

3D Simultaneous Seismic Refraction and Reflection Tomography of Wide-Angle Data

Colin A. Zelt (Rice University, Houston, TX, USA. e-mail: czelt@rice.edu)

The acquisition of 3D wide-angle data has become quite popular. For relatively sparse data or in areas with strong lateral variations, the development of a good starting model using prior information and the utilization of as much of the wide-angle data as possible is crucial to obtain geologically meaningful results. From 2D studies it is well known that using reflected arrivals in addition to refracted arrivals provides greater constraint on velocity and interface structure. 3D reflection times are normally used to constrain interface structure, either after the velocity structure above has been determined using refracted arrivals, or by alternating between solving for velocity using refracted arrivals and solving for depth using reflected arrivals. The disadvantages of these approaches are: (1) the reflection data have not been used to constrain velocity, and (2) a minimum-structure model cannot be assured since an objective function that measures the refraction and reflection data misfit and the velocity and interface structure simultaneously has not been minimized.

A method for 3D simultaneous seismic refraction and reflection tomography of wide-angle traveltime data to determine velocity and interface structure is presented. 3D traveltimes and raypaths are calculated using a finite-difference solution of the eikonal equation that is accurate for large velocity contrasts and capable of calculating reflection times from arbitrarily-shaped interfaces. The 3D tomographic method involves a simultaneous refraction and reflection inversion with regularization incorporating smoothness and perturbation constraints to the slowness and depth values so that a minimum structure model with minimum perturbation from the starting model can be obtained. Model space can be explored to estimate nonuniqueness by (1) varying the free parameters of the inversion, (2) allowing spatially-dependent regularization weights, and (3) clipping the velocity values in regions of relatively large total perturbation with respect to the starting model at each iteration. There are four free parameters, their values determined by systematic variation based on the ability to fit the data and an acceptable level and distribution of slowness and interface structure: (1) the relative weight of slowness and interface regularization, (2) the relative weights of smoothing and perturbation regularization for slowness, (3) the relative weights of smoothing and perturbation regularization for depth, and (4) the relative importance of maintaining vertical versus horizontal slowness smoothness. The total regularization is chosen such that the appropriate data misfit is achieved on the final iteration.

The reflection times constrain both the slowness and interface depth, but the first arrivals constrain only slowness because the model parameterization has no velocity discontinuities. The interfaces are not tied to the velocity model, which is defined on a uniform 3D grid of nodes; the interfaces are defined on the same 2D grid of nodes as that comprising (x,y) plane of the velocity model. The velocities are indirectly tied to the interfaces such that the updated velocity structure after each iteration is linearly stretched or compressed into the region between the updated interface positions to account for the increased or decreased thickness of each layer. This helps to maintain a velocity contrast associated with an interface in the starting model as the interface moves vertically with iteration.

Two synthetic examples are presented to illustrate the method. The first example shows the advantage of using reflections when there is a "blind" zone with no refracted ray bottoming points in the lower part of a layer. A comparison is made between a model recovered using only first arrivals and a model recovered using first and reflected arrivals. The second example uses first arrivals and two reflected phases from two interfaces to successfully recover both velocity and interface perturbations with respect to the starting model with local interface dips up to 20° in the true model.

Through a case study, a method for obtaining the most out of sparse 3D wide-angle data recorded across strongly-varying media is presented. The potential of such data is demonstrated by considering the large-scale geologic features of the study area and estimating model resolution. The data were recorded in a region of seamount subduction on the Chilean margin and consist of seven receivers and ten intersecting airgun profiles over a 90×90 km area providing constraint to 25 km depth. 14,448 first arrivals and 2738 reflected arrivals from three interfaces were used. The reflecting interfaces are the base of the Valparaiso forearc basin, the base of the accretionary wedge, and the subducting oceanic Moho. Pick uncertainties of 50-200 ms were assigned

based on the signal-to-noise ratio and the estimated timing accuracy. Poor signal propagation limited the picking of arrivals with offsets greater than about 50 km.

The approach to modeling these sparse 3D data was to: (1) use as much prior information as possible to develop the starting model, and (2) establish the minimum structure required beyond that contained in the starting model using as much of the 3D data as possible. A 2D starting model was developed for a dip profile at the southern edge of the 3D study area using (1) the known bathymetry, (2) sediment thickness from coincident reflection lines, (3) the nearest 2-D P-wave velocity model along the margin about 1000 km to the north, and (4) the dip of the subducting plate to 60 km depth (15°) based on regional seismicity. Refracted and reflected traveltimes from 20 ocean bottom receivers along the profile were inverted to obtain a 2D velocity and interface model. This model was extrapolated northward to obtain starting models for the remaining 9 airgun profiles of the 3D survey. Inline refracted and reflected traveltimes along the 10 profiles were inverted simultaneously such that consistency at the 10 intersection points of the 2D models was assured. The 3D starting model was obtained by fitting surfaces to the interfaces and upper and lower layer velocities defined by the ten 2D models.

The final 3D model shows the Valparaiso forearc basin, the accretionary wedge, the subducting plate, and possibly a subducting seamount. Using a simultaneous refraction and reflection inversion during all 2D and 3D inversion steps helped to honor the prior information and obtain the minimum structure beyond that contained in the starting model. Although the velocity expression of the subducted seamount is the only interpreted feature of the final 3D model not present in the 3D starting model, the results show that the other features contained in the starting model are consistent with the 3D inline and offline data. A checkerboard resolution test to assess the lateral velocity and depth resolution shows that the velocity resolution of large-scale features is excellent to about 10 km depth, but is somewhat smeared below this. The reflection-point distribution is sparse, and this is mirrored in the relatively poor lateral interface depth resolution. Overall, the results show the potential of relatively sparse 3D wide-angle data that may result from instrument failure, poor data quality, limited resources or site access, or a primarily 2D survey.

Reference:

Zelt, C.A., Hojka, A.M., Flueh, E.R. & McIntosh, K.D., 1999. 3D simultaneous seismic refraction and reflection tomography of wide-angle data from the central Chilean margin, *Geophys. Res. Lett.*, 26, 2577-2580, 1999.

Reflection and Refraction Imaging of Steeply Dipping Faults

John A. Hole
Virginia Tech, Department of Geological Sciences,
4044 Derring Hall, Blacksburg, VA, 24061-0420;
hole@vt.edu

To date, near-vertical strike-slip faults have not been directly imaged as reflectors in seismic reflection sections. Previous multichannel data across the San Andreas Fault (SAF) and across other major strike-slip faults observe a broad vertical zone with no reflectors (or only very short diffraction segments) that separates differing reflectivity on either side of the fault [*Lemiszki and Brown*, 1988; *Stern and McBride*, 1998]. Details such as the direction of dip of the fault, changes in dip at depth, and relations with other faults, which are all crucial to understand the tectonic behavior of the fault system, have not been well resolved. In addition to the problems of imaging vertical structures with techniques designed for horizontal structures, the interpretation of these data usually has been limited by a lack of seismic velocity information from coincident detailed refraction models.

While the petroleum industry has designed surveys and applied appropriate processing to image important steeply dipping targets, the academic research community has yet to adopt such techniques. COCORP and similar groups in the 1970's adapted multichannel reflection profiling, a tool developed by the petroleum industry, to geologic problems within the sub-sedimentary crust. The result was a revolution in our understanding of the structure and evolution of the continental crust. I propose to continue this philosophy of adopting industry techniques, with the goal of imaging steeply dipping structures in the crust. The new ability to image steeply dipping structures will prove particularly valuable in studies of complicated strike-slip fault systems.

An increase in seismic velocity with depth, the usual situation in the upper crust, refracts seismic energy into horizontal ray paths at a range of depths. These refracted (both turning and critically refracted) rays are the basis of refraction seismology, but are also at the correct orientation to be reflected by a vertical reflector and returned to the surface (Figure 1). Assuming similar reflection coefficients, similar ray lengths, and a reasonable upper crustal velocity gradient, the amplitudes of reflections in shot gathers should be similar for vertical and horizontal reflectors (Figure 1) [*Hole et al.*, 1996]. This is a consequence of the way energy is spread away from vertical ray paths by the velocity gradient.

The petroleum industry identified such "reflected refractions" from faults and salt domes more than 50 years ago. We draw a distinction between detection in shot or receiver gathers and imaging as part of a multichannel reflection section. Steep-dip reflections have not been imaged until recently because of limitations in conventional seismic acquisition and analysis. Source and receiver arrays, common-midpoint stacking, and most migration algorithms are designed to image reflections from sub-horizontal structures, eliminating other seismic arrivals as "noise". Recently, careful survey design and prestack processing and migration of multichannel data have allowed the imaging of reflectors from the steep sides of salt domes with dips up to 120° (overturned) [*Hale et al.*, 1992]. These images have provided important information for hydrocarbon exploration, delineating traps for oil and gas adjacent to salt domes and allowing accurate drilling of these targets.

Fault zones can reflect seismic energy due to velocity contrasts across the fault. In addition, low-velocity fault gouge, compositional layering, ductile mylonitic foliation, or retrograde metamorphism within the fault zone can all cause reflectivity due to one or more layers of different seismic velocity or anisotropy [e.g., *Mooney and Ginzburg*, 1986]. Numerous sub-horizontal extensional and compressional faults have been observed as major reflectors in multichannel seismic reflection images of the crust. There is every reason to expect strike-slip fault zones to have similar internal properties that will cause them to act as reflectors of seismic energy. Seismic reflections from the near-vertical SAF have been detected in shot and receiver gathers at Parkfield [*Louie et al.*, 1988] and near San Francisco [*Hole et al.*, 1996]. Neither these nor other crustal data sets across the SAF were acquired with the optimum parameters to produce a multichannel reflection image of vertical features.

Louie et al. [1988] developed a 3-D prestack Kirchhoff depth migration algorithm that allowed steep dips, and applied it to 1977 COCORP data across the SAF at Parkfield. To our knowledge, this was the first published steep-dip migration application in 2- or 3-D. Field acquisition parameters were typical for the early years of crustal reflection work, and were complicated by a very crooked line. *Louie et al.* [1988] produced an image of a 45°-

dipping reflection that they interpreted as due to a splay fault adjacent to the SAF. A vertical reflector was imaged in the upper kilometre, but was not directly correlated with any surface fault. They were unsuccessful at imaging the neotectonic SAF itself. This work was hampered by limited geometric coverage due to low data fold and the crooked line, by poor signal/noise, and by a lack of a good velocity model.

In addition to adopting the appropriate processing tools, the field survey must be properly designed. Five issues are crucial to the recording and subsequent migration of reflections from steeply dipping structures. First, longer lines incorporating longer source-receiver distances and longer recording times are needed due to the abnormal reflection moveout curve (Figure 1). Second, spatial aliasing of the wavefield must be avoided for migration of multifold data. Third, a crooked line and rugged topography must be either avoided or explicitly included in the analysis, for example through 3-D migration. Fourth, out-of-plane effects must be included by acquiring 3-D data or avoided by orienting the line perpendicular to geologic strike. Fifth, and most difficult, is that an excellent seismic velocity model must be available for the migration.

The ability to perform wide-angle or steep-dip migration depends strongly upon the accuracy of the seismic velocity model. The petroleum industry supplements velocity information contained in the seismic reflection data with borehole data to obtain the images of salt structures. This is aided by excellent continuity of seismic velocity in the relatively homogeneous and easily imaged sedimentary layers. For crustal targets, the detail provided from down-hole measurements is not available. In addition, lateral continuity of velocity is less consistent and more difficult to image by reflectivity. The best available velocity information must come from travel time modelling of refraction and wide-angle reflection data. The petroleum industry is now acquiring longer shot-receiver distances to take advantage of the improved velocity information from wider-angle data, an aspect in which the academic community is technologically more advanced.

A combined seismic reflection and refraction survey was acquired across the SAF at Parkfield in late 1998. Michael Rymer and Rufus Catchings (USGS, Menlo Park) are the PI's on the survey. The data were acquired to characterize the site of the proposed scientific drill hole through the SAF, providing a wide-angle velocity model of the upper kilometre and a multichannel reflection image of the upper 2-3 km. The survey design also satisfies all of the requirements for steep-dip imaging.

The line is 4930 m in length perpendicular to the SAF, extending 3.5 km southwest and 1.5 km northeast of the fault. Despite significant topography and brush, the data were acquired in a straight line across country to avoid crooked-line degradation of the modelling. Every shot and receiver station was surveyed after deployment with differential GPS. 494 shots were fired every 10 m along the line. The majority of the shots were 2 pounds of explosives buried in a shallow drill hole, although smaller shots or shotgun blasts were used where drilling was difficult. A fixed deployment of 840 seismometer channels was used to record every shot. The station spacing was 5 m in the central 3190 m of the line and 10 m in the westernmost 1160 m and the easternmost 580 m. The geophone frequency was 40 Hz. Seismic traces were recorded for 5 s at a 0.5 ms sampling rate.

This survey design is a true merger of seismic reflection spacings with seismic refraction shot-receiver distances. Only recently have the seismograph systems become available to achieve very long shot-receiver distances (relative to the desired depth of imaging) while maintaining dense shot and receiver samplings (relative to the shortest seismic wavelength). The requirements of steep-dip imaging are provided by the station spacing, line length, and straight line, and an excellent velocity model will be produced by refraction and wide-angle reflection travel time inversion.

Because of the timing of data archival work at the USGS, the data are not yet available for special processing to search for evidence of fault zone reflected waves. Usually data processing such as deconvolution and dip filtering is required to observe reflected arrivals in shot gathers [e.g., *Hole et al.*, 1996]. However, the raw shot gathers show strong events at the correct location and moveout for fault plane reflections from the SAF. We intend to supplement the standard data analysis with an attempt to image for the first time seismic reflections from the vertical San Andreas Fault. Due to the line length, steep dips will only be imaged to about 1 km depth.

The recent Parkfield survey does at a small scale what the crustal seismic community needs to consider at a larger scale. In many regions and for many geologic problems, conventional seismic acquisition and processing is unable to satisfactorily image the target of interest. A frequent cause of this failure is that steep dips are common in the crust. Examples are steep faults, complexly deformed metasediments, plutons, and dikes. Both the field and processing technologies are available to image steep dips, but some work is still required to adapt these tools to image the crystalline crust. The energy is in our seismic data; we should utilize it.

References:

Hale, D., N.R. Hill, and J. Stefani, Imaging salt with turning seismic waves, *Geophysics*, *57*, 1453-1462, 1992.

Hole, J.A., H. Thybo, and S.L. Klemperer, Seismic reflections from the near-vertical San Andreas Fault, *Geophys. Res. Lett.*, *23*, 237-240, 1996.

Lemiszki, P.J., and L.D. Brown, Variable crustal structure of strike-slip fault zones as observed on deep seismic reflection profiles, *Geol. Soc. Am. Bull.*, *100*, 665-676, 1988.

Louie, J.N., R.W. Clayton, and R.J. Le Bras, Three-dimensional imaging of steeply dipping structure near the San Andreas Fault, Parkfield, California, *Geophysics*, *53*, 176-185, 1988.

Mooney, W.D., and A. Ginzburg, Seismic measurements of the internal properties of fault zones, *Pure & Applied Geophys.*, *124*, 141-157, 1986.

Stern, T.A., and J.H. McBride, Seismic exploration of continental strike-slip zones, *Tectonophysics*, *286*, 63-78, 1998.

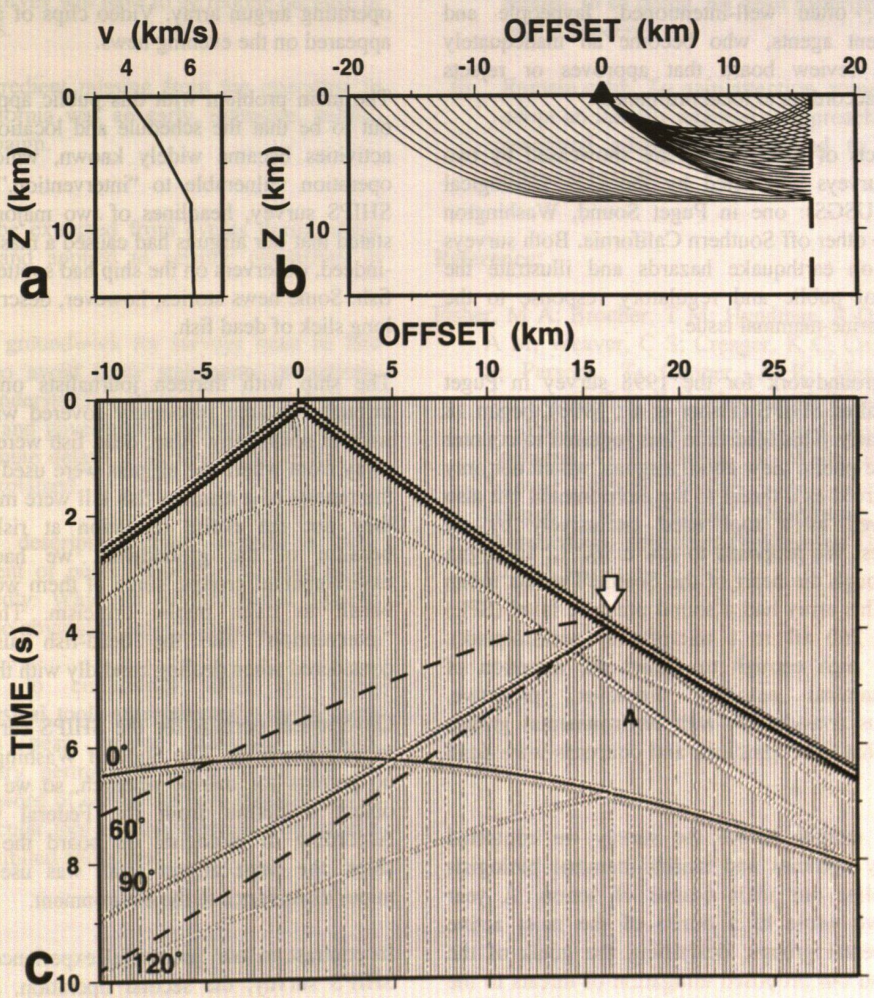

Figure 1. Synthetic San Andreas Fault reflections. (a) 1d velocity model with a moderate vertical gradient in the upper crust. (b) Vertical-fault reflection ray paths. (c) Synthetic reflections for a vertical fault at 17 km distance (labeled 90° dip) and a horizontal fault at 17 km depth (labeled 0°) with similar velocity contrasts, computed using finite-difference wave propagation. The faults are 100 m thick low-velocity (–10%) zones. At similar distances from the shot, the vertical and horizontal faults have similar reflection amplitudes. Dotted lines indicate the travel time curves (no amplitudes) for 60° and 120° fault dips. The arrow indicates the surface location of the dipping faults. A modeling boundary artifact is labeled A.

Figure from Hole et al., 1996.

Seismic Surveys and Environmental Concern

Michael A. Fisher
U.S. Geological Survey
345 Middlefield Rd
Menlo Park, CA 94025, USA
mfisher@usgs.gov

Recently, public concern about the environmental impact of seismic surveys that employ offshore airguns or onshore explosives has greatly increased. This contrary public opinion fosters government regulations that can stymie research or greatly increase its cost. Perhaps the greatest single threat to scientific inquiry that relies on seismic surveys is energetic, often well-intentioned, laypeople and government agents, who become an inadequately informed review board that approves or rejects research according to local ordinance.

The effects of local review are showcased by two recent surveys conducted by the U.S. Geological Survey (USGS): one in Puget Sound, Washington State, the other off Southern California. Both surveys focused on earthquake hazards and illustrate the breadth of public and regulatory response to the airgun/marine-mammal issue.

Laying groundwork for the 1998 survey in Puget Sound, called SHIPS (Fisher et al., 1998), began 18 months early. This lead time was required to counter a negative public view about airguns, which not only are perceived as a threat to the environment but also are viewed as a tool used exclusively by oil companies. We proposed to tow a 102 L, 16-airgun array through the heart of the Seattle/Tacoma urban region. This array had a sound pressure level (SPL) of about 260 dB re 1 microPa-m (peak-to-peak), which is high enough to attract the attention of marine-mammal activists. However, proactive, continuous consultation with environmental groups ensured that their questions and concerns were dealt with.

Eighteen months before the survey we contacted regulatory agencies and marine-mammal biologists to formulate our main course of action. A year before, we wrote to a dozen of the most active environmental groups, describing the goals of the survey and our proposed mitigation of threats to the environment. Most importantly, we solicited their advice on how best to minimize potential impacts. Six months before, we held public meetings to explain these goals and the mitigation. We brought onto the survey team a respected marine-mammal biologist, who helped design survey parameters and showed by his presence that we were serious in our mitigation. A few weeks before the survey we held press conferences with newspaper and TV reporters. In the few days before, we took media representatives on tours of the ship as geophysical gear was being installed, and we explained how airguns operate. Showing the airguns seemed to demystify them in the reporters', and hence the public's, mind. The day before the survey, thirteen reporters boarded the survey ship to observe the operating airgun array. Video clips of airguns firing appeared on the evening news.

The main problem with this public approach turned out to be that the schedule and locations of survey activities became widely known, which made the operation vulnerable to "intervention." During the SHIPS survey, headlines of two major newspapers stated that our airguns had caused a massive fish kill--indeed, observers on the ship had spotted a few dead fish. Some news stories, however, described a miles-long slick of dead fish.

The ship with thirteen journalists onboard sailed through the area reportedly covered with dead fish without seeing any. Also, dead fish were found miles away from where the airguns were used. In our view the reports of a massive fish kill were misguided, but they put the entire operation at risk. However, because of the groundwork we had laid with environmental groups, some of them worked on our behalf to calm public criticism. The threat of "intervention" like the dead-fish ruse must be considered when dealing candidly with the public.

Government permits for the SHIPS survey took six months to obtain. The State of Washington requires no permits for marine research, so we only had to obtain a permit from the Federal Government. According to biologists on board the two survey ships, the large airgun array was used with only minor disturbance to the environment.

In contrast to our successful experience during the SHIPS survey, the second operation, off southern California, became politically contentious. This survey area includes what must be the world epicenter for concern over marine mammals, and the USGS's proposed survey became embroiled in a larger controversy over the possibility that oil companies might choose to reactivate some offshore oil leases, which might in turn, endanger marine-mammal habitats. The single airgun the USGS

proposed to use was small (0.6 L; SPL about 220 dB re 1 microPa-m (RMS)).

The State of California denied our permit application, and in so doing, they decided not to follow the advice of their own technical staff, who had recommended accepting our proposed survey and mitigation plans. The State decided that Federal requirements were too lax, and they imposed stiffer conditions, some of which were onerous, such as not shooting at night. We informed the State about the successful outcome of the SHIPS survey but to no benefit. Because of contractual commitments made to reserve the survey vessel, the USGS acceded to these conditions. Ultimately, productive survey time amounted to about half of the total ship time. Also, some of this survey will have to be redone because of wide data gaps.

The main ingredient missing from the operation in southern California was an early, intensive, public-relations campaign.

Lessons can be extracted from events during these two surveys and applied to seismic operations in general:

1) Public groundwork for surveys must be laid early to avoid hasty statements or actions. Poor understanding of technical issues by the public and government regulators can lead to last-minute delays if important issues are not fully explained.

2) Survey descriptions must include a clear statement of public benefit. We were asked repeatedly: Why risk environmental damage when no obvious benefit will result?

3) Trying to circumvent laws by using geophysical tools surreptitiously, as in using airguns near marine mammals without necessary permits, is self-defeating for us. When word of outlaw surveys spreads, use of a particular tool can be narrowly constrained or prohibited altogether.

4) Articulate spokespeople should present science to environmental groups and the press. Lay questions need to be anticipated, and simple answers prepared. The spokespeople must remember that they represent a larger endeavor, not just their own project.

5) Hear, remember and speak the exact language of the public. A great benefit from our early, public discussions before SHIPS was that we heard people state their prime concerns, and we took literal note of their words and phrasing. During later interaction with the public, we repeated these concerns exactly as we had heard them and then provided simple replies. In so doing, we dealt forthrightly with public concerns.

6) Remain calm. To gain attention, some groups adopt an initially aggressive approach but are reassured when calmly invited to discuss important issues.

Reference:

Fisher, M A; Brocher, T M; Hyndman, R D; Trehu, A M; Weaver, C S; Creager, K C; Crosson, R S; Parsons, T; Cooper, A K; Mosher, D; Spence, G; Zelt, B C; Hammer, P T; ten Brink, U; Pratt, T L; Miller, K C; Childs, J R; Cochrane, G R; Chopra, S; Walia, R, 1999, Seismic survey probes urban earthquake hazards in Pacific Northwest: Eos, Transactions, American Geophysical Union, v. 80, p. 13-17.

Combined Active and Passive Seismic Studies to Determine 3D Lithospheric Structure – Report on Strategy and Experience

J. Ansorge[1], E. Kissling[1], F. Waldhauser[2], S. Solarino[3], R. Arlitt[1], R. Lippitsch[1], S. Sandoval[1]

(1) Institute of Geophysics, ETH Hoenggerberg, CH-8093 Zuerich, Switzerland,
(2) US Geological Survey, 345 Middlefield Rd, MS 977, Menlo Park, CA 94025, USA,
(3) Dipartimento di Science della Terra, Universita degli Studi di Genova, Via Benedetto XV, I-16132 Genova, Italy

Abstract

Active and passive lithospheric studies are a combination of specially planned seismic refraction and reflection measurements and forward or inverse 2D modelling methods with 3D tomographic inversion techniques applied to body-wave travel-time observations from local and teleseismic sources. Appropriate strategies are described for such a combination depending on type and amount of available data and on the target volume in the lithosphere.

Introduction

In this presentation we understand active and passive lithospheric studies as the combination of seismic refraction and reflection measurements and forward or inverse 2D modelling methods with 3D tomographic inversion techniques applied to body-wave travel-time observations from local and teleseismic sources. Each method is restricted to a certain depth range of the lithosphere with respect to applicability and resolution. Over the last years we have tried to develop appropriate strategies for such a combination depending on the type and amount of available data and on the target volume in the lithosphere.

Active seismic reflection and refraction methods lead to reliable 2D seismic velocity models for the crust. If the structure is not too complex and if a dense enough network of profiles is available, these active methods can provide reliable but simplified 3D models for major crustal interfaces (Kissling et al. 1997). The same is theoretically true for the lower lithosphere. It is hardly practical for financial and technical reasons, however, if one aims at a continuous coverage even along profiles or at detailed 3D structure. For similar reasons these surface-bound active seismic techniques fail to resolve the detailed picture even for the crust in cases of strong structural variations in all three directions where the lateral velocity gradient may equal or exceed the vertical gradient (Solarino et al. 1997).

The achievable resolution with passive local and teleseismic body-wave travel-time observations depends, of course, on the dominant wavelength of

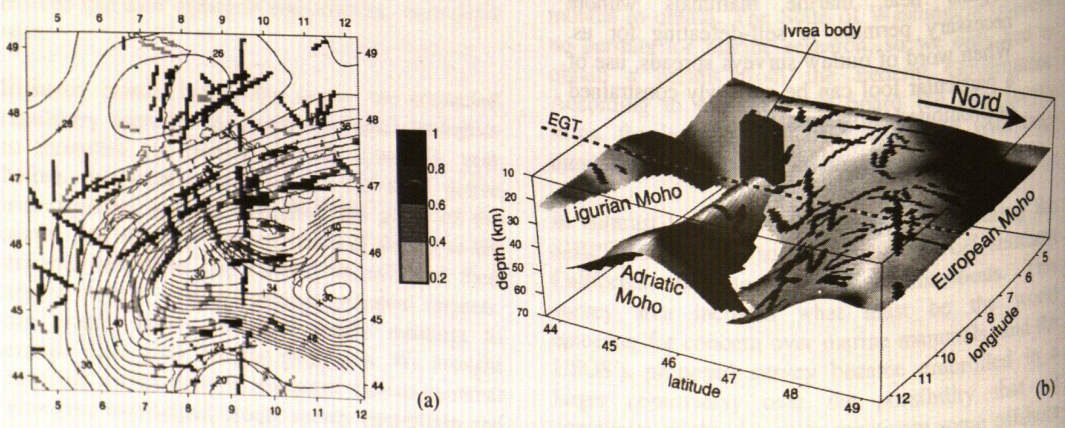

Figure 1: (a) Alpine Moho interface derived by smoothest interpolation of the 3D migrated active seismic data (after Waldhauser et al. 1998). Gray shading of the data base indicates weighting between 0.2 (poorly constrained) and 1 (highly reliable reflectors). The size of the elements indicates extension of Fresnel zone on the Moho. (b) Perspective SW view on the Moho below the Alpine region and the Ivrea body added schematically.

the seismic signals. Observations of local earthquakes with dominant wavelengths of 1 km or less provide reliable information on the crustal structure which is impossible to resolve with prevailing wavelengths of 10 km in first arrivals of teleseismic earthquakes. Besides, while signals from teleseismic sources may be recorded everywhere, local earthquake sources are sparse and shallow in many continental regions. Therefore, different strategies have to be followed depending on extension and depth of lithospheric target structure.

An appropriate combination of active and passive seismic techniques allows to resolve complex lithospheric structures within reasonable time and at affordable costs. The following chapters summarize a sequence of projects - aimed at a better knowledge of the lithospheric seismic velocity structure - where the practical approach develops with increasing experience and with improvement in interpretational techniques.

3D Alpine crust and Moho topography (crust; active survey): For 250 controlled-source reflection and refraction profiles in the greater Alpine region the crustal thickness and average crustal velocities were reviewed and weighted (Fig. 1a). The 2D–derived Moho reflector elements were migrated in space (Kissling et al. 1997) and interpolated to obtain a continuously gridded model for the Moho topography with least possible roughness and least amount of vertical offsets (Fig. 1). The quantitative control of these geometric features sets firm bounds to the evolution of the Alpine continental collision zone (Schmid and Kissling 1999). The crustal structure above the Moho is designed such that anywhere in the gridded model the average crustal velocity, sedimentary basins and the separation in upper and lower crust are preserved (see e.g. Fig. 3 for TOR) (Waldhauser et al. 1998). Spherical wavefronts are propagated from the base of this 3D model by FD methods to obtain traveltimes to the surface which can subsequently be used as corrections of teleseismic traveltimes when inverting for the structure of the lower lithosphere based on observations from permanent station networks (Waldhauser 1996).

Ivrea region (crust; active and passive surveys): Active surveys were carried out over many years to resolve the complex crustal structure of the Ivrea body in the inner arc of the western Alps (for more references see e.g. Ansorge et al. 1979, Thouvenot et al. 1990). These surveys were only able to detect locally the anomalous crustal structure but could never achieve a full 3D picture of the highly variable regional crustal system (Fig. 1b). Only the additional use of seismic tomography with travel-time data from local earthquakes recorded at existing station networks (western part of Fig. 2) has led to a complete 3D velocity model (Solarino et al. 1997) which covers the entire region and outlines the shape and contrasting velocity boundaries of the Ivrea body.

Project TOR (crust and upper mantle; active and passive surveys, respectively): This experiment is aimed at the structure of the lithosphere-asthenosphere system (LAS) across the northwestern part of the Trans-European Suture Zone (TESZ) (Fig. 3) by teleseismic tomography (TOR Working Group 1999). Earlier studies show a 200 km thick continental lithosphere in the north thinning to approximately 100 km south of the TESZ (Ansorge et al. 1992). As for the Alps, the crustal structure (Fig. 3) is fairly well known from active seismic experiments and was compiled similarly in an evenly gridded 3D velocity model of 3 km block size (Arlitt et al. 1999). Travel-time calculations through the 3D crustal model show significant travel-time residuals between –0.3 s and +0.5 s due to crustal structure. Based on the targeted depth range and desired resolution, and on the lack of a dense enough permanent station network in that area a seismic

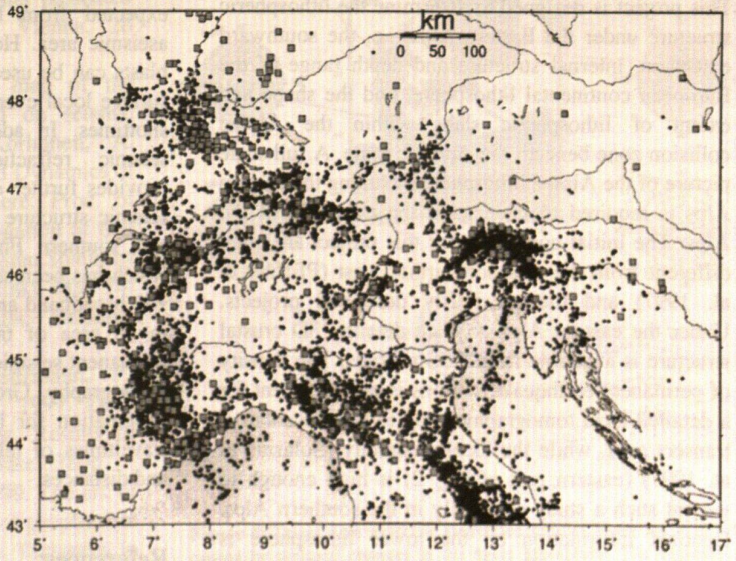

Figure 2: Permanent and temporary seismic stations of existing networks in the wider Alpine region (grey squares). Compilation of well locatable regional and local earthquakes recorded at these networks (Solarino et al. 1997). Triangles indicate temporary array of the TRANSALP project (Lippitsch et al. 1999).

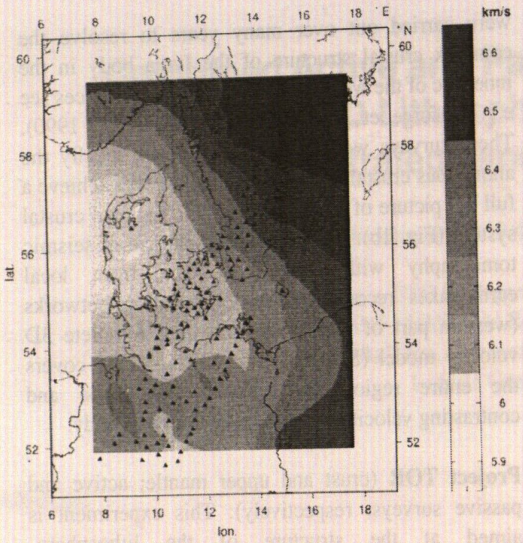

Figure 3: Temporary TOR array (black triangles) and average P-wave velocity in the TOR 3D crustal model (Arlitt et al. 1999). Thick line indicates Trans-European Suture Zone.

station array 1000 km long and 100 km wide with 140 short period and broadband stations (Fig. 3) was operated for about nine months to record teleseismic events from all azimuths. Out of 1200 recorded teleseismic events traveltimes from about 65 selected events were obtained. After correction for crustal contributions (Arlitt et al. 1999), the traveltime residuals (Fig. 4) serve as input to the tomographic inversion for the lithosphere-asthenosphere system (Arlitt 1999).

TRANSALP (crust and upper mantle; combined active and passive and passive surveys, respectively): This project is designed to determine the lithospheric structure under the Eastern Alps, i.e. the southward extension, internal structure and depth range of the European continental lithosphere, and the shape and extent of lithospheric slabs within the Alpine collision zone beneath the Adriatic plate. A full scale picture of the Alpine lithosphere including the eastern Alps is required to understand the evolution of the Alps. The initial conditions for this project are quite different from the situation further west (Pfiffner et al. 1997) and the previously described projects. Under the eastern Alps no such detailed 3D crustal structure is available from CSS profiles. The density of permanent earthquake stations is not sufficient for a detailed local tomography study in a representative transect area, while the local seismicity (Solarino et al. 1997) (eastern part of Fig. 2) is high enough to warant such a study especially in the southern Alps. Detailed information on the lower lithosphere is equally absent. Therefore, two complementary seismic surveys are performed along a N-S swath, 220 km long, across the eastern Alps (12°E). (I) An active seismic reflection and refraction survey is carried out which allows to extend the detailed Moho topography and 3D crustal model further east and to determine the internal crustal structure. (II) An array of 67 temporary seismic stations (Fig. 2) was operated for nine months with an average spacing of 15 km which recorded local and teleseismic earthquakes to supplement the crustal studies with local earthquake tomography and to reveal the lower lithosphere structure with high-resolution teleseismic tomography. For the latter recordings of the less dense permanent stations in the region are incorporated (Lippitsch et al. 1999).

SVEKALAPKO (crust and upper mantle; active and passive local surface bound and passive, respectively): This is still another project where active and passive surveys are combined to unravel the detailed structure of the lithosphere-asthenosphere system (LAS) again with different experimental and interpretational aspects. Of special interest is the lithosphere-asthenosphere boundary beneath an old craton and the variation of P and S velocities with depth and their ratio which is obviously not constant. The Fennoscandian shield (Hjelt et al. 1996) has not undergone major orogenic changes for the last 600 ma. It is an ideal place to study processes that control the evolution of the continental LAS. These processes, however, are overprinted by shortperiod depression and uplift of the shield caused by variable glaciation which provide information on the visco-elastic properties of the LAS. The successful and representative result of such a study requires a large enough target volume of the LAS and again a good knowledge of the crustal structure. Obviously, very little information can be expected from local earthquakes in this largely aseismic area. However, a large number of mining blasts can be used for a tomographic study as near-surface local events with known source location and shottimes. In addition, a long tradition of active seismic refraction and reflection experiments provides further excellent 3D information about the seismic structure of the crust in the area of central and southern Finland and Karelia (Luosto 1991) which has been selected for this study. A network of 143 broadband and shortperiod stations was installed in an area of 600 km by 600 km including the permanent seismic stations (SVEKALAPKO Seismic Tomography Group 1999). The main source of information for the lower LAS comes again from traveltimes of teleseismic events from all azimuths and distances.

References:

Ansorge, J., Mueller, St., Kissling, E., Guerra, I., Morelli, C. and Scarascia, S., 1979. Crustal

section across the zone of Ivrea-Verbano from the Valais to the Lago Maggiore. Bolletino di Geofisica Teorica ed Applicata, 21, 149-157.

Ansorge, J., Blundell, D. and Mueller, St., 1992. Europe's lithosphere - seismic structure. In: A continent revealed: The European Geotraverse (D. Blundell, R. Freeman, St. Mueller, Eds.) Cambridge Univ. Press, Cambridge, UK, 33-69.

Arlitt, R., 1999. Teleseismic body-wave tomography across the Trans-European Suture Zone in southern Scandinavia. PhD thesis, ETH-Zürich, in preparation.

Arlitt, R., Kissling, E., Ansorge, J. and TOR Working Group, 1999. 3-D Crustal Structure beneath the TOR Array and Effects on Teleseismic Wavefronts. Tectonophysics, in press.

Hjelt, S.-E., Daly, St. and SVEKALAPKO colleagues, 1996. SVEKALAPKO, Evolution of Paleoproterozoic and Archean Lithosphere. In: D.G. Gee and H.J. Zeyen (Editors), EUROPROBE 1996 - Lithosphere Dynamics: Origin and Evolution of Continents. Published by the EUROPROBE Secretariate, Uppsala University, 56-67.

Kissling, E., Ansorge, J. and Baumann, M., 1997. Methodological considerations of 3D crustal structure modeling by 2D seismic methods. In: Deep structure of the Swiss Alps. P. Heitzmann, P. Lehner, St. Mueller, A. Pfiffner, A. Steck (eds.), Birkhäuser, Basel, 31-38.

Lippitsch, R., Kummerow, J., Solarino, S., Sahli, M., Bopp, M., Ansorge, J., Eva, C., Gebrande, H., Kind, R. and Kissling, E., 1999. TRANSALP: Passive Seismic Tomography Experiment. Poster presented at TRANSALP Colloqium, Vienna, 26 April, 1999.

Luosto, U., 1991. Moho depth map of the Fennoscandian Shield based on seismic refraction data. In: H. Korhonen, A. Lipponen (eds.), Structure and Dynamics of the Fennoscandian Lithosphere. Proc. of the 2nd Workshop on Investigation of ther Lithosphere in the Fennoscandian Shield by Seismological Methods, Helsinki, May 14-18, 1990. Inst. Seismology, Univ. Helsinki, Report S-25, 43-49.

Pfiffner, O.A., Lehner, P., Heitzmann, P., Mueller, St. and Steck, A., 1997. Deep Structure of the Swiss Alps, Results of NRP 20. Birkhäuser Verlag Basel, 380p.

Schmid, S.M. and Kissling, E., 1999. The arc of the western Alps in the light of geophysical data on deep crustal structure. Tectonics, in press.

Solarino, S., Kissling, E., Selami, S. Smiriglio, G., Thouvenot, F., Granet, M., Bonjer, K.P. and Sleijko, D., 1997. Compilation of a recent seismicity data base of the greater Alpine region from several seismological networks and preliminary 3D tomographic results. Annali di Geofisica, 40, 161-174.

SVEKALAPKO Seismic Tomography Goup 1999. A Seismic Tomography Experiment in the Central Part of the Baltic Shield. Poster presented at EUG-X, Strasbourg, 28-31 April, 1999.

TOR Working Group, 1999. Important Findings Expected from Europe's Largest Seismic Array. EOS, 80/1, 1,6.

Thouvenot, F., Paul, A., Sénéchal, G., Hirn, A. and Nicolich, R., 1990. ECORS-CROP wide-angle reflection seismics: constraints on deep interfaces beneath the Alps. In: Deep Structure of the Alps, F. Roure, P. Heitzmann, R. Polino (eds.), Mém. Soc. géol. France, 156, 97-106.

Waldhauser, F., 1996. A parametrized three-dimensional Alpine crustal model and its application to teleseismic wavefront scattering. PhD thesis, No. 11940 ETH-Zürich, 173p.

Waldhauser, F., Kissling, E., Ansorge, J. and Mueller, St., 1998. 3D Interface Modeling with 2D Seismic Data: The Alpine Crust-Mantle Boundary. Geophys. J. Int., 135, 264-278.

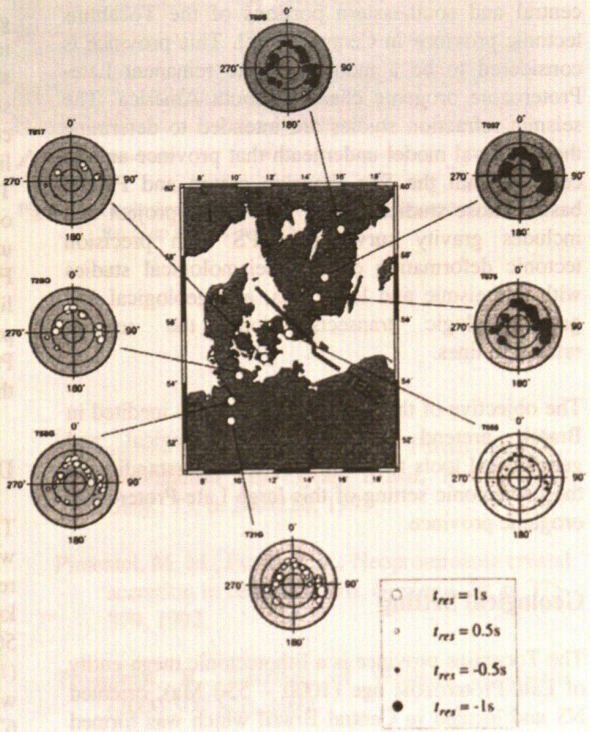

Figure 4: Travel time residuals at selected stations along the TOR array caused by strutural changes in the lower lithosphere. The residuals are plotted with respect to backazimuth and angle of incidence of the incoming wave. Open circles: positive residuals; full circles: negative residuals; diameter of circle proportional to size of residual (Arlitt 1999).

Deep Seismic Refraction Experiment in the Tocantins Tectonic Province in Central Brazil

J. Berrocal[(1)], W. Mooney[(2)], J.E. Soares[(3)], F.A. Perosi[(1)] & C. Fernandes[(1)]

[(1)] Instituto Astronômico e Geofísico, Universidade de São Paulo
[(2)] United States Geological Survey, Menlo Park, CA
[(3)] Observatório Sismológico Universidade de Brasília

Introduction

Deep refraction experiments in the continental portion of South American are scarce, especially in the Brazilian territory that occupies a very large proportion of this continent. We present in this work the data acquisition stage of a deep refraction experiment that has been carried out in September 1999, by using mainly seismographs borrowed from the PASSCAL program and with the participation of technical staff linked to the USGS refraction group of Menlo Park-CA.

Three deep seismic refraction lines, with a length of around 300 km each, have been deployed in the central and southeastern portions of the Tocantins tectonic province in Central Brazil. This province is considered to be a more complete remanent Late-Proterozoic orogenic chain in South America. The seismic refraction studies are intended to determine the structural model underneath that province and its contacts with the São Fransico craton and Parana basin. Those studies belong to a larger project that includes gravity surveying, GPS high precision tectonic deformation control, seismological studies with teleseismic and local data, and geological and geomorphologic transects along the seismic refraction lines.

The objective of the larger project, that is inedited in Brazil, pretend to use both geological and geophysical tools to obtain a better understanding of the geotectonic setting of this large Late-Proterozoic orogenic province.

Geological Setting

The Tocantins province is a lithotectonic mega-entity of Late-Proterozoic age (1000 – 550 Ma), oriented NS and located in Central Brazil which was formed between the São Francisco and Amazon cratons during the Brasiliano orogenic cycle. It was originated by the collision of continental blocks, representing a locked system of a passive margin oceanic basin. Considering its dimensions (~ 1000 km in length and ~ 400 km wide) and the diversity of its geological terrain's, it represents the more complete remanent Late-Proterozoic orogenic chain in South America, compatible with present similar orogenic chains like the Himalayas and Alps mountains.

That province contains the metasediments of three folded belts, Brasilia to the east, and Paraguay and Araguaia, to the west, distributed around a central segment constituted by the older median massive of Goias that shows the highest degree of metamorphism (geologically complex) with characteristics of continental portions and island arcs. Despite the high level of knowledge about its geology, (Pimentel & Fuck, 1992; Fuck et al., 1994 Hasui et al., 1994; Trompete, 1994) and a good gravimetric surveying (Marangoni et al., 1995), the tectonic and structural evolution of this province is still controversial. That region has also a fair level of seismic activity, representing its modern dynamic condition that it is not known in detail. Two of the lines have been executed in the Central Portion of the Tocantins Province, as shown in the geological map of Fig. 1, that are transversal to the main lithologic units of that province and to its interface with the São Francisco craton, in the eastern extreme. The third line is located in the Southeastern portion of the province, to define its interface with the Fanerozoic Parana basin and with the São Francisco craton in this portion.

Description of the Seismic Lines

The three lines of this experiment were deployed with the same characteristics. Each line had 120 recording points, located at approximately every 2.5 km. Seven explosions were fired in each line at every 50 km, with the larger explosions at the extremes (1000 kg of emulsion explosives) and the middle one with only 500 kg. The explosives were placed inside 6" diameter x 60 to 40-m deep holes, filling up to 2/3 of the hole and the rest tamped with gravel. The seven explosions in each line were fired during two night periods.

The equipment used was 111 SGRs and L4-C short period vertical seismometers borrowed from

PASSCAL, together with Toshiba laptops and Master Clock to program the SGRs and automatic fire units to initiate the explosions. The remaining points were occupied with digital seismographs and L4-Cs belonging to the São Paulo University.

The Central Portion lines of the Tocantins Province were named as L1 and L2, for the western and eastern lines respectively. They are also shown in Fig. 2 together with the Bouguer anomaly map. The Southwestern Portion line is called L3 line. The explosions are named according to the line, such as Ex11, for explosion 1 of line L1.

Data Processing

The data recorded in the field was pre-processed at the Seismological Laboratory of USGS at Menlo Park-CA. The individual tapes of each recording point was played back to transfer the data to a larger tape, making also time correction for each station and converted to SEG-Y format. This converted data is being processed in Brazil by using the SU package. Some of the sections are presented in Fig. 3 (for line L1) and in Fig. 4 is presented a reduced section of the explosion Ex11 of this line. In Fig. 5 we present the seismic section of explosion Ex34 (for line L3) that shows a poor quality data. In Figs. 6 and 7 we present the reduced sections for explosions Ex31 and Ex34, respectively, and in Figs. 8 and 9 are the theoretical models of these sections.

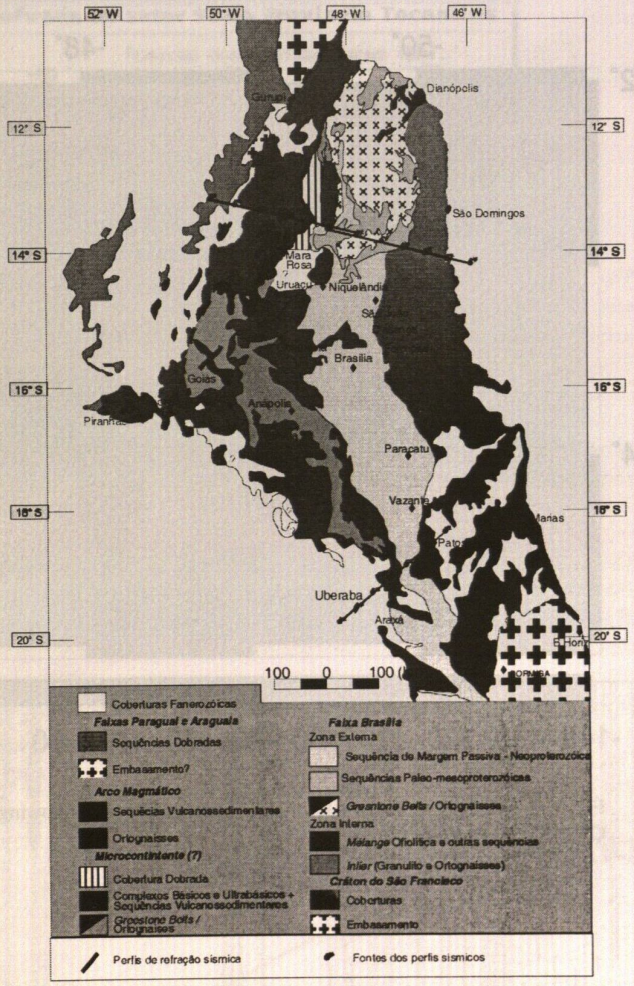

Figure 1 - Geological map of the Tocantins Province showing the deep seismic refraction lines.

Bibliography

Fuck, R.A.; Pimentel, M.M.; Silva, L.J.H.D.. Compartimentação tectônica na porção oriental da Província Tocantins. In: SIMPÓSIO DE GEOLOGIA DO CENTRO -OESTE, 4, Anais, Brasília, SBG, p 215-216, 1994.

Hasui, Y.; Costa, J.B.S.; Haralyi, N.L.E.. Estrutura em Quilha Brasil Central, uma feição fundamental na geologia de Goiás e Tocantins. *Revista Bras. Geociênc.*, São Paulo, v.13, p. 2, p. 463-97, 1994.

Marangoni, Y.R.; Assumpção, M.; Fernandes, E.P.. Gravimetria em Goiás, Brasil, *Revta. Bras. Geof.*, *13*, p. 205-220, 1995.

Pimentel, M. M.; Fuck, R. A.. Neoproterozoic crustal accretion in central Brazil, *Geology*, *20*, p. 375-379, 1992.

Trompette, R.. Geology of Western Gondwana (2000-500 Ma), 1994.

This research is being supported by grants from FAPESP, PADCT/FINEP and CNPq.

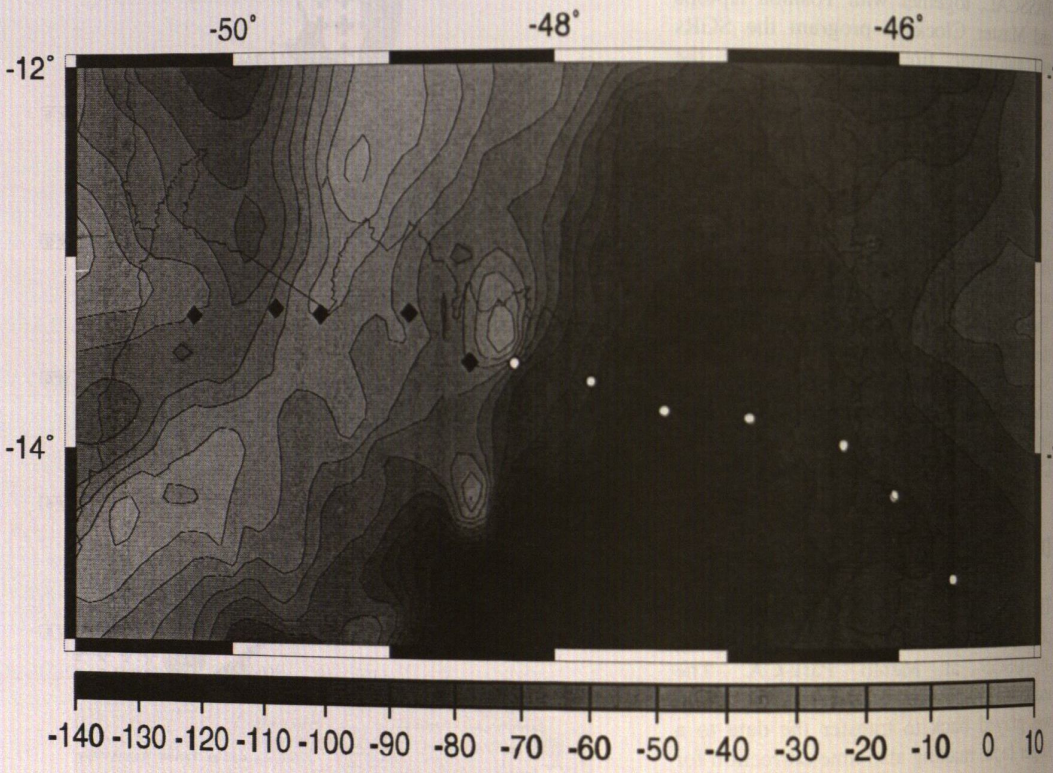

Figure 2 – Bouger anomaly map of the Tocantins Province showing the two deep refraction lines (L1 and L2) at the Central Portion of this province.

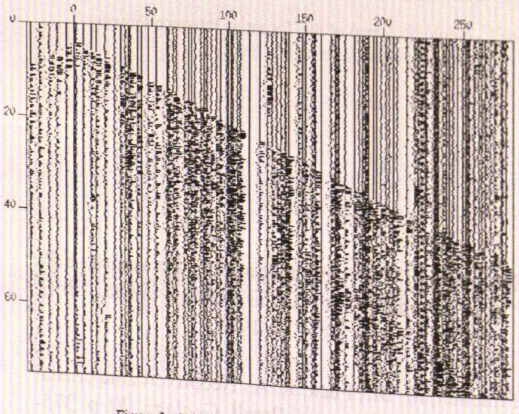

Figure 3 - Seismic section of explosion Ex11 of line L1

Figure 3 – Seismic section of shotpoint Ex11 of line L1.

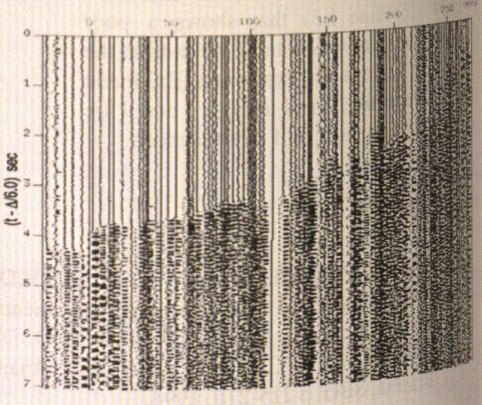

Figure 4 – Reduced seismic section of shotpoit Ex11 of line L1.

Figure 5 - Seismic section of shotpoint Ex34 of line L3

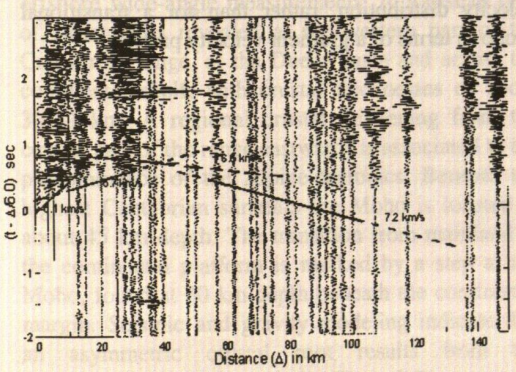

Figure 6 - Reduced seismic section of explosion Ex31 of line L3

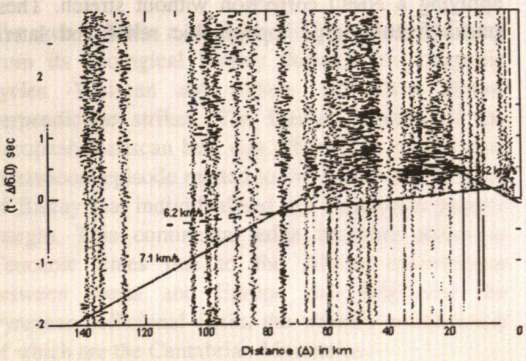

Figure 7 - Reduced seismic section of explosion Ex34 of line L3

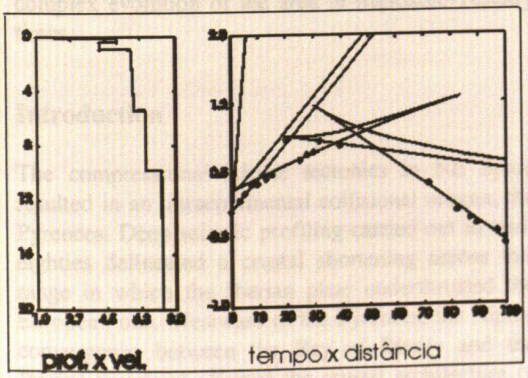

Figure 8 - Theoretical model of section shown in Fig.6

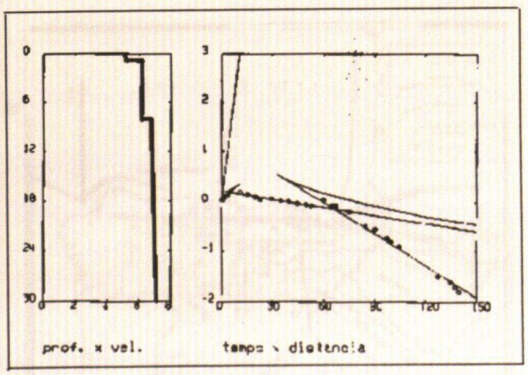

Figure 9 - Theoretical model of section shown in Fig.7

Featuring the Moho Beneath the Urals by Wide-Angle Modelling of P and S Data

R. Carbonell, J. Gallart and A. Pérez-Estaún.
Dept. of Geophysics, Inst. of Earth Sciences "Jaume Almera", CSIC, Barcelona, Spain

The Mohorovicic discontinuity in the southern Urals was imaged by the normal incidence URSEIS'95 seismic data beneath the European plate and the Siberian terranes, while it was not resolved underneath the core of the orogen. In constrast, the wide-angle reflection-refraction component of that experiment and particularly the combination of the P- and S-wave data acquired by the three component geophones place important constraints on the shape, internal structure and possible nature of the Moho. The PmP and SmS phases are characterized by low frequencies (1-6 Hz) and their signature changes along the transect. P- and S-wide-angle sections were obtained by producing a conventional stack after applying a NMO correction without stretch. These stacks feature large topographic relief and lateral changes in the seismic Moho, as well as arcuate features suggesting boudin like structures. High amplitude sub-Moho events present at the horizontal components seem to indicate further structural complexity in the upper mantle. These probably correspond to important crust mantle interactions (i.e., equilibration processes) beneath the root zone. The coda of the PmP phase, the amplitude behavior of the PmP with offset and the existence of a high frequency Pn arrival place further constraints on the internal structure of the Moho. One-dimensional reflectivity modeling of the PmP and Pn phases provides evidence for a 6 km-thick Moho consisting of approximately 600 m thick layers with a bimodal velocity distribution, rather than for a transitional Moho in terms of a gradient velocity profile.

Wide-angle seismic measurements from the Pyrenees to the Cantabrian Mountains and the North Iberian margin: evidence for the lateral extent of an Alpine crustal thickening

Josep Gallart [1], Javier A. Pulgar [2], David Pedreira [2], Jorge Gallastegui [2], Jordi Díaz [1], and Ramón Carbonell [1]

[1] Dept. Geophysics, Institute of Earth Sciences-CSIC, Barcelona, Spain
[2] Dept. Geology, Universidad de Oviedo, Spain

Abstract

The crustal architecture at the western ending of the Pyrenees, in the Cantabrian Mountains and their foreland basins has recently been studied by extensive seismic profiling on land and by onshore-offshore wide-angle measurements. A Variscan type of structure is revealed at the western part of the Cantabrian range, at the Duero basin and across the continental shelf, with crustal thicknesses of about 30-32 km. A regional crustal thickening from the central part of the range eastwards is associated to the predominance of the Alpine tectonics. Beneath the highest Cantabrian summits the Moho is located at about 45 km depth. The transition from mainland to the continental platform is marked by a step at the Moho, found at 30 km depth beneath the continental margin. Seismic and gravity modeling indicate that an asymmetric crustal root results from the southwards interaction of the Bay of Biscay crust, indenting the Iberian crust that is underthrusted towards north. Such a Pyrenean structural image is also retrieved beneath the Basque-Cantabrian basin, where further lateral variations must be related to the complex evolution of the area in Mesozoic-Tertiary times.

Introduction

The compressional Alpine tectonics in NE Spain resulted in an intracontinental collisional orogen, the Pyrenees. Deep seismic profiling carried out in mid-eighties delineated a crustal shortening across this range in which the Iberian plate underthrusted the European one. Westward of the Pyrenees, the Alpine convergence between the Bay of Biscay and the Iberian mainland affected the crustal architecture of the Cantabrian Mountains and the North Iberian continental margin. In the last 7 years, extensive controlled seismic soundings have been performed in this area, particularly refraction profiling on land and onshore-offshore wide-angle recordings (Figure 1). Most relevant data and results are reported here. The E-W and N-S seismic transects obtained provide the first 3-D image on a crustal scale of the velocity-depth distribution at the western prolongation of the Pyrenees, along the Cantabrian Mountains and their foreland basins (Fernández-Viejo et al., 1998; 1999).

The area exhibits a complex 3-D structure resulting from its geological history through two orogenic cycles -Variscan and Alpine- that show almost perpendicular strikes. The Iberian segment of the European Variscan belt was affected by a Mesozoic extensional episode related to the opening of the Bay of Biscay that individualized the Cantabrian passive margin. This continental edge becomes active in Cenozoic times due to the Alpine convergence between Iberia and Europe that originated the Pyrenean collisional chain, the western prolongation of which are the Cantabrian Mountains.

E-W transect

Profile 1 provides a 700 km long E-W transect that

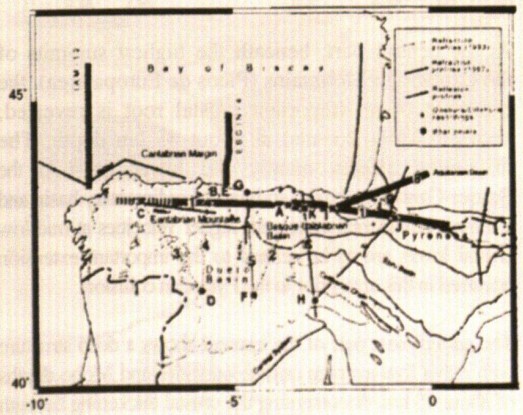

Figure 1. Simplified geological map of the study area and location of seismic profiles.

reveals the significant structural variations in the Northern Iberian Peninsula. Reversed refraction profiles have been gathered from 5 shotpoints: C, B, A, I and J (Fig. 1). Each shot (1.5 T of chemical explosives) was recorded by about 100 portable stations deployed along the profile up to 200 km offsets.

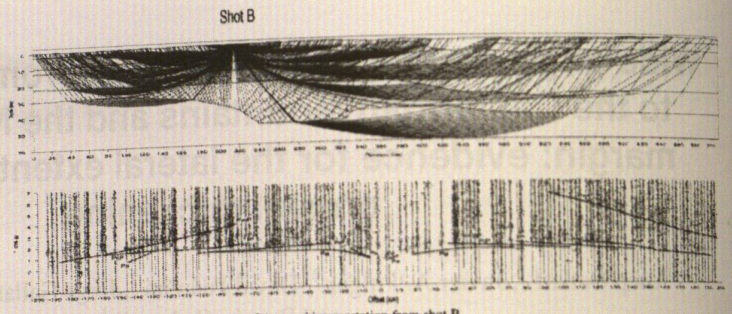

Figure 2. Refraction profile 1. Example of data and interpretation from shot B

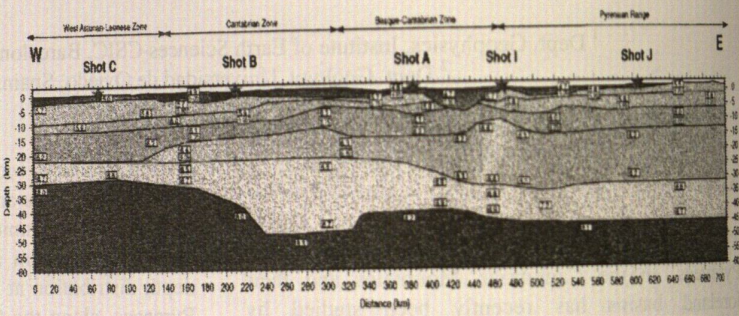

Figure 3. Velocity-depth model along profile 1, from the combined interpretation of all the data sets.

An example of these data is presented from shot B at the Cantabrian zone (Fig. 2). Panels show the ray-tracing along the interpreted model and the data with the correlated seismic phases. Ps, Pg and Pn denote refractions at the sediments, basement and upper mantle. PiP, P*, PcP and PmP mark reflections within the crust and at the Moho, respectively.

Significant lateral variations of crustal structure are documented by the differences in arrival times and relative amplitudes of deep crustal seismic phases. Note in particular the outstanding delay of about 2 s observed in the PmP arrivals towards the East with respect to the analogous phase to the West.

The final velocity-depth model is shown in Fig. 3. The western part of the Cantabrian Mountains, towards the Variscan hinterland zones and beneath the foreland Duero basin shows a Variscan-type of crustal structure. Three main levels, upper, mid and lower crust are differentiatied, with average velocities of 6.0, 6.25 and 6.8 km/s. The total crustal thickness is 30-32 km.

At the central part, beneath the highest summits of the Cantabrian Mountains (Picos de Europa area), the existence of an important crustal root is revealed, with the Moho located at about 45 km depth. The thickening affects mainly the lower crust.At the Basque-Cantabrian basin, an inverted sedimentary basin and a thinner continental crust with higher velocities at mid-low crustal levels are to be related to the important extension occurred in this area prior to the Pyrenean collision.

The easternmost part of the transect shows a deep structure with rather low-average crustal velocities and Moho depths of about 45 km, documenting the crustal thickening beneath the Pyrenean range due to the Alpine convergence between the Iberian and European plates.

N-S transects

The wide-angle data obtained from the marine reflection profiles IAM-12 and ESCIN-4 (Fig. 1) provide two North-South transects covering respectively the Variscan and the Alpine domains of NW Iberia. Examples of seismic data (receiver gathers from wide-angle recordings onshore of air-gun shots of marine profiles) are shown in trace-normalized amplitudes, 3-12 Hz band-pass filter and Vr=6 km/s (Fig. 4). Note the strong delays in arrival times and diffractions produced by the abrupt continental slope. CL marks the coastline. Main seismic phases labeled as in Fig. 2.

On the left side: western transect. Example of data obtained at station no.32 from the seismic profile IAM-12. On the right side: eastern transect. Station no. 25 illustrate the recordings on land from the marine profile ESCIN-4. Note that in this case a late phase, PmP' is observed and interpreted as a reflection on a northward deepening Iberian Moho.

Velocity-depth models (upper panel), density models (middle panel) and fitting of the gravity anomalies (lower panel) are also shown for the IAM-12 (left) and ESCIN-4 (right) transects (Figure 5). The dashed boxes in gravity models indicate the parts constrained from the seismic models. CL marks the coastline.

NE –SW transect

The seismic refraction profile 8 provides a NE-SW transect at the Western Pyrenees. The correlation of

main deep seismic phases has been established after a combined analysis of P- and S-wave data sets as illustrated in Figure 6. Note that on the P-wave section (vertical component, left panel) the dominant seismic energy between 50-120 km offsets is observed around 2 s reduced time. In the velocity-depth modeling, these arrivals will constrain an interfase at around 20-25 km depth which is doubtful to correspond to the Iberian Moho. However, the S-wave data, shown on the right panel (E-W horizontal component with a velocity reduction of 3.46 km/s and with a $\sqrt{3}$ factor at the time scale relative to the P-section), illustrate that another seismic phase, later than the previously discussed one, can be correlated with higher energy at arrival times that correspond to arrivals visible also on the P-section between 4 to 3 seconds. They can more likely mark the Moho boundary.

The velocity-depth model interpreted for profile 8 shows an imbrication between the European and Iberian crusts, analogous to that found in the ECORS-Pyrenees profile as well as in the Cantabrian Mountains transect.

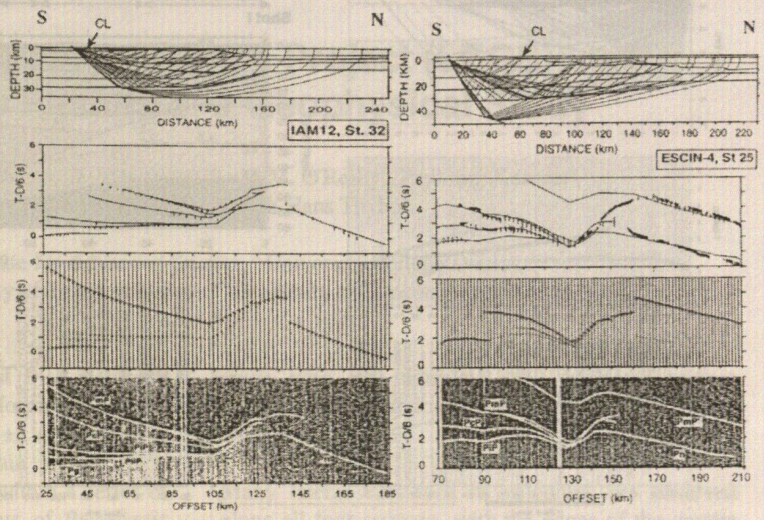

Figure 4. Examples of wide-angle data and interpretation for profiles IAM-12 (left) and ESCIN-4 (right).

Discussion and Conclusions

The new seismic data in NW Iberia constrain the westward lateral extent of the Alpine deformation that has reworked and thickened the preexisting Variscan crust. The E-W and N-S velocity-depth

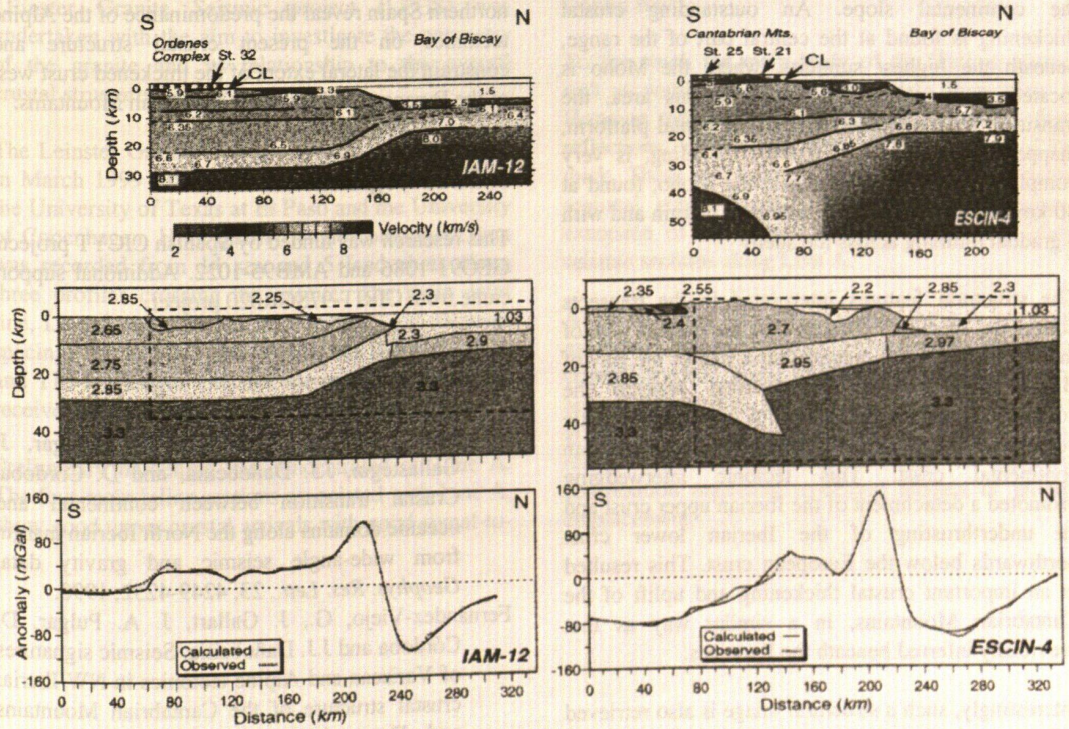

Figure 5. Velocity-depth models (upper panel), density models (middle panel) and fitting of the gravity anomalies (lower panel) in the IAM-12 (left) and ESCIN-4) transects. Velocities in km/s and densities in g/cm^3. The dashed boxes in gravity models indicate the parts constrained from the seismic models. CL marks the coastline.

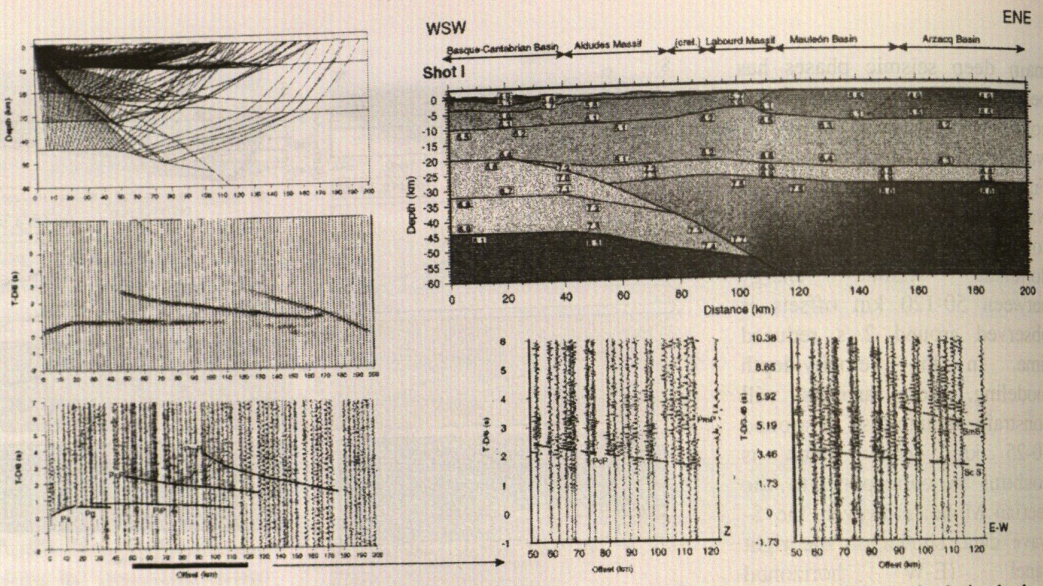

Figure 6. Data and interpretation of refraction profile 8. The upper part shows the P-record section, ray-tracing and velocity-depth model. The lower part displays for comparison a blow-up of the P-section (vertical component) and the corresponding S-section (E-W component). See text for further explanation.

transects reveal marked 3-D heterogeneities in the crustal structure. In some cases the deep crustal features could only be constrained by a combined interpretation of P- and S-wave data sets.

At the western part of the Cantabrian range, at the Duero basin and across the continental shelf a Variscan type of structure is found, with crustal thicknesses of 30-32 km and a transition to the oceanic domain marked by a rapid thinning beneath the continental slope. An outstanding crustal thickening is found at the central part of the range, beneath the highest summits, where the Moho is located at about 50 km depth. In this area, the transition from mainland to the continental platform, mapped by seismic and gravity modeling, is very complex, with a marked step at the Moho, found at 30 km depth beneath the continental margin and with a gradual thinning across the shelf.

The structural features interpreted in the transects across the western Pyrenees and the central part of the Cantabrian zone suggest that a slab of the Bay of Biscay domain was underthrusted beneath the continental margin giving rise to anomalous mantle velocities and indenting southwards the Iberian continental crust. This tectonic interwedging promoted a detachment of the Iberian upper crust and an underthrusting of the Iberian lower crust northwards below the European crust. This resulted in an important crustal thickening and uplift of the Cantabrian Mountains, in a similar way as that previously inferred beneath the Pyrenees.

Interestingly, such a structural image is also retrieved in between the Pyrenees and the Cantabrian ranges, at the Basque-Cantabrian basin. In this area, the seismic results show also significant lateral variations within upper, middle and lower crustal levels that can be related to the complex interaction between the Iberian and European plates in Mesozoic-Tertiary times, including an important crustal extension related to the opening of the Bay of Biscay and an inversion of former extensional basins during the Pyrenean orogenesis.

In summary, the new seismic data collected in northern Spain reveal the predominance of the Alpine tectonics on the present crustal structure and constrain the lateral extent of the thickened crust west of the Pyrenees, beneath the Cantabrian Mountains.

Acknowledgments

This research was funded by Spanish CICYT projects GEO91-1086 and AMB95-1022. Additional support came from CIRIT-97SGR020 project.

References

Fernández-Viejo, G., J. Gallart, J.A. Pulgar, J. Gallastegui, J.J. Dañobeitia, and D. Córdoba, Crustal transition between continental and oceanic domains along the North Iberian margin from wide-angle seismic and gravity data, *Geophys. Res. Lett.*, 23, 4249-4252, 1998.

Fernández-Viejo, G., J. Gallart, J. A. Pulgar, D. Córdoba and J.J. Dañobeitia, Seismic signatures of Variscan and Alpine tectonics in NW Iberia: crustal structure of the Cantabrian Mountains and Duero basin. *Journal of Geophysical Research* (1999) (in press).

Leinster Granite Seismic Project (LEGS): Preliminary Results of a Geophysical Study

James A. Hodgson[1], Peter W. Readman[1], Brian M. O'Reilly[1], Padhraig Kennan[2], Steve Harder[3], Randy Keller[3] & Hans Thybo[4].

[1] Dublin Institute for Advanced Studies, [2] University College Dublin, [3] University of Texas at El Paso, [4] University of Copenhagen.

The Leinster Granite is the largest Irish Batholith intruded during the Caledonian deformation. It is a post-tectonic intrusion ca 405 Ma ±2 *(O'Connor et al. 1989)*, and consists of five main plutons. It is generally poorly exposed and lies within a series of folded and thickened metasediments of Palaeozoic age.

Geological mapping has delineated the boundaries of the granite and some internal structure although its the overall geometry and depth are unknown. Gravity data shows a large low associated with the granite, generally trending NE-SW, with a minimum value of -30 mGals centred on the Tullow pluton. This negative anomaly clearly defines the surface outcrop of the granite but also continues towards the southwest, which strongly suggests that there is a substantial subsurface extension of the granite to the southwest. Structural interpretations based on gravity modelling are not well constrained, therefore the LEinster Granite Seismic project (LEGS) was undertaken with the aim to investigate the geometry of the granite and its relationship to the overall crustal structure.

The Leinster Granite Seismic project was conducted in March 1999 using 300 REFTEK TEXANS from the University of Texas at El Paso and the University of Copenhagen. High quality single component data was recorded from 14 sea and 5 land shots along three profiles crossing the granite. The main axial line, Line A was 185 km long with a 1 km receiver spacing. The two traverse lines, Lines B and C, of 70 and 110 km length intersect the axial line and have receiver spacing of 1.5 and 1.3 km respectively.

Preliminary modelling has concentrated on Line A. The four main inline sections associated with Line A, show good upper crustal arrivals with good signal-to-noise ratio that correlate well with the surface geology, and clear lower crustal and mantle phases were also observed.

Many lateral variations in velocities are observed along all four sections, with the edges of the granite well defined. A step between phases on shots 10 from Dublin Bay and A1 inland from Blessington, show the steep gradient associated with the northern units of the granite, and a slightly shallower gradient associated with the Tullow pluton is also visible. Clearly noticeable from these shots is the dramatic increase in velocity when crossing from the granite into higher velocity volcanics, which split the two main bodies of the granite. A series of shallow reflections are observed with most energy confined above 4.5 km depth, within the Northern Units of the granite. This suggests the granite in the north has a maximum depth of 4.5 km. In addition modelling also suggests the granite thins northward towards Dublin Bay.

To the south the main body of the Tullow pluton, isn't as well constrained by the data from Line A. However depths around 5 km are calculated from reflections, with the main body again at about 4 km thick. These observations are consistent with broad regional gravity trends. However the southwestern extension of the granite can not be inferred from seismic sections along Line A.

At present only the upper crust of Line A has been modelled, but with further modelling of the entire crustal structure along all three lines, and with the help of gravity data, a conclusive model of the entire granite and crustal structure will be produced. The results from this study will also make an important contribution regarding structural models of granite emplacement.

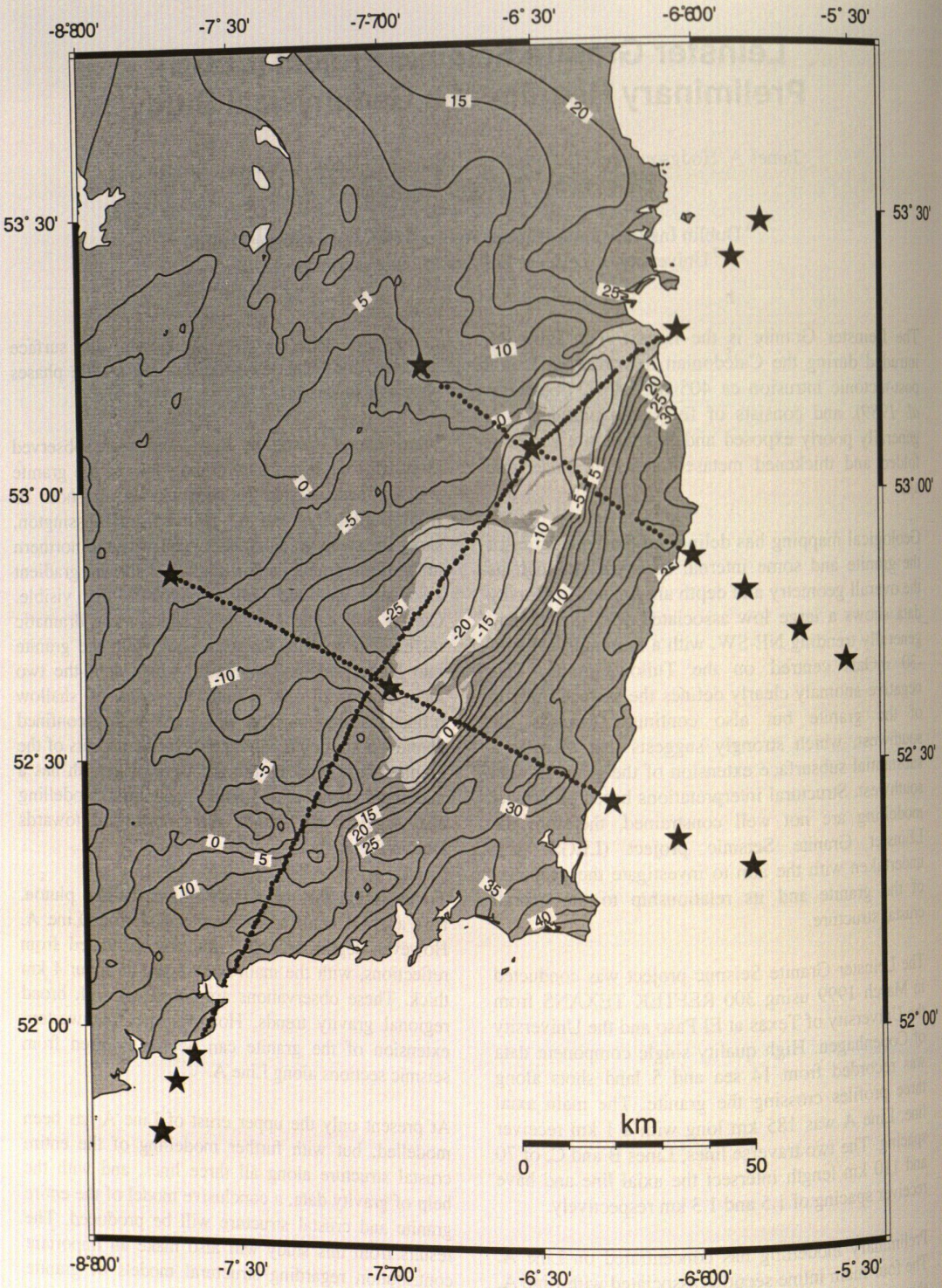

Figure 1: LEGS Experiment Layout

Low-Velocity Reflective Zone in the Upper Mantle Imaged along Peaceful Nuclear Explosion Seismic Profile Kraton

L. Nielsen (University of Copenhagen, ln@seis.geol.ku.dk)
H. Thybo (University of Copenhagen)
A. V. Egorkin (GEON Centre)

Global studies of high-density controlled source seismic data collected to offsets beyond 1000 km have revealed the "8° discontinuity" at about 100 km depth in continental areas (Thybo & Perchuc, 1997). The 100-200 km depth range below the 8° discontinuity is characterised by low seismic velocities, and scatterers inside this zone produce a long lasting coda of strong reflected secondary arrivals, which can be observed in the 700-1200 km offset range. Supplementary to the seismic interpretations Thybo & Perchuc (1997) carried out thermal modelling studies, and they propose that a partially molten zone extends from the 8° discontinuity at ~100 km depth to the Lehmann Discontinuity. The Lehmann discontinuity is detected at varying depths, depending on the thermal state of the mantle. It is shallow in "cold", cratonic regions and deep in "hot", tectonically active regions, where the partially molten zone may extend to the 400 km discontinuity. Global earth models based on earthquake sources indicate slightly reduced seismic P-wave velocities in the ~100-200 km depth range (Dziewonski & Anderson, 1981; Kennett & Engdahl, 1991). However, this low-velocity zone is a less pronounced feature in global models based on earthquake data. Ryberg et al. (1996) used ray tracing and travel time inversion of refracted and reflected seismic travel times to derive a two-dimensional P-wave velocity model for the crust and upper mantle along the ~4000 km long deep seismic sounding profile Quartz situated in northern Eurasia. At offsets larger than 800-900 km Ryberg et al. (1996) observe first arrival travel time delays of about 2.5 s in the PNE recordings, and they interpret an approximately 25 km thick lithospheric low-velocity zone below ~105 km depth along the northernmost 2000 km of profile Quartz. In the ~2000 southernmost kilometres of profile Quartz they interpret a low-velocity zone at ~150-180 km depth.

Tomographic inversion studies of Russian peaceful nuclear explosion (PNE) data collected along the 3500 km east-west striking profile Kraton (Fig. 1) has provided new information about the two-dimensional P-wave velocity structure of the upper mantle beneath the Siberian platform area (Nielsen et al., 1999). The average receiver spacing along profile Kraton is about 15 km, and the seismic data under study contain strong signals above 3 Hz. Thus, the PNE data along profile Kraton provide a unique high-resolution seismic data set for investigating the upper mantle. A striking feature in this tomographic model is a zone in the 100-200 km depth range characterised by reduced velocity and zero to

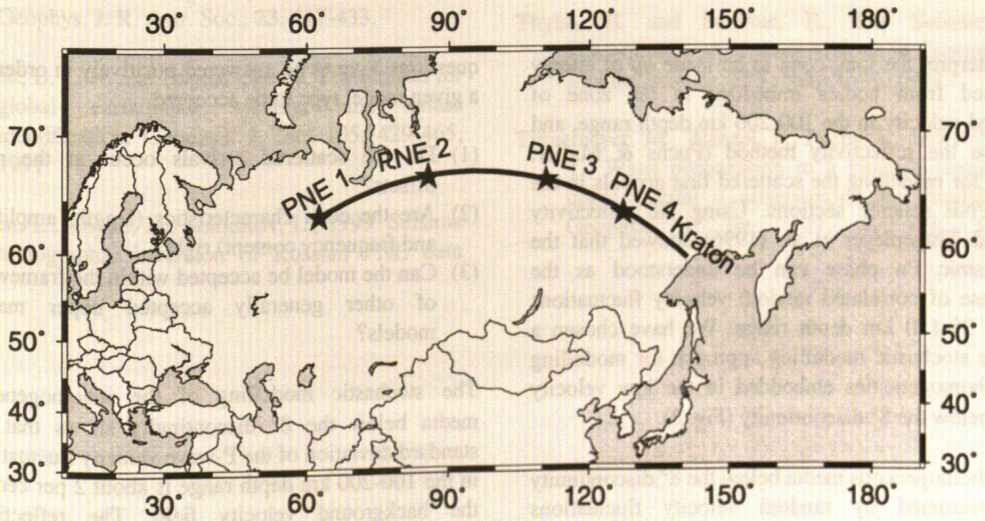

Fig. 1. Location of "Peaceful Nuclear Explosion" seismic profile Kraton. Numbered PNE's denote shot points providing data for this study.

negative vertical velocity gradient. We interpret the top of this low-velocity zone to be the 8° discontinuity.

The low P-wave velocities in the 100-200 km depth range are mainly controlled by delayed first arrivals in the 800-1300 km offset range. In the four PNE sections collected along profile Kraton these first arrivals are scattered and have an up to 5 s long coda of high amplitude (Fig. 2).

inversion. By choosing different correlation functions and standard deviations for the velocity fluctuations we generate stochastic one-dimensional velocity models for which we calculate synthetic seismograms. The calculated seismograms are compared to the four PNE sections of profile Kraton, and we judge which group(s) of stochastic models can be accepted for representing the inhomogeneous reflecting media below the 8° discontinuity and which model types have to be ruled out. Three

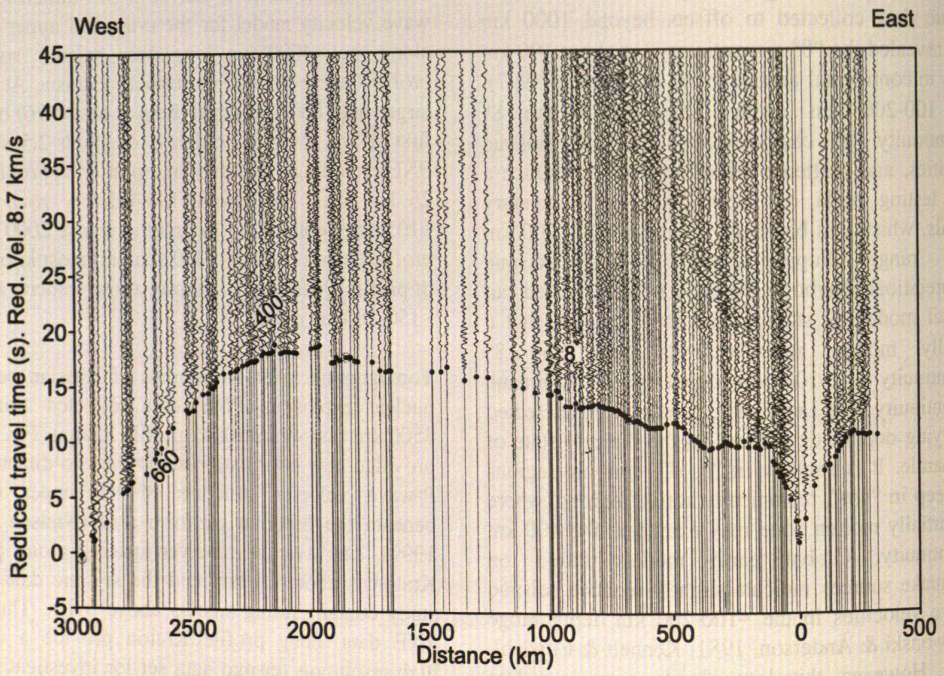

Fig. 2. Seismogram montage and first arrival travel time picks (dots) from PNE 4 plotted in reduced travel time (reduction velocity 8.7 km/s) versus offset. Secondary reflected arrivals from the 8° and the 400 km discontinuities have been marked by "8°" and "400", respectively. Please note that the digitisation of the traces starts up to 10 s before the first arrival.

We interpret the long coda to be made up of energy reflected from bodies imbedded in the zone of reduced velocity in the 100-200 km depth range, and we use the reflectivity method (Fuchs & Muller, 1971) for modelling the scattered first arrivals in the four PNE seismic sections. Using the reflectivity method Tittgemeyer et al. (1996) showed that the teleseismic Pn phase can be understood as the response of correlated random velocity fluctuations in the 35-110 km depth range. We have chosen a similar stochastic modelling approach for modelling the inhomogeneities embedded in the low velocity layer below the 8° discontinuity (Fig. 3).

The inhomogeneous media below the 8° discontinuity is represented by random velocity fluctuations superimposed onto the more smooth background velocity structure found by the tomographic

questions have to be answered positively in order for a given model type to be accepted:

(1) Do the scattered arrivals occur at the right offsets?
(2) Are the coda characteristics (length, amplitude and frequency content) right?
(3) Can the model be accepted within the framework of other generally accepted upper mantle models?

The stochastic modelling of the inhomogeneous media below the 8° discontinuity shows that the standard deviation of the P-wave velocity fluctuations in the 100-200 km depth range is about 2 per cent of the background velocity field. The reflectivity modelling indicates that the reflecting bodies are less than 15 km in thickness.

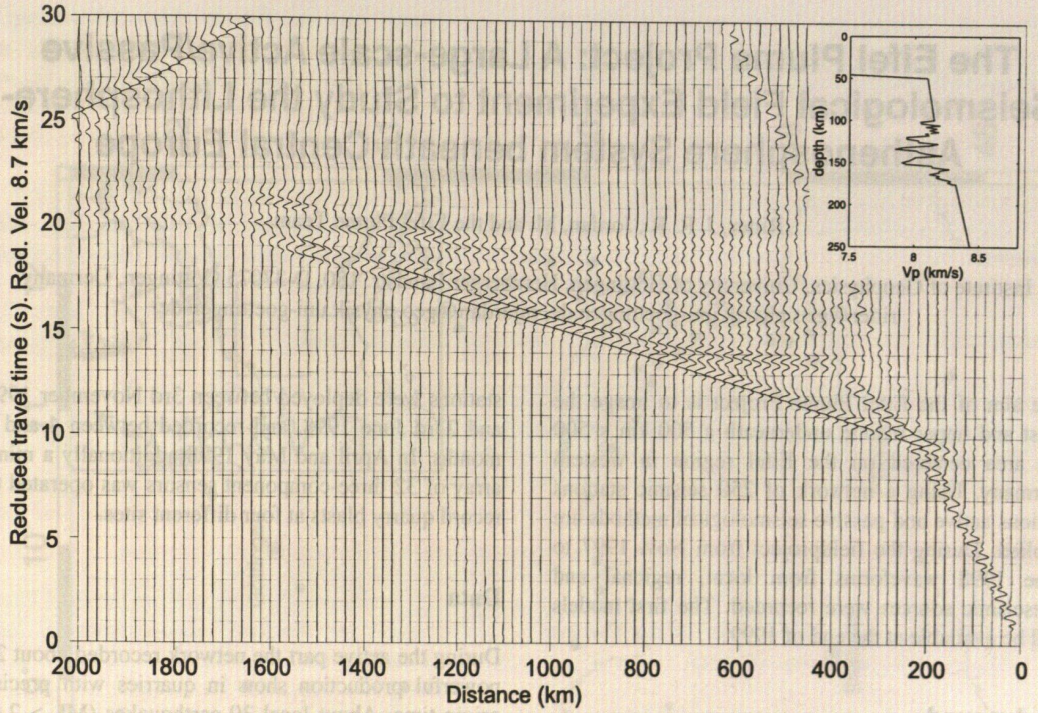

Fig. 3. Synthetic seismogram calculated by the reflectivity method. Upper right corner: Example of a 1D velocity model plotted from 0 to 250 km depth. Note random velocity fluctuations in the 100-176 km depth interval.

References

Dziewonski, A. M. & Anderson, D. L., 1981. Preliminary reference Earth model. Phys. Earth Planet. Interiors, 25, 297-356.

Fuchs, K. & Müller, G.,1971. Computation of synthetic seismograms with the reflectivity method and comparison with observations. Geophys. J. R. Astr. Soc., 23, 417-433.

Kennett, B. L. N. and Engdahl, E. R., Traveltimes for global earthquake location and phase identification, Geophys. J. Int., 105, 429-465, 1991.

Nielsen, L., Thybo, H., Solodilov, L., 1999. Seismic tomographic inversion of Russian PNE data along profile Kraton. Geophysical Research Letters. (In press).

Ryberg, T., Wenzel, F., Mechie, J., Egorkin, A., Fuchs, K. and Solodilov, L., Two-Dimensional Velocity Structure beneath Northern Eurasia Derived from the Super Long-Range Seismic Profile Quartz, Bulletin of the Seismological Society of America, 86, 857-867, 1996.

Thybo, H. and Perchuc, E., The Seismic 8° Discontinuity and Partial Melting in Continental Mantle, Science, 275, 1626-1629, 1997.

Tittgemeyer, M., Wenzel, F., Fuchs, K. and Ryberg, T., Wave propagation in a multiple-scattering upper mantle – observations and modelling, Geophys. J. Int., 127, 492-502, 1996.

The Eifel Plume Project: A Large-scale Active/Passive Seismological Field Experiment to Study the Lithosphere-Asthenosphere System beneath Central Europe

Ritter, J. R. R., Jordan, M. and the Eifel Plume Team

Institute of Geophysics, University of Göttingen, Herzberger Landstr. 180, D-37075 Göttingen, Germany
ritter@geo.physik.uni-goettingen.de, mjordan@geo.physik.uni-goettingen.de

The aim of the Eifel Plume Project is to image the crust and upper mantle underneath a 500 km x 500 km area centered on the Eifel region in western Germany. Using a network of 250 seismic stations various active and passive seismological methods are applied. During the fieldproject from Nov. 1997 to June 1998 waveforms from local, regional and teleseismic sources were recorded. The first models will be available at the end of 1999.

Background

Since 45 Ma B.P. volcanic eruptions happened in the Eifel mountains in the western part of Germany. Two volcanic fields evolved in the last 600 ka and the last eruptions occurred only 11-12 ka B.P. (e.g. Schmincke et al., 1983). At the same time strong uplift (up to 250 m in 600 ka) occurred in the region (Meyer and Stets, 1998). A previous teleseismic tomography study by Raikes and Bonjer (1983) revealed a broad zone of low-velocity material at 50 to 200 km depth beneath the Eifel region. This seismic anomaly was interpreted as hot mantle diapir or mantle plume which melts at the base of the lithosphere and provides the magmas (Neugebauer et al., 1983). A model by Granet et al. (1995) proposed that several such plumes could be found underneath the Cenozoic volcanic fields in Central Europe (e.g. Massif Central, Bohemian Massif, ...).

Field Project

The distribution of the seismic stations is displayed in Figure 1. About 160 mobile recorders were deployed in the spatial gaps between the 85 permanent stations. The closest station spacing (10-15 km) is in the centre of the network and is adjusted for crustal studies and high resolution in the mantle. At the outer areas of the network the station spacing was increased to 30-40 km. This is enough to get data required for a tomography study with a resolution of 30-50 km in the lower half of the upper mantle. A broadband array in the form of a cross consisting of 35 stations operated within the network. The mobile stations were deployed between 3rd November 1997 and 23rd June 1998, and recorded between 4 and 8 months. In April and May 1998 additionally a mini-array of 32 three-component sensors was operated to record quarry blasts at four different sites.

Data

During the active part the network recorded about 20 powerful production shots in quarries with precise origin time. About local 30 earthquakes (ML > 2.4) occurred within the network during the total recording time. More than 100 teleseisms (mb > 5.5) were recorded for the seismological studies. In Figure 2 we show two examples of the recordings. Azimuthal gaps in the teleseismic source distribution are filled with recordings at the permanent stations with events from the last decade.

Planned Investigations

The records of the few local earthquakes are used for seismo-tectonic studies. Together with the data from the quarry blasts crustal tomography models will be determined. The teleseismic recordings are the basis for a regional seismic tomography down to at least 400 km depth. Receiver function analyses will show possible 3D topography of seismic discontinuities. S-wave splitting can determine anisotropy in the mantle. The teleseismic data are also used for an analysis of the scattering strength of the lithosphere. The final model for the lithosphere-asthenosphere system will be determined by integrating results from seismology, deep electromagnetic sounding, petrology and geodynamic modelling.

Eifel Plume Team

U. Achauer (Strasbourg), G. Bock (Potsdam), G. Bokelmann (Stanford), M. Budweg (Göttingen/Potsdam), T. Camelbeeck (Bruxelles), U. Christensen (Göttingen), F. Collin (Bruxelles), N.

Fig. 1

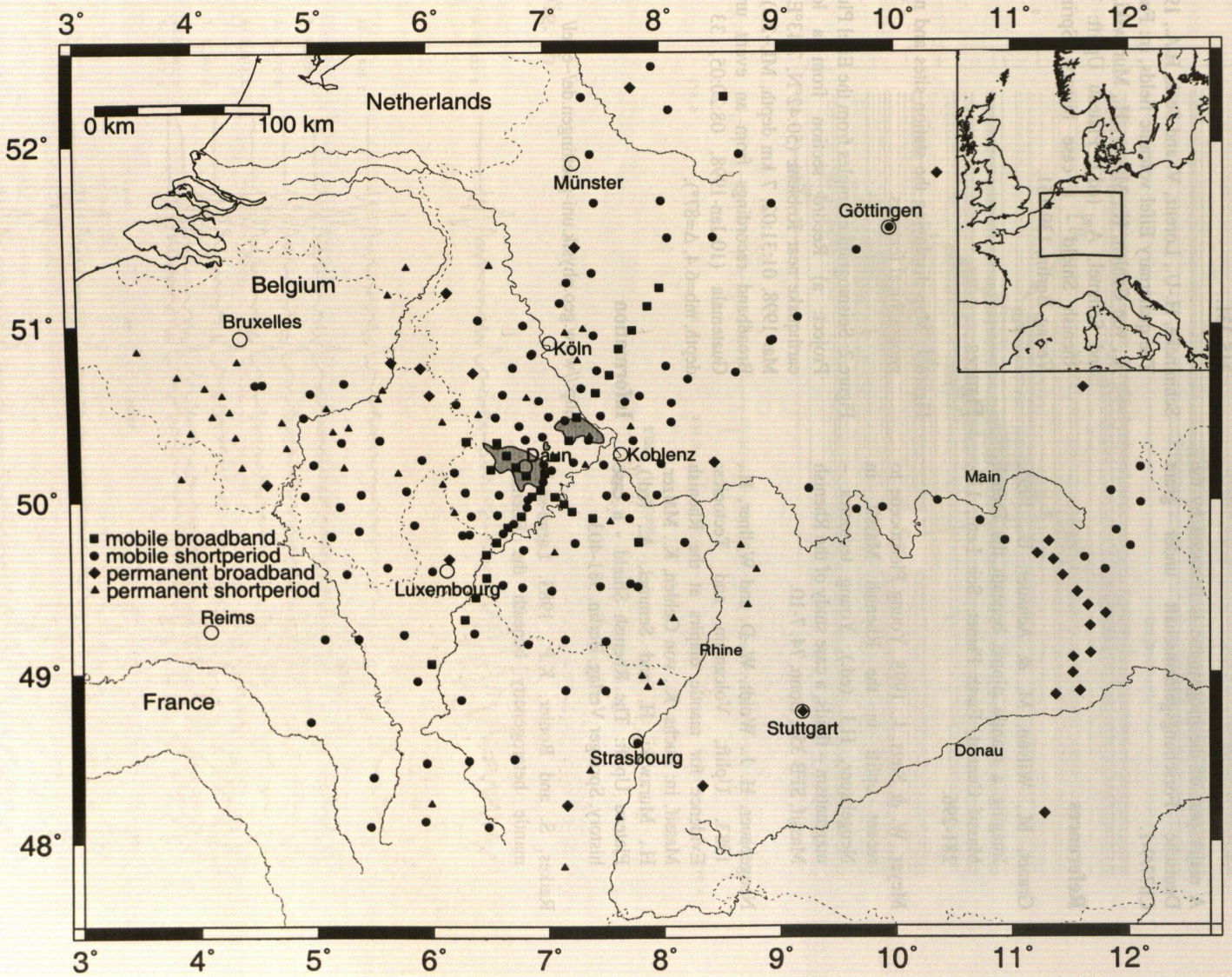
3°
4°
5°
6°
7°
8°
9°
10°
11°
12°
52°
51°
50°
49°
48°
0 km
100 km
Netherlands
Belgium
France
Münster
Göttingen
Bruxelles
Köln
Bonn
Koblenz
Main
Rhine
Luxembourg
Reims
Stuttgart
Strasbourg
Donau
mobile broadband
mobile shortperiod
permanent broadband
permanent shortperiod

d'Oreye de Lantremange (Walferdange), I. Eschghi (Daun), K.-G. Hinzen (Köln), M. Jordan (Göttingen), T. Kaspar (Göttingen/Köln), R. Pelzing (Krefeld), J. Ritter (Göttingen), Y.-F. Temme (Göttingen/Potsdam), M. Weber (Potsdam).

A major part of the programme is financed by the Deutsche Forschungsgemeinschaft under grant Ch77/9-1.

References

Granet, M., Wilson, M. & Achauer, U., 1995. Imaging a mantle plume beneath the French Massif Central, Earth Planet. Sci. Lett., 136, 281-296.

Meyer, W. & Stets, J., 1998. Young Pleistocene to recent uplift in the Rhenish Massif, in Neugebauer, H.J. (ed.), Young tectonics – magmatism – fluids, a case study of the Rhenish Massif, SFB 350, Bonn, 74, 7-10.

Neugebauer, H. J., Woidt, W.-D. and Wallner, H., 1983. Uplift, Volcanism and Tectonics: Evidence for mantle diapirs at the Rhenish Massif, in: Fuchs, K., von Gehlen, K., Mälzer, H., Murawski, H. and Semmel, A., (ed.), Plateau Uplift: The Rhenish Shield - a case history, Springer Verlag, Berlin, 381-403.

Raikes, S. and Bonjer, K.P., 1983. Large-scale mantle heterogeneity beneath the Rhenish Massif and its vicinity from teleseismic P-residuals measurements, in: Fuchs, K., von Gehlen, K., Mälzer, H., Murawski, H. and Semmel, A., (ed.), Plateau Uplift: The Rhenish Shield - a case history, Springer Verlag, Berlin, 315-331.

Schmincke, H.-U., Lorenz, V. and Seck, H.A., 1983. The quaternary Eifel volcanic fields, in: Fuchs, K., von Gehlen, K., Mälzer, H., Murawski, H. and Semmel, A., (ed.), Plateau Uplift: The Rhenish Shield - a case history, Springer Verlag, Berlin, 139-151.

Figures

Figure 1: Map displaying the station sites and main geographical features.

Figure 2: Seismogram examples from the Eifel Plume Project: a) Record section from a local earthquake near Koblenz (50.42°N, 7.43°E, 1-Mar-1998, 01:31:02, 7 km depth, ML~2.3), b) Broadband recordings from an event under Guatemala (10-Jan-1998, 08:20:05, 33 km depth, mb=6.4, Δ=87°).

Information

http://www.geo.physik.uni-goettingen.de/~eifel/

Fig. 2a

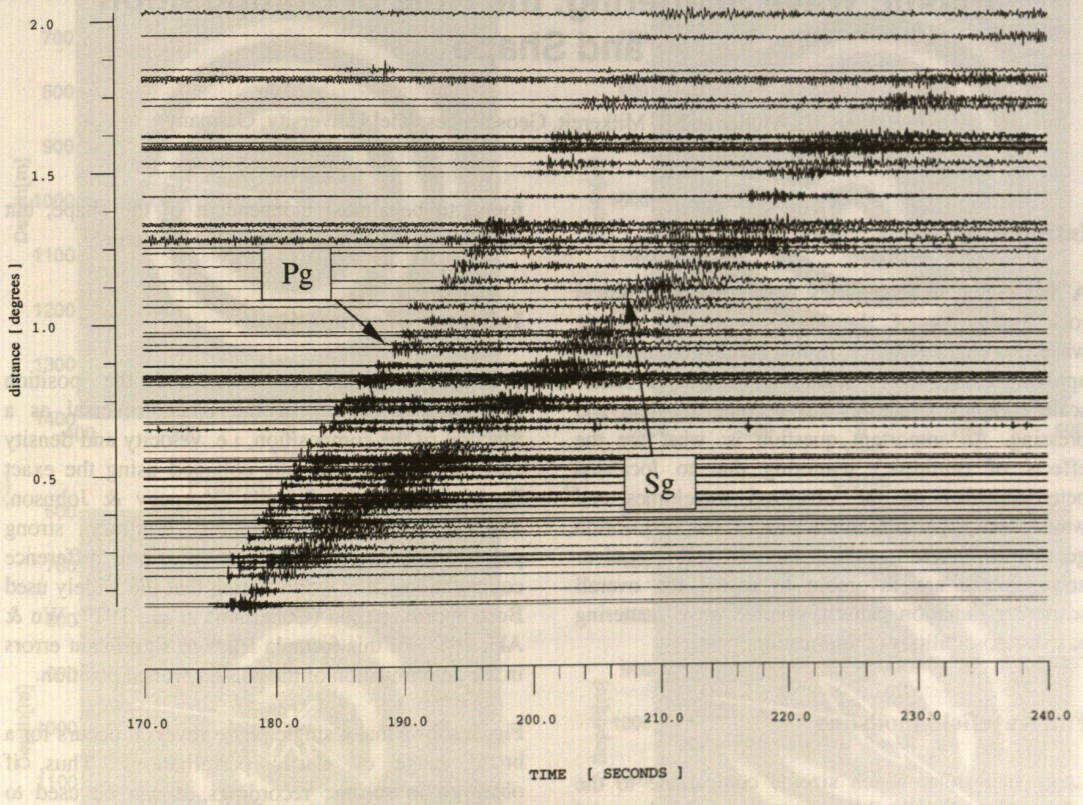
2.0
1.5
1.0
0.5
distance [degrees]
Pg
Sg
170.0
180.0
190.0
200.0
210.0
220.0
230.0
240.0
TIME [SECONDS]

Fig. 2b

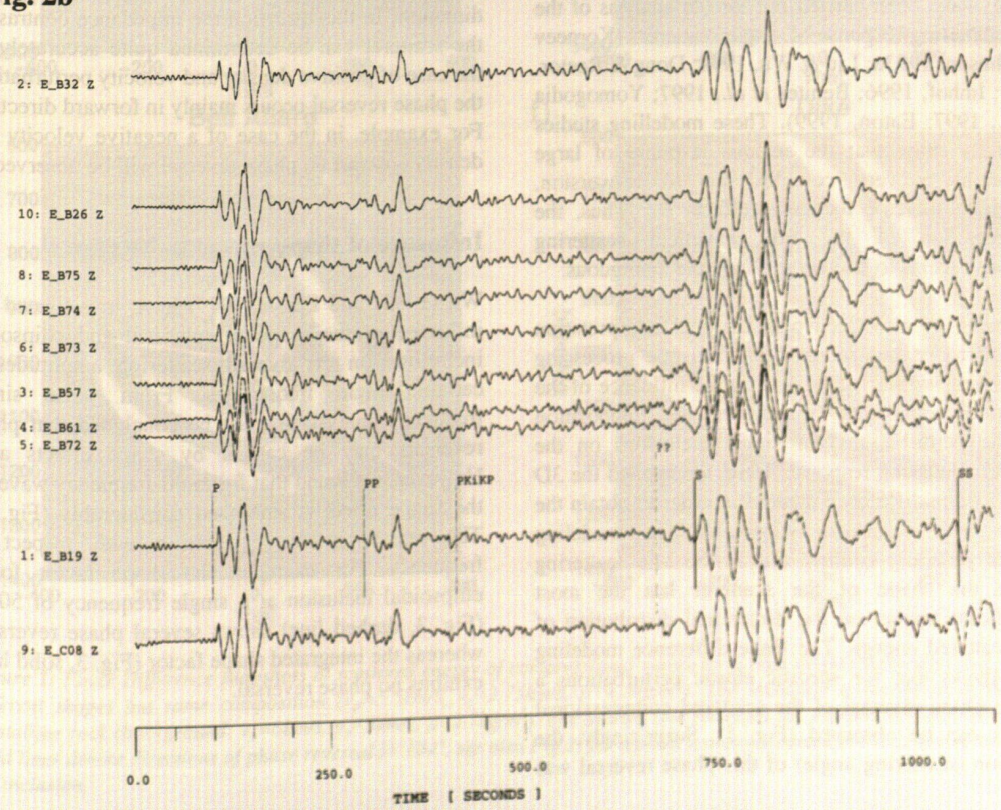
2: E_B32 Z
10: E_B26 Z
8: E_B75 Z
7: E_B74 Z
6: E_B73 Z
3: E_B57 Z
4: E_B61 Z
5: E_B72 Z
??
P
PP
PKiKP
S
SS
1: E_B19 Z
9: E_C08 Z
0.0
250.0
500.0
750.0
1000.0
TIME [SECONDS]

Elastic Wave Scattering: the Role of Composition and Shape

T. Bohlen, Cf. Müller and B. Milkereit, Geosciences, Kiel University, Germany

Introduction

A major goal in seismology is to correlate physical rock properties of the earth's crust to seismic wavefield characteristics. In this context the need for applying elastic wave scattering to analyze small-scale complex structures has become apparent and pressing. An important question is: what are the effects of (multiple) scattering due to localised heterogeneities on the observed traveltimes and waveforms. Especially in the case of VSP acquisition geometries, where the source and receiver arrangements are favorable to assess the overall scattering radiation pattern, seismic wave scattering has vast possibilities of application.

Full wavefield modeling

Large inclusions which size is comparable to the seismic wavelength (Mie scattering) are of special economical interest for example in mineral exploration. Some full wavefield forward modeling studies have been carried out for the analysis of the Mie scattering response of single scatterers (Korneev & Johnson, 1993a; Liu & Wu, 1994; Dong & Rector, 1995; Imhof, 1996; Benites *et al.*, 1997; Yomogodia *et al.*, 1997; Eaton, 1999). These modelling studies generally show that the seismic response of large inclusions is very complex due to conversion, "creeping waves", focussing effects etc. Thus, the interpretation of the full wavefield scattering response seems to be very difficult and ambiguous.

In search of an effective and robust interpretation method to be incorporated into seismic processing algorithms we started to analyze the influence of the structural complexity (shape) and the composition (elastic perturbations) of single inclusions on the seismic scattering response. Here, we applied the 3D elastic finite difference method in order to obtain the exact three-component wavefield. The modeling results generally confirm that in the Mie scattering range the shape of the scatterer has the most significant impact on the directional distribution of the scattered energy. The finite difference modeling also shows that for specific elastic perturbations a single phase reversal of the scattered compressional waves can be observed (Fig. 1). Surprisingly, the position (scattering angle) of this phase reversal was found to be almost independent of the shape, but sensitive to the composition of the scatterer.

Influence of composition

We analyzed the occurance and the position (scattering direction) of the phase reversal as a function of the composition, i.e. velocity and density contrasts (Fig. 2). Results obtained using the exact Rayleigh scattering formula (Korneev & Johnson, 1993a), which is valid for arbitrary strong perturbations, agree well with the finite difference computations. It is worth noting that the widely used Born approximation (Gubernatis *et al.*, 1977; Wu & Aki, 1985) of this formula leads to significant errors in the determination of the phase reversal position.

Fig. 2 shows that a single phase reversal occurs for a broad range of elastic perturbations. Thus, if observed in seismic recordings, it can be used to characterize the composition of the inclusion. For example, in the case of weak impedance contrasts, the phase reversal occurs mainly in backward direction. In this direction the impedance contrast of the scatterer can be determined quite accurately. In the case of positive density and velocity perturbations the phase reversal occurs mainly in forward direction. For example, in the case of a negative velocity and density contrast no phase reversal will be observed.

Influence of shape

Wu (1985) and Eaton (1999) have investigated the influence of the shape of spherical and ellipsoidal inclusions on the overall scattering amplitudes at certain single frequencies. From these single frequency analysis it must be concluded that phase reversals may be caused by shape effects also. However, we found that for multi-frequency wavelets the shape effect is smoothed considerably (Fig. 3). The reason is the integration with respect to frequency. For example, the shape factor for a ellipsoidal inclusion at a single frequency of 50 hz (Fig. 3, dashed line) shows several phase reversals, whereas the integrated shape factor (Fig. 3, solid line) exhibits no phase reversal.

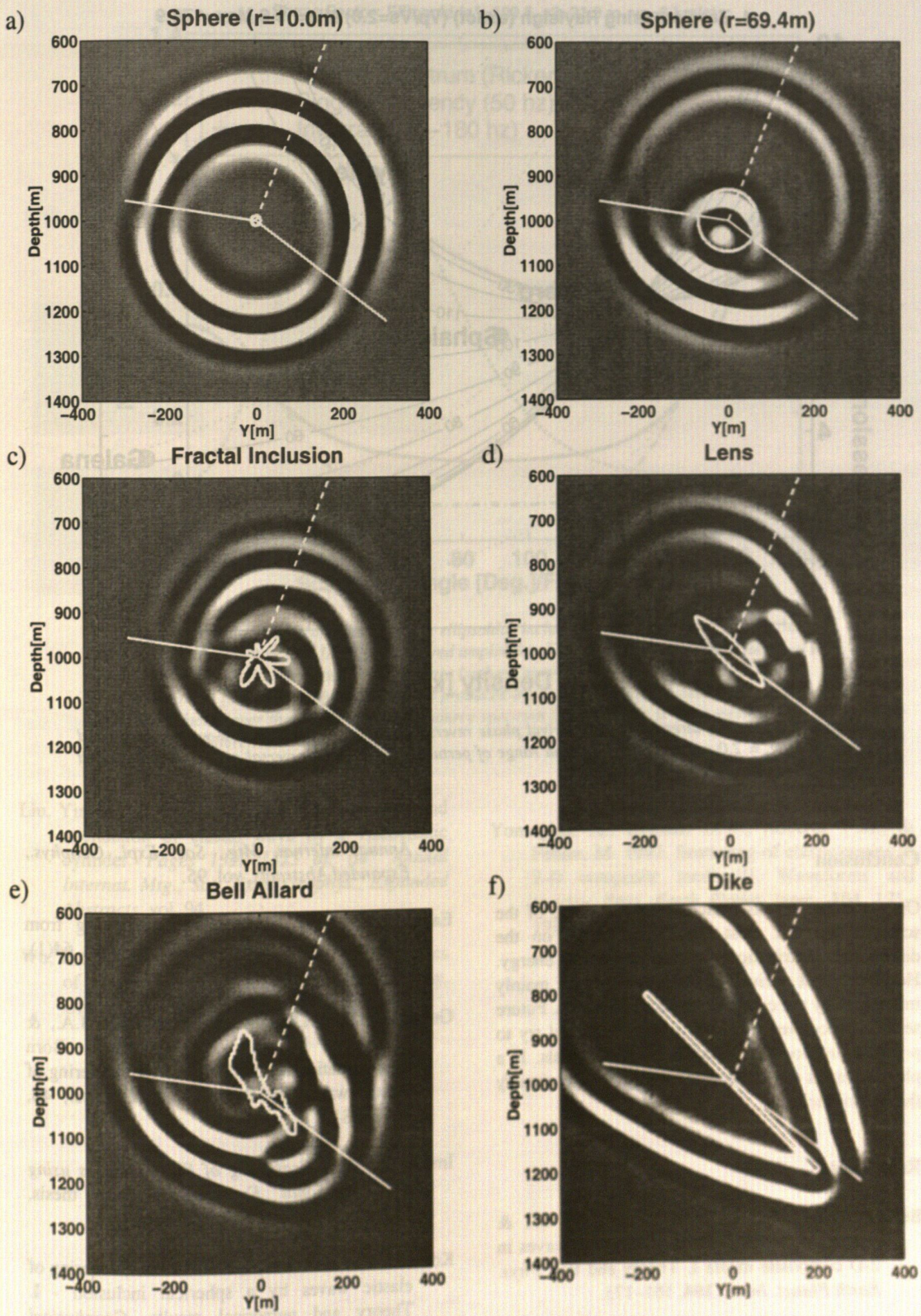

Figure 1: Finite Difference snapshots of scattered energy of compressional waves for 6 high-density inclusions (a-f) with different shapes but same composition (v_p=5.5km/s, v_s=2.75km/s, ρ=4.3kg/m^3). The inclusion is hosted in a typical crystalline rock (background: v_p=6km/s, v_s=3km/s, ρ=2.7kg/m^3). The dashed line indicates the incident ray direction, the solid lines denote directions of phase reversal (≈ 104°, see also Fig.2) for a point scatterer located at the centre of mass of the inclusion.

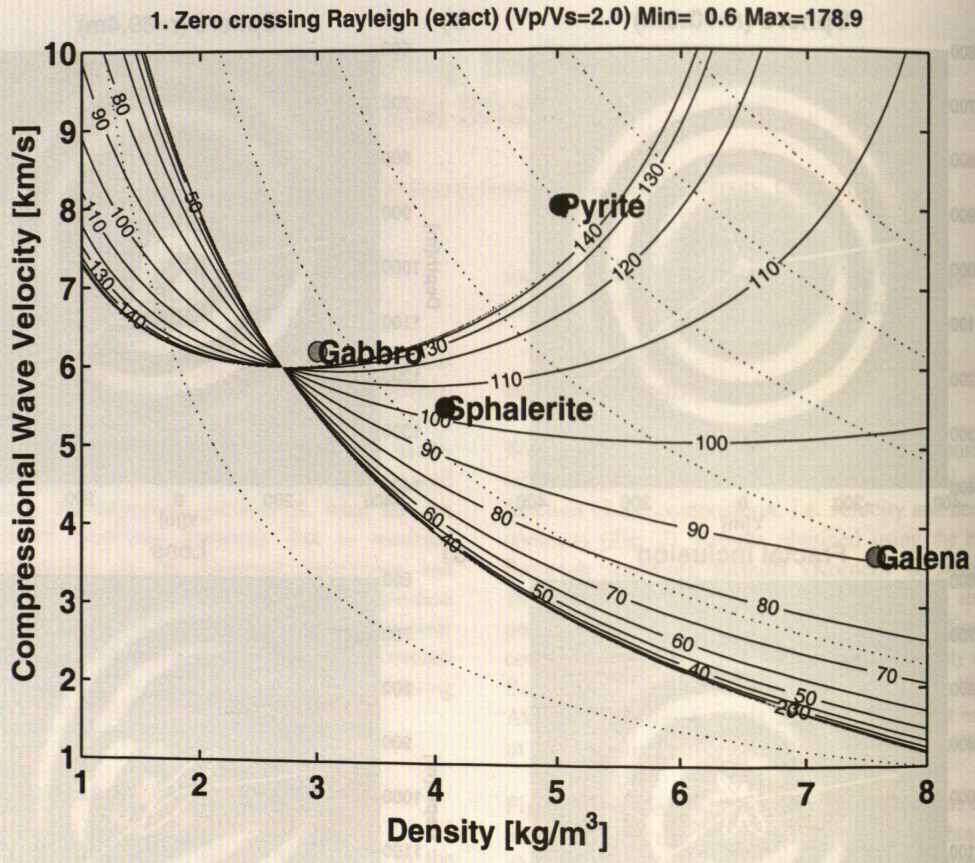

Figure 2: *Scattering direction of first arrival phase reversal as function of inclusion P-wave velocity and density (v_p/v_s = 2.0 assumed). For a broad range of perturbations a phase reversal occurs. If observed, it may help to classify the type of inclusion.*

Conclusion

Our modeling results indicate that the shape of the scatterer has the most significant impact on the directional distribution of the scattered energy. However, first arrival phase reversals are mainly influenced by the composition of an inclusion. Future seismic processing of single scatterers should try to preserve and localize possible phase reversals. If a phase reversal can be detected it may help to classify the type of inclusion.

References

Benites, D.W., Roberts, P.M., Yomogida, K., & Fehler, M. 1997. Scattering of elastic waves in 2-D composite media I. Theory and test. *Phys. Earth Planet. Inter.*, **104**, 161–173.

Dong, Q., & Rector, J.W. 1995. Seismic scattering from inclusions. *Pages 1317-1320 of: 65th Annual Internat. Mtg., Soc. Expl. Geophys., Espanded Abstracts*, vol. 95.

Eaton, D.W. 1999. Weak elastic scattering from massive sulfide orebodies. *Geophysics*, **64**(1), 289–299.

Gubernatis, J.E., Domany, E., Krumhansl, J.A., & Thompson, R.M. 1977. The Born approximation in the theory of the scattering of elastic waves by flaws. *J. Appl. Phys.*, **48**, 2812–2819.

Imhof, M. 1996. *Scattering of Elastic Waves using Non-Orthogonal Expansions*. Ph.D. thesis, Massachusetts Institute of Technology.

Korneev, V.A., & Johnson, L.R. 1993a. Scattering of elastic waves by a spherical inclusion - I. Theory and numerical results. *Geophysical Journal International*, **115**, 230–250.

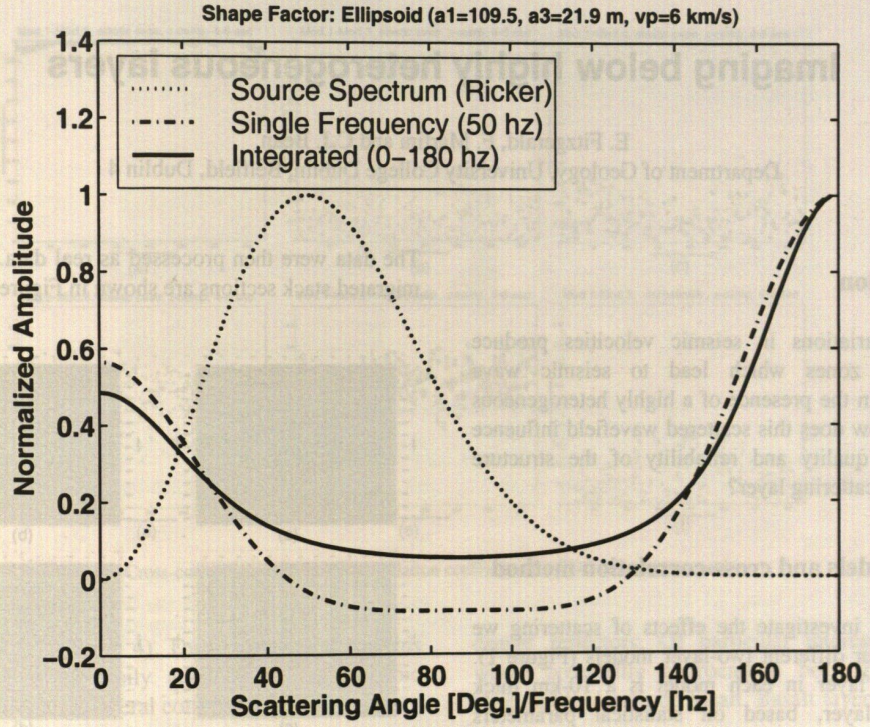

Figure 3: *Influence of the shape of the ellipsoidal inclusion (semimajor axes a_x=109.5m, a_z=21.9m) shown in Fig. 1d on the scattered amplitudes. The single frequency shape factor at 50hz (dashed line) shows two zero crossings (=phase reversals), whereas in case of a Ricker-type source function no phase reversal is produced because of a weighted summation of the shape factor over the bandwidth of the source spectrum (dotted). This is in agreement with the finite difference wavefield (Fig. 1d).*

Liu, Yin-Bin, & Wu, Ru-Shan. 1994. Scattering and attenuation of elastic wave by a viscoelastic cylinder. *Pages 1322–1325 of: 64th Annual Internat. Mtg., Soc. Expl. Geophys., Expanded Abstracts*, vol. 94.

Wu, R-S., & Aki, K. 1985. Scattering characteristics of elastic waves by an elastic heterogeneity. *Geophysics*, **50**, 582–595.

Yomogida, K., Benites, D.W., Roberts, P.M., & Fehler, M. 1997. Scattering of elastic waves in 2-D composite media II. Waveforms and spectra. *Phys. Earth Planet. Inter.*, **104**, 175–192.

Imaging below highly heterogeneous layers

E. Fitzgerald, F. Martini and C.J. Bean
Department of Geology, University College Dublin, Belfield, Dublin 4

Introduction

Random variations in seismic velocities produce anomalous zones which lead to seismic wave scattering. In the presence of a highly heterogeneous structure how does this scattered wavefield influence the image quality and reliability of the structure below the scattering layer?

Initial models and cross-correlation method

In order to investigate the effects of scattering we generate four different two-layer models (Figure 1). The upper layer in each model is a 10-km thick stochastic layer, based on statistical parameters obtained from well logs. The lower layer in each model is also 10 km thick and represents the mid to lower crustal "target" layer. It is also statistically defined but is "less scattering" then the upper crust. The layers are characterised by different values of standard deviation of the velocity fluctuations (σ) and Hurst exponent (H). In some cases they are substituted with a homogeneous layer (see below).

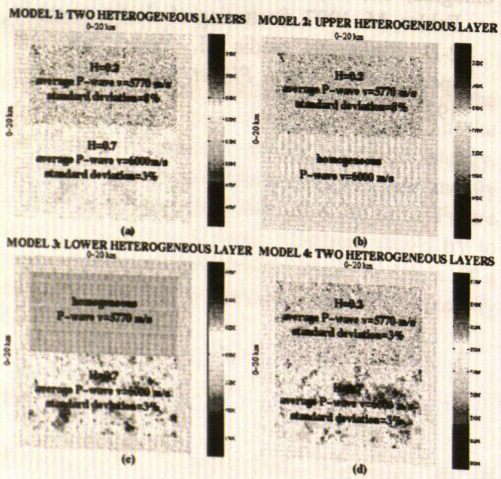

Figure 1: (a) model 1, (b) model 2, (c) model 3 and (d) model 4.

Shot gathers were generated on those models with a finite difference viscoelastic wave simulator, 8th order in space, 2nd order in time on staggered grid (Igel, 1993), for both the elastic and the viscoelastic cases. The data were then processed as real data. The final migrated stack sections are shown in Figure 2.

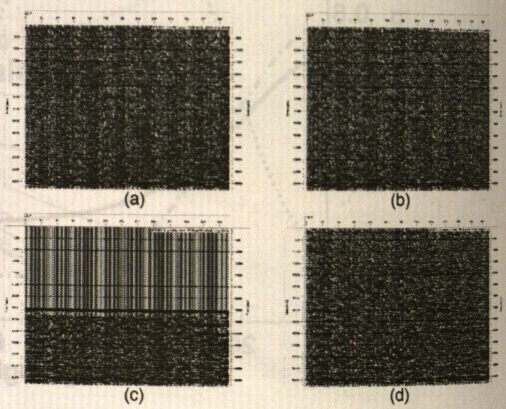

Figure 2: Final seismic sections, elastic case, (a) model 1, (b) model 2, (c) model 3 and (d) model 4.

To compare results from different models we calculated the cross-correlation coefficient between correspondent traces in the sections, in a 4-6 sec window, corresponding to the bottom layer: if the two datasets are similar, the cross-correlation tends to one, if they are unlike, it tends to 0. The results are shown in Figure 3.

From the results it is evident that multiple scattering in the top layer ensures waves continue to be recorded at time/depths corresponding to the bottom layer, which is then not properly imaged: 4-6 TWT sec window in Model 1 and 2 are almost identical. The amount of multiple scattering is controlled by the standard deviation of the velocity fluctuations in overlying layers, values of which can be obtained from superdeep borehole data. Important observation is that viscoelasticity reduced the degree of contamination: therefore it seems that in a strong scattering regime, a low intrinsic Q can improve imaging of lower structures.

To see how this scattering influences the imaging of a deep reflector, we add a strong deep reflector to our first model. The reflector is a 160-m thick homogeneous layer and has an average reflection coefficient of 0.1. Following the same procedure to generate and process the data, we obtained a final stack section: the reflection associated with the thin layer at depth shows variation in amplitude, timing

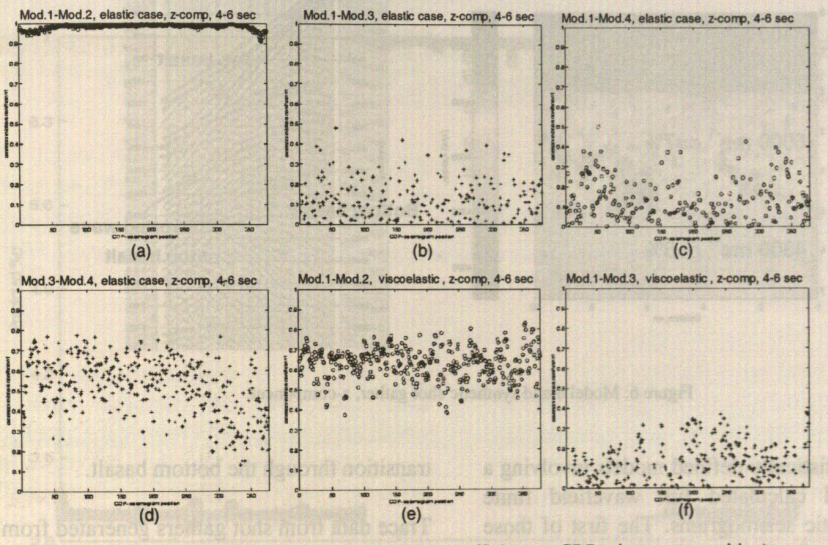

Figure 3: Cross-correlation plots (cross-correlation coefficient vs. CDP-seismogram position).

and thickness (Figure 4). During interpretation this character can be easily attributed to topographic variation or lack of lateral continuity.

deeper reflectors. Of particular interest are areas where potentially hydrocarbon bearing strata are obscured by layers of basalt. Basalt layers are highly

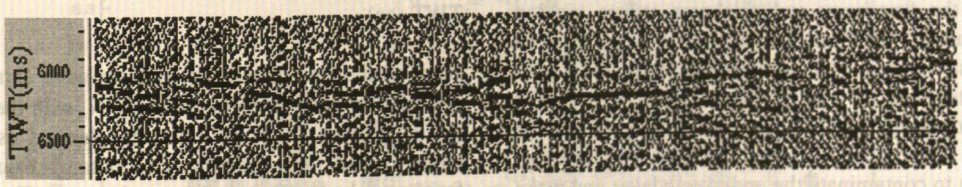

Figure 4: Final-stack section, 5.6-6.7 seconds window from model 1 with a strong deep reflector added.

A specific example: imaging below basalt layers

In many areas of the world the presence of high velocity layers makes it difficult to seismically image reflective and heterogeneous, Conventional seismic techniques usually fail to image not only reflectors below the basalt but even the bottom basalt. Here, we aim to investigate the role played by internal scattering in controlling image quality and what are the controlling factors in the amount of scattering generated.

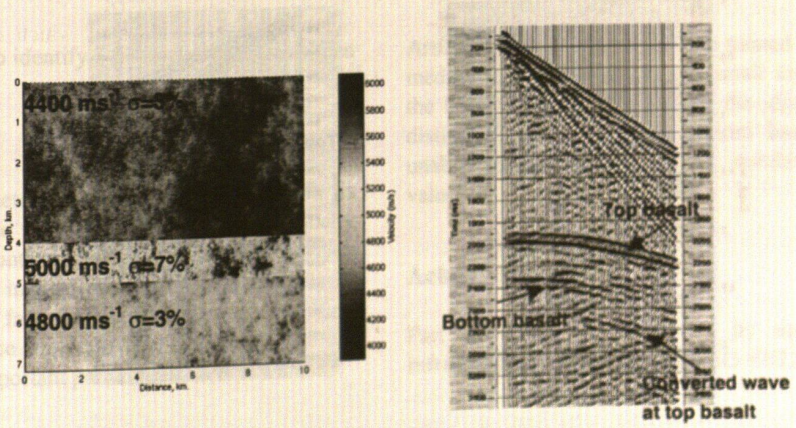

Figure 5: Model 5 and synthetic shot gather, z-component.

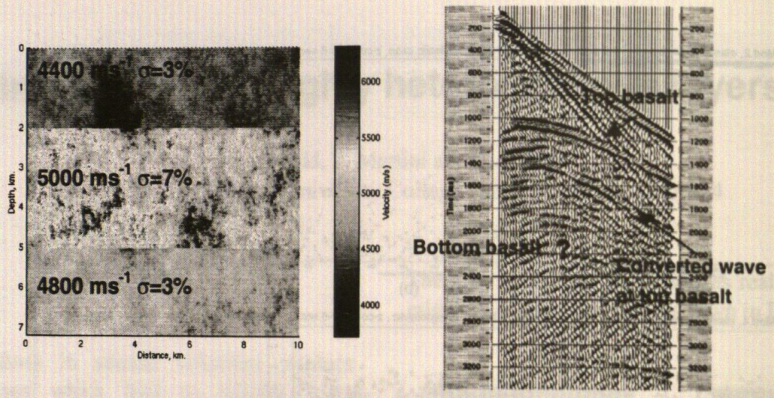

Figure 6: Model 6 and synthetic shot gather, z-component.

We produced statistically defined models involving a basalt layer and calculated full wavefield finite difference synthetic seismograms. The first of those models (model 5, fig.5) has a basalt thickness of 1 km and a source frequency of 12 Hz: in this case we can identify the bottom basalt. In the model 6 (fig.6) we changed the basalt thickness to 3 km and in model 7 (fig.7) the source frequency to 35 Hz: in both cases the bottom basalt is not identifiable. This is controlled by the number of cycles within the basalt layer: the frequency and thickness values yield a maximum of 4.8 P-wavelengths in the basalt layer in the first case and 14 P-wavelengths in the other two. Our interpretation is as follows: in the first case there are not enough wavelengths propagating within the basalt to produce a large amount of scattering, enough to contaminate the underlying layer and make it difficult to identify the bottom basalt.

Use of Artificial Neural Networks (ANN)

Given the difficulty in identifying the bottom basalt in some of the scenarios, above, we wanted to see if we can invert for medium statistics based on seismic character using ANN as a way of identifying transition through the bottom basalt.

Trace data from shot gathers generated from Model 7 were used to train a neural network to invert for medium statistics beneath the basalt layer on the shot gathers. We used a dataset of 18 NMO corrected shot gathers. The trace data for ANN training were divided in three sections to represent the three different layers in the model (layer 1: 0.3-0.7 TWT sec, layer 2: 0.75-1.16 TWT sec, layer 3: 1.17-1.35 TWT sec).

Horizontal slices of the shot gathers were extracted and used as input patterns to the ANN, with the σ of the layer from which the data were derived used as target output. The training set contains examples from each layer. The results are shown in Figure 8. The ANN has clearly identified 3 distinct layers.

We then decided to restrict the training examples to data from layer 1 and 2 only. By restricting the training set we investigate the ability of an ANN to predict vertically on seismic data for which it has no a-priori information on. This ANN was unable to predict the correct σ for each layer but the trained

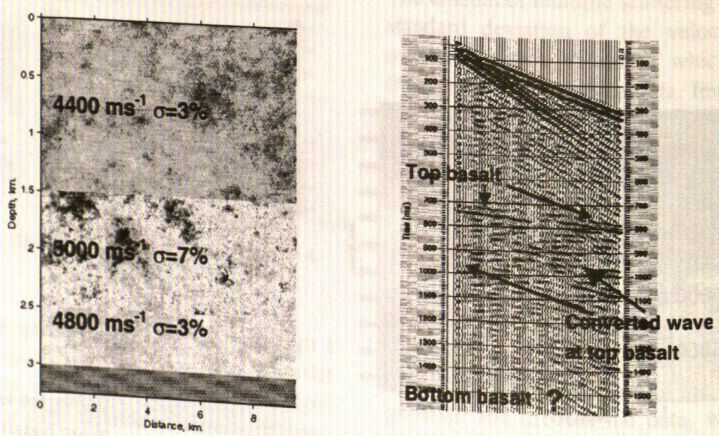

Figure 7: Model 7 and synthetic shot gather, z-component.

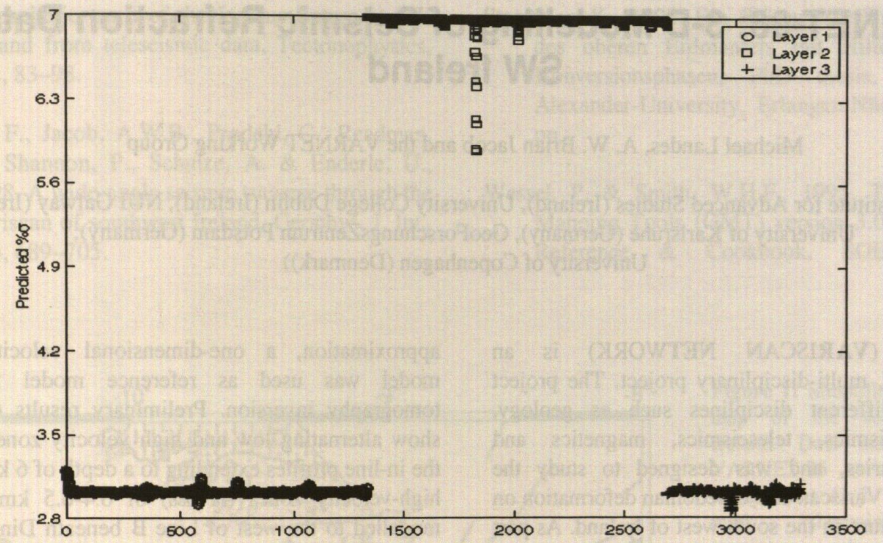

Figure 8: Standard deviation prediction results for the total dataset, using the ANN trained on a quarter of the available data.

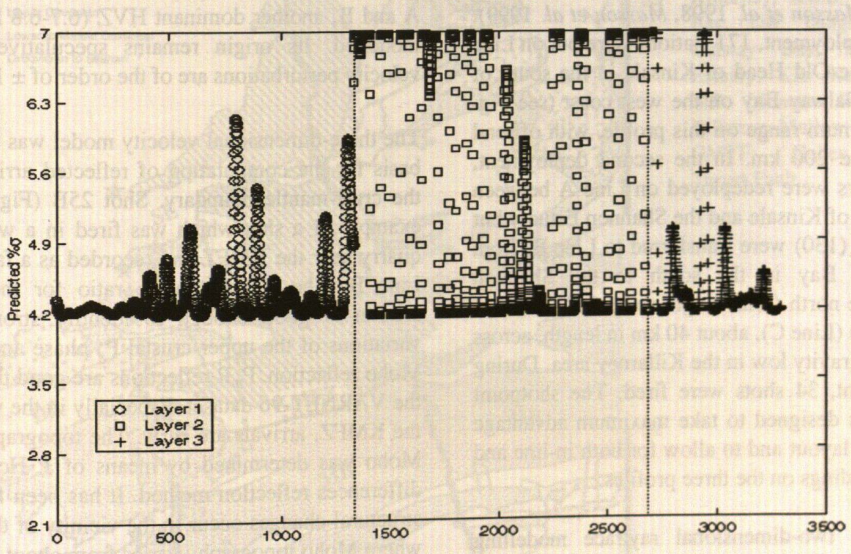

Figure 9: Standard deviation prediction results for the total dataset, using the ANN trained on a restricted subset of the data.

ANN was able to identify 3 distinct packages, as seen in Figure 9.

Conclusions

Scattering in heterogeneous structures –which is controlled by the standard deviation of the velocity fluctuations – contaminates deeper structures, which are not properly imaged. The number of cycles/layer is a controlling factor for the amount of scattering generated. Source frequency and layer thickness are consequently important parameters.

Artificial Neural Networks were trained to invert for medium statistics beneath the basalt layer and find the bottom basalt. This enabled the identification of distinct layers, and hence bottom basalt, even if unable to predict the correct standard deviation values.

Acknowledgements

Part of this work is funded by the Petroleum Infrastructure Project, project RSG 97/21.

VARNET-96: 3-D Modelling of Seismic Refraction Data, SW Ireland

Michael Landes, A. W. Brian Jacob and the VARNET Working Group

(Dublin Institute for Advanced Studies (Ireland), University College Dublin (Ireland), NUI Galway (Ireland), University of Karlsruhe (Germany), GeoForschungsZentrum Potsdam (Germany), University of Copenhagen (Denmark))

VARNET (**VARI**SCAN **NET**WORK) is an international, multi-disciplinary project. The project integrates different disciplines such as geology, gravity, seismics, teleseismics, magnetics and magnetotellurics, and was designed to study the influence of Variscan and Caledonian deformation on crustal structure in the south-west of Ireland. As part of the seismic survey, three refraction / wide-angle reflection profiles were completed in two deployments in June 1996 (Lines A, B and C; *Landes et al.* 1999, *Masson et al.* 1998, *Masson et al.* 1999). In the first deployment, 171 stations were put on Line A between the Old Head of Kinsale in the south of Ireland and Galway Bay on the west coast (see Fig. 1). The maximum range on this profile, with off-end shots, is some 200 km. In the second deployment, some receivers were redeployed on Line A between the Old Head of Kinsale and the Shannon Estuary but most of them (130) were transferred to Line B, from Roaringwater Bay in the south to the Shannon Estuary in the north (total length some 140 km), and a short profile (Line C), about 40 km in length, across a prominent gravity low in the Killarney area. During the experiment, 34 shots were fired. The shotpoint geometry was designed to take maximum advantage of the profile layout and to allow for both in-line and fan shot recordings on the three profiles.

Results from two-dimensional raytrace modelling indicate a multi-layered crust. The upper crust, extending to a depth of about 14 km, is laterally variable. South of the Shannon Estuary sedimentary basins alternate with uplifted basement (5.8-6.0 km/s). This correlates well with the surface geology. The middle crust shows structural changes beneath the Shannon Estuary which coincide with the proposed location of the Iapetus Suture Zone. The total crustal thickness varies from 29-32 km.

The target region for the three-dimensional raytrace and inversion modelling was confined to the area to the south of the Shannon Estuary. Checkerboard resolution tests for the survey geometry have indicated that the spatial resolution of the area is about 30 km, while boundaries of resolved bodies are defined to within about 10 km. As a first approximation, a one-dimensional velocity-depth model was used as reference model for the tomography inversion. Preliminary results (Fig. 2) show alternating low and high velocity zones along the in-line profiles extending to a depth of 6 km. Two high-velocity zones (HVZs) of 6.4-6.5 km/s were modelled to the west of Line B beneath Dingle Bay and the mouth of the Kenmare River. The HVZs may be associated with major east-west trending Variscan features. In the South Munster Basin, between Lines A and B, another dominant HVZ (6.7-6.8 km/s) was modelled. Its origin remains speculative. Overall velocity perturbations are of the order of ± 10%.

The three-dimensional velocity model was taken as a basis for the computation of reflected arrivals from the crust-mantle boundary. Shot 25B (Fig. 3) is an example of a shot which was fired in a water-filled quarry near the KMFZ and recorded as a fan shot on Line B. The signal-to-noise ratio for the seismic section is good enough to identify strong lateral variations of the upper crustal P_g phase and the P_mP Moho reflection. P_mP reflections are good throughout the VARNET-96 dataset. Especially in the vicinity of the KMFZ, arrivals are early. The topography of the Moho was determined by means of J. Hole's finite differences reflection method. It has been found that structural changes occur in the vicinity of the KMFZ where Moho topography varies from about 27-28 km in the south of Ireland to about 32-33 km towards the Shannon Estuary (Fig. 3).

References

Hole, J.A. & Zelt, B.C, 1995. 3-D finite-difference reflection traveltimes, Geophys. J. Int., 121, 427–434.

Landes, M., Prodehl, C., Hauser, F., Jacob, A.W.B., Vermeulen, N.J. & Mechie, J., 1999. VARNET-96: Influence of Variscan and Caledonian orogenies on crustal structure in SW Ireland. Submitted to Geophys. J. Int.

Masson, F., Hauser, F. & Jacob, A.W.B., 1999. The lithospheric trace of the Iapetus Suture in SW Ireland from teleseismic data, Tectonophysics, 302, 83–98.

Masson, F., Jacob, A.W.B., Prodehl, C., Readman, P., Shannon, P., Schulze, A. & Enderle, U., 1998. A wide-angle seismic traverse through the Variscan of southwest Ireland, Geophys. J. Int., 134, 689–705.

Stammler, K., 1992. Ein Beitrag zur Untersuchung des oberen Erdmantels mit Hilfe von PS-Konversionsphasen, PhD thesis, Friedrich-Alexander-University, Erlangen-Nürnberg, 175 pp.

Wessel, P. & Smith, W.H.F., 1995. The Generic Mapping Tools (GMT) version 3.0: Technical Reference & Cookbook, SOEST/NOAA.

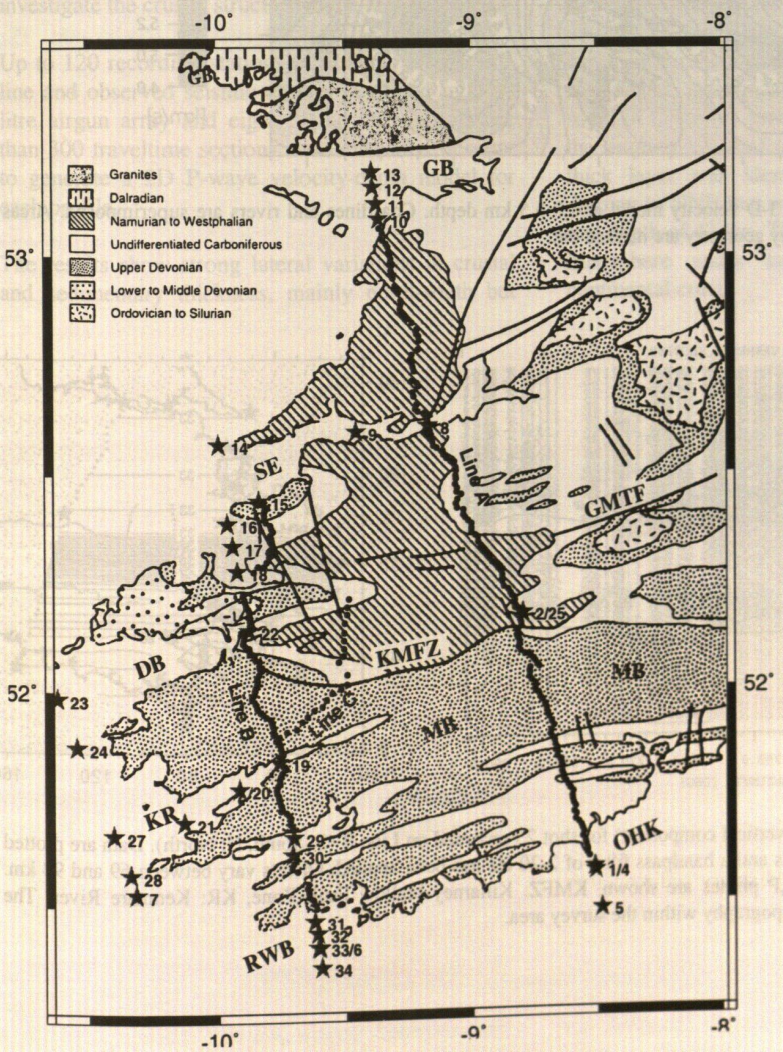

Figure 1: Simplified geological map of the south-west of Ireland. Dots mark sites of VARNET-96 seismic stations along Lines A, B and C, stars mark shotpoints. Thin continuous lines indicate mapped surface faults. OHK: Old Head of Kinsale, K: Killarney, RWB: Roaringwater Bay, DB: Dingle Bay, GB: Galway Bay, SE: Shannon Estuary, KR: Kenmare River, MB: Munster Basin, KMFZ: Killarney-Mallow Fault Zone, GMTF: Galtee Mountains Thrust Fault.

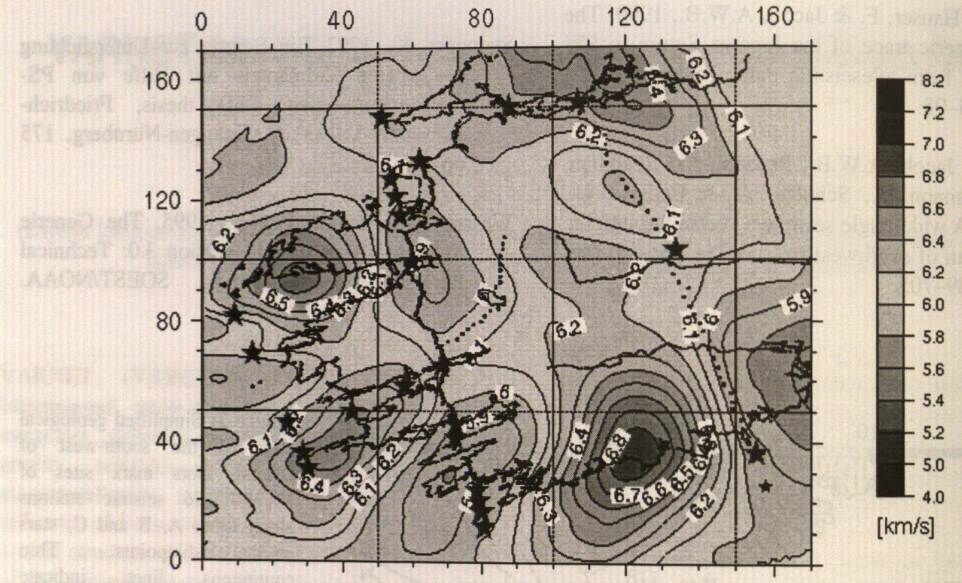

Figure 2: Horizontal slice of the 3-D velocity model at 6.0-6.5 km depth. Coastlines and rivers are superimposed. Areas which are not covered by the survey geometry are masked out.

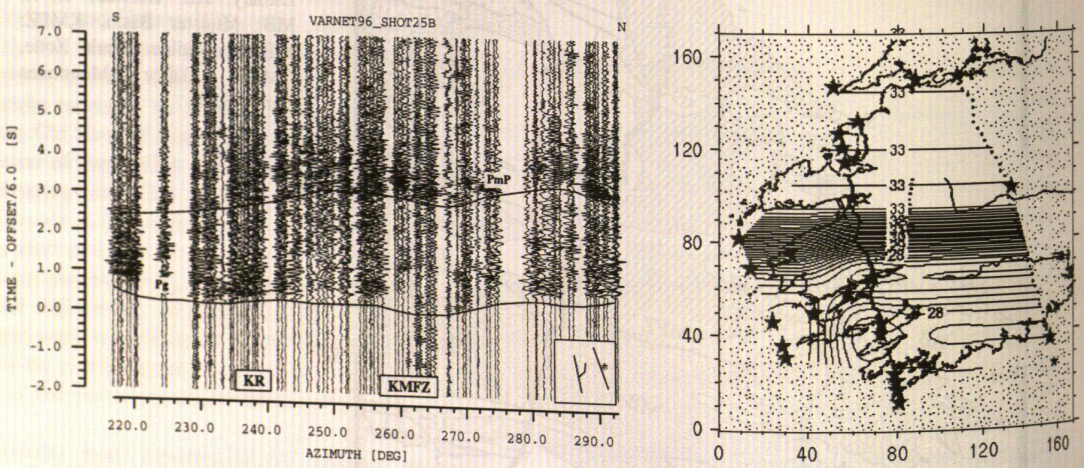

Figure 3: P-wave record section (vertical component) for shot 25 recorded on Line B (S: South, N: North). Data are plotted with a reduction velocity of 6 km/s and a bandpass filter of 2-20 Hz has been applied. Offsets vary between 69 and 94 km. Correlated arrivals for P_g and P_mP phases are shown. KMFZ: Killarney-Mallow Fault Zone, KR: Kenmare River. The picture to the right shows Moho topography within the survey area.

Crustal Investigation of the Hellenic Subduction Zone Using Wide Aperture Seismic Data

Jannis Makris, Marco Bohnhoff

University of Hamburg, Institute of Geophysics, 20146 Hamburg, Germany
E-mail: mb@gpm.dkrz.de

Three wide-aperture seismic onshore-offshore lines were carried out on and around Crete in order to investigate the crustal structure of the region.

Up to 120 recording stations were deployed on each line and observed seismic energy generated by a 48 litre airgun array and eight 20 kg landshots. More than 300 traveltime sections were evaluated in order to generate a 2D P-wave velocity-depth model for each profile.

The results show strong lateral variations in crustal and sedimentary thickness, mainly north-south but also east-west, along strike. The continental crust below Crete has a maximum thickness of 32.5 km. Below the Cretan Sea the crust thins to a minimum of only 15 km while south of Crete the stretched continental crust reaches a minimum of 17 km. The continental margin and continent-ocean transition south of Crete are located approximately 100 km off the southern coast of the island. Below Crete, a 7 km thick layer was identified on each of the lines, dipping to NNE that could be followed by reflections to a depth of 42 km. This layer is the oceanic African lithosphere under subduction below the Agean continental crust.

A Comparison between Statistical and Deterministic Deconvolution

Scott Pearse (e-mail: pearse@esc.cam.ac.uk)
Richard Hobbs (e-mail: hobbs@esc.cam.ac.uk)

Bullard Laboratories, Madingley Rise, Madingley Road, Cambridge, CB3 0EZ

Obtaining reliable images beneath sills and basalts is a major restriction for the exploration of the western margin of Britain and elsewhere. We present here a simple and economical method to significantly improve the sub-sill image in areas of moderately deep water. The basis of the method requires the in-field measurement of the source wavelet by a single hydrophone beneath the source array. A projection of this recorded wavelet into the far field yields a source that is shown to provide a reliable wavelet for bandlimited deterministic deconvolution. We therefore remove the ambiguity inherent in statistical deconvolution a.k.a. Wiener filtering. The final image shows a significant improvement over standard processing for this area, especially in the near surface and beneath a basalt sill.

The problem is shown to lie in the assumptions of statistical deconvolution. The sill preferentially scatters the high-frequency energy allowing only the low-frequency to be transmitted. This low-frequency is largely carried in the bubble pulse tail of the source which is highly reverbatory. Statistical deconvolution does not differentiate between the low-frequency bubble and the low-frequency primary reflection so it tends to remove both leaving a confused image of weak energy.

Introduction

The British Institutions Reflection Profiling Syndicate (BIRPS) has acquired over 250,000 km of near normal incidence deep seismic reflection profiles around the British Isles and further afield over the last 18 years (Snyder and Hobbs, 1999). WESTLINE (England and Hobbs, 1997) is the only one to have the source wavelet recorded for deterministic deconvolution and multiple removal (Ziolkowski, 1991).

The airgun array used in the experiment measured 21.3 m in length by 50 m across and contained 40 airguns ranging in size from 40 to 460 cu in giving a total volume of 9390 cu in. The source was rich in low frequencies as described in Hobbs & Snyder (1992), and was designed to be towed at a depth of 10m (actual depth 11.65 m). As part of the experiment, the source signatures were measured using a towfish hydrophone while in deeper water. The signatures were recorded at a sample interval of 0.2 ms and a record length of 2 seconds. The hydrophone was situated beneath the airgun array. Exact positioning was achieved by firing the airguns at the corners of the array in sequence every hour. This procedure allowed the location of the hydrophone to be calculated. The cable length was then altering accordingly to position the hydrophone beneath the airgun array. Weather conditions were such that the ship's speed needed to be maintained at 4.1 knots. At this speed the hydrophone was towed at a depth of 65-70 m, 12 m behind the array centre.

The objective was to determine the far field source for multiple suppression (Ziolkowski, 1991), but as we show here, the source information can be used for deterministic deconvolution with a standard radon multiple suppression scheme, yielding exceptional results.

We compare statistical and deterministic deconvolution using data processed at a 4 ms sample interval, using a radon multiple suppression regime. Unlike statistical deconvolution, the deterministic deconvolution filters have been produced independently of the data, so there is no possibility that the primary information will be harmed. The recorded source wavelet cannot be used for deconvolution directly as it needs to be corrected for the receiver ghost, the effect of the instrument response, as well as the correct source ghost.

Wavelet Manipulation

The recorded source wavelet already contains a source ghost as it is a convolution of the source function and the effective reflection coefficient of the sea-surface. However, as the recording was not made in the true far field, the source ghost needs to be manipulated to have the correct amplitude. The time of the source ghost arrival is obtained from the recorded source using $t_d = f_n^{-1}$ where f_n is the notch frequency and t_d is ghost delay time. Deconvolution of the recorded source with a reflectivity series containing a spike of calculated amplitude at this

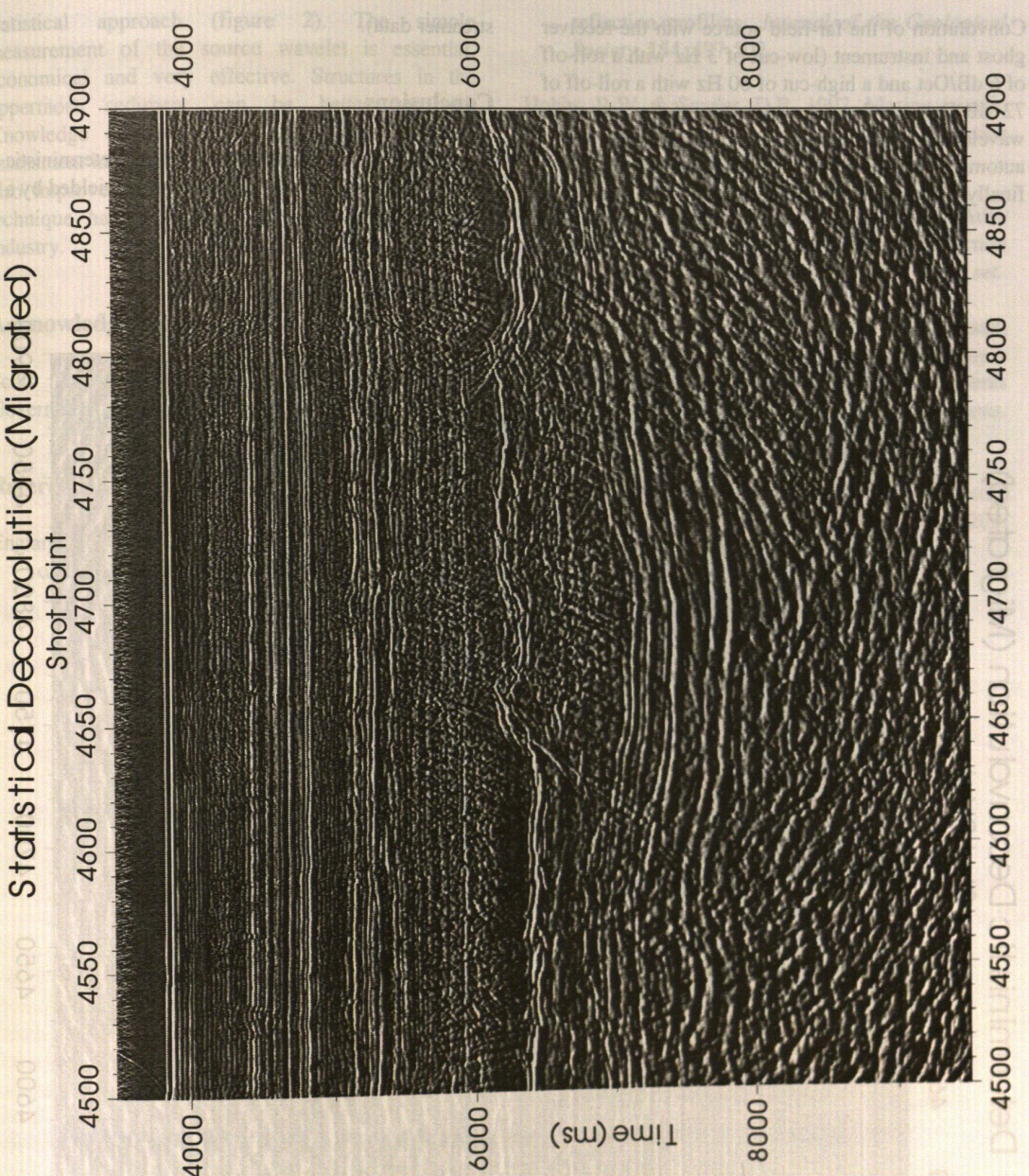

Figure 1. After statistical deconvolution the whole section is reverbatory in character. The migration suffers terribly from smiles typically caused by over-migration even though the migration velocities used are close to those used in the NMO correction applied before stacking. If lower velocities are used then most of the diffraction tails are under-migrated. The cause of the migration smiles is that the assumed statistical wavelet is incorrect. The statistical deconvolution operator changes on a trace by trace basis, so it introduces a trace by trace variation.

ghost delay time, gives the notional source (Ziolkowski *et al.*, 1982).

The notional source contains a high frequency oscillation, due to unknown sea-surface parameters and source directivity. This disturbance is of no consequence as it is beyond the specification of the anti-alias filter for the seismic data. The effect of the source and receiver ghosts can be determined from notches in the frequency spectrum of a shot gather which can be transformed into delay times for the respective ghosts. The correct source ghost notch can now be added to the frequency spectrum of the source using the source ghost delay time. The resulting wavelet is an estimate of the far-field source.

Convolution of the far-field source with the receiver ghost and instrument (low-cut of 3 Hz with a roll-off of 6 dB/Oct and a high-cut of 80 Hz with a roll-off of 72 dB/Oct) produces an estimate of the complete wavelet used for deterministic deconvolution. An automated process repeats the steps on every shot and finally resamples them to 4 ms (the sample rate of the streamer data).

Conclusions

The level of detail preserved after deterministic deconvolution (figure 1) far exceeds that yielded by a

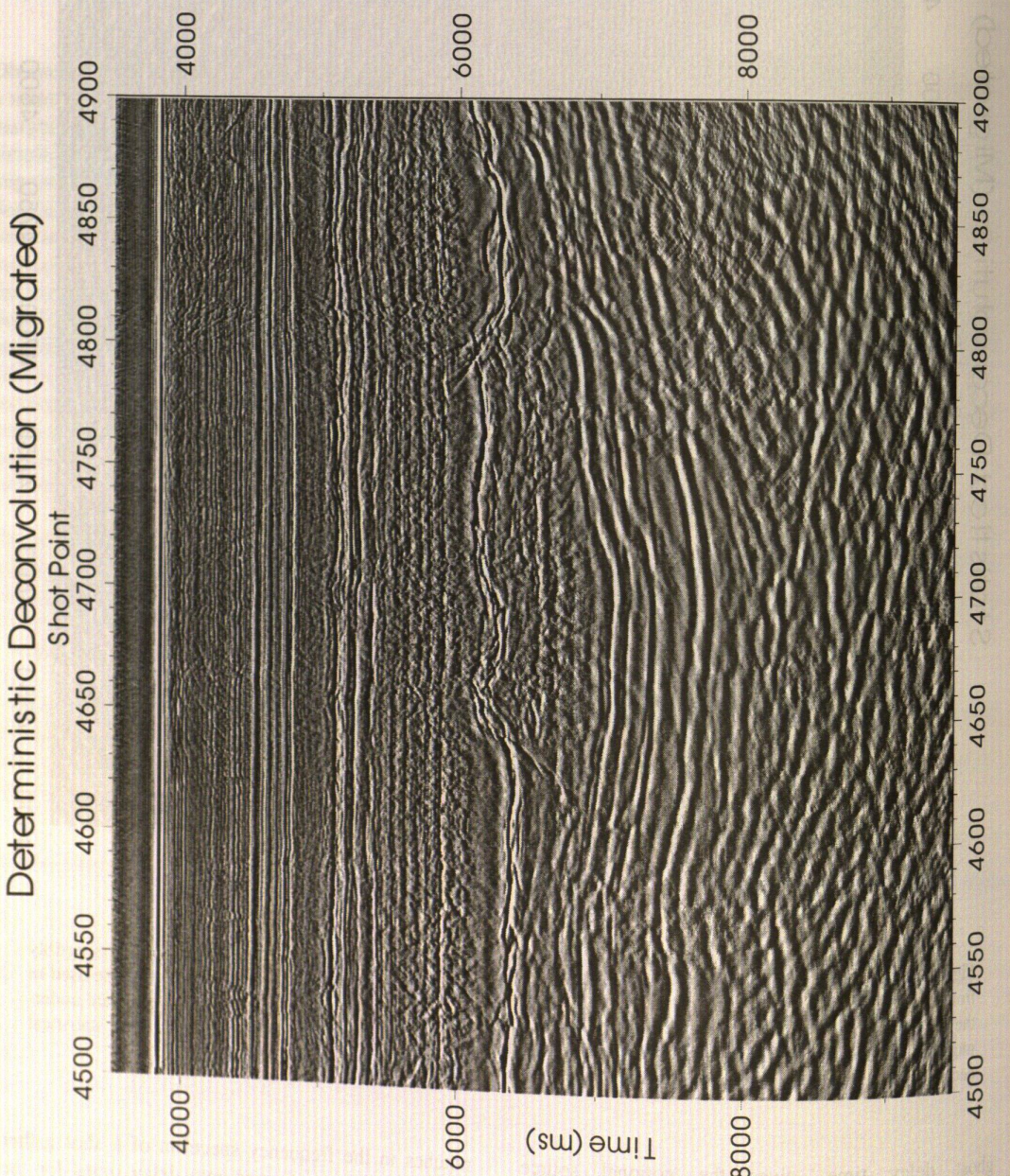

Figure 2. After deterministic deconvolution and migration, the result is a clean, crisp image with well-resolved faults and bed terminations. Almost all of the diffraction tails have migrated well with little over- or under-migration. The zero phase output from the deterministic deconvolution means that the section directly represents the reflectivity of the sub-surface. Black and white represent positive and negative impedance changes respectively. The top of the sill gives a positive impedance change from sediment to basalt and the base equally gives a negative impedance change. From the onset of the positive event to the end of the negative is now only 50 ms; 25 ms from peak to trough. This is equivalent to 75 m at 6 km/s.

statistical approach (figure 2). The simple measurement of the source wavelet is essential, economical and very effective. Structures in the uppermost sediment can be better resolved. Knowledge of such structures is vital for risk assessment in oil exploration. The sub-basalt image is also improved, as are deep crustal reflectors. This technique has applications in both academia and industry.

Acknowledgements

Scott Pearse is funded by the Isle of Man Government.

References

England, R.W. & Hobbs, R.W. 1997. The structure of the Rockall Trough imaged by deep seismic reflection profiling. *Journal of the Geological Society*, **154**, 497-502.

Hobbs, R.W. & Snyder, D.B. 1992. Marine seismic sources used for deep seismic reflection profiling. *First Break*, **10**, 417-426.

Snyder, D.B. & Hobbs, R.W. 1999. The BIRPS Atlas II: A second decade of deep seismic reflection profiling. *Geological Society London, 3 CD set.*

Ziolkowski, A., Parkes, G., Hatton, L. & Haugland, T. 1982. The signature of an airgun array - Computation from near-field measurements including interactions - Practical considerations. *Geophysics* **47**, 1413-1421.

Ziolkowski, A.M. 1991. Why don't we measure seismic signatures? *Geophysics* **56**, 190-201.

2-D Traveltime Inversion and Full-Wavefield Modelling Applied to Marine Reflection/Refraction Data across the Chicxulub Impact Crater

Paolo Primiero (primiero@ic.ac.uk), Jo Morgan, Mike Warner
T.H. Huxley, Imperial College, London SW7 2BP, UK.

Introduction

Quantitative images representing geophysical characters such as elastic and acoustic properties of the sub-surface are provided by inverting seismic data. Commonly used travel-time tomography attempts to find models that reproduce particular phases recognized in the seismic dataset. Full-wavefield tomography has many potential advantages compared to this technique. It can resolve structure that is of the order of the seismic wavelength, whereas travel-time methods are limited to resolving structure of the order of the Fresnel zone. In many seismic datasets, solving for the full-wavefield represents an order of magnitude improvement in resolution. The principal disadvantage to full-wavefield methods is that they require a better physical description of wave propagation, and are therefore computationally more expensive.

A full-wavefield inversion has been developed and successfully applied to cross-borehole data (Pratt et al., 1996); it involves the numerical solution of the wave equation by finite differences in the frequency domain. The algorithm performs a local search to reduce non-linearity, and the step length for each iteration is small. Hence the starting velocity model should be close to the "real" model, and synthetic travel-times of individual phases must arrive within half a wavelength of the observed travel-times. In addition, the input model must be smooth. We intend to apply full-wavefield inversion to near-normal-incidence reflection data acquired across the Chicxulub impact crater in Mexico. We used travel-time tomography to provide a smooth starting model. Some preliminary resolution tests are also presented to assess the potential of this technique.

Data were acquired on a 6 km multi-channel streamer, shots were fired every 50 m, channels 1-120 were spaced at 12.5 m, channels 121-240 at 50 m (Figure 1). We observe direct arrivals, wide-angle reflections and refractions, and diffractions as first arrivals. The main problems we have encountered in adapting the inversion codes to these data have been: 1) the handling of large amplitude variations between near and far offsets, 2) the handling of surface waves (the code is currently acoustic only), and 3) the handling of near-surface generated multiples. All three are potential problems with wide-angle data, but items 1) and 3) are exacerbated by the shallow water depth (20–30 m along much of the profile).

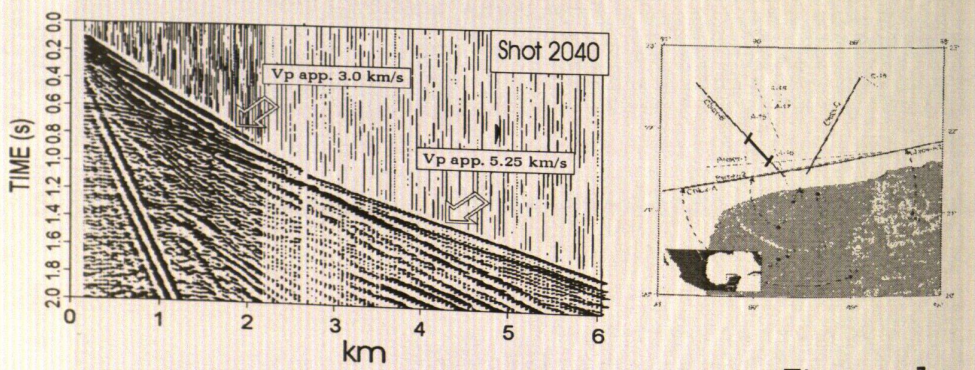

Figure 1.

Fig.1) Example shot gather. The near offsets are dominated by strong direct arrivals and reflections. The tick line on the map shows the location of the seismic profile.

FAST travel-time inversion

We used the FAST tomography code (Zelt and Barton,1998) to invert for the first-arrival travel-time.

The ray paths constrained by the acoustic solution of the eikonal equation are recalculated at each iteration, and a smoothness parameter is included in the regularized inversion scheme. As a start to modelling the data across Chicxulub we have chosen a subset of the data. The data spans a 41 km section of the Chicx-B profile, it runs across a topographic high in the Tertiary section and into the deep post-impact basin. The profile ends above the peak-ring, a topographic ring observed within the basins of large impacts. From well data, semblance plots and ray-tracing we know that the Tertiary section has significantly lower velocities (2 to 3.5 kms^{-1}), than the deeper Cretaceous and impact-related deposits which have velocities > 5 kms^{-1}.

We started each non-linear iteration with 20 values of λ ranging from 1000 to 1. Models on the left side have the minimum misfit errors but are rougher than models on the right side. On the other hand smoother models require a bigger number of iteration to converge to a minimum misfit. We propose that the preferred model lies approximately at the point of inflection on λ versus misfit plots. For the subsequent non-linear iteration we choose the model corresponding to the point of inflection. The corresponding best models are plotted in Figure 3. With this procedure the misfit approached a 6^2 value of 1.0 after 4 iterations.

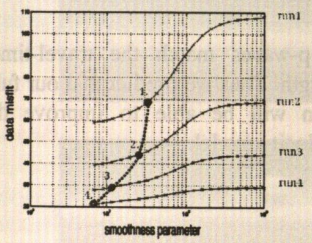

Figure 2.

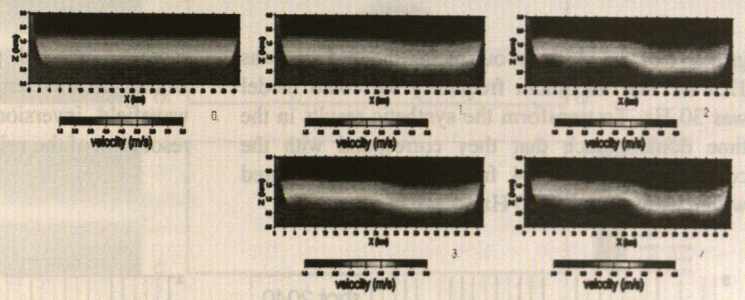

Figure 3.

Fig. 2) Crosses in the diagram represent each model as a function of the trade-off parameter λ and the data misfit.
Fig. 3) Averaged 1-D starting model. Fig.3.1, 3.2, 3.3, 3.4 are the corresponding models selected after each run (Figure 2).

In our preliminary modelling of these data Brittan et al. (1999) used RAYINVR (Zelt and Smith, 1992) and the recovered velocity models contained sharp boundaries. There is no advantage in using a starting velocity model with sharp boundaries: 1) if the boundaries are incorrectly positioned then, with a small step-length, many iterations will be required to correct the boundary location, and 2) with consideration of the Fresnel width our velocity models should represent a smoothed version of the real structure.

We took a 1-D average of the Brittan et al. (1999) recovered velocity model. We calculate the ray paths for this model. The velocities were smoothed using a cubic spline interpolator such that arrivals were not being modelled as head-waves and shadow zones for the ray paths due to the sharp interfaces were avoided. The starting model was parameterised as a rectangular matrix 41 km wide and 2.5 km deep, and with a node spacing of 20 m (Figure 2.0). In computing a slowness model for inversion the model was regridded with a 100 m spacing; the updated model was regridded back to 20 m spacing for the forward model.

The final model was obtained after 4 non-linear iterations. The velocities increase from 2.1 km/s in the shallow part of the basin to 5.8 km/s at the bottom. The model has a minimum structure but some smeared features can be recognised (Figure 4.):

A) The low velocities in the Tertiary sediments overlaying the crater floor.
B) The high velocity structures in the outer part.

Full-wavefield modelling

The final tomographic image is used as a starting model for the finite difference propagation of the waveform (Pratt et al., 1996). The algorithm is completely implemented in the frequency domain and a Fourier transform must be calculated in the end to reverse the results in time. To calculate the solution for the wave-field we use a direct matrix solver such as the LU decomposition method. This is a central point in the algorithm because the resulting matrix of factors can be re-used to calculate the forward solution for a large number of sources. Since the solution is calculated for one frequency at a time, modelling the attenuation effects, which are frequency dependent, is straightforward. A limit for the maximum modelling frequency is imposed by the

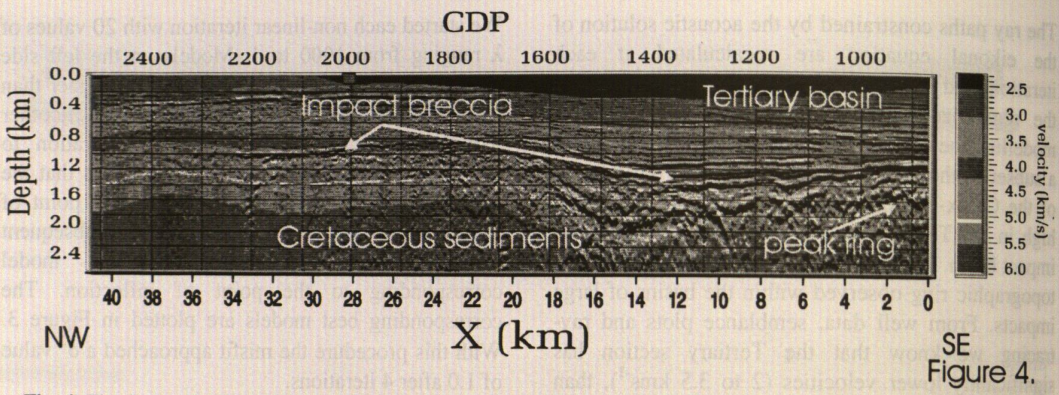

Fig. 4) The final model obtained after 4 non-linear iterations corresponding to Fig3c).

grid size of the mesh. In our model the grid size was 12.5 m. The maximum frequency we could model was 30 Hz. To transform the synthetic results in the time domain such that they correspond with the correct trace length 64 frequencies were required within a range of 1 to 30 Hz.

synthetic derived p-waves match the travel-times within half wavelength. Thus we predict that our full-wavefield inversion will be able to improve the resolution of the velocity model.

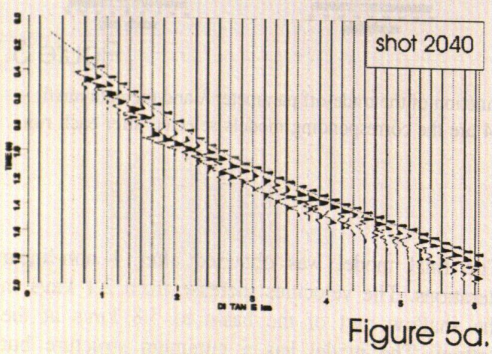

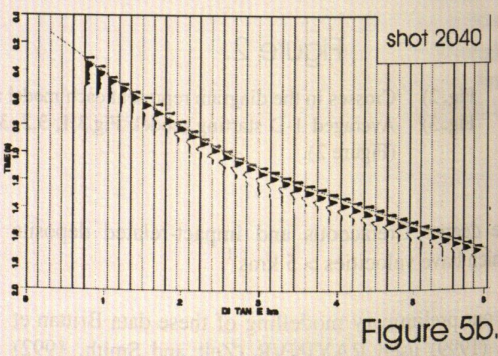

Fig. 5) Comparison between synthetic finite difference results and pre-processed data after the windowing procedure. The small triangles represent the picked arrivals and the straight line the calculated travel-time arrivals interpolated along the offsets.

We have pre-processed the observed data. The shots were band-pass filtered to 0–30 Hz and re-sampled to 16 millisecond. A predictive deconvolution was applied within ensembles in two steps: 1) in the shot domain; 2) in the constant offset domain. This process attenuates coherent noise and first order multiple that is not easily modelled, and improves the signal coherence of the first arrivals.

Synthetic results show in acoustic p-wave arrivals and some strong direct arrivals. At this stage we do not intend to invert for the entire dataset, just for the first arriving waveforms. Hence the data has been windowed to remove late arrivals. Reflections and later phases could be added later to the data. Windowing the data is an important step and the length of the window must be carefully chosen: we try to avoid to introduce unwanted high (infinite) frequencies cutting the data. In this window the

Full-wavefield inversion: preliminary test

To test the full-wavefield inversion we simulated an experiment on a rectangular grid of 485x160 points corresponding to a model 6 km wide and 2.5 km deep. Shot are spaced every 50 m at a depth of 250 m. 119 shots were modelled and the receivers were positioned at each grid point.

- The true model (Figure 6a) consists in an anomaly of the dimension of a wavelength and 10% increase in velocity superimposed to a constant gradient background model.

- A smeared anomaly superimposed to the background model (6b) is used as a starting model for the inversion. The difference between model (6a) and (6b), in (6d) is of the order of 300 ms^{-1}.

The final model after 15 iterations using 3 groups of 5 frequencies each (6c). The difference between model (6a) and (6c) is of the order of 10 ms^{-1} (6e).

Pratt, R. G., Zong Z.M., Williamson P. and Warner, M., (1996) Two-dimensional velocity models from wide-angle seismic data by wavefield inversion. Geophys. J. Int. 124, 323-340.

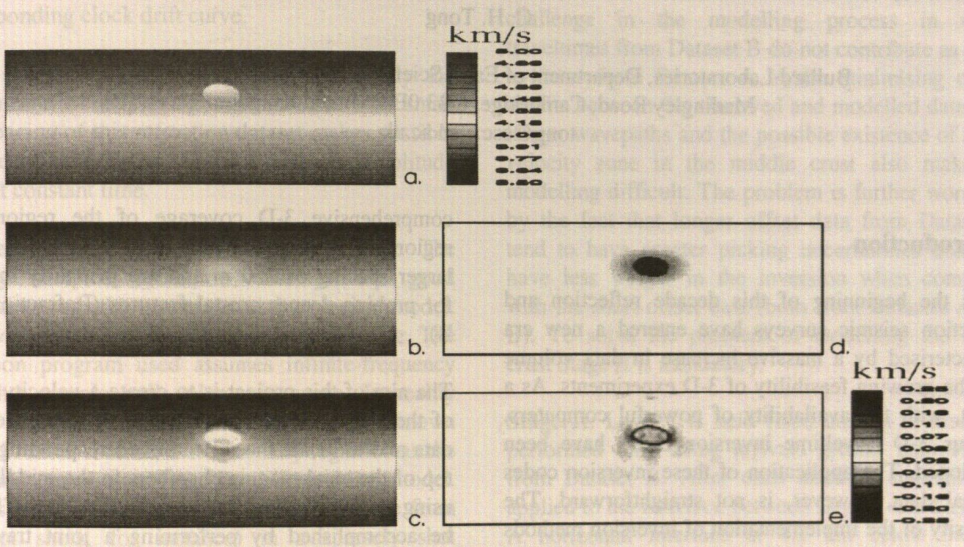

Figure 6

Conclusions

Travel-time tomography produces a smoothed velocity model that is appropriate as a starting model for the finite difference propagation of the waveform. Waveform modelling shows acoustic p-wave arrivals and some strong direct arrivals. At a first stage we intend to invert only for the first arriving waveforms and have muted the data to remove later phases. The derived p-waves match the travel-times within the order of half wavelength. Simulation tests prove that a high resolution image is achieved after a small number of iteration using "packets" of only few frequencies at time. On the base of these results our waveform inversion potentially would improve the resolution of the velocity model when the real data will be inverted.

References

Brittan, J., Morgan, J. V., Warner, M. R., Marin, L. and the Chicxulub Working Group, 1999, Chicxulub seismic experiment: The first two seconds: Geological Society of America Special Paper (in press).

Tarantola A., (1984). Inversion of seismic reflection data in the acoustic approximation. Geophysics 49, 1259-1266.

Zelt, C. A. and Smith, R. B., (1992). Seismic traveltime inversion for 2-D crustal velocity structure. Geophys. J.Int. 108, 16-34.

Zelt, C. A. and Barton, P. J., (1998) Three-Dimensional seismic refraction tomography: A comparison of two methods applied to data from Faeroe Basin, J. Geophys. Res., 103, B4, 7187-7210.

Modelling three-dimensional seismic data: Case study on the 9° 03' N overlapping spreading centre on the East Pacific Rise

C. H. Tong

Bullard Laboratories, Department of Earth Sciences, University of Cambridge,
Madingley Road, Cambridge, CB3 0EZ, United Kingdom.
tong@esc.cam.ac.uk

I Introduction

From the beginning of this decade reflection and refraction seismic surveys have entered a new era characterised by a massive increase in data volume and the growing feasibility of 3-D experiments. As a result, with the availability of powerful computers, various 3-D traveltime inversion codes have been developed. The application of these inversion codes to real data, however, is not straightforward. The diversity of the implementation of inversion methods and the uniqueness of each dataset make any modelling process a highly original activity. Previous work on inversions of 3-D seismic data (e.g. Toomey et al., 1994; Zelt et al.; 1996, Zelt and Barton, 1998) clearly exemplify this point.

Making reliable geological models for interpretation is the ultimate goal of any investigation and this can only be achieved by simultaneously exploiting certain important characteristics inherent in the experiment and the resulting data, and having a sound modelling strategy. This paper presents the methods and strategy used in a 3-D crustal study of the East Pacific Rise with refraction and reflection data.

II Overview of the study

The ARAD (Anatomy of a Ridge Axis Discontinuity) cruise was undertaken in 1997 to provide the first joint reflection and wide-angle seismic data for the study of the structure of the overlapping spreading centre at 9° 03' N on the East Pacific Rise (Singh et al., 1999).

Eleven regional shot lines and 201 parallel reflection profiles with a lateral spacing of 100m were shot and simultaneously recorded by a grid of 30 ocean bottom hydrophones, some of which were also equipped with geophones (Figure 1). More than 158,000 densely spaced airgun shots (37.5m shot spacing) were fired and the recordings of these shots provide both ample amounts of wide-angle data for investigating the upper velocity structure (Refraction Data A) and a reflection dataset with a comprehensive 3-D coverage of the region. The regional OBS lines consist of 2000+ shots with a larger spacing of 250 m and are primarily intended for probing deeper crustal features (Refraction Data B).

The aim of this project is to create a velocity model of the upper and middle crust using the wide-angle data and to locate the reflectors corresponding to the top of the axial magma chambers in the middle crust using stacked and unstacked reflection data. This can be accomplished by performing a joint traveltime inversion of the data from shots fired within the study area marked in Figure 1 using an inversion code developed by J. Hobro. The inversion code uses two-point ray tracing for forward modelling data and employs regularised inversion by invoking the conjugate gradient method.

There are essentially two 'sets' of refraction data available (albeit both collected from the same experiment) that possess very different characteristics. The main obvious differences lie in the spatial density of shots and the amount of data. Also, Refraction Dataset A is characterised by shorter offset arrivals (up to 12 km) due to the noisy sea environment caused by the short shot intervals. On the other hand, seismic arrivals from up to 29 km offset have been identified from Refraction Dataset B. 28,979 and 3301 arrivals corresponding to Datasets A and B respectively have been picked from 12 seismometers and are used for initial testing.

III Data preparation: exploiting the uniqueness of the dataset

Clock drift correction: One of the most critical steps in data processing is to relocate the seismometers with high accuracy. In traditional 2-D experiments the success of relocating OBSs accurately relies on having crossing shot lines. The 3-D dataset poses extra constraints by providing direct water arrivals from all azimuths. However, the unique strength of having a 3-D geometry lies in the fact that the drifts of the OBS clocks, which would otherwise be assumed to be linear, can be deduced by

considering water arrivals from a number of shot lines collected at different times during the cruise. A code has been written that searches for the minimum root mean square misfit between the observed water arrival times and the modelled arrival times and hence finds the actual location of an OBS and the corresponding clock drift curve.

Time slices: Record sections are traditionally the only means of displaying seismic data. The small shot spacing of this refraction dataset makes possible the use of time slices, which are spatial amplitude plots at constant time.

Fresnel volume and decimation of data: The densely sampled refraction data provide good constraints on the upper crustal velocity model. However, this has to be achieved with due care. The inversion program used assumes infinite-frequency rays that sample null volume in space. In reality waves from sources sample a finite volume, known as the Fresnel volume, that is usually regarded as the maximum resolution limit in the resulting model. This is true for near-parallel wavepaths (those from adjacent shots, for instance) in a sparsely shot experiment because they rarely have overlapping Fresnel volumes.

If 3-D full waveform inversion is performed, the existence of overlapping near-parallel Fresnel volumes will undoubtedly offer potential to resolve velocity anomalies smaller than the Fresnel radius. Such an inversion would, however, be far beyond the capability of present-day computers. Since traveltime inversion is performed in this study, decimation of data may be required in order to avoid the problem of having potentially significant differences between the traveltimes calculated based on ray theory and those observed. The extent of decimation applied can be determined by first using relatively fewer data to construct a model and then to add the decimated data back gradually to see if the model is sufficient to satisfy these added data within the picking uncertainties.

IV Inversion algorithm

The inversion comprises three stages, in which the first two are primarily for producing velocity models that are close enough to the final model to save computation time and to boost the "hit rate", or in other words, the proportion of observed data that can be modelled. It is worth noting that the typical runtime for one iteration including forward modelling and inversion is in the order of 0.5 to 1 day on a workstation with a single 533MHz processor and at least 10 iterations are required to produce the final model.

Stage I: Both Refraction Datasets A and B (truncated at offsets up to 12 km) are used in this stage of iterative inversion. The final model consists of a well-constrained upper crust (down to 4.5 km depth from the sea surface, marked L I in Figure 1). However, the sheer size of Dataset A creates a challenge in the modelling process in which traveltimes from Dataset B do not contribute as much as those from Dataset A in the minimising of the misfits between the observed and modelled data. The longer wavepaths and the possible existence of a low velocity zone in the middle crust also make the modelling difficult. The problem is further worsened by the fact that longer offset data from Dataset B tend to have greater picking uncertainties and thus have less weight in the inversion when compared with the short offset data (both from Datasets A and B). To solve the problem of modelling the lower crust Stage II is mandatory.

Stage II: Layer I is held fixed and an inversion is performed only using arrivals greater than 12 km from Dataset B. After each iteration smoothing is applied to the interface between Layer I and Layer II. A horizontal interface at 4.5 km below the sea surface between the two layers is sufficient as the main concern at this stage is to construct a lower crustal model that will serve as the starting model for Stage III. It is important to obtain a model that closely resembles the final model to be produced by the final joint inversion of all the seismic data. The problems encountered in Stage I are solved using this procedure.

Stage III: Starting with the final model from Stage II unstacked reflection data will be incorporated into the final joint inversion of all refraction data. The unstacked data contain both depth information on the reflectors, which lie 0.5 km to 1 km below the interface between Layers I and II, and velocity constraints on the region above the reflectors.

The problem of the smaller contribution of the large offset data still persists in this stage, although the starting model is closer to the final model. The way to alleviate the problem is to introduce some degree of scaling, which involves comparing frequency distribution of offset in the combined refraction dataset (Datasets A and B) with that in an ideal dataset. An ideal dataset can be obtained by forward modelling using the final model from Stage II and hence, producing a set of synthetic traveltimes. The ideal dataset has more data at larger offsets than the combined refraction dataset and provides an objective standard for weighting of large offset data.

A migration of the stacked reflection data is then used to define the geometrical distribution of the reflectors, which are not continuous across the study area.

V Conclusion

The work presented above shows the technical problems encountered in inverting a large combined 3-D marine seismic dataset and solutions are offered. The inversion algorithm described has been adopted for inverting the most densely sampled 3-D seismic dataset collected to date. Initial results show the strengths of employing a two-stage process for producing a good starting model based on inverting subsets of data. This improves the "hit rate" of the large offset data and also bears significant advantage on the total computation time. Other exploitations of the 3-D nature of the experiment and data explained have also facilitated the modelling process. This case study has implications for the design of future seismic experiments: shot spacing plays an important role in the modelling procedure. The stage-by-stage approach to analysing 3-D joint refraction and reflection experiments has also been demonstrated.

Acknowledgements

I would like to thank my supervisors P. J. Barton, M. C. Sinha, S. C. Singh and R. S. White for their guidance. I also thank A. J. Harding, G. M. Kent, J. A. Orcutt, R. W. Hobbs, J. Pye and S. Bazin, who are involved in the ARAD project.

References

Hobro, J, Ph.D. Thesis, University of Cambridge, in preparation.

Singh, S. C., M. C. Sinha, A. J. Harding, G. M. Kent, P. J. Barton, J. A. Orcutt, R. S. White, and R. W. Hobbs, Preliminary Results Are in from Mid-Ocean Ridge Three-dimensional Seismic Reflection Survey, EOS, Volume 80 Number 16, pp. 181, 185, 1999.

Toomey, D. R., S. C. Solomon, and G. M. Purdy, Tomographic imaging of the shallow crustal structure of the East Pacific Rise at 9° 30', J. Geophy. Res., 99, 3031-3041, 1994.

Zelt, B. C., R. M. Ellis, R. M. Clowes, and J. A. Hole, Inversion of three-dimensional wide-angle seismic data from the southwestern Canadian Cordillera, J. Geophy. Res., 101, 8503-8529, 1996.

Zelt, C. A. and P. J. Barton, Three-dimensional seismic refraction tomography: A comparison of two methods applied to data from the Faeroe Basin, J. Geophy. Res., 103, 7187-7210, 1998.

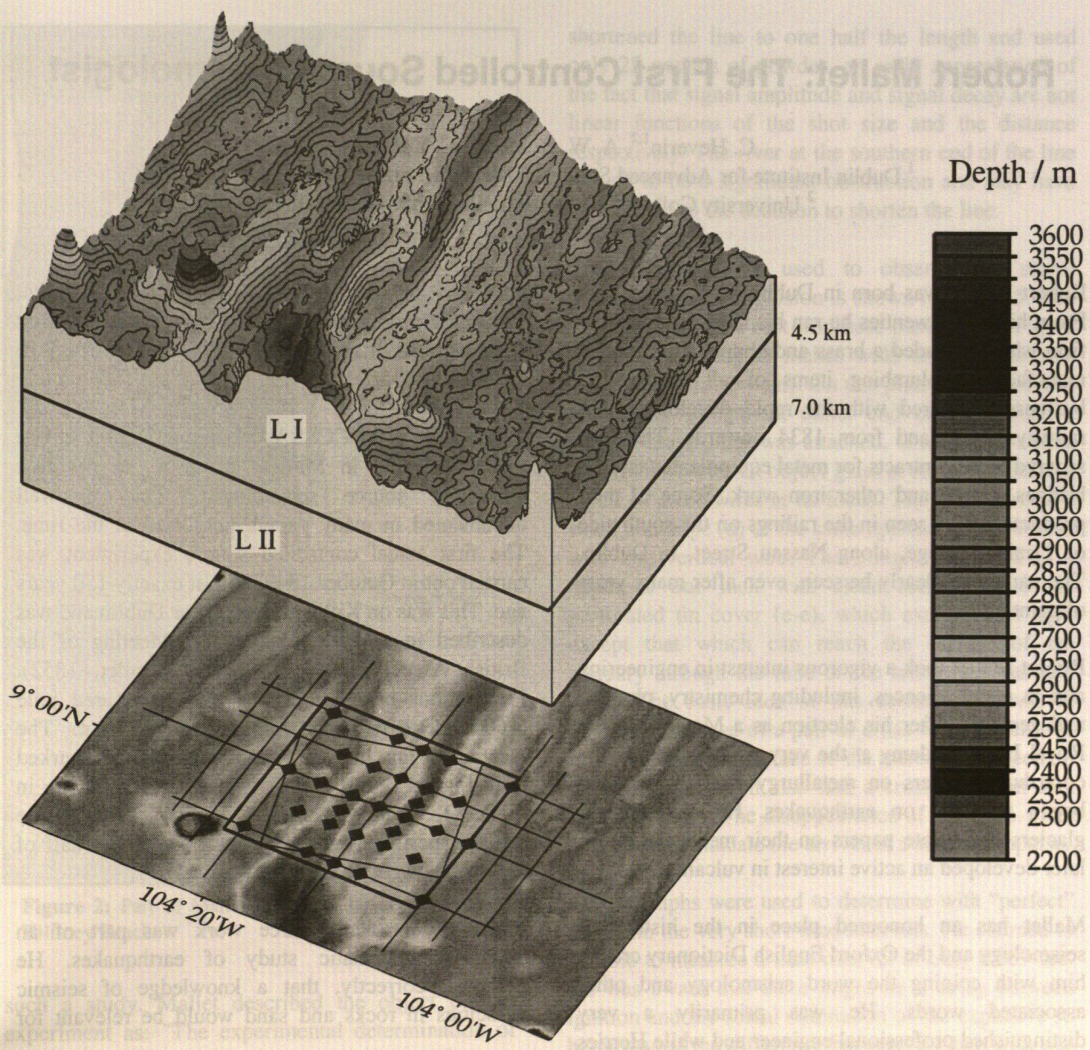

Figure 1 The bathymetry map shows the geometry of the experiment. The thick lined box defines the region of this study (measured 27.9 km by 25.6 km) and the 30 ocean bottom seismometers are represented by the filled rhombuses. The tilted box (measured 23 km by 20 km) contains 201 parallel shot lines with line spacing of 100 m (Refraction Dataset A and reflection dataset) and the eleven lines that form a grid correspond to the more sparsely shot lines (Refraction Dataset B). The velocity structure of Layers I and II (marked L I and L II in the Figure) is constrained by different subsets of the refraction data (see text for explanations). Please note that these two layers are by no means related to the conventional layering of oceanic crust and the thickness of the layers shown here is not to scale.

Robert Mallet: The First Controlled Source Seismologist

C. Heverin[1,2], A. W. B. Jacob[1], C. J. Bean[2]
[1] Dublin Institute for Advanced Studies, 5 Merrion Square, Dublin 2, Ireland
[2] University College Dublin, Belfield, Dublin 4, Ireland

Robert Mallet was born in Dublin on 3 June 1810. From his early twenties he ran his father's successful firm which included a brass and copper foundry and manufactured plumbing items of all kinds. The business prospered with the rapid development of railways in Ireland from 1834 onwards. The firm secured large contracts for metal equipment, cast-iron bridges, cranes and other iron work. Some of their products can be seen in the railings on the south side of Trinity College, along Nassau Street, in Dublin. The name can clearly be seen, even after many years of painting.

Robert Mallet took a vigorous interest in engineering and in many sciences, including chemistry, physics, and geology. After his election as a Member of the Royal Irish Academy at the very early age of 21, he contributed papers on metallurgy and geology and began to write on earthquakes. He also studied glaciers and wrote papers on their mechanisms. He later developed an active interest in vulcanology.

Mallet has an honoured place in the history of seismology and the Oxford English Dictionary credits him with coining the word seismology and other associated words. He was primarily a very distinguished professional engineer and while Herries Davies (1982) considered him merely to be 'an amateur earth-scientist' he noted that he was of international repute in that field.

His influence can be seen in every aspect of seismology. He developed plans for a seismometer but, unusually for him, he did not actually build it, though his drawings are said to have influenced the design of a seismometer built by Palmieri in 1855. Between 1852 and 1854 he published an earthquake catalogue. He used the catalogue to produce a map of earthquakes throughout the world which still looks remarkably good, though the events along the mid-ocean ridges are, of course, absent.

He also made plans for a systematic study of the effects of a major earthquake. His chance came when a large earthquake occurred in the Naples area on 16 December 1857. The Royal Society contributed 150 pounds and Mallet spent three months between January and April 1858 observing and measuring the effects of the earthquake on buildings and other objects throughout the region. The results were published in 1862 in two large volumes (Mallet, 1862). He produced a splendid isoseismal map with the directions of motion indicated from his study of the damage.

Participants in the CCSS Workshop in Dublin will be more interested in Mallet's claim to be the first controlled source seismologist. This is well documented in many papers published at the time. The first actual controlled source experiment was carried out in October 1849, almost exactly 150 years ago. This was on Killiney Beach near Dublin and was described in a report to the 21st Meeting of the British Association in July 1851 (Mallet, 1852). Preparations began in July, with a measured mile (1600 metres) being carefully staked out. The location of this line, just south of Dublin, is marked A in Figure 1, and is also shown in the drawing in Figure 2, which appeared in Mallets paper. In the actual experiment he used only the northern half of the line, between B and C in Figure 2.

Mallet's controlled source work was part of an extensive systematic study of earthquakes. He believed, correctly, that a knowledge of seismic velocities in rocks and sand would be relevant for

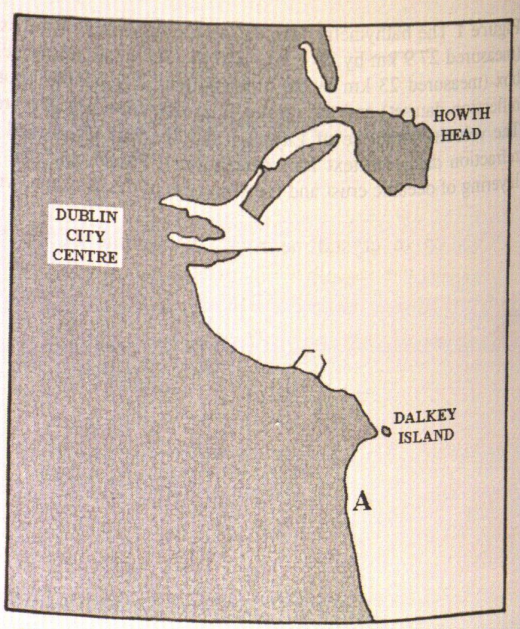

Figure 1: A map of the greater Dublin area. 'A' marks the site of Mallet's first controlled source experiment.

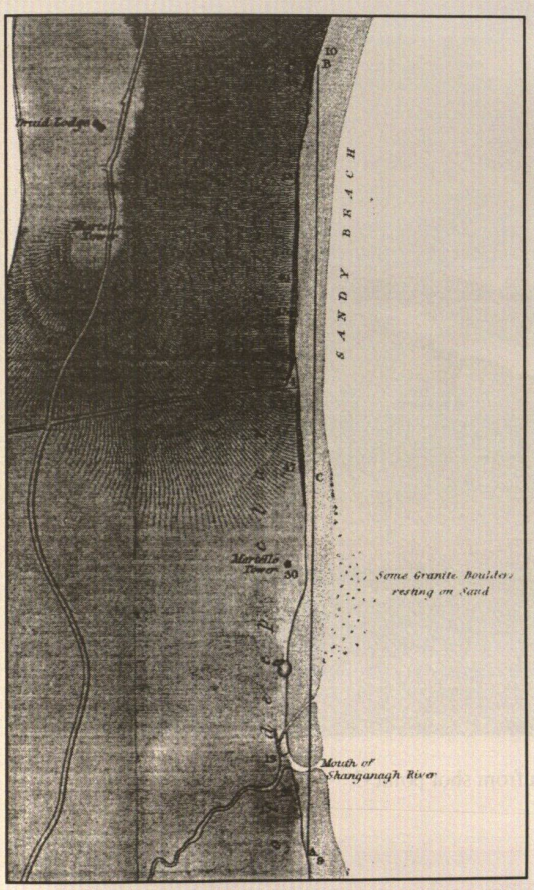

Figure 2: Part of Mallet's map of the experiment on Killiney Beach.

such a study. Mallet described the object of this experiment as: "The experimental determination of the limits of transit rate of the propagation of waves or pulses, analogous to those of earthquakes through solid materials."

He chose Killiney Beach to measure what he expected to be slow waves in discontinuous media (sand) and later moved to Dalkey Island nearby (Figure 1) to measure what he expected to be faster propagation in crystalline rock, the granite of the island. The view south from near his shot-point is shown in Figure 3 with Bray Head in the background. Some late twentieth century seismologists can be seen in Figure 3, working on a much smaller scale than Mallet did. The view north is shown in Figure 4 and the eastern end of Dalkey Island can be seen with a Martello tower apparent on the skyline.

The beach is straight and level and consists of sand resting on a bed of hard clay and gravel. The measured line was one mile long and he calculated that 128 pounds (about 58 kg) would be needed to produce an observable pulse at that distance. This was thought to be too large an explosion so he shortened the line to one half the length and used only 25 pounds of powder, an early appreciation of the fact that signal amplitude and signal decay are not linear functions of the shot size and the distance respectively. The river at the southern end of the line proved to be a significant obstruction and may have contributed to the decision to shorten the line.

The instrument he used to observe the signal generated by the explosion is shown in Figure 5. The seismoscope had a cast iron base plate (a-a in Figure 5) 20 inches long, 8 inches wide and half an inch thick (1 inch = 2.54 cm). On this plate was a cast iron rectangular trough. At either end of this trough a vertical brass pillar was attached. One carried a tube (c) provided with an object glass at its lower end and a pair of cross wires at its focus. The other carried a small telescope (d) of the same aperture and provided with one vertical wire. The trough was filled to a depth of one inch with clean mercury, and the perforated tin cover (e-e), which excluded all light except that which can reach the surface of the mercury through the tube or the telescope, was laid on it. The basic idea of this seismoscope was to observe the image of a pair of cross wires which was reflected from the surface of the mercury and seen on the telescope which also had a cross-wire, but at a different angle. The disappearance of the cross-wires was taken to indicate the arrival of a seismic impulse.

Chronographs were used to determine with "perfect" precision the very short time intervals. He claimed to be able to measure a time interval of only 0.007 sec. He was aware that there might be a delay between ignition and the actual detonation of the explosive so he measured the difference between the two with one chronograph and then the arrival time at the seismoscope with another. The firing pulse started both chronographs. The shot-point observer, close to the source, stopped his chronograph as soon as he saw evidence of the explosion at the surface (the powder was buried 6 feet, almost 2 metres, below the surface). The seismoscope observer stopped his chronograph when the cross-wires disappeared. The difference between the two readings gave the travel time of the wave from the source to the seismoscope.

Mallet made some rather questionable, but very small, corrections to the travel time and it may be that these were unnecessary. He made eight successive measurements and, even though the timing system was rather crude, he achieved fairly consistent results. The travel time was almost 3 seconds, the average being 2.91 seconds (he gave the figure as 2.911639, amazing precision!). This represents about 900 feet per second, about 270 m/s. His "correction" increased this value to about 290 m/s but this may not be valid. He considered this to be a very low value. It

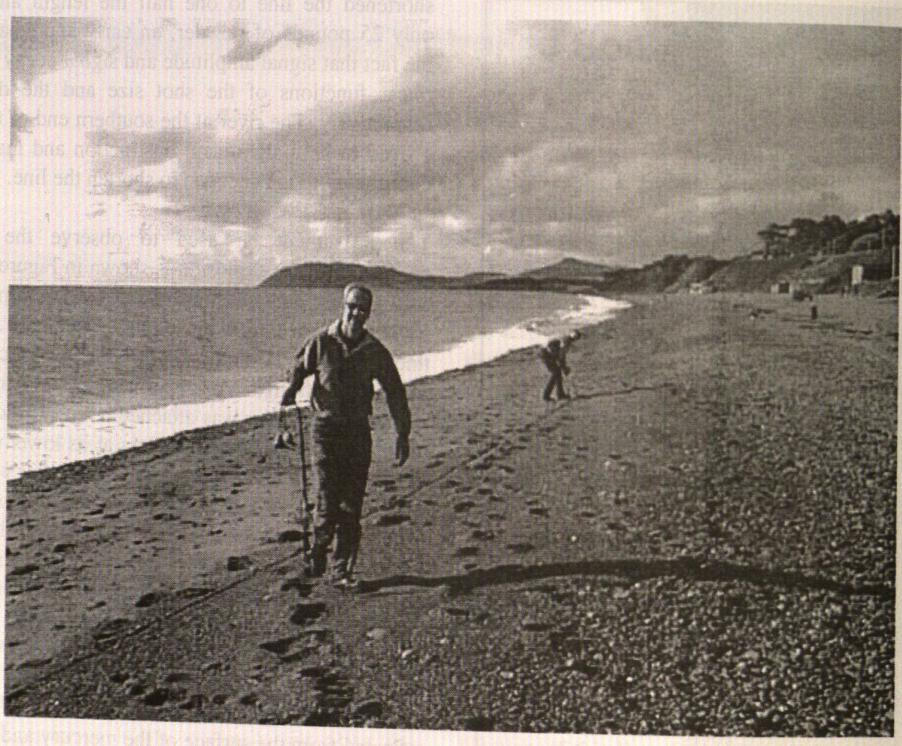

Figure 3: The view south from shot point C.

Figure 4: The view north from shot point C. Dalkey Island is on the horizon on the right.

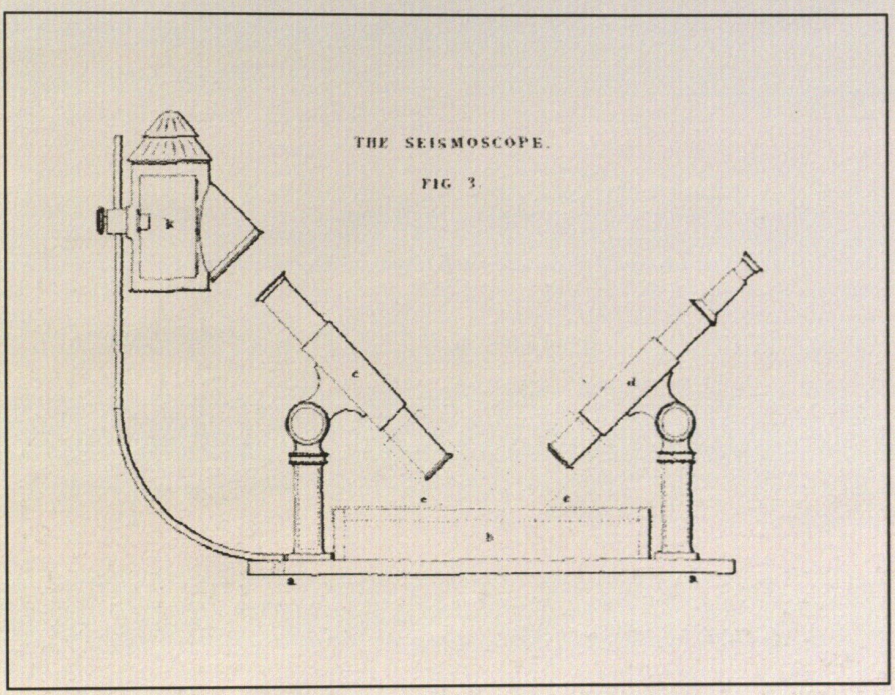

Figure 5: Mallet's Seismoscope as portrayed in his 1852 paper (see text for details).

is worth noting that he carried out tests (using a musket) that proved that the signal was not transmitted through the air. The greatest velocity he measured, even in the solid granite of Dalkey Island, was a little less than 500 m/s. He knew enough about the properties of matter to believe that he was not observing compressional waves. He could be excused for not knowing what waves he had measured because it is likely that the waves were surface waves, probably Rayleigh waves. Rayleigh did not predict the existence of these waves until about forty years later.

Some hammer seismics were carried out in August 1999 to cheek on the P wave velocities under the beach. We would not have been allowed to use barrels of gun-powder! These profiles were very short and were carried out in the vicinity of Mallets shot point. The data indicated that the sand is very thin, about 1.5 metres, with a very low velocity of about 220 m/s at this point. Immediately below this is clay with a velocity of about 1.4 km/s, though that seems to increase with depth, and below the clay there is rock at about 3 km/s.

Mallet's observed velocity of about 270 m/s is much too low to be a P wave velocity for either the clay or the underlying rock and it is rather high to be a surface wave purely in the sand. It is likely that short-period Rayleigh waves were observed and that the cross-wires did not disappear on the arrival of earlier, but probably very small, P waves.

References

Herries Davies, G. L., 1982. *Robert Mallet: Earth-scientist.* In: R. C. Cox (Editor), Robert Mallet 1810-1881, Centenary Seminar Papers, published by the Institution of Engineers of Ireland and the Royal Irish Academy, 35–52.

Mallet, R., 1852. Report to the British Association for the Advancement of Science, Part 1, 272–320.

Mallet, R., 1862. Great Neapolitan Earthquake of 1857: The first principles of observational seismology, publ. John Murray, London, in two volumes, pp. 456 and pp. 408.

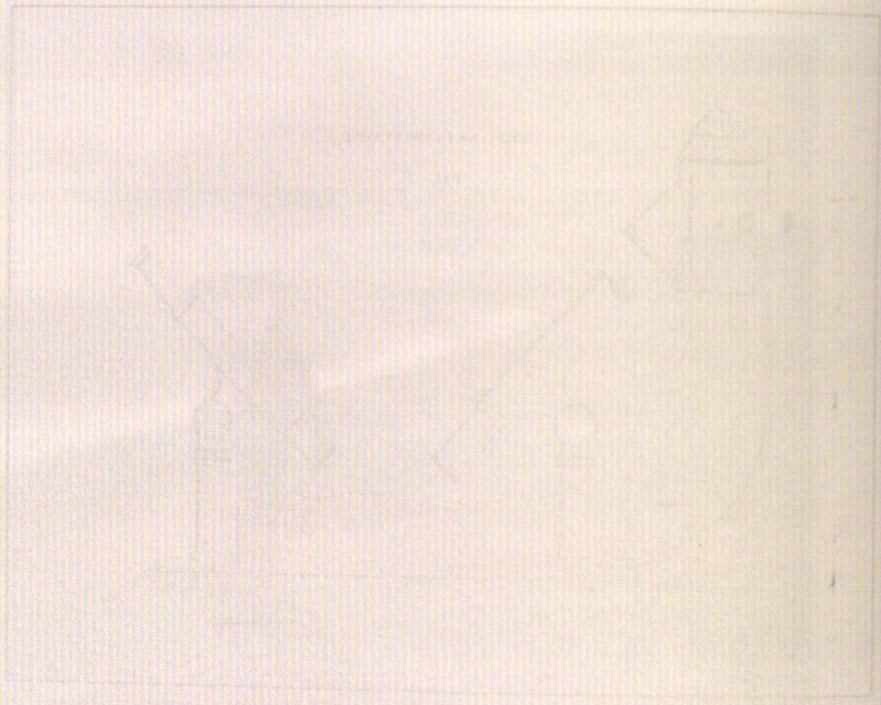

COMMUNICATIONS OF THE

DUBLIN INSTITUTE FOR ADVANCED STUDIES

Series D, Geophysical Bulletin No. 49

DUBLIN 2000

DUBLIN INSTITUTE FOR ADVANCED STUDIES

ISBN 1-85500-958-7